MODELLING AU CATALYST FROM BULK TO NANOSCALE

Alberto Roldán Martínez

ISBN: 978-84-693-7669-0
Dipòsit Legal: T-1748-2010

UNIVERSITAT ROVIRA I VIRGILI
MODELLING AU CATALYST FROM BULK TO NANOSCALE
Alberto Roldán Martínez
ISBN:978-84-693-7669-0/DL:T-1748-2010

UNIVERSITAT ROVIRA I VIRGILI
MODELLING AU CATALYST FROM BULK TO NANOSCALE
Alberto Roldán Martínez
ISBN:978-84-693-7669-0/DL:T-1748-2010

UNIVERSITAT ROVIRA I VIRGILI
MODELLING AU CATALYST FROM BULK TO NANOSCALE
Alberto Roldán Martínez
ISBN:978-84-693-7669-0/DL:T-1748-2010

Alberto Roldán Martínez

Modelling Au catalyst from bulk to nanoscale

TESI DOCTORAL

dirigida pel Prof. Josep Manel Ricart Pla i
pel Prof. Francesc Illas Riera.

Departament de Química Física i Inorgànica

UNIVERSITAT ROVIRA I VIRGILI

Tarragona
2010

UNIVERSITAT ROVIRA I VIRGILI
MODELLING AU CATALYST FROM BULK TO NANOSCALE
Alberto Roldán Martínez
ISBN:978-84-693-7669-0/DL:T-1748-2010

UNIVERSITAT ROVIRA I VIRGILI
MODELLING AU CATALYST FROM BULK TO NANOSCALE
Alberto Roldán Martínez
ISBN:978-84-693-7669-0/DL:T-1748-2010

UNIVERSITAT ROVIRA I VIRGILI
Departament de Química Física i Inorgànica

Josep Manel Ricart Pla, Catedràtic de Química Física, del Departament de Química Física i Inorgànica de la Universitat Rovira i Virgili, i **Francesc Illas Riera**, Catedràtic de Química Física, del Departament de Química Física de la Universitat de Barcelona

CERTIFIQUEM que la present memòria, que porta per títol:

Modelling Au catalyst from bulk to nanoscale

ha estat realitzada sota la nostra direcció, en el programa de doctorat en Química Teòrica i Computacional pel llicenciat en Química **Alberto Roldán Martínez** per a obtenir el grau de Doctor en Química amb Menció Europea.

Tarragona, Setembre de 2010

Prof. Josep Manel Ricart Pla Prof. Francesc Illas Riera

UNIVERSITAT ROVIRA I VIRGILI
MODELLING AU CATALYST FROM BULK TO NANOSCALE
Alberto Roldán Martínez
ISBN:978-84-693-7669-0/DL:T-1748-2010

UNIVERSITAT ROVIRA I VIRGILI
MODELLING AU CATALYST FROM BULK TO NANOSCALE
Alberto Roldán Martínez
ISBN:978-84-693-7669-0/DL:T-1748-2010

UNIVERSITAT ROVIRA I VIRGILI
MODELLING AU CATALYST FROM BULK TO NANOSCALE
Alberto Roldán Martínez
ISBN:978-84-693-7669-0/DL:T-1748-2010

UNIVERSITAT ROVIRA I VIRGILI
MODELLING AU CATALYST FROM BULK TO NANOSCALE
Alberto Roldán Martínez
ISBN:978-84-693-7669-0/DL:T-1748-2010

Agradecimientos

Antes de nada quisiera agradecer muy sinceramente a mis directores de tesis: el Prof. Francesc Illas y el Prof. Josep M. Ricart por la paciencia, la constancia y la didáctica que me ha dedicado, además de haberme alentado, ayudado y guiado en este difícil tramo final. Sin ellos dos no me podría haber iniciado en la comunidad científica.

To all people in "Dipartamento di Scienzia dei Materiali dell'Università Milano-Bicocca". To Prof. Gianfranco Pacchioni for always being patient and kind to me. To Livia, Cristiana, Gloria, Federico, Umberto and others for being very friendly to me and also for sharing your own friends playing football or having a party.

Gracias a quienes me ayudaron a dar los primeros pasitos entre teóricos: Javi C. y Dani T. con quien tuve la oportunidad de realizar mis primeros cálculos. Por supuesto a quien me abrió al mundo de las nanopartículas mientras me mostraba videos del *calico electrónico* y de *el niño loco alemán*, un gran compañero Francis V.

Por supuesto a todos el Grupo de "Computational Materials Science Laboratory", itinerantes y permanentes, muy especialmente a Pablo R. con quien he compartido este largo camino desde la *iniciación a Linux* de Javi C. a la ardua escritura de la memoria. También una ovación especial a Victor M. por nuestras conversaciones más allá de lo meramente científico y responder a mis preguntas como quien habla de la climatología local.

Al área de Química i Física de la URV, desde el primer profesor al último doctorando, alumno del "treball experimental" o visitante, por ser una comunidad ejemplar. También a José O., Archimago de los clusters, al refugio otorgado por lady Elisenda M. y a la siempre alegre ayuda de Moises A. A *La Comunidad de los Cuantiquillos,* a todos en general y a cada uno en particular, pues a cada uno tengo algo en concreto que agradecer y aunque no los cite expresamente ya saben quienes son. Especialmente mencionar a los miembros del nidito de amor en el despacho 204 donde celosamente se guarda la lista de los *Cuantiquillos*. Más allá de la Tierra Media, agradecer a Idoia M, Vane del R. y Miriam D. por todos los momentos divertidos y las entrañables conversaciones que hemos mantenido juntos.

A la *Hermandad d20*, que decir de vosotros esquizo-paranoico-obsesivos, gracias por mostrarme cosas que ojos normales no pueden ver y hacerme viajar a mundos donde las leyes de la física no son lógicas ecuaciones. Espero impacientemente *El Reencuentro*, mientras, caminaremos siguiendo otros códigos de honor. Doy gracias también a las parejas por tener que aguantar vuestras frikadas.

A mis familias por su apoyo incondicional y los buenos momentos que me hacen desconectar del día a día.

Finalmente, mis más calurosos agradecimientos a Elena V. por todo, por ser como es, por escuchar mis dudas y delirios, por aguantar lo que ha aguantado, por todos y cada uno de los momentos que hemos compartido, compartimos y compartiremos, GRACIAS.

UNIVERSITAT ROVIRA I VIRGILI
MODELLING AU CATALYST FROM BULK TO NANOSCALE
Alberto Roldán Martínez
ISBN:978-84-693-7669-0/DL:T-1748-2010

UNIVERSITAT ROVIRA I VIRGILI
MODELLING AU CATALYST FROM BULK TO NANOSCALE
Alberto Roldán Martínez
ISBN:978-84-693-7669-0/DL:T-1748-2010

UNIVERSITAT ROVIRA I VIRGILI
MODELLING AU CATALYST FROM BULK TO NANOSCALE
Alberto Roldán Martínez
ISBN:978-84-693-7669-0/DL:T-1748-2010

Contents

UNIVERSITAT ROVIRA I VIRGILI
MODELLING AU CATALYST FROM BULK TO NANOSCALE
Alberto Roldán Martínez
ISBN:978-84-693-7669-0/DL:T-1748-2010

UNIVERSITAT ROVIRA I VIRGILI
MODELLING AU CATALYST FROM BULK TO NANOSCALE
Alberto Roldán Martínez
ISBN:978-84-693-7669-0/DL:T-1748-2010

UNIVERSITAT ROVIRA I VIRGILI
MODELLING AU CATALYST FROM BULK TO NANOSCALE
Alberto Roldán Martínez
ISBN:978-84-693-7669-0/DL:T-1748-2010

Introduction

This introductory chapter justifies the main reasons for the research presented in this thesis. Catalytic processes on metal surfaces are of great importance, not only in industry, but also in daily life. Therefore, there is considerable interest in furthering knowledge of surface reactions at the elementary level of physisorption, chemisorption, molecular diffusion, bond breaking and bond formation. This requires the most advanced experimental techniques and theoretical descriptions available: spectroscopy, computational chemistry and kinetic mechanisms. Reaction profiles are also of great importance to understand how processes take place in the macroscopic world. In this thesis we focus, in particular, on gold, its different forms and its catalytic activity. Computational chemistry can be an important support for experimental researchers, facilitating the interpretation of phenomena at molecular level and the prediction of the properties of promising systems.

UNIVERSITAT ROVIRA I VIRGILI
MODELLING AU CATALYST FROM BULK TO NANOSCALE
Alberto Roldán Martínez
ISBN:978-84-693-7669-0/DL:T-1748-2010

UNIVERSITAT ROVIRA I VIRGILI
MODELLING AU CATALYST FROM BULK TO NANOSCALE
Alberto Roldán Martínez
ISBN:978-84-693-7669-0/DL:T-1748-2010

1.1 Background

Gold bulk

Gold bulk has fascinated mankind ever since it was first discovered. It is the most noble of metals, it does not tarnish on exposure to the atmosphere and retains its beautiful luster undiminished forever.

For chemists, until recently, gold has been of very little interest, although it did fascinate alchemists before the advent of modern chemistry. The reason is that its chemical inertness as a bulk metal appeared to provide very limited opportunities for opening up new chemistry. It was almost as though the fact that gold is the most noble of metals precluded anyone from really searching for new interesting discoveries. So the chemistry of gold was relatively undeveloped, and in chemistry text books the chapters dealing with gold were usually the shortest.

Gold surfaces

Historically, gold was discounted as a base-metal catalyst because of the low reactivity of gold surfaces. They are highly inefficient at dissociating molecular oxygen, a key stage in many oxidation reactions [1] such as the partial oxidation of alkenes. This selective oxidation yields epoxide, a product appreciated by many industries. It is a reactive chemical intermediate and it is used principally in the manufacture of polyether polyols, propylene glycols, glycol ethers and polyalkylene glycols. The epoxides of the simplest alkenes, ethene and propene, are in great and ever-increasing demand. Ethene oxide (EO) has an estimated world consumption of 20 million tonnes per year, and the world production of propene epoxide (PO) is more than 6 million tonnes per year.

Propene oxide is traditionally made using chlorohydrin, which is obtained from propene and chlorine reacting in the presence of water. However, this method produces a large amount of waste [2, 3, 4]. Other techniques that use electrochemical oxidation on a Pt-black anode, and photochemical oxidation over SiO_2-based catalysts can produce PO [5]. However, selectivities are not sufficiently high (50% at most). Commercially available catalysts for partial ethene oxidation have been reported to operate with selectivities in the 80% range, although some patents and academic studies have claimed experimental selectivities over 85.7% [6].

Making a heterogeneous catalysis study of alkene epoxidation in an ultra high vacuum (UHV) requires the use of high molecular weight olefins with desorption activation barriers that are above the activation barrier for partial oxidation [7]. For instance, styrene was used to study ethene because they are chemically analogous, but styrene has a higher molecular weight and, therefore, a relatively high desorption temperature [8, 9, 10, 11, 12]. Partial oxidation of styrene to styrene oxide has been observed on $Ag(100)$ [9], $Ag(111)$ [8, 12], $Cu(110)$ [13], and $Cu(111)$ [14], and recently gold-based catalysts have attracted considerable attention due to their potential utility for oxidative reactions, including propene epoxidation [15].

The oxidant species in heterogeneous catalysis has been widely discussed in the scientific community. Basically there are two hypotheses: one is that adsorbed dioxygen is the epoxidation agent whereas oxygen adatoms (adsorbed atoms) are responsible for combustion [16]; the other, also based on classical measurements, was that

UNIVERSITAT ROVIRA I VIRGILI
MODELLING AU CATALYST FROM BULK TO NANOSCALE
Alberto Roldán Martínez
ISBN:978-84-693-7669-0/DL:T-1748-2010

all the chemistry is due to oxygen adatoms [17]. Single crystal measurements demonstrated how oxygen adatoms react with adsorbed ethene to yield both the epoxide and combustion products on silver surfaces [18]. Therefore, it is concluded that oxygen adatoms are responsible for both the combustion and selective oxidation of co-adsorbed alkenes [19, 20, 21, 7, 15].

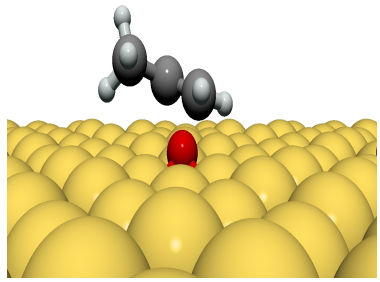

Figure 1.1.1: Propene and oxygen adatom on $Au(111)$ surface.

The first step in the oxidation reaction should include the adsorption and dissociation of molecular oxygen where the activation barrier towards oxygen dissociation seems to play a crucial role in determining the respective kinetic relevance of the elementary steps [20, 21]. On several transition metal surfaces the dissociation of oxygen molecules at low temperature is mediated by molecular chemisorption as a precursor [22] but they usually strongly perturb the electronic structure of co-adsorbed organic molecules as well and thereby give rise to 'burning' [23].

It is well-established that gold surfaces are inactive toward oxygen adsorption unless activated by the deposition of atomic O or sufficient energy is provided to break the $O-O$ double bond. Several methods for preparing oxygen pre-adsorbed surfaces have been developed. One of them is to use NO_2 to generate atomic oxygen [24]. The high reactivity of NO_2 with metals enables the chemisorbed atomic O coverage on the surface to be accurately controlled, and avoids potential contamination problems caused by the high pressures needed to prepare adsorbed O when molecular O_2 is used [7]. The use of a supersonic beam of oxygen atoms produced from a radio-frequency generated plasma source can deposit oxygen atoms on $Au(111)$ [25]. Atomic oxygen has also been prepared on $Au(111)$ by exposure to ozone [26], the thermal dissociation of gaseous O_2 using hot filaments [27] or O^+ sputtering [26].

Atomic oxygen can act both as an electrophilic reagent at $C=C$ double bonds [28, 29] and as a nucleophilic reagent, attacking electrophilic C atoms in co-adsorbed hydrocarbons [30, 31].

It has previously been shown that on $Ag(110)$ [32], $Ag(111)$ [33] and $Cu(111)$ [34] propene and other alkenes adsorb with the $C=C$ bond almost parallel to the metal surface [35]. Also, the surface-mediated ethene addition to oxygen seems to be the rate-determining step [18, 20].

The nature of the reaction intermediates is important for understanding the alkene epoxidation mechanism. There are two ways of adding oxygen to the $C=C$ bond. One is when the O atom forms bonds with both C atoms simultaneously.

Evidence for the sequential addition with the formation of an oxametallacycle intermediate has been provided by both theoretical [36, 37, 21] and experimental studies [38, 39, 20, 40]. In the case of styrene oxide, the existence of two distinct desorption peaks from clean $Ag(111)$ provides evidence of two different oxametallacycle configurations [7]. These oxametallacycles are intermediates to epoxide or to acetaldehyde, the latter being identified as the first step on the downhill path to total combustion [37, 21]. So the alkene epoxidation selectivity is determined by the difference between the *Gibbs* free energies of the oxametallacycles activated in the two reaction pathways [37].

Aldehydes are derived from allyloxy intermediates that are formed by inserting oxygen into the allylic $C-H$ bond. The mechanism on Ag is generally thought to involve the addition of chemisorbed, atomic oxygen to the $C=C$ bond [41]. However, silver catalysts are not as effective as epoxidation catalysts for alkenes with allylic $C-H$ bonds because combustion predominates. One example is that while Ag catalysts epoxide ethene with selectivities around 80%, propylene epoxidation occurs with only 5% selectivity [42]. The oxidation of styrene on chemisorbed oxygen-covered $Au(111)$ selectively yields styrene oxide, benzoic acid, and benzene-acetic acid. In most cases only 20% of the styrene is selectively oxidized [27].

The fundamental reason for the superior performance of copper is that its *Lewis* basicity is lower than that of silver [43]. Adsorbed ethene oxide is expected to bond more strongly to group VIII metals than to silver, which eventually might lead to the destruction of the alkene. This argument is consistent with the observations made about $Pd(110)$ [44, 45], $K/Ni(111)$ [46], and $Pt(111)$ [47], in which the adsorption of ethene oxide resulted in its being destroyed and the formation of either CO and H on $Pt(111)$ and $Pd(110)$ or acetaldehyde on $K/Ni(111)$ [20, 21].

There are two probable pathways for forming an allyloxy intermediate when propene is activated by oxygen on $Au(111)$: oxygen activates allylic hydrogen (forming an allyl) followed by oxygen addition to allyl or oxygen is inserted into the $C-H$ followed by allylic hydrogen transfer to an oxygen [15]. The presence of allylic H atoms in the alkene yields a stable adsorbed allyl species and adsorbed $O-H$, thus precluding selective oxidation and leading only to combustion [35]. When allylic hydrogen atoms are present (propene, allylbenzene and their isomers), $Cu(111)$ surpasses $Ag(111)$ by an even greater margin: copper continues to catalyze selective oxidation effectively, whereas silver simply burns these allylic alkenes [35, 11, 15]. The theoretical results imply that the key difference between silver and copper resides in the primary chemistry: silver favors allylic hydrogen stripping and copper favors metallocycle formation. This difference suggests that attempts to further improve the selectivity of copper catalysts should focus on the primary chemical processes, possibly altering the structure and/or composition of the metal surface. The propensity to strip hydrogen atoms is driven by the basic character of adsorbed oxygen.

The partial oxidation of propene is also induced by atomic oxygen bound to $Au(111)$, although epoxidation is not the favored pathway [15]. Instead, allylic $C-H$ bond activation leads to the formation of an aldehyde, which is subsequently oxidized to other products. Therefore, propene epoxide is not formed from propene oxidation on $Au(111)$, probably because of the facile activation of allylic $C-H$ bonds [15].

UNIVERSITAT ROVIRA I VIRGILI
MODELLING AU CATALYST FROM BULK TO NANOSCALE
Alberto Roldán Martínez
ISBN:978-84-693-7669-0/DL:T-1748-2010

Gold Nanowires

One-dimensional systems, such as wires, have attracted tremendous interest because of their size-dependent properties. However, several areas require further development. In particular, the fabrication of desired 1D nano-materials with tailored atomic structures and their assembly into functional devices are still major challenges for nano-technologists.

Nowadays, research is paying particular attention to the formation of metallic nanowire structures, semiconductors and metal oxide materials with an emphasis on the structural characterization of nucleation, initial growth, defects and interface structures, and the theoretical analysis of nano-crystal formation, reactivity and stability. There are several self-organized growth techniques: for example, vapor–liquid–solid growth, oxide-assisted chemical vapor deposition, laser ablation, thermal evaporation, metal-catalyzed molecular beam epitaxy, etc. [48]. One way of obtaining metallic nanowires is self-assembly, which involves attaching nanoparticles with a large surface-to-volume ratio [49]. Thus, nanowires grow stepwise by adding nanoparticles and reducing their surface energy. Only with a proper understanding of these processes will it be possible to produce crystal with the desired shape.

One-dimensional nanostructures grown by these technologies have been observed to exhibit unusual growth phenomena and unexpected properties: e.g. diameter-dependent and temperature-dependent growth directions, structural transformation by enhanced photo-thermal effects and phase transformation induced by the point contact reaction in ultra-thin semiconductor nanowires. Metal nanowires are components in nanoelectronic devices. They exhibit highly tunable optical properties that make them attractive candidates for several applications. One-dimensional Au nanostructures, especially ultra thin nanowires (diameter $< 2\,nm$), are of great interest because of their unusual transport properties and promising applications in nanoscale electronics and sensors.

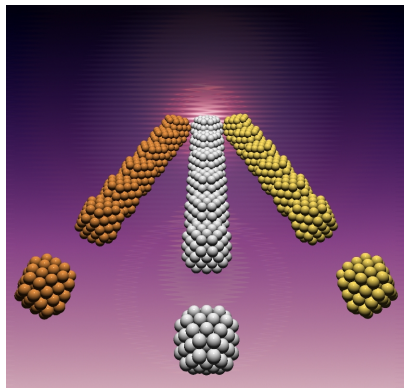

Figure 1.1.2: Metal nanowires representation growing at [111] direction.

In the case of gold nanowires, [111] is the thermodynamically favorable growth direction which is reasonable for fcc metal [50, 51, 52]. Experimental Au nanowires have an inter-layer spacing (d) of 2.35 Å which corresponds to the (111) crystal plane of gold. X-ray diffraction peaks confirm that nanowires are made up of pure gold

UNIVERSITAT ROVIRA I VIRGILI
MODELLING AU CATALYST FROM BULK TO NANOSCALE
Alberto Roldán Martínez
ISBN:978-84-693-7669-0/DL:T-1748-2010

[50, 53, 51, 52], and they show a small, short and "twisted" rod-like structure [51] and a wire-diameter distribution of about 2 nm [50, 54, 51].

The chemical inertness and high conductivity of Au nanowires make them ideal candidates for connecting molecular devices. At room temperature, Au nanowire exhibits electron conduction and conventional ohmic behaviour. For example a $9\,nm$ wire resistance $450\,nm$ long was measured to be $1.85\,k\Omega$ without constant resistance correction. This corresponds to the resistivity of $260\,ohm \cdot nm$, much lower than has been measured for polycrystalline Au wires ($1000\,ohm \cdot nm$) [49].

Gold nanoparticles

The number of papers on nanoparticles published annually clearly shows that the field has achieved both substantial importance and a certain degree of maturity. Overall, it is an active research field of great current interest and expectations are high.

The properties of materials change as their size approaches nanoscale. The fact that the properties of ultra small pieces of material differed from those of the same bulk material was known by artisans as far back as the 9th century, who used this knowledge to create a glittering effect on the surface of pots. Metal nanoparticles whose plasmon resonance falls in the visible range of the spectrum are also interesting as pigments. But it was *Michael Faraday* who provided the first scientific description of the optical properties of nanometer scale metals.

There are a wide variety of synthetic methods that can be used to obtain nanoparticles: grinding methods, gas-phase methods, liquid-phase syntheses, etc. Of these, colloidal deposition is an attactive way to synthesize highly dispersed supported gold catalysts, since it decouples gold particle synthesis and deposits on the support. Aspects other than the particle size itself must be taken into account for high-quality nanoparticles: for example, they must be as monodisperse as possible, the surface functionalization must be well controlled and agglomeration processes must be effectively suppressed. The formation of infinite solids is always energetically favored over nanoparticles with their large surface areas, unsaturated bonding sites and unoccupied coordination sites. The agglomeration of nanoparticles is then energetically favored, as it minimizes surface areas and saturates bonding and coordination sites.

The deciding factor for the use of nanoparticles in catalysis is the large surface area to volume ratio, which means that there are many catalytic active centers on the surface and relatively few inactive inner atoms. As gold nanoparticles of different sizes and shapes are easy to obtain, they play a central role in furthering our understanding of size-dependent and shape-dependent catalytic properties. For example, polyhedral gold nanoparticles with an exceptionally high activity can be prepared *in situ* by reduction with citric acid or citrate under mild conditions without using surfactants or templates at all.

The qualitative differences between nanoparticles and extended materials can be found in the following properties:

- Surface-dependent particle properties: These are properties which, in principle, the bulk material also displays, but which only become dominant in nanoparticles because of the high surface-to-volume ratio.

UNIVERSITAT ROVIRA I VIRGILI
MODELLING AU CATALYST FROM BULK TO NANOSCALE
Alberto Roldán Martínez
ISBN:978-84-693-7669-0/DL:T-1748-2010

- Size-dependent particle properties: Many properties of nanoparticles are directly related to their small size. Among these are optically transparent layers, interference effects, superparamagnetic nanoparticles, and applications in molecular biology and medicine.

- Size-dependent quantum effects: The electronic structure of nanoparticles is influenced directly by their size. These effects are caused by the transition from an atom or molecule with defined energy levels to the dispersed bands of groups of atoms and finally to the bulk material.

Structures of nanoparticles

Since the catalyzed reaction occurs only on the surface, the catalyst surface area directly correlates with the turnover of material. Specially in the case of the noble metals, the cost advantage of nanoparticles is obvious. In retrospect, heterogeneous catalysis is one of the first examples of nanoparticles being used for major industrial benefit. A further example is the drastic increase in the chemical reactivity of nanoparticles as the particle diameter decreases.

Nanoparticles need to be characterized if nanoparticle syntheses and applications are to be understood and controlled. This characterization is done by a variety of different techniques, mainly drawn from materials science. Common techniques are electron microscopy (TEM, SEM), atomic force microscopy (AFM), scanning tunneling microscopy (STM), X-ray photoelectron spectroscopy (XPS) and powder X-ray diffraction (XRD), among others.

A variety of studies on gold nanoparticle structures containing 2 to 20 atoms have reported structural transitions from planar to near three-dimensional structures at around 13 metal atoms. For larger clusters, the lowest energy isomer was the tetrahedral pyramid shape and the next most stable was an amorphous structure [55, 56]. So, the thermodynamically most stable configuration of small crystallites is determined by the free energy of the surface facets and the interface with the support, and cluster structure can be derived by *Wulff* construction [57]. It is assumed that the distance from the surface of a specific plane to the center of the moiety is proportional to the surface energy. Thus, if we have a surface plane with little energy, it will be at a short distance from the center of the crystallite and it will cut the other planes and form a polyhedron.

To model nanoparticles, three-dimensional metal crystallites cut from metal bulk by low-index planes are a suitable starting point and they lead to a tic and appropriate representation of catalyst models [58, 59, 60, 61, 62, 63, 64]. The fcc metals are cut by low index planes to expose (111) and (001) faces, which gives the clusters octahedral, cuboctahedral and icosahedral structures. For Au_{13} the cuboctahedral symmetry is found to be the most stable, while for Au_{55} the icosahedral structure is preferred although the energy difference with the cuboctahedral is rather small, $\sim 0.1\,eV$ [65]. Initially the metal–substrate interactions can be neglected and only the bare clusters considered [58]. It should be noted that non-supported gold nanocrystals can be active for oxidation reactions [66].

The discovery of the phosphine-stabilized Au_{55} cluster in 1981 marks the beginning of a paradigm shift from classic colloidal science to chemical nanotechnology.

UNIVERSITAT ROVIRA I VIRGILI
MODELLING AU CATALYST FROM BULK TO NANOSCALE
Alberto Roldán Martínez
ISBN:978-84-693-7669-0/DL:T-1748-2010

The ability to obtain extremely stable gold nanoparticles in aqueous solution has led to a renaissance in the use of gold for life science applications.

From a qualitative point of view, many of the new phenomena encountered in gold chemistry are experimentally well diagnosed and theoretically fully interpreted, but quantitative data, such as bond energies and their dependence on the interatomic distances and on the substitution pattern, are still scarce. This means that it is still rather difficult to make a stringent evaluation of physical properties, and further studies are required. Once these limitations have been overcome, rapid progress could be made in the most promising applications of new gold-containing compounds in materials and nanoscience.

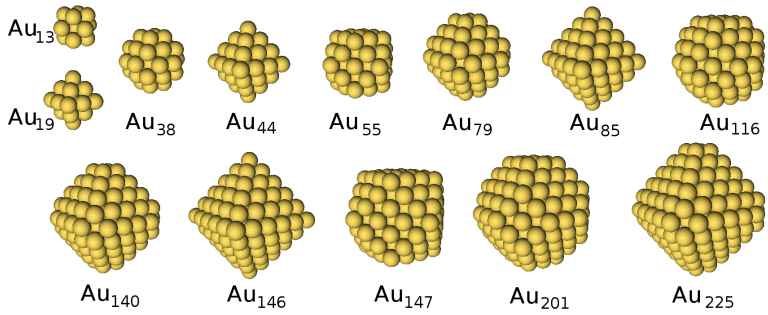

Figure 1.1.3: Polyhedral nanoparticles.

One of the goals of cluster science is to clarify how various properties observed in the bulk state differ from those in smaller nanoparticles, and the extent to which these cluster properties approach their bulk values. Ligand-free metal clusters are commonly studied in gas phase by means of supersonic molecular beams and are characterized by electron and mass spectroscopy techniques. Hence, bare clusters could be useful for studying the transition from atom or molecule to the solid state on the nanoparticle scale.

When the cluster size is increased, properties follow a monotonous trend and eventually converge to the bulk values. The use of scalable models makes it possible to predict the properties of larger particles of a tic size without carrying out rather demanding calculations.

Reactivity of nanoparticles

A significant number of heterogeneous catalytic processes are performed by transition metal catalysts supported on metal oxides. Several of these metals belong to the platinum group and are quite expensive. Therefore, if smaller amounts of these metals could be used, the cost of technological processes could be significantly reduced. The fact that the size of materials depends on their electronic structure, then, is of great importance in the nanoscience of gold, which has attracted considerable attention as a nanoparticle catalyst.

UNIVERSITAT ROVIRA I VIRGILI
MODELLING AU CATALYST FROM BULK TO NANOSCALE
Alberto Roldán Martínez
ISBN:978-84-693-7669-0/DL:T-1748-2010

Haruta et al. demonstrated that high selectivity in the heterogeneous oxidation of propene to propene oxide could be achieved by gold on titania [67]. Several reactions are also attributed to gold nanoclusters such as herbicides, numerous polymers, and fine chemicals or the reduction of functionalized nitroaromatic compounds to aniline derivatives, which are important intermediates for pharmaceuticals. *Serna and Corma* have shown that Au nanoparticles on TiO_2 or Fe_2O_3 substrates catalyze the hydrogenation of functionalized nitroarenes under mild reaction conditions with high selectivity [68].

Small gold nanoparticles in the size range $1-5\,nm$ can be prepared using the colloidal deposition method [69, 70]. Although *Herzing et al.* showed that the active species in Au/FeO_x catalysts consist of subnanometer clusters, numerous other studies have identified 2 to 5 nm particles as the critical "nanostructure". Determining the exact number of atoms in this kind of structure is complicated by several factors, one of which is the slight contraction of the Au–Au bond distance known to occur in particles of this size [71].

Some experimental studies of the structural features of nanosized Au clusters on MgO show that, in many cases, perfectly regular particles are able to grow on the substrate. The macroscopic surface and interface free energy lead to geometrical *Wulff* construction [72]. Gold clusters are likely to be adsorbed on oxygen vacancies on the $MgO\,(100)$ surface, where interaction with this color center involves partial electron transfer. The cluster-support interaction determines the width and the position of the gold $d-$band in the energy region. Also structural dynamic fluxionality of the Au cluster plays an important role in the adsorption of the reactants and in lowering the reaction activation barriers [73]. Au_{20} supported on defect-poor and defect-rich $MgO\,(100)$ films revealed that charging clusters via partial electron transfer from the oxide support plays an essential role in the activation of nanosize gold model catalysts. Surprisingly, defect-rich MgO increases Au oxidation activity [74].

There has been much debate about the nature of the active site of $Au/support$ catalysts. Some authors have pointed out the special role of the metal/support interface as a region of high activity. By decreasing the size of the gold particle the overall activity can be increased because the active interface increases [75]. In 2000, a model was proposed in which Au atoms at the interface between the Au particle and the oxide are the active oxidation centers [76]. Indeed the electronic nature of very small gold particles can be expected to be significantly influenced by the nature of the support, especially the availability of defect sites. All researchers agree that the catalyst activity of supported gold nanoparticles increases as the mean particle size decreases. As the particle diameter decreases, the proportion of gold atoms in contact with the support increases and the electronic nature of these atoms will be influenced by the support. This effect is highly significant for particle diameters less than $2\,nm$, which coincides with a dramatic enhancement in activity. Neither the electronic properties of the interface nor the valence band of the nanoparticles were subject to separate experimental investigations.

Recently *Valden et al.* suggested that the anomalously high reactivity of small gold particles is due to quantum–size effects. Using scanning tunneling microscopy they showed that gold particles form disc-like structures on a TiO_2 surface and that the reactivity depends strongly on the disc height [77]. For instance, Au/CeO_2 catalysts with gold clusters $\leqslant 1\,nm$ were more active than those containing larger

UNIVERSITAT ROVIRA I VIRGILI
MODELLING AU CATALYST FROM BULK TO NANOSCALE
Alberto Roldán Martínez
ISBN:978-84-693-7669-0/DL:T-1748-2010

gold clusters [78]. Furthermore, a microscopy study of Au/FeO_x catalysts demonstrates that the origin of the activity is associated with bi-layer nanoclusters that are $\sim 0.5\,nm$ in diameter, whereas mono-layer clusters (which have only three to four atoms) and isolated Au atoms appear to be essentially inactive for CO oxidation [71]. Theoretical studies indicate that an isolated neutral Au_{10} cluster is able to catalyze the CO oxidation reaction even below room temperature [79].

The catalytic properties of Au, then, depend on the support, the preparation method, and particularly the size of the Au clusters [77]. Several scientists and engineers are working to explain this dependence. Various key issues need to be considered:

- The relative abundance of low- and high-coordinate sites as a function of particle size [80].
- The metal–support interactions [74, 81].
- The electronic structure of very small metal particles [82].

One of the most studied catalytic processes is CO oxidation by O_2. Highly dispersed gold catalysts with particle sizes of $2-5\,nm$ supported on reducible metal oxides, in particular on TiO_2, Fe_2O_3, CeO_2, Co_3O_4, are well known for their high activity towards CO oxidation at low temperatures. Nevertheless, this process only takes place at temperatures below $-70\,^{\circ}C$ on supported gold clusters with sizes below $1\,nm$ [70]. Hence, the activity of a supported Au particle is very sensitive to its structure, which determines the proportion of low-coordinated sites, their character and the features of the $Au/oxide$ perimeter interface. The crucial role of low-coordinated edge and corner sites in the catalytic activity of Au particles is evident [75].

An important step in catalytic oxidation processes is the activation of molecular oxygen. Because of the high activity in oxidation reactions, the reactivity of gold clusters with oxygen has been extensively analyzed. However, no clear picture has emerged from the work done about the reaction mechanism of O_2 dissociation. Unlike on the surface, the interaction of O_2 with both neutral and ionic ultra-small clusters has been subject to in-depth study [73, 83]. The interaction energy is largest for the anionic gold ultra-small clusters in which it presents a distinct odd-even behavior as a function of the number of gold atoms. The bonding mechanism involves charge transfer to oxygen molecules with a concomitant activation of the $O-O$ bond to a superoxo state [73]. The dissociated adsorption is predicted to induce large relaxations in the gold part of the complex which could be detected by mobility measurements or electron diffraction spectroscopy. Ultra-small neutral and cationic gold clusters also bind oxygen, although the interaction is much weaker and does not induce $O-O$ bond activation [73].

Clusters that are larger than just a few atoms have also been studied theoretically [84]. Density functional theory (DFT) has been used to investigate the interaction of oxygen with free gold particles. *Luo et al.* performed a study for Au_{24} clusters and concluded that the oxygen adsorption was dependent on particle shape and the coordination number of the interacting gold atoms [85]. Besides, Au_{55} shows very weak interactions with O_2 but substantial bonding with Au_{13} [86]. In the case of supported clusters, theoretical studies suggest that the interface between the metal particle and oxide support is the most probable active site [87, 88].

UNIVERSITAT ROVIRA I VIRGILI
MODELLING AU CATALYST FROM BULK TO NANOSCALE
Alberto Roldán Martínez
ISBN:978-84-693-7669-0/DL:T-1748-2010

In all cases the adsorbed molecule is found to be activated as a peroxo species molecule with an intramolecular bond length that is weaker and more stretched than in the free molecule [74]. The nature of the active gold-oxygen complex remains unclear, and detailed kinetic measurements are required to determine its role in the reaction mechanism.

1.2 Surface science in catalysis

Nowadays, surface processes are unconsciously used by millions of people in the world: they are present in the chemical industry, in cars, in a simple bike, etc. Research into surface science has made great efforts to further understanding of the characterization and reactivity of catalysts, because of their importance in industrial processes. Catalysts are the workhorses of chemical transformation in several processes [89], and they are indispensable in:

- Production of transportation fuels in oil refineries
- Production of bulk and fine chemicals in all branches of the chemical industry
- Prevention of pollution by avoiding the formation of waste

Most current chemical products, then, are yielded by catalysts, and without them our society would not have reached the present standard of living. For instance, all modern cars have catalysts in the end of the exhaust pipe to reduce their polluting emissions. This catalyst is known as the three-way catalyst and it is a mixture of platinum, rhodium and palladium. Although it is less selective for a particular reaction than homogeneous catalysts, condensed matter is used in industry because of its ability to separate the final products (normally in gas or liquid phase) from the catalysts. Surface science, however, is not only heterogeneous catalysis. The world of microtechnology and nanotechnology has become of particular interest in the last decades, especially for computer science, because chips are getting smaller and smaller, and the properties of matter on a molecular scale are therefore more important. Finally, other important events in the field of surface science are corrosion, adhesion, electrochemical reactions, etc.

Surface science, then, has developed into a scientific discipline with a solid conceptual basis [90]. The relation between the catalytic activity of a certain reaction, and the composition and structure of a surface is, in general, qualitatively well understood.

1.2.1 Experimental techniques in surface science

Understanding how adsorbed molecules behave on a catalyst is crucial to understanding how a process takes place. Table 1.2.1 shows some experimental techniques that allow scientists to study catalysts and their adsorbed molecules.

Some of these techniques mainly provide information about surface structure and/or adsorbates. AFM or STM have been developed in recent decades, and are very sophisticated devices. RAIR spectroscopy has been used for more than 50 years and it is one of the most powerful surface techniques. RAIR is a non-destructive, inexpensive technique, and it is very sensitive to the structure of the adsorbed molecule. NEXAFS spectroscopy is a powerful, non-destructive technique which is highly sensitive to the adsorption mode of the molecule and its chemical environment. Despite the power of these techniques, their results depend on the capability of experimentalists to assign and resolve their spectra. The theoretical simulation of these spectra can be a great help for the assignation of the bands and the interpretation of the results.

UNIVERSITAT ROVIRA I VIRGILI
MODELLING AU CATALYST FROM BULK TO NANOSCALE
Alberto Roldán Martínez
ISBN:978-84-693-7669-0/DL:T-1748-2010

Table 1.2.1: Experimental techniques used in surface science.

Name	Type	Information
Low-energy electron diffraction (LEED)	Electron diffraction	Surface structure
Reflection-adsorption infrared spectroscopy (RAIRS) Electron energy loss spectroscopy (EELS)	Vibrational spectroscopy	Adsorbate vibrations
X-ray photoelectron spectroscopy (XPS) Ultraviolet photoelectron spectroscopy (UPS) Photoelectron microscopy (PM) Near-edge X-ray adsorption fine structure (NEXAFS)	Electron spectroscopy	Determination of elements Bonding adsorbate-surface Surface images Structure of the adsorbate
Scanning tunneling microscopy (STM) Atomic force microscopy (AFM)	Scanning probe techniques	Surface images
Temperature programmed desorption (TPD)	Temperature technique	Adsorption energies

1.2.2 Tools in computational techniques

Computational techniques and theoretical calculations are carried out by computers, one of the most important inventions of the 20th century which have led to a revolution in science, education and industry. The impact of this revolution is comparable to the industrial revolution in the 19th century. To understand computer science, it is necessary to be aware of the events that have led to its development.

From Stonehenge to Marenostrum

Ancient civilizations created a variety of mechanical devices to assist in the automation of tasks. The ancient stone monument of *Stonehenge*, south of England, was built between 1900 and 1600 BC, and it seems to be an astronomical calculator that can predict seasonal changes. In Western Europe, logarithm tables were designed by the mathematician *John Napier* to simplify calculations, subsequently leading to the rule of calculus. The young French mathematician *Blaise Pascal* invented the first mechanical adding machine, a device that used a system of gears and wheels similar to those found in a mileometer. A large number of other mechanical calculators were created by refining *Pascal*'s design. In the late nineteenth century, these calculators became important as scientific and commercial tools.

The second fundamental idea that emerges in the history of computing was the concept of stored programs to control calculations. A prime example of an automatically controlled device is a loom invented by *Joseph Marie Jacquard*, which used

metal cards with holes. A collection of these cards formed a program that ran the loom. The two fundamental concepts, automatic calculation and stored program control, were combined by the mathematician *Charles Babbage*, who began work on what was called the difference engine.

The first fully electronic computer was developed by *John Atanasoff*. The best known of the first electronic computers was ENIAC, built at the University of Pennsylvania. It consisted of more than 18000 vacuum valves and 1500 relays, filling a room that measured $6x12\,m^2$. It was used by the army to calculate projectile trajectories.

The actual physical computer components are called hardware. Different generations of computers can be identified by the type of hardware they use. The ENIAC is an example of a first-generation computer and is characterized by the use of vacuum tubes. Advances in electronics brought about changes in computer systems and in the sixties IBM introduced the first second-generation computer, which used transistors as a valves. Later, in the nineties personal computers integrated silicon chips to become the fourth generation.

The continuous advances in technology have produced an extensive collection of computer systems, from laptops to parallel supercomputers, such as *Marenostrum* in Barcelona or *Maginet* at the *Universitat Rovira i Virgili* (see figure 1.2.4). Simulation methods in condensed matter have made it possible for computers to evolve and continuous research into mathematics has led to the old semi-empirical methods evolving into the current highly parallelizable *ab initio* methods.

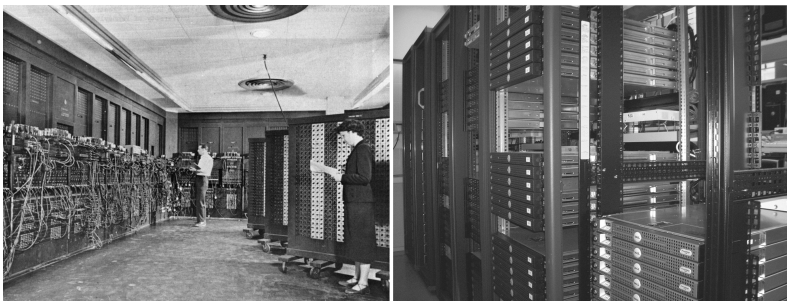

Figure 1.2.4: ENIAC, a first generation computer (http://grupo1044331.files.wordpress.com), and Maginet cluster.

UNIVERSITAT ROVIRA I VIRGILI
MODELLING AU CATALYST FROM BULK TO NANOSCALE
Alberto Roldán Martínez
ISBN:978-84-693-7669-0/DL:T-1748-2010

1.3 Objectives of this thesis

This thesis uses a periodic density functional methodology to study several gold structures and their catalytic activity. The study focuses on bulk gold, the bi-dimensional gold surface and its reactivity towards propylene epoxidation, the self-assembly of nanoparticles with a mono-dimensional structure, and nanoparticles and their catalytic activity towards O_2 activation.

The results further our knowledge of condensed matter, and in particular its structure and reactivity. We have also tried to be useful for new researchers in computational studies and we have provided a brief guide to preparing any-dimensional systems.

The general objectives of this work are:

- To model bulk, surface, wire and nanoparticle metal structures.
- To study the metal-adsorbate interaction and to establish the adsorption properties.
- To use vibrational frequencies to characterize structures that are minima or saddle points.
- To simulate the reaction profiles and to determine the transition states that connect various minima.
- To use microkinetic models to simulate reaction profiles in real catalytic conditions.

In the case of nanoparticles, we shall attempt to provide an approach that bridges the gap between the traditionally separate electronic structure and solid-state science.

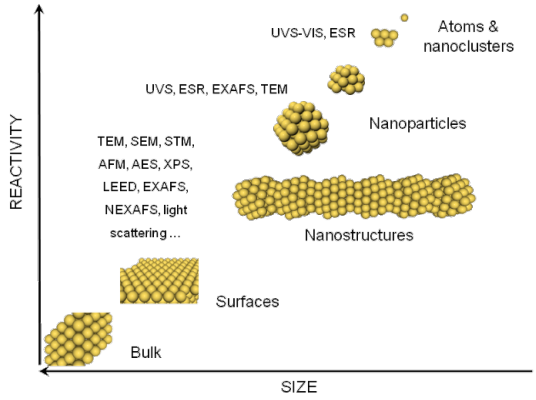

Figure 1.3.5: The general scheme, which describes the relatives chemical activity of metals species versus their size and some experimental techniques used in its characterization.

UNIVERSITAT ROVIRA I VIRGILI
MODELLING AU CATALYST FROM BULK TO NANOSCALE
Alberto Roldán Martínez
ISBN:978-84-693-7669-0/DL:T-1748-2010

1.4 Contents of this thesis

This thesis is structured as follows:

- In the present chapter (chapter 1) we introduce the thesis, describe its objectives and state its scope.
- Chapter 2 summarizes the methodology and the models used for calculations and their foundations.
- Chapter 3 presents the results as a function of system periodicity.
  - The aim of the first section is to explain the steps taken to obtain an accurate three-dimensional structure and some of the properties derived from bulk.
  - Taking into account the background, we describe a theoretical study of the primary chemistry of propene epoxidation on $Au(111)$.
  - Below, in the section on one-dimensional systems, we describe an example of self-assembled metal nanowires built with nanoparticles with sizes of $\sim$1.5 nm and different cluster orientations.
  - Given the importance of nanoscale materials, the last subsection sheds light on the nanoparticle structure model as well its unexpected catalytic activity towards oxygen activation. This subsection also explains the dependence of the activity on the nanoparticle charge and gives information about these catalytic processes with a microkinetic simulation.
- Chapter 4 provides a brief summary and the conclusions.
- The last chapter contains a list of publications and the bibliography used during this thesis.

UNIVERSITAT ROVIRA I VIRGILI
MODELLING AU CATALYST FROM BULK TO NANOSCALE
Alberto Roldán Martínez
ISBN:978-84-693-7669-0/DL:T-1748-2010

UNIVERSITAT ROVIRA I VIRGILI
MODELLING AU CATALYST FROM BULK TO NANOSCALE
Alberto Roldán Martínez
ISBN:978-84-693-7669-0/DL:T-1748-2010

Theoretical models

In this chapter we introduce the theoretical methods, models and tools that are used in this thesis.

All calculations used are based in quantum chemistry methods, where the well-known Schrödinger equation is solved in the frame of some approaches. We have used the density functional theory (DFT), where the Schrödinger equation is solved by means of the system electronic density. DFT has demonstrated to be a reliable and low-time consuming method, which is suitable for the study of materials. The bulk, surface or wires of materials may be modeled by unit cell replication where an unit cell is periodically reproduced or by cluster models, were a small piece is modelled as an isolated system. Zero-dimensional shapes, nanoparticles, may be also modelled by both cluster and periodic models.

The calculations carried out in this thesis have been made with a periodic model using the VASP code. This method uses plane-waves as the basis sets for the electronic expansion. This modelling way has demonstrated to evaluate properly the adsorption energies, the adsorption geometries, the coverage effects and the vibrational frequencies of adsorbates on metal surfaces.

UNIVERSITAT ROVIRA I VIRGILI
MODELLING AU CATALYST FROM BULK TO NANOSCALE
Alberto Roldán Martínez
ISBN:978-84-693-7669-0/DL:T-1748-2010

2.1 The *Schrödinger* equation

Schrödinger equation is the key equation of quantum mechanics. Developed by the physicist *Erwin Schrödinger* in 1926, has the same importance to quantum mechanics as *Newton's* laws of motion have to the large-scale phenomena of classical mechanics or the *Maxwell* equations to electromagnetism. For a system composed of N electrons and M nuclei, it is expressed as: (equation 2.1):

$$\hat{\mathcal{H}}\Psi_n\left(\{\overrightarrow{r_i}\}\left\{\overrightarrow{R_\mu}\right\}\right) = E_n\Psi_n\left(\{\overrightarrow{r_i}\}\left\{\overrightarrow{R_\mu}\right\}\right) \tag{2.1}$$

where $\hat{\mathcal{H}}$ is the time-independent $\hat{\mathcal{H}}$amiltonian, Ψ_n is the wave-function of the system associated to the energy level E_n and $\overrightarrow{r_i}$and $\overrightarrow{R_\mu}$ are the spatial coordinates of the electrons and the nuclei, respectively. All properties (except for relativistic effects) of the electron-nuclei system are described by equation 2.1. By solving this equation we therefore obtain all the physic-chemical properties of the target system. Unfortunately, this involves dealing with a system of (N+M) interactive particles. Even for a very small system, this process is too complex to be solved and several approximations are needed.

For systems with many variables, a common way to simplify complicated equations is to separate the variables. One such separation step, universally accepted in electronic structure theory, is the so-called *Born-Oppenheimer* approximation [91]. This approximation is based on the difference in mass between nuclei and electrons. The lightest nucleus, the one of the hydrogen atom, is actually 1,836 times heavier than an electron. We can therefore consider nuclear and electronic motion as independent. Electrons follow nuclei instantaneously during the motion of the latter, i.e. they change their wave-function very quickly with respect to the time-scale of nuclei. This fact makes the equation easier to be solved, because nuclei may be considered frozen, and the number of freedom degrees are decreased in a huge amount. In spite of that, even for the smallest polielectronic atoms and molecules, this equation is impossible to be solved, because the potential interaction between two electrons (V_{ee}) is difficult to evaluate, and other approximations are required. These approximations try to solve this electron-electron interaction and results depend on the capability of this approximation to describe each term [92, 93].

As all performed calculations in this thesis were carried out in the frame of density functional theory (DFT), the following description is focused on this methodology instead of all methods [92] developed to solve the Schrödinger equation.

UNIVERSITAT ROVIRA I VIRGILI
MODELLING AU CATALYST FROM BULK TO NANOSCALE
Alberto Roldán Martínez
ISBN:978-84-693-7669-0/DL:T-1748-2010

2.2 Density Functional Theory (DFT)

To solve the *Schrödinger* equation two different ways may be chosen, one based on wave-function methods and the other one based on electronic density. The former, which can provide extremely accurate results if a high level of Configuration Interactions is included, are limited to 10-100 electrons because of the great scaling with the system size. For transition metal systems its application is therefore restricted to quite small systems. The alternative to the wave-function methods is the Density Functional Theory (DFT) [94, 95], which is based on the electronic density of the system.

In 1964 *Hohenberg and Kohn* demonstrated that for every chemical system, the energy is a function of its electronic density. It makes that two theorems were enunciated [96, 97]:

"Any observable magnitude of a stationary non-degenerated groundstate can be calculated exactly from its electronic density."

"The electronic density of a stationary non-degenerated groundstate can be calculated exactly determining the density that minimizes the energy of the ground-state."

This allow to reconstruct the *Schrödinger* equation, and express the energy of the system as a function of the electronic density [93]:

$$E[\rho] = T[\rho] + V[\rho] + W_{CL}[\rho] + W_{NCL}[\rho] \tag{2.2}$$

where T is the kinetic energy, V is the nucleus-electron potential, W_{CL} is the coulombic and non-coulombic, W_{NCL}, electron-electron potential and ρ is the electronic density. This energy must be minimised, and the expression found is:

$$F_{HK}[\rho] = T[\rho] + W_{CL}[\rho] + W_{NCL}[\rho] \tag{2.3}$$

$$\frac{\delta E[\rho]}{\delta \rho(\vec{r})} = V_{ext}(\vec{r}) + \frac{\delta F_{HK}[\rho]}{\delta \rho(\vec{r})} \tag{2.4}$$

2.2.1 *Kohn-Sham* equation

Expression 2.4 is known as the fundamental density equation and allows us to minimise the energy and to find the electronic density of the system. Here two problems are presented. We do not know the exact expression of T and W.

The expression of T, the first problem, was solved by *Khon* and *Sham* in 1965 [98]. The kinetic energy is easy to calculate from the wave-function. Therefore they proposed to use a reference system of N electrons that interact with an external potential V_{ext}. This external potential has a special property, the electrons in V_{ext} create a potential that has the same density as the real system. In this system the electrons do not interact among them but interact with the nuclei. In these terms the energy minimised is:

$$\frac{\delta E\left[\rho\right]}{\delta\rho\left(\vec{r}\right)} = \frac{\delta T_s\left[\rho\right]}{\delta\rho\left(\vec{r}\right)} + \int \frac{\rho\left(\vec{r_2}\right)}{r_{12}} d\vec{r_2} + V_{ext}\left(\vec{r}\right) + \frac{\delta E_{XC}}{\delta\rho\left(\vec{r}\right)} \tag{2.5}$$

The problem is that the kinetic energy of this reference system $T_s\left[\rho\right]$ and the real one $T\left[\rho\right]$ are not the same. The difference of kinetic energies expression and the energy of coulombic repulsion are joined in one only term, the exchange-correlation energy (E_{XC}).

E_{XC} includes all terms that are not easily calculated like exchange energy, correlation energy, the difference of the kinetic energies and the auto-interaction correction. It makes the equation to be:

$$\hat{h_{KS}}\psi_i = \varepsilon\psi_i \qquad \hat{h_{KS}} = -\frac{1}{2}\nabla^2 + V_{eff}\left(\vec{r}\right) \tag{2.6}$$

These equations are very similar to the *Hartree-Fock* (HF) equations, and they are called the *Kohn-Sham* (KS) equations. Like in HF method, this equation is solved iteratively and could be calculated KS orbitals. These orbitals and their energies have not a real physical sense, because these orbitals come from the calculation of an external potential where the particles are non-interacting among them.

Another important difference between DFT and the wave-function based methods (for instance HF method), is that DFT uses an approximated $\mathcal{H}$amiltonian, but the electronic density for the system is exact. On the other hand, in HF the $\mathcal{H}$amiltonian is exact, but the wave-function is an approximated solution.

2.2.2 Exchange-correlation potential

The therms not easy to solve in equation 2.5 are included in exchange-correlation potential, now the problem is how to calculate the part of the energy that comes from this exchange-correlation potential. Many kind of methods are used to evaluate this term: local density approximation (LDA), gradient generalized approximation (GGA), hybrid functionals, and exact exchange are discussed below.

LDA

Local density approximation (LDA) was the first way to evaluate the exchange-correlation energy and the easiest one nowadays. In this approximation the exchange-correlation energy is evaluated for a uniform gas of electrons. For the exchange part, the homogeneous density gives an expression for the energy [93, 96]:

$$E_X^{LDA}\left[\rho\right] = -\frac{3}{4}\left(\frac{3}{\pi}\right)^{\frac{1}{3}} \int \rho\left(\vec{r}\right)^{\frac{4}{3}} d\vec{r} \tag{2.7}$$

Several possibilities are available. The most common one is the functional by *Vosko*, *Wilk* and *Nusair* (VWN) [99] developed interpolating a sample of correlation energies values obtained by Monte-Carlo calculations, equation 2.7.

The results provided by this method are satisfactory, however, this model does not evaluate accurately the exchange-correlation hole. In special, it works extremely

well for systems where the density remains constant, like metals with a large number of electrons. Geometries, vibrational frequencies and charge densities are very good, but binding energies tend to be overestimated.

For open shell calculations, alpha and beta densities must be treated independently and local spin density approximation (LSDA) is used to evaluate independently the alpha and beta equations, like in unrestricted HF calculations.

GGA

In LDA the exchange-correlation effects are punctual and depend only on the value of the electronic density in a point. The next step is to introduce density gradients in the description of the exchange-correlation effects, which makes that exchange-correlation potential not only depends on a value of the density in a point, also how it variates on the near points:

$$V_{XC} = \frac{\delta E_{XC}[\rho]}{\delta \rho(\overrightarrow{r})} - \nabla \frac{\delta E_{XC}[\rho]}{\delta (\nabla \rho(\overrightarrow{r}))} \tag{2.8}$$

Several approximations on the gradient have been implemented, and all of them give better results for geometries, vibrational frequencies and charge densities than LDA. However, its computational cost is higher. The main reason for using GGA is the increase of the quality of binding energies. Some implemented functionals are [100, 101, 102, 103, 104, 105, 106]:

- Perdew-Wang 86 (PW86)
- Becke-Perdew (BP)
- Lee-Yang-Parr (LYP)
- Perdew-Wang 91 (PW91)
- Perdew-Burke-Enzerhof (PBE)
- Revised Perdew-Burke-Enzerhof (RPBE)

Often, these functionals contain experimental parameters to adjust the energy of a series of atoms. The only one that is strictly ab-initio is the PW91 functional, which was built using data of LDA. PBE and RPBE correct the PW91 functional to improve results.

In this thesis most of the calculations are made by PW91 functional, which tends to be a good functional for the description of chemical bonds. Additionally we have checked different types of functional.

Hybrid Functionals

Even for GGA, some chemical features are still not well described. For example, the band gap between the bonding band and the conduction band in semiconductors is too small from GGA calculations. In the case of HF calculations, this gap tends to be overestimated. These two results give the idea of mixing both methods to improve the unknown part of V_{XC} and therefore increase the quality of the results.

UNIVERSITAT ROVIRA I VIRGILI
MODELLING AU CATALYST FROM BULK TO NANOSCALE
Alberto Roldán Martínez
ISBN:978-84-693-7669-0/DL:T-1748-2010

The exchange part of this exchange-correlation potential is in these models the exact exchange of the HF method. The correlation part comes from the DFT treatment. This makes these methods to be a hybrid between DFT and HF.

The problem of hybrid method is that HF exchange potential does not take into account the dynamical correlation, so a new term of dynamical correlation must be added into the functional, and this is made through the adiabatic connection. Depending on how this part is treated, and the used percentage of each method, some functionals appear [107, 108]:

- B3LYP
- B3PW91

These functionals work extremely well for atoms and molecules, but some numerical problems appear for solid state calculation when periodical conditions are required.

Exact exchange

The last innovation on exchange-correlation functional development is given by the exact exchange, E_{XX}, with the especial contribution in solid state by *Görling* implementation [109]. Using a molecular orbital is possible to derive mathematically the exact exchange expression, and correct the auto-interaction problem, therefore, only the electronic correlation remains unknowns. E_{XX} allows to obtain very accurate results in band gaps and it is very useful to describe excited states with Time Dependent DFT, TDDFT. On the other hand, E_{XX} has drawbacks such as the treatment of *Van der Waals* interactions, which remain bad described due to bad correlation accuracy. Hence, although E_{XX} is more exact but also more expensive computationally, the applicability to big systems is reduced. The exact exchange is not implemented yet into used program to carry out this thesis.

2.2.3 *Hubbard* approximation

An approach of local density, that contains the *Hubbard* expression, adds an additional term known as LDA+U method. The added value is the U of *Hubbard*, which is similar to *Anderson* impurity method [110] that was developed by *Anisimov et al.* during the nineties [111]; an accurate DFT methodology adding a potential that depends of orbital occupancy and modifies the coulombic repulsion between d- or f-electrons. This modification is needed to correct the $d \longleftrightarrow d$ (or $f \longleftrightarrow f$) mean field contribution in systems with strong electronic correlation.

The added U represents the orbital polarization that corresponds to coulombic interaction in the *Hubbard* model. Therefore, the approximation improves the distance between occupied and unoccupied bands and increases the orbital localization.

2.2.4 DFT problems

DFT methods have very favorable characteristics and it is employed to carry out different kind of systems by a huge number of scientific. However, there are many areas where the currents functionals are known to perform poorly.

UNIVERSITAT ROVIRA I VIRGILI
MODELLING AU CATALYST FROM BULK TO NANOSCALE
Alberto Roldán Martínez
ISBN:978-84-693-7669-0/DL:T-1748-2010

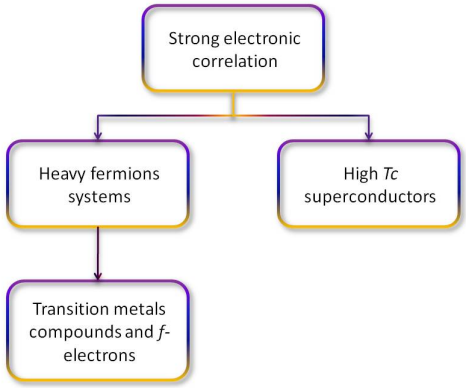

Figure 2.2.1: Scheme of high electronic correlated systems.

- Current DFT methods describe poorly weak interactions due to dispersed forces such as *Van der Waals* type interactions. However, hydrogen bonding in mainly electrostatic and is reasonably well accounted for many DFT functionals.
- Exchange-correlation functionals that do not include self-interaction corrections or give an incorrect potential behaviour lead to loose bound electrons, such as anions arising from systems with a relatively low electron affinities. Nevertheless, a medium-sized basis set with a single set of diffuse functions will give a reasonable estimation of experimental electron affinity.
- Dissociation of a charge odd-electron systems takes place with dissociation energy profile displaying an artificial barrier. Transition structures are similarly predicted to be stable by functionals that do not included exact exchange. Since HF overestimates activation barriers, hybrid methods often give reasonable barriers.
- Excited states properties have to be calculated by time-dependent-DFT methods, the accuracy of energies is typically $\sim 0.5\,eV$ for valence states.
- Charge transfer description is inherently unsuitable for DFT methods because exchange-correlation functionals is inherently local, only electron density depending.
- DFT describes different spin multiplicity by exchange-correlation functional, different way that HF theory that describes it by the exchange integral on the occupied orbital. Therefore, relative energy of states are often poorly described. Hybrid methods with a suitable parametrized amount of exact exchange perform better results [112, 113].

2.3 Calculations using VASP

Vienna Ab-initio Simulation Package (VASP) [114, 115, 116, 117] is a package developed by *G. Kresse*, *J. Furthmüller* and *J. Hafner*, which uses DFT and periodical using planes-waves. Due to the periodicity of the ideal solids, without defects and infinite lenght, this package is highly efficient for material simulation. Surfaces are simulated by a slab model, which is repeated in the three dimensions of the space. It is also possible to simulate nanoparticles that, like surfaces, are repeated in the three dimensions but the model contains a large vacuum in all directions to isolate the moiety. VASP allows the calculation of adsorption energies, equilibrium geometries of minimum and transition states, charge distributions, density of states and projected density of states (DOS and PDOS), vibrational frequencies and dipole moments.

VASP can use several functionals to evaluate the energy of a system. One can choose between LDA and several GGA implementations: PW-B, PW, PW91, PBE, RPBE, LMH.

The basis set for a common chemistry calculation package are localized on the atoms, but VASP uses plane-waves, that are not localized on an atom, in spite of, they have the periodicity of the cell used. This fact allows to work easier with periodicity.

Moreover, VASP code uses pseudopotentials to decrease the number of electrons to be treated, because it is demonstrated that core electrons do not take part in chemical bonds. Projector Augmented Wave-functions (PAW) and ultra-soft (US) pseudopotentials are implemented on VASP package.

2.3.1 Plane-waves and *Blöch* theorem

The best way to simulate an ideal solid, surface or wire is to create an unit cell, which is repeated in three, two or one dimensions. Repeating the unit cell reproduces a periodic structure. This means that a translation operator ($\hat{T}$) is being used, and this operator must commute with the $\mathcal{H}$amiltonian of the system:

$$\left[\hat{H}, \hat{T}\right] = 0 \tag{2.9}$$

Blöch theorem [118, 119] uses the translational symmetry to reduce the infinite number of the one-electron wave-functions computing the number of electrons in the unit cell. Then the one-electron wave-functions can be expressed as the product of a periodic part and a wave-like part.

Blöch functions can be chosen as eigenvectors for the $\mathcal{H}$amiltonian, and *Schrödinger* equation can be solved from the crystalline orbitals. Then, eigenfunctions of $\mathcal{H}$amiltonian will contain the translational symmetry.

The crystalline orbitals can be expanded using a linear combination of basis set functions. In VASP, this expansion is made with plane-waves which are usually used in physics and in electromagnetic fields to simulate the band structure of solids. Every periodic function can be expanded as an addition of plane-waves, and *Blöch* functions are expanded as a linear combination of plane-waves:

$$\Psi_{n,\vec{k}}\left(\vec{R}\right) = \sum_{\vec{g}} a_{n,\vec{g}\,\vec{k}} \exp^{\left(i\left(\vec{g}+\vec{k}\right)\vec{R}\right)} \tag{2.10}$$

UNIVERSITAT ROVIRA I VIRGILI
MODELLING AU CATALYST FROM BULK TO NANOSCALE
Alberto Roldán Martínez
ISBN:978-84-693-7669-0/DL:T-1748-2010

The sum runs over all vectors of the reciprocal space, and the wave-vector determines one point in the first *Brillouin* zone. The expansion coefficients tend to zero when the kinetic energy of the plane-waves is high enough. This makes possible to cut the energy of the plane-waves, and only use a few of them up to a restricted energy. Therefore it is possible to use a finite basis to calculate the system obtaining accurate results. A negative consequence of this method is that the number of plane-waves included in every k-point is different. The k-points are those points in the limit of the *Brillouin* zone, or alternatively, are the point where one can reach from the origin of the zone crossing no *Bragg* planes (first *Brillouin* zone). Of course, it is not possible to calculate for every k-point in the *Brillouin* zone, but a mesh of k-points can be created and the energy is evaluated on them.

2.3.2 Reciprocal space

Some aspects regarded with periodic structures are easily understood introducing a reciprocal lattice as a mathematical tool. Reciprocal space is an alternative space of *Bravais* lattice without real existence in the crystal but really useful to simplify the physical description.

The reciprocal lattice build up from a given direct lattice is also a *Bravais* lattice. Therefore, knowing the direct primitive vectors $\overrightarrow{a}$ the reciprocal primitive ones $\overrightarrow{b}$ can be obtained by equation 2.11,

$$b_i = 2\pi \frac{a_j \times a_k}{a_i \left(a_j \times a_k\right)} \qquad \forall_{i,j,k} \in \{1,2,3\} \tag{2.11}$$

Primitive cell takes the name of first *Brillouin* zone or *Wigner Seitz* cell in reciprocal space. Although a finite basis of plane-waves is used and, therefore, the subset wave-vectors of *Wigner Seitz* cell has a finite number of states, the wave-vectors number is also infinite. The symmetry elements of *Brillouin* zone are took in advantage to study a discrete number of wave-vectors (*k-points*).

The reciprocal space vectors are perpendicular to direct lattice planes, useful for diffraction theory. Thus, for each vector in reciprocal lattice there is family of planes in real space perpendicular to this vector. A perpendicular plane bisector of a line joining the origin of the reciprocal space to a point of the reciprocal lattice is the *Bragg* plane seen with diffraction theory.

2.3.3 *Miller* index

The correspondence between reciprocal lattice vectors and families of lattice planes provides a way to specify the orientation of a lattice plane. It is natural to pick a reciprocal lattice vector to represent a lattice plane. The *Miller* indexes $\{h,k,l\}$ of a lattice plane are the coordinates of the shortest reciprocal lattice vector normal to that plane, with respect to a specified set of primitive reciprocal lattice vectors.

The *Miller* indexes are related with the points that intersects with direct vectors lattice by equation 2.12:

$$h = \frac{1}{x_1}\,; \quad k = \tfrac{1}{x_2}\,; \quad l = \frac{1}{x_3} \tag{2.12}$$

UNIVERSITAT ROVIRA I VIRGILI
MODELLING AU CATALYST FROM BULK TO NANOSCALE
Alberto Roldán Martínez
ISBN:978-84-693-7669-0/DL:T-1748-2010

In this way, when a *Miller* index is 0 there is no intersection point with a lattice vector, the plane is extended to infinity and parallel to the vector.

2.3.4 Pseudopotentials. The PAW method

To solve the problem of huge number of plane-waves necessary to have a good description of core electron of an atom, even using the *Blöch* theorem and calculating only the plane-waves that have up to a certain kinetic energy, pseudopotentials have to be used.

It is known that core electrons do not intervene in chemical bonds and these electrons are not necessary to be explicitly described if we only want to deal with chemical processes. This justifies the use of the so-called frozen-core electron approximation, where core electrons are calculated in a reference configuration and remain invariable in the calculations. Then, the wave-functions for valence electrons are substituted by pseudo-wave-functions, which reproduce the energy levels obtained by an all-electron calculation. These pseudo-wave-functions are different from the all-electron wave-functions because in the inner zone, near the nucleus, are designed not to have any node. This makes decrease in a substantial way the number of plane-waves required.

Several kinds of pseudopotentials are available, like ultrasoft pseudopotentials (US) [120], non-conserving pseudopotentials [119] or projected augmented wave pseudopotentials (PAW)[119, 121] which are the ones used in the present thesis.

The PAW pseudopotentials have demonstrated to give high quality results in solid state chemistry, despite being more time-demanding than other pseudopotentials. The biggest difference between PAW pseudopotentials and the other ones is that PAW tries to reproduce the nodal structure of the upper core states in addition to valence states in the self-consistent iterations, so PAW is a frozen-core method, but it tries to introduce the advantages of all-electron calculations by equation 2.13.

$$|\Psi\rangle = \left|\tilde{\Psi}\right\rangle - \sum_{N,i} \left|\tilde{\phi}_{N,i}\right\rangle c_{N,i} + \sum_{N,i} |\phi_{N,i}\rangle\, c_{N,i} \tag{2.13}$$

This means that, PAW describes core electrons with a frozen nodal structure and valence electrons by an all-electron wave-function. Thus, the quality of results improves substantially speciallyfor first row atoms.

2.3.5 Reaching steady states.

To perform total-energy calculations a global minimization of energy is needed. It implies a first minimization to find the electronic ground state and a second one to find the nuclei arrangement which minimizes the energy. Only the relaxation of the system to its ground state is considered in this short section.

In the steepest descents method, the direction, g^{-1}, moves from a point x^1 corresponds to minus the gradient of the function [122, 123]:

$$g^1 = -\left.\frac{\partial F}{\partial x}\right|_{x=x^1} = -\varsigma x^1 \tag{2.14}$$

UNIVERSITAT ROVIRA I VIRGILI
MODELLING AU CATALYST FROM BULK TO NANOSCALE
Alberto Roldán Martínez
ISBN:978-84-693-7669-0/DL:T-1748-2010

where ς is a gradient operator acting on the vector $\overrightarrow{x^1}$. Now, moving from x^1 along the direction of the steepest descent to the point $x^1+b^1g^1$, an appropriate value of b^1 can be chosen so that the function reaches a minimum. This process minimizes only the value of the function along a particular line in the multidimensional space, so one must perform a set of minimization along different lines to find the absolute minimum, using $x^1+b^1g^1$as a starting point for the next iteration step and leading to next point x^2. A set of vectors $\{x^m\}$ are generated so that the value of the function decreases at each iteration. With the steepest descent algorithm there is no guarantee that the minimum will be reached in a finite number of iterations. The method works particularly bad when the minimum lies in a long narrow valley. In this case, each steepest-descent vector is orthogonal to the vector of the previous iteration step. The main problem with the steepest descents methods holds in the fact that after a minimization is performed along a given gradient direction, a new minimization along a new direction introduces errors proportional to the previous gradient. A method in which each minimization step is independent on the previous one would be very useful. The conjugate-gradients method provides a simple procedure for implementation of such a minimization approach [122].

The initial direction is taken to be $g^1 = -\frac{\partial F}{\partial x}\big|_{x=x^1}$. A conjugate direction is constructed using a combination of initial direction and the new gradient. The direction is obtained from the algorithm 2.15.

$$d^m = g^m + \gamma^m d^{m-1} \tag{2.15}$$

where

$$\gamma^m = \frac{g^m \cdot g^m}{g^{m-1} \cdot g^{m-1}} \tag{2.16}$$

and $\gamma^1 = 0$. Since the conjugate directions are independent, the dimensionality of the vector space is reduced by one at each iteration. When the dimensionality of the function space is reduced to zero the trial vector must be at the position of the minimum.

The difference between the conjugate-gradient and the steepest-descent method holds in the fact that each direction is chosen only from the information about the function at the present sampling point in the steepest decedents but using information from all the sampling points along a path in the conjugate-gradient method.

In VASP, the *Kohn-Sham* equations are solved self-consistently with an iterative matrix diagonalization combined with the *Broyden/Pulie* [124, 125] mixing method for charge density. The combination of these two techniques makes the code very efficient, especially for transition metals, which present a complex band structure around *Fermi* level. The algorithms implemented in VASP are based on a conjugate gradient scheme, the block *Davidson* scheme or a residual minimization scheme (RMM). These algorithms work as follows: Firstly they calculate the electronic ground state for a particular geometry, then they evaluate the forces of this geometry, and finally predict a new geometry based on these forces.[1] This process is iterative until a

[1] Three different algorithms are available in VASP to calculate this new geometry:

1. Quasi-Newton calculation.
2. Conjugated gradients (CG).[126]

UNIVERSITAT ROVIRA I VIRGILI
MODELLING AU CATALYST FROM BULK TO NANOSCALE
Alberto Roldán Martínez
ISBN:978-84-693-7669-0/DL:T-1748-2010

convergence parameter is achieved.

Transition states

The steady state higher in energy that links two minimum along a path is a transition state. The path is referred as the lowest energy way for the rearrangement of a atoms group from one stable configuration to another. It is frequently used to define a reaction coordinate for transition such as chemical reactions or diffusion processes in solids and it is often referred to as the minimum energy path. The energy difference between the initial state and the potential energy maximum (saddle point) is the activation energy barrier.

Many different methods have been developed for finding the reaction path and saddle points. Some of them starts at a local minimum of the potential energy and follow the lowest path. However, this path does not always lead to the saddle point. Another common used method involves the calculation of normal modes of the atoms arrangement at each step along the path, and the following of each mode until a saddle point is reached. This procedure requires evaluation and diagonalization of the second derivative matrix and it is limited to small systems.

Other methods make use of two points boundary condition. Two local minimum of the potential energy surface corresponding to the initial and the final state for the transition state is needed. The simplest of them is a *Drag* method where a coordinate is chosen as a progress variable. This degree of freedom is varied stepwise during the transition form the initial to the final step. In each step a minimization is carried out over the remaining degrees of freedom. This method works well for a simple cases and fails on the description of some trickily systems, leading sometimes to discontinuous paths. On another class of two point methods, a set of replicas of the system is generated between the initial and final step. All intermediate images are optimized at the same time in some concerted way.

Some other algorithms are implemented. Quasi-Newton algorithm allows calculate saddle points on hypersurface of potential energy. NEB algorithm [127] and DIMER algorithm [128] are useful to find transition states. Besides, VASP package permits to evaluate numerically vibrational frequencies using a harmonic approximation by finite displacements of the atoms of a system. A combination of these algorithms must be used to find good descriptions for the hypersurface of potential energy.

3. Damped molecular dynamics (MD).

UNIVERSITAT ROVIRA I VIRGILI
MODELLING AU CATALYST FROM BULK TO NANOSCALE
Alberto Roldán Martínez
ISBN:978-84-693-7669-0/DL:T-1748-2010

2.4 Steady state analysis

Steady state is defined as a point of potential energy on hypersurface characterized by the gradients of each vibrational mode equal to zero. It could be a local or total minima on the hypersurface or a saddle point, therefore it has to be characterized. Some properties such as electronic configuration or forces between atoms could be reached directly from electronic density, others like vibrational modes needs to scan the hypersurface closer to the point. During this section, some tools and methods are described to study steady state points.

2.4.1 Vibrational frequencies

Vibrational calculations are necessary for two purposes: The first one is to localize the steady state on the hypersurface and ensure that the optimized stationary point is a minimum on the potential energy surface (or a transition state (TS) if it is desired). The other purpose is to simulate the infrared (IR) or Raman spectrum and *High Resolution Energy Loss (*HREELS*)* to be compared with the experimental one, and therefore assign the bands of the spectra.

It is necessary to remark that vibrational calculations only have sense on the optimized geometries (the forces or first derivatives of the potential energy are zero), because vibrational frequencies are related directly with the force constants, which are the second derivatives of the potential. Mathematical analysis ensures that a stationary point is a minimum if all second derivatives are positive (one negative for a TS), namely, the vibrational frequencies are all real (one imaginary frequency for TS) [129].

Second derivatives of the potential can be carry out by two mathematical methods: the analytical method and numerical ones. The analytical method calculates explicitly the second derivative of the potential. VASP does not uses this analytical method. The numerical method, which is used by VASP, takes finite displacements for every cartesian coordinate, and then evaluates the second derivatives from the energy gradients variation in these displacements. In the harmonic approximation, these displacements have to be big enough to make a substantial variation of the energy in order to minimize the numerical errors in the calculation of the derivatives, but they have to be small enough to ensure that we are in the harmonic zone. For adsorbates on a solid structure it is considered that phonons of the surface and vibrational frequencies of the adsorbate are decoupled. This decreases the number of steps to be calculated and the calculation is focused on desired frequencies. When second derivatives are calculated, the *Hessian* matrix [130] is created:

$$H\,f\,(x_1,...,x_n) = \begin{pmatrix} \frac{\delta^2 f}{\delta x_1^2} & \cdots & \frac{\delta^2 f}{\delta x_1 \delta x_n} \\ \vdots & \ddots & \vdots \\ \frac{\delta^2 f}{\delta x_n \delta x_1} & \cdots & \frac{\delta^2 f}{\delta x_n^2} \end{pmatrix} \tag{2.17}$$

Once the *Hessian* matrix is computed, it is necessary to weight the *Hessian* up by the mass. Then, the Hessian matrix is diagonalized. The eigenvalues are the vibrational frequencies and the eigenvectors are the vibrational normal modes (VNMs) of the system [131].

2.4.2 Density of states

One of the principal aims of computational chemistry is to understand how chemical bonds are created and how the molecules interact. Density of states (DOS) is the representation of the number of states in a specified energy.

Inside the *Brillouin* zone, each k-point defines energy levels that form energy bands which can be represented by means of a band diagram plot. When the number of atoms increase and the energy levels are enough close, discrete levels become a continue band. Commonly there are two characteristic bands, the valence band that is below the *Fermi* level (E_F) and contains all occupied states, and the conduction band, which is above the *Fermi* level and has unoccupied states, valence and conduction bands are parallel to the *Highest Occupied Molecular Orbitals (*HOMO*)* and *Lowest Unoccupied Molecular Orbital (*LUMO*)* respectively in molecules. This kind of diagrams could be very complicated and difficult to interpret, for this reason the DOS plot are more interesting.

The density of states are obtained carrying out the number of possible states for each level energy including all states on k-points of the *Brillouin* zone and divided by the *Brillouin* cell volume. DOS is represented versus a range of energy.

Mathematically, the DOS is the number of electrons for energy level ε_n^k for a close shell:

$$n(\varepsilon) = 2\sum_{n,k}\delta\left(\varepsilon - \varepsilon_n^k\right) \tag{2.18}$$

Where δ is the *Dirac* function. The huge number of k-points leads to integrate over *Brillouin* zone:

$$n(\varepsilon) = 2\sum_{n,k}\int \delta\left(\varepsilon - \varepsilon_n^k\right) dk \tag{2.19}$$

Open shell system density of states plot contains both alpha and beta states representable individually, where each state is occupied only by one electron.

A consequence of using plane-waves is that the electrons are delocalized. This can be solved projecting DOS into the spherical harmonics. These spherical harmonic orbitals have a specific radius, called *Wigner-Seitz* radius. *Wigner-Seitz* radius depends on the element and the chemical embedding of every atom. Projected Density Of States (PDOS) allows us to analyze the bands implied in bonds. Charge transfers, ionic interactions and covalent interactions can be analyzed on the displacement and intensity changes of the bands.

2.4.3 Atoms in molecules. *Bader*

At first of 90s *Richard Bader* developed a theory that allows to justify mathematically the *Lewis* model and the *Valence Shell Electron Pair Repulsion* (VSEPR) by a topological analysis of the electronic density, *atoms in molecules* (AIM) [132, 133, 134, 135]. Firstly, it was though for isolate molecules but is easily applied to condensed matter and it may be useful to interpret the electronic density.

The theory starts with the proposal that electrons are into an attractive external field by the nucleus corresponding to a local maximum of the electronic density. The

UNIVERSITAT ROVIRA I VIRGILI
MODELLING AU CATALYST FROM BULK TO NANOSCALE
Alberto Roldán Martínez
ISBN:978-84-693-7669-0/DL:T-1748-2010

nucleus are embedded by a electron cloud. From the physic point of view not only the electronic density has to be considered, also the field derived from density gradients vectors, $\nabla\rho(r)$. These vectors take the direction of rising density, and all trajectories have to finish in other atomic centers. Therefore, an important consequence on the description of delimiting space around the nucleus, the cavity, can be derived by this density gradients vectors: the limit between two atoms is defined by zero flux surfaces, which fulfill:

$$\nabla\rho(r_s)\,\vec{n}(r_s) = 0 \tag{2.20}$$

where $\vec{n}(r_s)$ is the unitary vector normal to the surface in r_s point. Between two atoms there is only one direction with the highest density, which is known as a bonding way assigned on the basis of chemical considerations such as *Lewis* and VSEPR models. However, AIM does not give explanation to non-bonding electron pairs, which requires to include a density laplacian $\nabla^2\rho(r)$. Density laplacian gives information about where the charge concentration is.

However, the important advantages of AIM is the non-arbitrary and systematic atomic hole definition, therefore, the integration over this space gives the *Bader* charges besides of previous value of radius as *Mulliken* charges. Also, other properties can be measurable over the *Bader* hole such as Spin Density.

2.4.4 Electronic density

The study of electronic density gives information about interacting species, for example in the case of a molecule adsorbed on a surface. This analysis could be difficult due to the high density closer to atomic nucleus. However, the electronic density shows only the adsorbate effect as derived from the electronic density of the system minus the isolate components density, substrate and molecule.

Therefore, it is possible to obtain an electronic density map where density of charge build-up and charge depletion is shown explaining charge transfers or covalent bonds when the electronic density raises is the interatomic zone.

2.4.5 Work-function

Work function is the minimum energy needed to remove an electron as well as the required energy to move an electron from the higher energy occupied level, *Fermi* level, E_F, to vacuum. Mathematically:

$$\phi = V - E_F \tag{2.21}$$

where V is the electron density in the vacuum. The work-function is related to the charge transfer that takes place between a substrate and an adsorbed molecule. A large value of the work-function means less transfer charge, and a small work-function means a charge transfer between adsorbate and substrate easily.

Inside the bulk the potential energy oscillates, this fact corresponds to atomic positions due to core-electron attractive interaction. Nevertheless, the potential energy remains constant outside the solid. An adsorption can modify the work-function value.

UNIVERSITAT ROVIRA I VIRGILI
MODELLING AU CATALYST FROM BULK TO NANOSCALE
Alberto Roldán Martínez
ISBN:978-84-693-7669-0/DL:T-1748-2010

2.5 Solid models

In this section we will raise different models to represent the condensed matter. There are two approaches: periodic models and non-periodic models, each one with advantages and disadvantages to give information about material behaviour. In addition, there are other methodologies that combines, for example, a high-level cluster embedded by less accurate region. The combination of isolated cluster on a periodic system can be useful to study superstructures.

2.5.1 Bulk models

Crystalline compounds show an organized structure that can be expressed at macroscopic aspect as common salt and at nanoscale as nanoparticles. The importance of continuous model is the imposition of periodic conditions simplifying the extended materials study. An ideal solid can be observed as an infinite 3-dimensional repetition of a small piece. For example, the copper bulk (Fm3m structure) is the infinite repetition in the three space directions of a cube, where Cu atoms are placed on the vertexes of the cube and on the face center. In this case, the unit cell would be this cube. Therefore, the number of atoms on the unit cell is small and the *Schrödinger* equation is solved faster, under wave-function conditions or electronic density in determinate points, which are not affected by translational operators (*Blöch* theorem 2.3.1).

The presence of a perturbing element in the system, as a defect, does required a supercell to eliminate the interaction between perturbing elements on reply cells.

2.5.2 Surface models

As commented in the introduction of this section, two different surface models exist, each one with its advantages and disadvantages. Following, we are going to explain the features of each one applied to surfaces and why they have been chosen for every purpose.

Periodic surface. Slab

In the case of surfaces, the repetition of the unit cell only in two directions of the space is desired , but not in the third one. In order to avoid the problem of the repetition in the third space direction imposed by plane-waves, one large vacuum region is added in one direction (normally the Z-direction). Then the unit cell is repeated infinitely: this is the slab model. The cell larger than its primitive, namely, that contains more than one primitive cell, is denoted as $p(n\times n)$, where n is the times of primitive cell replicated in surface directions. The vacuum region must be large enough to avoid undesirable interactions between consecutive slabs in Z-direction, usually $\geq 10\,$Å [136, 137, 93]. In figure 2.5.2 is presented the slab model.

Disadvantages

- It could be inappropriate to study, for example, dispersed particles on a surface, which contains an amount of aggregate atoms, because this system leads to very large cell and needs very expensive calculations.

UNIVERSITAT ROVIRA I VIRGILI
MODELLING AU CATALYST FROM BULK TO NANOSCALE
Alberto Roldán Martínez
ISBN:978-84-693-7669-0/DL:T-1748-2010

Advantages

- It gives a correct descriptions of extended surfaces.
- Small cell is required to reproduce an infinite ideal surface due to periodicity.
- It allows the study non-local properties such as *Fermi* level, elastic constants, coverages effects and adsorption energies, that could be calculate by equation 2.22:

$$E_{ads} = E_{total} - \left(E_{slab} + E_{adsorbate(g)}\right) \tag{2.22}$$

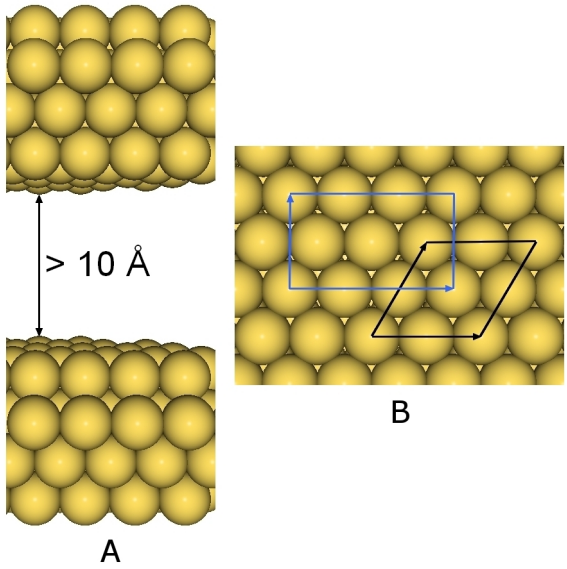

Figure 2.5.2: A: four layers slabs and 10 Å vacuum region. B: two possible cells, in black 2×2 unit cell; in blue $3 \times \sqrt{3}$ unit cell.

Non-periodic surface. Cluster Model

Another strategy to simulate a surface is to use the cluster model. This is a much simpler method than the slab one. In the cluster model the solid is "cut" and only a small piece of the total system is used for the calculation. In figure 2.5.3 a cluster of 29 atoms is presented. In this case, all the surface is reduced to only three layers.

Sometimes the cluster is embedded into a grid of charge points that represent the *Madelung* potentials and simulate lateral interactions with the rest of surface, it is specially useful for ionic systems. Besides, the charge points could polarize the edge atoms and modifying the electrostatic potential. Polarization can be considered for ionic systems using the ionic potential model, non-ionic system may be really difficult to compute.

UNIVERSITAT ROVIRA I VIRGILI
MODELLING AU CATALYST FROM BULK TO NANOSCALE
Alberto Roldán Martínez
ISBN:978-84-693-7669-0/DL:T-1748-2010

Disadvantages.

- It is inadequate to study metallic systems where the electronic density is highly delocalized, reached only from determinate size.
- Model size is into nanometric scale where each atom has to betaken into account and leads to different electronic structure.
- It allows to study local properties such as adsorption geometries or adsorbed molecules vibration frequencies. But non-local properties could not converge with the size of the cluster [138, 139].
- Size dependent properties like adsorption energy are not accurate due to edge effects. The problem is not solved increasing the cluster size because of the number of edge atoms increase too.

Advantages.

- The model has demonstrated be effective to obtain local properties [140, 141], besides avoid interaction with other like fictitious periodic systems does.
- The small size allows to use different very accurate quantum chemistry methods such as wave-function or density function including excited states.

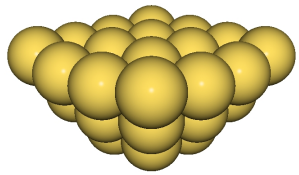

Figure 2.5.3: Cluster of 29 atoms, 16 atoms are in the upper layer, 9 in the second one and 4 in the last one.

2.5.3 Nanoparticle models

Commonly isolated particles may be modelled as normal clusters. Other possibility to study confined systems is using periodic conditions and adding vacuum on all cell directions to avoid interactions between bonded cell aggregates (see figure 2.5.4). The origin of this models is the same that for slabs, which are computed adding vacuum between layers. Like for slabs a vacuum about 10 Å is enough to have consistent results.

Disadvantages.

- Cluster shape could be very similar to real supported catalytic particles, although the support usually is neglected.
- Periodic conditions limits to DFT methodology.

UNIVERSITAT ROVIRA I VIRGILI
MODELLING AU CATALYST FROM BULK TO NANOSCALE
Alberto Roldán Martínez
ISBN:978-84-693-7669-0/DL:T-1748-2010

Advantages.

- It allows to study metallic systems [142, 143], as well as covalent or ionic ones [144].
- In well defined 3D nanoparticles, both size depending and non-size depending properties are well described.
- Symmetry is not restricted and therefore reactivity at low coverage can be studied.

It is possible to take advantage of periodic conditions to study superstructures like nanowires [145] or zeolites [146] that are extended in less than the three space directions.

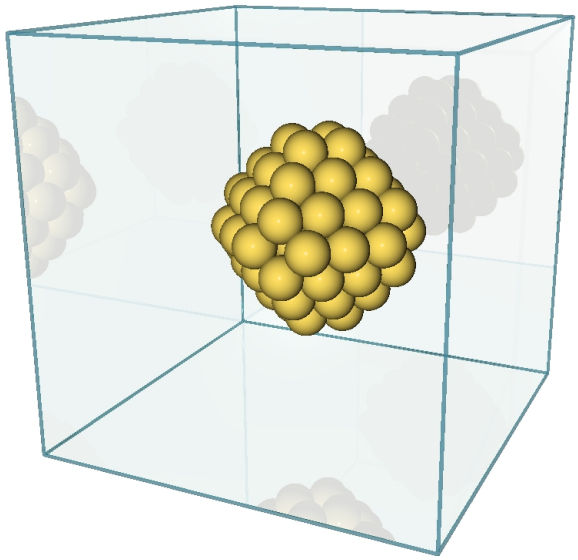

Figure 2.5.4: Isolated cluster on a periodic environment.

2.6 Catalysis

Catalysis is the process in which the rate of a chemical reaction is either increased or decreased by means of a chemical substance which is not consumed in the reaction [147]. This concept was used before *Berzelius*, who gave an appropriate definition at 1836. Afterward, at the XXth century *Paul Sabatier* wrote about the catalytic phenomena [148]. Along this century the catalysis had a huge importance in industrial development [149, 150, 151, 152] but it is not after 70s when this science left to be empirical and gave more importance to reaction thermodynamics and kinetics. Nowadays, catalysis is not only important for industry but also for the environment safety.

There are three parameters to determine the catalytic effectiveness: activity, selectivity and stability.

Activity determines the powers of magnitude that a catalyst increases the reaction rate. In catalysis it is important to take into account that reactive phase has to be in contact with the active site. The activity could be increased by the presence of other substance named promoter, which speed up certain elementary reaction steps, for example, alkali promoters are employed to modify activity and selectivity patterns in a variety of heterogeneous catalytic processes.

Selectivity means that the catalyst is more specific to catalyze one characteristic reaction and not others. To be selective, one reaction pathway could be benefit and/or others reactions be poisoned by catalyst.

Catalyst is not spent in a reaction and it is useful during a lot of reaction cycles but there are phenomena that do lost his activity, such as poisons or sintering in the case of dispersed catalyst. The number of cycles is the catalyst life and indicates his stability.

There are many kind of catalytic process depending of number and types of systems phases. This process could be classified into three big groups: homogeneous, enzymatic and heterogeneous catalysis.

In homogeneous catalysis, all the components, reactants, products and catalyst, are in the same phase. It also includes reactions where the reactive gas is dissolved into a liquid where the process takes place. Commonly, the homogeneous catalyst are organometallic compounds with a high selectivity following a simple pathway. The principal disadvantage is the difficulty to separate products and catalyst.

Enzymatic reactions take place in all living organisms by specific chains of amino-acids with a complicate third level of packaging which derives in a superselective and superactive catalyst that works in a colloidal environment. The weak point of this enzymatic proteins is that they only works in a very specific conditions of temperature and pH media, a variation of twice degrees could denature the enzyme and it become effectiveless.

Briefly summarized, in heterogeneous catalysis there are, at least, two phases, the reactants and products are in one phase and catalyst is usually in solid phase.

2.6.1 Heterogeneous catalysis

Lots of efforts in the research of surface science have made towards the understanding of heterogeneous catalysis, because of its importance in industrial processes. Most

UNIVERSITAT ROVIRA I VIRGILI
MODELLING AU CATALYST FROM BULK TO NANOSCALE
Alberto Roldán Martínez
ISBN:978-84-693-7669-0/DL:T-1748-2010

important industrial reactions and an amount of the actual chemical products are yielded by heterogeneous catalysts, and without them our society would not have reached the present standard of life. In spite of, and being less selective for a concrete reaction than the homogeneous catalysts, heterogeneous catalysis is used in industry because of it is easy to separate the final products (normally gas or liquid phase) from the catalysts (commonly solid phase). One example of this is the *Haber-Bosch* process, where N_2 and H_2 react to yield NH_3 on metallic iron, or the *Fischer-Tropsch* reaction, where H_2 and CO react to yield methanol or other hydrocarbons on some metallic oxides.

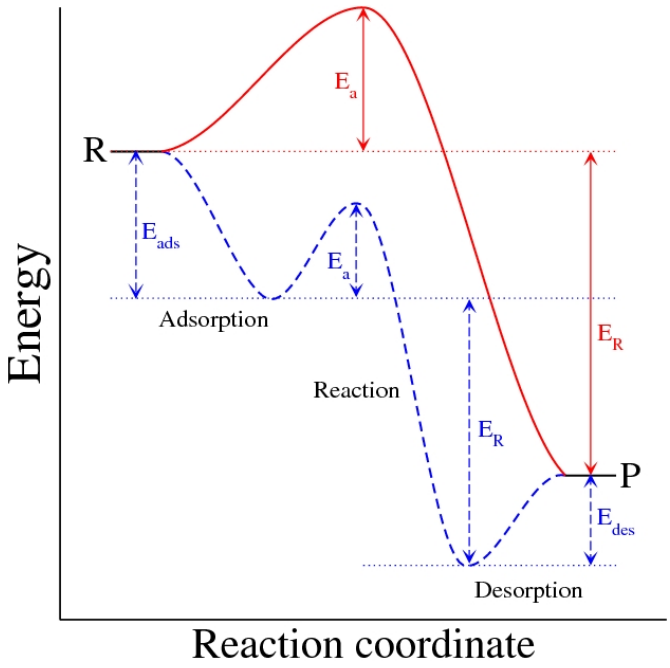

Figure 2.6.5: Profile representation for both non-catalytic (red-line) and catalytic (blue-line) reactions. Where E_{ads} is the adsorption energy, E_a is the activation energy, E_{des} is the desorption energy and E_R represents the reaction energy, in this case, exothermic.

On heterogeneous catalysis, reactants as well as products interact with catalyst, which makes the study of the process more complicated. Since *Paul Sabatier* publications [148], the catalyst is considered as a reactant forming an unstable species on the surface. The situation with a maximum reaction rate would be when intermediate species has both non-strong and non-weak interaction with catalyst.

Usually five steps could be distinguished in heterogeneous catalytic process:

- Reactants diffusion to reach the catalyst surface.
- Reactants adsorption on an available catalyst site.
- Reaction taking place on catalyst.
- Products desorption.

- Products diffusion to fluid phase.

The reaction process is represented schematically on figure 2.6.5. Therein, the catalyst allows other reaction path with a lower transition state energy, then reaction takes place faster than without catalyst. Global rate will depend of the limiting step that has the higher energy barrier, usually it is the reaction process.

UNIVERSITAT ROVIRA I VIRGILI
MODELLING AU CATALYST FROM BULK TO NANOSCALE
Alberto Roldán Martínez
ISBN:978-84-693-7669-0/DL:T-1748-2010

2.7 Microkinetic study

Although we may be able to describe a catalytic reaction on a well-defined single crystal of a metal under well-defined and simplified conditions, this becomes tremendously more complicated when the same reaction runs over small catalyst particles on a support in a tic reactor environment. The world of the ideal surface science and industrial practice are not only separated by the often cited pressure gap, but also by structural, and material gaps. The complexity of small supported crystallites environment is only beginning to be explored.

Catalysis is a very broad field of study that is closely interwoven with numerous other scientific disciplines. This becomes immediately evident if we realize that catalysis encompasses many length scales. Understanding reactions at the elementary level of the rupture of bonds in reactants and the formation of bonds in products is at the heart of the matter, and requires the most advanced experimental techniques and theoretical descriptions available. This is the domain of spectroscopy, computational chemistry, kinetics. Subtle details are taken into account, such as the effect of the orientation of molecules in a collision that may result in a reaction, and the distribution of energy over a molecule's degrees of freedom. This is the fundamental level of study needed if we want to link reactivity to quantum mechanics, which is really what rules the game at this fundamental level. The length scales of interest are in the subnanometre region. The next level is that of small catalytic active particles, with typical dimensions of between 1 and 10 nm, and inside the pores of support particles. The questions of interest are the size, the shape, the structure and the composition of the active particles, in particular of their surfaces, and how these properties relate with catalytic reactivity. Transport phenomena such as the diffusion of molecules inside pores may affect the rate at which products form and become an important consideration on this level. The next level is that of shaped catalysts, in the form of extrudes, spheres, or monoliths on length scales varying from millimeters to centimeters, and occasionally even larger. Typical issues of interest are porosity, strength, and attrition resistance such that catalysts are able to survive the conditions inside industrial reactors [89].

There are two types of reactor, the flow and the batch reactor. The flow reactor is typically used in large-scale industrial processes. Reactants are continuously fed into the reactor at a constant rate, and products appear at the outlet, also at a constant rate. Such reactors are said to operate under steady state conditions, implying that both the rates of reaction and concentrations become independent of time (unless the rate of reaction oscillates around its steady state value). The batch reactor is generally used in the production of fine chemicals. At the start of the process the reactor is filled with reactants, which gradually convert into products. As a consequence, the rate of reaction and the concentrations of all participants in the reaction vary with the time. We will assume that our batch reactor behaves as a well stirred tank reactor, such that all participants are well mixed and concentration gradients do not occur.

Then, kinetic studies provide the framework for describing the rate at which a chemical reaction occurs and it enables us to relate the rate with the reaction mechanism. This mechanism describes how the molecules react via intermediates to the eventual product. It also allows us to relate the rate to macroscopic process pa-

UNIVERSITAT ROVIRA I VIRGILI
MODELLING AU CATALYST FROM BULK TO NANOSCALE
Alberto Roldán Martínez
ISBN:978-84-693-7669-0/DL:T-1748-2010

rameters such as concentration, pressures, and temperatures. Namely, these studies provide us with the tools to link the microscopic world of reacting molecules to the macroscopic world of industrial reaction engineering [89].

2.7.1 Equation rate

The reaction rate is defined as the rate of reactants disappearance, or the rate of production:

$$\nu_a A + B \xrightarrow{k} A_{\nu_a} B \tag{2.23}$$

$$r = -\frac{1}{\nu_a}\frac{\delta\left[A\right]}{\delta t} = +\frac{\delta\left[A_{\nu_a}B\right]}{\delta t} \tag{2.24}$$

where $[X]$ is the concentration of component X with stoichiometric constant ν_X, r is the rate and k the rate constant. If the reaction occurs in the gas phase, we may replace the concentrations by partial pressures.

A reaction is elementary if occurs in a single step that cannot be divided into further sub-steps, and proceeds exactly as expressed by the reaction equation (equation 2.23). For an elementary step:

$$r = k\left[A\right]^{\nu_a}\left[B\right]^{\nu_b} \tag{2.25}$$

in which stoichiometric constants (ν_X) equal the orders of the reaction in the respective molecules. A reaction mechanism is a sequence of elementary steps, which temperature dependence of the rate constants is given by the *Arrhenius* equation:

$$k(T) = A\, e^{\left\{-\frac{E_a}{k_B T}\right\}} \tag{2.26}$$

where A is called the pre-exponential factor, E_a is the activation energy and k_B is the *Boltzmann*'s constant. The physical interpretation of the *Arrhenius* equation is that of an event in which a potential energy barrier has to be surmounted to achieve a completed reaction.

Heterogeneous catalysis involves reactants and products in the three-dimensional space of gases or liquids, but with intermediates on a two-dimensional surface. Thus we cannot simply use concentrations as in the case of uncatalyzed reactions. We can think of a catalyst as a collection of active sites (denoted by $*$) located at a surface. The total number of sites is constant and the adsorption of the reactant is formally a reaction with an empty site. We assume that all sites are equivalent and each can be occupied by a single species only. We will use the symbol θ_A to indicate the fraction of occupied sites by the species A. Hence, the fraction of unoccupied sites available for reaction will be $1-\sum_i \theta_i$, where i denotes each adsorbed species.

The macroscopic rate of a catalytic reaction is expressed in concentration per unit of time but also can be seen as a characteristic activity per weight or per volume unit of catalyst in all its complexity with regard to shape, composition, etc. Note that the rates of product formation and reactant conversion indeed have the dimensions of mol per unit of time, and that these rates are proportional to the number of sites, or, in fact, the amount of catalyst present in the reactor.

UNIVERSITAT ROVIRA I VIRGILI
MODELLING AU CATALYST FROM BULK TO NANOSCALE
Alberto Roldán Martínez
ISBN:978-84-693-7669-0/DL:T-1748-2010

2.7.2 Reaction mechanisms

The catalytic process is a sequence of elementary steps that form a cycle from which the catalyst emerges unaltered. Identifying which steps and intermediates have to be taken into account may be difficult, requiring spectroscopic tools and computational approaches. From computational results we will know elementary steps, which may describe in detail the rate equation for such processes.

Commonly we can talk about two reaction mechanism: *Langmuir–Hinshelwood* or *Eley–Rideal*. In *Langmuir–Hinshelwood* kinetics is assumed that all species are adsorbed and accommodated (in thermal equilibrium) with the surface before they take part in any reactions. Hence, species react in the chemisorbed state on the surface. Another possibility is the so-called *Eley–Rideal* mechanism, in which one of the reactants reacts directly out of the gas phase, without being accommodated at the surface. Whether a catalytic reaction proceeds via a *Langmuir–Hinshelwood* or *Eley– Rideal* mechanism has significant implications for the kinetic description, as in the latter case one of the reactants does not require free sites to react.

To solve the kinetics for the most general case, in which, for example, we allow the variation of partial pressures with time,

$$A_2(g) + 4* \overset{k_1}{\rightarrow} A_2(ads) \tag{2.27}$$

$$A_2(ads) \overset{k_2}{\rightarrow} 2A(ads) \tag{2.28}$$

$$2A(ads) \overset{k_3}{\rightarrow} A_2(ads) \tag{2.29}$$

$$A_2(ads) \overset{k_4}{\rightarrow} A_2(g) + 4* \tag{2.30}$$

we need a full set of differential equations describing the coverage of all species that participate in the reaction set:

$$\frac{dP_{A_2}}{dt} = -k_1 P_{A_2} \theta_*^4 + k_4 \theta_{A_2} \tag{2.31}$$

$$\frac{d\theta_{A_2}}{dt} = k_1 P_{A_2} \theta_*^4 - k_2 \theta_{A_2} + k_3 \theta_A^2 - k_4 \theta_{A_2} \tag{2.32}$$

$$\frac{d\theta_A}{dt} = 2k_2 \theta_{A_2} - 2k_3 \theta_A^2 \tag{2.33}$$

$$\theta_* = 1 - 4\theta_{A_2} - 2\theta_A \tag{2.34}$$

These equations can be solved numerically by a computer, without making any approximations. Naturally all the involved kinetic parameters need to be either known or estimated to give a complete solution capable of describing the transient (time dependent) kinetic behavior of the reaction. However, there are many approximations to reduce the complexity such as: steady state, quasi-equilibrium, steps with similar rates, irreversible step, etc.

UNIVERSITAT ROVIRA I VIRGILI
MODELLING AU CATALYST FROM BULK TO NANOSCALE
Alberto Roldán Martínez
ISBN:978-84-693-7669-0/DL:T-1748-2010

2.7.3 Reaction rate theory

Many reaction rate theories are based on the concept that reacting molecules acquire energy to reach an activated state (the top of the activation barrier) from which the product forms. Transition State Theory (TST) includes the vibrations and rotations of reacting molecules, which are heavily involved in the exchange of energy when molecules collide, but are also degrees of freedom that are excited when a reacting complex passes over the activation barrier.

Without enter in detail, the *Boltzmann's* distribution leads to a partition function. It is a thermodynamical function of state which, through the sum over all the energy levels, contains all properties of the system. Although work with large sums with many terms is too labored, infinite mathematical series often yield simple expressions. Partition functions are very important to estimate equilibrium constants and rate constants in elementary reaction steps.

Therefore, we shall take a look at the partition functions of molecules. Molecules possess translational, vibrational, rotational and electronical degree of freedom, the last three as internal degrees. We will be interested in how the velocities of molecules are distributed and we will need to transform the *Boltzmann's* distribution of energies into the *Maxwell–Boltzmann's* distribution of velocities, changing the variable from energy to velocity.

We consider a molecule for which the different degrees of freedom are independent and the energy is simply the sum of the energies contained in the different degrees of freedom. Then we can write the global partition function as the product of the partition functions.

$$Q = q_{translation} \cdot q_{rotation} \cdot q_{vibration} \cdot q_{electronic} \tag{2.35}$$

Translational partition function

Starting with the partition function of translation, we consider a particle of mass m moving in a plane xy of dimension A with velocity v_{xy}. Its kinetic energy is $\varepsilon_{xy} = \frac{p_{xy}^2}{2m}$. The coordinates available for the particle are xy, then p_{xy} can be divided into small cells, each of size h, which is the *Planck*'s constant. We can integrate over the space and calculate the partition function [89].

$$q_{translation}^{2D} = \frac{2\pi m\, k_B T}{h^2} A \tag{2.36}$$

Rotational partition function

Rotational partition function is derived as a function of rotational quantum number as well as inertia moment. The last depends of molecule geometry. For both kind of molecule, linear and non-linear, the rotational function is explained below.

Rotational energy, equation 2.37, leads to the rotational partition function for linear structures, equation 2.38.

$$\varepsilon_J = \frac{h^2 J(J+1)}{8\pi^2 I} \tag{2.37}$$

UNIVERSITAT ROVIRA I VIRGILI
MODELLING AU CATALYST FROM BULK TO NANOSCALE
Alberto Roldán Martínez
ISBN:978-84-693-7669-0/DL:T-1748-2010

$$q_{rotation}^{linear} = \frac{1}{\sigma}\frac{8\pi I\, k_B T}{h^2} \tag{2.38}$$

where I is the moment of inertia defined as $I = \mu r^2$, being μ the reduced mass and r the atoms distances to the center of mass (CM) and σ is the symmetry factor, see table 2.7.1.

Table 2.7.1: Symmetry factor (σ) for different symmetry groups.

Symmetry Group	Types of molecule	Symmetry factor
C_1, C_i and C_s	CO, CH_3OH, ...	1
C_2, C_{2v} and C_{2h}	O_2, H_2O, ...	2
C_3 and C_{3h}	NH_3, $B(OH)_3$, ...	3

When the molecule is non-linear we need three angular coordinates resulting in three values of inertia moments. The position of each atom is expressed in a coordinate system whereby the center of mass is the origin. Each atom is along these axes, usually labeled as a, b and c. The principal moments of inertia are [153]:

$$I_a = \sum_i^N m_i(b_i^2 + c_i^2) \tag{2.39}$$

$$I_b = \sum_i^N m_i(a_i^2 + c_i^2) \tag{2.40}$$

$$I_c = \sum_i^N m_i(a_i^2 + b_i^2) \tag{2.41}$$

for all atoms (i) in the molecule and distance to new axis: a_i, b_i and c_i. The rotational partition function for a non-linear molecule is given by equation 2.42 [153].

$$q_{rotation}^{non-linear} = \frac{1}{\sigma}\left(\frac{8\pi^2 k_B T}{h^2}\right)^{\frac{3}{2}}\sqrt{\pi I_a I_b I_c} \tag{2.42}$$

Vibrational partition function

The vibrational energy levels using the harmonic oscillator approximation are given by equation 2.43, from the bottom of iso-surface potential and with frequency $h\upsilon$ [89].

$$\varepsilon_i = \left(i + \frac{1}{2}\right)h\upsilon \tag{2.43}$$

$$q_{vibration} = \sum_{i=0}^{\infty} e^{\left\{-\frac{\left(i+\frac{1}{2}\right)h\upsilon}{k_B T}\right\}} = \frac{1}{1 - e^{\left\{-\frac{h\upsilon}{k_B T}\right\}}} e^{\left\{-\frac{\left(\frac{1}{2}\right)h\upsilon}{k_B T}\right\}} \tag{2.44}$$

UNIVERSITAT ROVIRA I VIRGILI
MODELLING AU CATALYST FROM BULK TO NANOSCALE
Alberto Roldán Martínez
ISBN:978-84-693-7669-0/DL:T-1748-2010

The second exponential factor is regarded with the energy contribution at bottom point defined as $-\left(\frac{1}{2}\right)h\nu$, see figure 2.7.6. Hence we can work with the first term of equation 2.44 if the system energy is corrected by Zero Point Energy (ZPE).

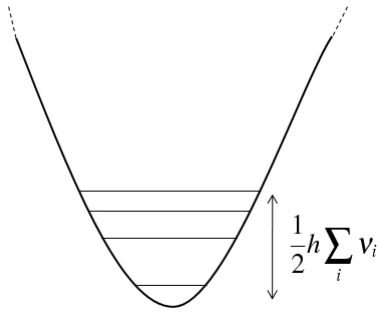

Figure 2.7.6: Zero Point Energy correction at steady state energy.

Electronic partition function

Usually this partition function does not contribute to the global partition function and can therefore be taken as unity. Nevertheless, it is not the case when an unpaired electron is in the highest occupied molecular orbital, i.e., a triplet where the orbital momentum can assume two orientations with respect to the axis. Thus, there are two orientations for the spin, giving four different configurations with a relatively small difference in energy between them [89].

Electronic partition function is done by equation 2.45.

$$q_{electronic} = \xi_{\varepsilon_0} + \sum_{i>0} \xi_{\varepsilon_i} e^{\left\{-\frac{\varepsilon_i}{k_B T}\right\}} \tag{2.45}$$

where ξ is the degeneracy of state ε_i, and $i > 0$ refers to excited electronic states. To obtain excited states energy is possible to use time dependent DFT or get in directly from experimental values. Instead of, we assume that energy separation between excited states is large enough compared with $k_B T$, and the contribution of excited states is irrelevant, thus $q_{electronic} = \xi_{\varepsilon_0}$.

Transition State Theory (TST)

Transition state theory was developed by *H. Eyring*, and independently also by *M.G. Evans* and *M. Polanyi*, around 1935 [154, 155]. In qualitative terms TST describes the reaction via an activated complex located at the top of the energy barrier between reactants and products.

Reacting molecules are activated to the transition state by collisions with surrounding molecules. TST is a canonical approach that assumes rapid energy randomization in the reactant configuration and all trajectories that pass through the transition state valley lies to products without recrossing, crossing the barrier is

UNIVERSITAT ROVIRA I VIRGILI
MODELLING AU CATALYST FROM BULK TO NANOSCALE
Alberto Roldán Martínez
ISBN:978-84-693-7669-0/DL:T-1748-2010

only possible in the forward direction [156]. These two assumptions limit the theory to describe adsorption and desorption process and recrossing of trajectories with insufficient energy. They have to be explicitly accounted for this theory.

The reaction event is described by a single parameter, called the reaction coordinate, which usually is a vibration mode, i.e. If the reaction is a dissociation of a diatomic molecule, the reaction coordinate would be the stretching vibration between the two atoms. The activation of this vibration would weaken the bond between them. The reaction can thus be visualized as a journey over a potential energy surface where the transition state lies at the saddle point.

The partition functions, $Q^{\mp}$ (activated complex) and Q (reactants), must be given with respect to the same zero of energy. The energy difference between the ground state and the transition state is the barrier or activation energy, E_a, used in collision theory. Incorporating it into the rate expression, we automatically obtain a constant rate expression, 2.46, that bears great resemblance to the *Arrhenius* equation 2.26:

$$k = \frac{k_B T}{h} \frac{Q^{\mp}}{Q} e^{\left\{-\frac{E_a}{k_B T}\right\}} \tag{2.46}$$

Once the kinetic parameters of elementary steps are available, we can construct a microkinetic model to describe the overall reaction. Otherwise, one has to rely on fitting a rate expression that is based on an assumed reaction mechanism: adsorption, desorption and/or reaction. Although this theory is restricted in its ability to describe adsorption and desorption, it does not mean that other influences upon these process can not be usefully described with TST.

Adsorption process

In the adsorption of molecules we need to distinguish between two cases: physisorption and chemisorption. Physisorption is a weak interaction characterized by the lack of a true chemical bond between adsorbate and surface, also the molecule is poorly disturbed. The other extreme is chemisorption, in which the molecule lands immediately at its final adsorption site without the possibility of moving over the surface.

As a part of adsorption process we are particularly interested in the rate of collisions between gas and surface. For a surface of area A, the molecules that will be able to hit this surface must have a velocity component orthogonal to the surface v_z. All molecules with velocity v_z, given by the *Maxwell–Boltzmann's* distribution $f(v_z)$ in cartesian coordinates, at a distance $v_z \triangle t$ orthogonal to the surface, will collide. Then, we can obtain the total number of collisions in time interval Δt on the area A as a function of molecule pressure (P_i), equation 2.47 assumes an ideal gas behaviour [89].

$$r_{collision} = \frac{P_i}{k_B T} \int_0^{\infty} v_z \sqrt{\frac{m}{2\pi k_B T}} e^{\left\{-\frac{m v_z^2}{2 k_B T}\right\}} \delta v_z = \frac{P_i}{\sqrt{2\pi m\, k_B T}} \tag{2.47}$$

The rate of gas adsorption on a surface is determined by the gas-surface rate of collision and by the sticking coefficient (S). The sticking coefficient (S) is a measure of the fraction of incident molecules which adsorb upon the surface, the probability

UNIVERSITAT ROVIRA I VIRGILI
MODELLING AU CATALYST FROM BULK TO NANOSCALE
Alberto Roldán Martínez
ISBN:978-84-693-7669-0/DL:T-1748-2010

lies in the range $[0, 1]$ corresponding to none and all impinging stick molecules on surface respectively. S depends upon many variables such as coverages (θ), crystal face, steric factor between molecules, energy transference when molecule-surface interaction takes place, molecule orientation [157, 158, 159]... To determine all this parameters is practically impossible, nevertheless we can consider the temperature dependency of S by equation 2.48 where a free molecule moves perpendicular to the surface towards activated species ($\mp$). This species is anchored (chemisorbed) and its translation and rotation are frustrated.

$$S_0(T) = \frac{q^{\mp}_{vibration} q^{\mp}_{electronic}}{q^{2D}_{translation} q_{vibration} q_{rotation} q_{electronic}} e^{\left\{-\frac{\triangle E}{k_B T}\right\}} \tag{2.48}$$

The rate adsorption becomes 2.49:

$$r_{ads} = \frac{A_{cat}}{\sqrt{2\pi m\, k_B T}} P_i \theta^* S_0(T) \tag{2.49}$$

where A_{cat} is the effective area of catalyst and θ^* is the coverage of free sites.

Reaction process

We consider a surface with adsorbed molecules distributed randomly over the surface that react. The rate constant towards products is given by equation 2.50.

$$k_{reac} = \frac{k_B T}{h} \frac{Q^{\mp}}{Q} e^{\left\{-\frac{\triangle E}{k_B T}\right\}} = \frac{k_B T}{h} \frac{q^{\mp}_{vib}\, q^{\mp}_{elec}}{q_{vib}\, q_{elec}} e^{\left\{-\frac{E_a}{k_B T}\right\}} \tag{2.50}$$

Desorption process

Desorption is important due to it represents the last step in a catalytic cycle and is also the basis of temperature-programmed desorption (TPD), a powerful tool used to investigate the adsorption, decomposition and reaction of species on surfaces.

If the pumping speed is infinitely high readsorption may be ignored. The desorption rate is defined as the change in adsorbate coverage per unit of time. Then this constant rate could be derived by 2.51 considering the 2D-translational, once the third direction is the reaction coordinate.

$$k_{des} = \frac{k_B T}{h} \frac{Q^{\mp}}{Q} e^{\left\{-\frac{\triangle E}{k_B T}\right\}} = \frac{k_B T}{h} \frac{q^{2D}_{trans}\, q_{rot}\, q_{vib}\, q_{elec}}{q_{vib}} e^{\left\{-\frac{E_{des}}{k_B T}\right\}} \tag{2.51}$$

If the desorption is not activated, E_{des} is equals to the adsorption energy. The heating rate is defined as $\frac{\delta T}{\delta t}$ and TPD curve is defined as $\frac{\delta P_i}{\delta t}$.

2.7.4 Units

To skip mistakes is strongly recommended to take care with the units in the whole microkinetic scheme. To facilitate the understanding we will clarify some units conversion.

All energies have to be corrected by the zero point energy (ZPE) means equation 2.52 if vibrational partition function is defined as 2.53.

UNIVERSITAT ROVIRA I VIRGILI
MODELLING AU CATALYST FROM BULK TO NANOSCALE
Alberto Roldán Martínez
ISBN:978-84-693-7669-0/DL:T-1748-2010

$$E_T = E_Q + ZPE = E_Q + \frac{1}{2}\frac{hc}{\kappa}\sum_{i=1}^{NMV}\nu_i \Rightarrow eV \tag{2.52}$$

$$q_{vibrational} = \frac{1}{1 - e^{\left\{-\frac{hc\nu}{k_B T}\right\}}} \Rightarrow no\ units \tag{2.53}$$

where E_T is the useful energy in eV, E_Q is the energy obtained by quantum calculations in eV, $\frac{c}{\kappa}$ is a factor to adapt the frequencies (ν_i) to be in cm^{-1}, also h is the *Planck's* constant $\left(6.626069311E^{-34} J\,s^{-1}\right)$, c is the light speed $\left(29979245800\,cm\,s^{-1}\right)$, the *Boltzmann's* constant (k_B) is $1.380650524 \cdot 10^{-23}\,J\,K^{-1}$ and κ converts eV to J ($1\,eV = 1.6021765314E^{-19} J$ and $J = kg\,m^2 s^{-2}$) [160].

The adsorption process takes place means equation 2.49 where A_{cat} is the active area of support in m^2, pressure (P_i) is given in Pa and m is the molecule mass in kg. Although it is complicated to find the adsorption activate complex using DFT the $\triangle E$ in equation 2.48 could be the ZPE difference between the free molecule and the molecule moving on 2D.

In a multiple steps process that contains rates evolving pressure, it is recommended add the factor RT to normalize the rate units, concentration per second, assuming that one m^2 of catalyst has one m^3 of volume of gas phase, where R is the ideal gas constant $8.31447215\,J\,K^{-1} mol^{-1}$, equation 2.54.

$$r_{ads} = \frac{1}{RT}\frac{dP_i}{dt} \Rightarrow \frac{mol}{m^3\,s}\frac{m^3}{m^2} = \frac{mol}{m^2 s} \tag{2.54}$$

Contained on desorption process, the moment of inertia I is given in $kg\,m^2$.

Finally, the parameter c is added into vibrational partition function (eq. 2.53) to do the exponential adimensional as well as the parameter κ must to be added into energetic exponential $\left(e^{\left\{-\frac{E_{des}}{k_B T}\kappa\right\}}\right)$ to remove the units.

UNIVERSITAT ROVIRA I VIRGILI
MODELLING AU CATALYST FROM BULK TO NANOSCALE
Alberto Roldán Martínez
ISBN:978-84-693-7669-0/DL:T-1748-2010

Results

Chapter 3 reports the results obtained in this thesis, ordered by the space dimensionally of the subject under study and presented as in the publications derived of the present work.

First section is devoted to three-dimensional systems: the bulk. Where bulk modeling is the first step to develop following studies such as surfaces or nanoparticles.

Next section contains results about two-dimensional studied systems. It exposes published results concerning to Au surface activity towards propylene epoxidation.

Briefly, the third section reports the study of nanowires, as monodimensional systems.

The last section is devoted to zero-dimensional systems. This contains information about gold nanoparticles and its catalytic properties towards O_2 activation as a function of cluster sizes.

UNIVERSITAT ROVIRA I VIRGILI
MODELLING AU CATALYST FROM BULK TO NANOSCALE
Alberto Roldán Martínez
ISBN:978-84-693-7669-0/DL:T-1748-2010

UNIVERSITAT ROVIRA I VIRGILI
MODELLING AU CATALYST FROM BULK TO NANOSCALE
Alberto Roldán Martínez
ISBN:978-84-693-7669-0/DL:T-1748-2010

3.1 Three-dimensional systems: Bulk

"The comet is mostly empty, mostly porous. Probably all way in, there is no bulk ice. The ice is all in the form of tiny grains"

Michael A'Hearn [1]

3.1.1 Metallic bulk

Materials properties derive from its inner structure. This properties can be simulated by computational models reproducing the whole material behaviour as compressibility or conductivity.

To modelize the bulk, usually, we have to known its staking structure to develop a replicable cell. It shall be the smallest one to reduce the computational resource but large enough to have accurate results. This primitive cell is characterized by cell vectors and package system deriving interatomic distances. To obtain the optimum distance between atoms and also for cell parameters, the system has to be in a bottom of hypersurface potential energy. This point is reached modifying the cell parameter by a single point calculations, starting from the experimental value and going up and down close to it. Afterward, the total energy trend has to be minimized by equation 3.1 and represented in figure 3.1.1.

$$\left.\frac{\partial E}{\partial a}\right|_{a_0} = 0 \tag{3.1}$$

where a is the cell parameter.

The optimum cell parameter (a_0) provides the interatomic distance where atoms are in equilibrium between attractive and repulsive forces. These forces are determined by the exchange-correlation potential and hence the distance a_0 vary with the used functional.

Another parameter comparable to experimental results is the bulk modulus (B_0) that is defined as the inverse of compressibility. Therein, the bulk modulus gives information about which is the pressure to compress (or expand) the material over a differential volume. For a general point of view, matter with small bulk modulus is easily compressible.

[1] Astronomer and professor of the University of Maryland.

UNIVERSITAT ROVIRA I VIRGILI
MODELLING AU CATALYST FROM BULK TO NANOSCALE
Alberto Roldán Martínez
ISBN:978-84-693-7669-0/DL:T-1748-2010

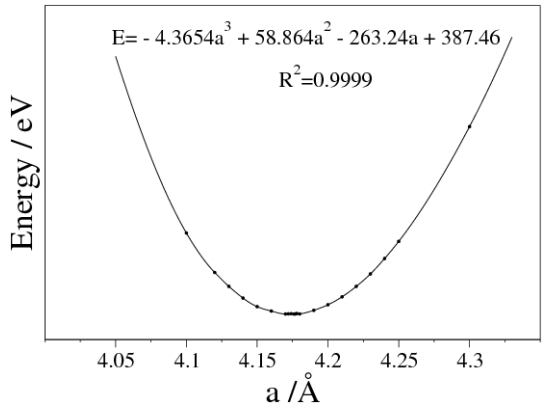

Figure 1: Total energy representation as a function of cell parameter (a) for Au bulk using GGA (PW91) as exchange-correlation functional.

Bulk modulus (B_0) is derived from pressure (P) plotted as a function of volume (V), where trend-line is used to solve the equation 3.2.

$$B_0 \equiv -\left(\frac{\partial P}{\partial LnV}\right)_T = V_0 \left.\frac{\partial P}{\partial V}\right|_{V_0} \tag{3.2}$$

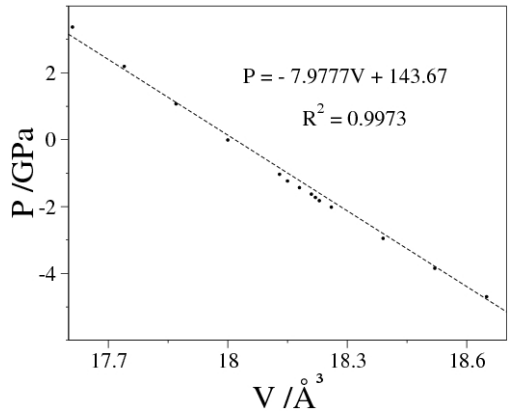

Figure 2: Pressure vs volume plot of Au bulk using functional GGA (PW91). Linear trend-line is added.

The cohesion energy (E_{coh}) property gives an idea about the energy to coalesce from the amount of atoms in gas phase without interaction among them. The cohesive energy is expressed by equation 3.3 where the bulk energy is E_{bulk}, the number of atoms into bulk cell is N and E_m is the energy of isolate atoms.

$$E_{coh} = \frac{E_{bulk} - N \cdot E_m}{N} \tag{3.3}$$

Cu, *Ag* and *Au* bulks

In this thesis, we have studied different metallic bulks with face cubic centered *(fcc)* structure : *Cu*, *Ag* and *Au*. Results are summarized in table 3.1.1 for two exchange-correlation functional: LDA and GGA with Vosko, Wilk and Nusair (VWN) and Perdew Wang 91 (PW91) approximations respectively.

Table 1: Optimized cell parameter (a_0), bulk modulus (B_0) and cohesive energy (E_{coh}) as a function of LDA (VWN) and GGA (PW91) functional.

	a_0, Å		B_0, GPa		E_{coh}, $eV/atom$	
	LDA	GGA	LDA	GGA	LDA	GGA
Cu	3.52	3.65	182	118	-4.54	-3.52
Cu_{exp}	3.61^a		142^b		-3.50^b	
Ag	4.01	4.15	108	103	-3.63	-2.56
Ag_{exp}	4.09^a		101^b		-2.96^b	
Au	4.07	4.17	194	145	-4.30	-3.06
Au_{exp}	4.07^a		220^b		-3.78^b	

^{a} Experimental values are in references [161, 162], ^{b} in [163, 164, 165].

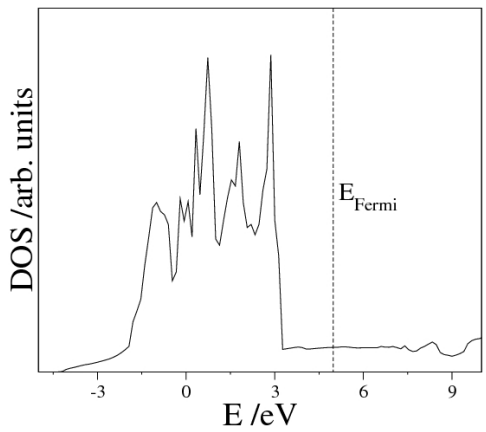

Figure 3: *Au* bulk density of states using GGA (PW91) as a V_{xc}. Dashed line shows the *Fermi* level energy, also the energy of d-band center and the density of states at *Fermi* level are indicated with an arrow and a number respectively.

Density of state (DOS) plot is useful to analize the electronic structure of the system. In the case of metals, they have a good conductivity and this property has to be expressed on DOS plot as an available states to transfer electrons from valence to conduction band without a band gap.

UNIVERSITAT ROVIRA I VIRGILI
MODELLING AU CATALYST FROM BULK TO NANOSCALE
Alberto Roldán Martínez
ISBN:978-84-693-7669-0/DL:T-1748-2010

3.2 Two-dimensional systems: Surface

"After 1980, you never heard reference to space again. Surface, the most convincing evidence of the descent into materialism, became the focus of design. Space disappeared."

Arthur C. Erickson [2]

The catalytic effectiveness of extended gold surfaces on the partial oxidation of olefins containing an allylic C–H bond is studied by means of periodic density functional calculations applied to slab models representing Au(111). Results show that the H-stripping, leading to an adsorbed allyl and OH radicals, is by far more probable than the one leading to the formation of oxametallacycle intermediates, which is the necessary step towards the partial oxidation of propylene. Our observations suggest that the failure of extended gold surfaces arises from the high sensitivity of the molecular mechanism toward changes in the basic character of adsorbed oxygen, in line with previous findings.

[2] Architect and professor in McGaugh Hall, University of California.

UNIVERSITAT ROVIRA I VIRGILI
MODELLING AU CATALYST FROM BULK TO NANOSCALE
Alberto Roldán Martínez
ISBN:978-84-693-7669-0/DL:T-1748-2010

UNIVERSITAT ROVIRA I VIRGILI
MODELLING AU CATALYST FROM BULK TO NANOSCALE
Alberto Roldán Martínez
ISBN:978-84-693-7669-0/DL:T-1748-2010

3.2.1 On the effectiveness of partial oxidation of propylene by gold: A density functional theory study

Corresponding to: Roldan, A.; Torres, D.; Ricart, J. M.; Illas, F. Journal of Molecular Catalysis A-Chemical 2009, 306, 6-10.

Introduction

Heterogeneous epoxidation of olefins, especially ethylene and propylene, continues to be an enticing subject for both scientific and practical reasons [1,2]. Although metals such as Ag, Cu or Au are capable of activating oxygen and carrying out catalytic partial oxidation, only silver is employed to produce several millions tons of ethylene oxide (EO) annually [3]. Moreover, the molecular mechanism of olefin epoxidation by Ag is well known [4–7] and also the effect of the metal surface on the selectivity has been explored [8,9]. Propylene oxide (PO) is even more valuable than EO [10–12]; however, the heterogeneously catalyzed epoxidation of propylene is a much tougher problem to solve. The industrial production of PO is based on the use of propenechlorohydrine, [13] the oxidation of propylene with organic peroxides [14,15] or the oxidation of propylene with hydrogen peroxide [16]. Recent attempts to avoid the use of organic oxidants, that produce a large amount of waste, rely on the use of Ag or Cu-based catalyst [17,18]. While the use of Ag for propylene epoxidation delivers very low selectivity over a wide range of experimental conditions and catalyst formulation [17], Cu-based catalysts have shown a better performance, reaching very large values of selectivity, at least under laboratory conditions [18]. Supported gold nanoparticles have also attracted considerable attention in epoxidation studies [19–24] due to their unusual catalytic properties [25–29]. For instance, it has been shown that Au nanoparticles supported on Ti-silicates in the presence of molecular hydrogen and oxygen produce PO with a selectivity greater than 90% at relatively low temperatures and at atmospheric pressure [19,20] and, recently, it has been found that Au nanoparticles are able to epoxide cyclohexene, cis-cyclooctene, styrene and cis-stilbene although with the help of an initiator [21]. Just last year, Turner et al. [22] have reported epoxidation of styrene by Au nanoparticles derived from Au_{55} without co-fed molecular hydrogen and without any initiator. Also early this year, Lee et al. [30] proposed a way of avoiding the use of hydrogen by means of gas mixtures involving oxygen and water.

It seems to be generally agreed that the difficulty to epoxide higher alkenes increases when allylic hydrogen atoms, which may be stripped from the molecule, are present. This elementary step is undesirable since it shuts off the epoxidation channel and results in total combustion [31]. Recently, experimental

UNIVERSITAT ROVIRA I VIRGILI
MODELLING AU CATALYST FROM BULK TO NANOSCALE
Alberto Roldán Martínez
ISBN:978-84-693-7669-0/DL:T-1748-2010

results proved that partial propylene oxidation readily occurs on an oxygen precovered Au(111) surface, although the formation of the epoxide is not the most favored [32]. The reaction pathways proposed by Deng et al. [32] lead to acrolein, through an allyloxy intermediate, or to propylene epoxide. The results suggested that small changes in the acid–base activity of adsorbed oxygen had the potential to tune the selectivity towards propylene epoxidation and that this is likely to be the case for other higher alkenes containing allylic C-H bonds.

Motivated by the work of Deng et al. [32] we carried out a systematic density functional theory based study to investigate the role of atomic oxygen chemisorbed on Au(111) as a partial oxidation agent for olefins containing allylic C-H bonds. Results show that the formation of propylene epoxide on Au(111) is highly inhibited with the route to allyl radical being by far more probable than the formation of oxametallacycle intermediates. The later is a necessary step towards partial oxidation [33,34]. Kinetic and thermodynamic arguments regarding the amphoter character of adsorbed oxygen are employed to analyze the failure of extended gold surfaces to epoxide this type of alkenes.

Computational approach

Periodic density functional (DF) calculations have been carried out to study of the molecular reaction mechanism involved in the partial oxidation of propylene on a oxygen covered Au(111) surface. The Au(111) surface is modelled by slabs containing 4 atomic layers with a full relaxation of the two outermost ones, the repeated slabs being separated by a vacuum width corresponding to 5 atomic layers. A p(3×3) supercell is employed to describe a situation with 0.11 ML coverage of both reactants, PO and adsorbed O. The DF calculations have been carried out within the usual Kohn–Sham (KS) implementation of density functional theory and using the PW91 version of the generalized gradient approximation (GGA) for the exchange-correlation potential [35]. The inner electrons have been described by the projector augmented wave (PAW) method [36] and the KS valence states expanded in a plane-waves basis set with a cut-off at 315 eV for the kinetic energy. The reciprocal space of the p(3×3) cell was described with a Monkhorst–Pack mesh with 4×4×1 k-points [37]. All minima on the potential energy surface were relaxed until calculated forces on relaxed atom are lower than 0.01 eV/Å. The optimized structures have been then refined using a higher cut-off or 415 eV and a 7×7×1 grid of k-points. The calculated adsorption energies thus obtained are within 0.05–0.07 eV larger than those obtained with the smaller cut-off. Consequently, the 315 eV value was used in the computationally expensive nudged elastic band (NEB) calculations necessary to locate the transition state structures and in the subsequent characterization by frequency analysis. Minima and TS structures were fully characterized with a pertinent vibration analysis, through diagonalization of the corresponding block of Hessian matrix obtained by numerical difference of analytical gradients, neglecting coupling with the surface phonons, and making sure that the former have only positive eigenvalues and the TS structures show a single normal mode associated with an imaginary frequency.

All calculations were carried out using the VASP code and transition state (TS) structures were located through the climbing image version of the NEB algorithm [38]. The spurious energy contribution due to the dipole arising from

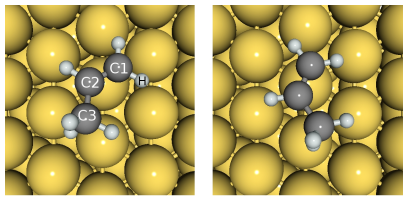

fcc-top-fcc hcp-top-hcp

Figure 1: Molecular arrangements for propylene adsorbed on Au(111). Carbon atoms in the molecule are labeled as C_1, C_2 and C_3, C_1 and C_2 being the carbon atoms involved in the double bond and H stands for the hydrogen atom of the methyl group pointing up or down. See caption of Table 1 for more details.

Table 1: Adsorption energy (E_{ads} in eV) and relevant geometric parameters (z in Å and α in degrees) for propylene adsorbed on the clean Au(111) surface. Adsorption energies are given with respect to gas phase molecule and the clean surface. The calculated geometry of the gas phase propylene is given for comparison. The name for the different adsorption arrangements stands for the adsorption sites of the carbon atoms (*fcc*, *top* or *hcp*) in propylene and the pointing direction of the methyl group (down toward the surface or up to the vacuum).

Arrangement	E_{ads}	$z(C_1)$	$z(C_2)$	$d(C_1-C_2)$	$\alpha(H-C_1-C_2-C_3)$
fcc-top-fcc up	-0.04	3.100	3.414	1.346	0.7
fcc-top-fcc down	-0.05	2.955	3.220	1.348	1.1
hcp-top-hcp up	-0.03	3.115	3.402	1.345	0.2
hcp-top-hcp down	-0.04	3.029	3.351	1.346	0.5
Gas phase C_3H_6	-	-	-	1.335	0.1

the adsorption of reactants in one of the surfaces was removed using the standard dipole correction [39].

Results and discussion

Firstly, we consider the adsorption of propylene on the clean Au(111) surface. The molecule adsorbs via a di-bonded conformation, parallel to the surface. Although a systematic exploration of the different adsorption modes was carried out, we only report here four configurations corresponding to two arrangements for propylene on the surface (*fcc–top–fcc* and *hcp–top–hcp*). For each of these two arrangements, two different conformations have been considered for the methyl group pointing either toward down the surface or up to the vacuum. Two of the four different adsorption modes are shown in Fig. 1 and the geometry and adsorption energies are summarized in Table 1. For all arrangements considered, the unsaturated C_1-C_2 bond lies nearly parallel to the surface, being the average height of the molecule ∼3.1 Å. Two geometric parameters were employed to characterize the degree of distortion of the adsorbed molecule. While the C_1-C_2 distance is directly related to the activation of the double bond, the (H-C_1-C_2-C_3) dihedral angle informs about the loss of planarity of the molecule. The average value for the C_1-C_2 distance is ∼1.3 Å, being almost equal to the corresponding for free propylene. In a similar way, the (H-C_1-C_2-C_3) dihedral angle for the adsorbed propylene is similar to that of the free molecule and also remains unchanged for the different arrangements considered. Values for adsorption en-

ergies correspond to a weak adsorption. Here, it is important to point out the adsorption energies discussed above are not described to the desired accuracy because of the limitations of the PW91 (and in general of DFT methods) to describe weak interactions. The accurate description of propylene adsorption on the clean Au(111) is, of course, a problem. However, the main goal of the present work is to analyze the changes induced by co-adsorbed atomic oxygen. This means comparing adsorption energies with and without co-adsorbed O and the resulting relative energies are much less affected by the GGA inherent errors (see Refs. [40–43] and references therein) and, hence, the present study provides meaningful results.

The adsorption of atomic oxygen on Au(111) has been the subject of previous work and therefore [44], we will now consider the interaction of propylene with the oxygen covered gold surface. We analyzed a broad set of co-adsorption arrangements, shown in Fig. 2, in which oxygen was located on the most stable threefold hcp hollow site and the propylene molecule close enough so that the two adsorbates can react. Situations with atomic oxygen far from the alkene may also stabilize this species but further reaction will require oxygen diffusion above the surface, this is the step not considered in the present work. Geometric parameters as well as adsorption energies are shown in Table 2 where results in parenthesis correspond to those obtained with more stringent numerical thresholds (see above). The presence of propylene on the surface slightly modifies the geometric properties of oxygen, with a small increase in the perpendicular distance to the surface. The adsorption properties of propylene are also modified by the presence of co-adsorbed oxygen. The adsorption energy of propylene is increased by $\sim$0.1 eV although the geometry of the molecule suffers minor changes only. From the data in Table 2, one can also conclude that the difference in adsorption energy between conformations of propylene with hydrogen pointing down or away from the surface is small, even in the presence of adsorbed oxygen.

Once propylene and atomic oxygen are both adsorbed on Au(111) and close enough, they can undergo different reaction pathways, leading either to the dehydrogenation of the hydrocarbon or to the formation of oxametallacycle-type intermediates (OMMP) [31,5,4]. From configuration I-Down (see caption of Figs. 1 and 2 for details), a search for the minimum-energy path leads to the stripping of hydrogen atoms to yield allyl and hydroxyl radicals, whereas configurations II, III, and IV (Fig. 2) have been found to lead to the formation of OMMP intermediates (see Fig. 1 for atomic labels). There are two possible structures for the OMMP intermediate. The first one, hereafter referred to as OMMP1, is linked to the surface through C_2, while C_1 is bounded to oxygen; reducing the distance between C_2 and O will lead to the TS towards PO (see Fig. 3 for details). The second intermediate (OMMP2) is linked to gold through C_1 and with C_2 bounded to oxygen and, eventually can evolve to PO. Following previous work [31], we will refer to the first step in the energy profile of Fig. 4 leading to these type of intermediates from the adsorbed reactants as primary chemistry of the propylene partial oxidation mechanism. In a similar way, we define the secondary chemistry as the steps involving evolution from the OMMP1 intermediates to either propanal or propylene oxide. The secondary chemistry has not been considered here since previous work involving Cu(111) and Ag(111)

UNIVERSITAT ROVIRA I VIRGILI
MODELLING AU CATALYST FROM BULK TO NANOSCALE
Alberto Roldán Martínez
ISBN:978-84-693-7669-0/DL:T-1748-2010

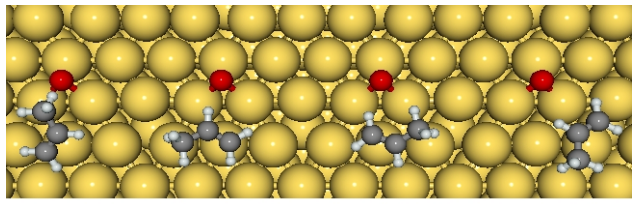

Figure 2: Molecular arrangements for co-adsorbed propylene and atomic oxygen on Au(111). Four arrangements were considered and for each one, two conformations of the methyl group were tested. See caption of Fig. 1 for further details.

Table 2: Adsorption energy (E_{ads} in eV) and relevant geometric parameters (z in Å and α in degrees) for co-adsorbed propylene and O on Au(111). Adsorption energies are given with respect to gas phase propylene molecule and the oxygenated surface; values in parenthesis correspond to calculations with a cut-off of 415 eV a 7×7×1 grid of k-points.

Arrangement	E_{ads}	z(C_1)	z(C_2)	d($C_1 - C_2$)	$\alpha(H - C_1 - C_2 - C_3)$
I-up	-0.11 (-0.18)	2.932	3.299	1.352	1.5
I-down	-0.13 (-0.18)	2.836	3.241	1.353	1.5
II-up	-0.15 (-0.20)	2.757	3.076	1.356	2.2
II-down	-0.15 (-0.20)	2.929	3.251	1.351	2.3
III-up	-0.13 (-0.19)	2.724	3.053	1.356	0.4
III-down	-0.14 (-0.19)	2.720	3.029	1.537	0.3
IV-up	-0.05 (-0.10)	3.308	3.542	1.343	0.4
IV-down	-0.04 (-0.10)	3.319	3.543	1.343	0.0

shows that the main difference between ethene and propene epoxidation lies precisely in the primary chemistry [4,31].

The minimum-energy path for the formation of OMMP1 corresponds to a rotation of the double bond through an axis perpendicular to the surface placed on the C_2 atom. The formation of this intermediate implies the creation of two new bonds: one between C_1 and adsorbed O and a second one between C_2 and a gold surface atom. The C_1-C_2 distance elongates from 1.357 to 1.518 Å, with an intermediate value of 1.353 Å at the TS (Fig. 5). The other relevant change involves the C_2-Au distance, which changes from 3.029 Å in the initial state to 2.759 Å in the TS state and to 2.489 Å in the OMMP1. The energy barrier for this reaction (E_{TS} OMMP1) is 0.52 eV, and the intermediate lays 0.95 eV below the energy of adsorbed reactants. Energy barriers and additional geometrical parameters for the TS involved in this reaction path are given in Table 3. In a very similar way, the formation of OMMP2 implies the same molecular movement, but in this case the intermediate is bounded to oxygen through C_2 and to the gold surface though C_1. The C_2-O distance changes from 3.317 to 1.428 Å, with an intermediate value of 2.366 Å at the TS and the C_1-Au distance changes from 3.442 Å in the initial state to 2.295 Å in the TS state and to 3.071 Å in the OMMP2. The energy barrier for this reaction is 0.78 eV, significantly larger than the one leading to OMMP1 from the same reactants, and the intermediate lays 0.70 eV below the energy of adsorbed reactants.

The large difference between the en-

UNIVERSITAT ROVIRA I VIRGILI
MODELLING AU CATALYST FROM BULK TO NANOSCALE
Alberto Roldán Martínez
ISBN:978-84-693-7669-0/DL:T-1748-2010

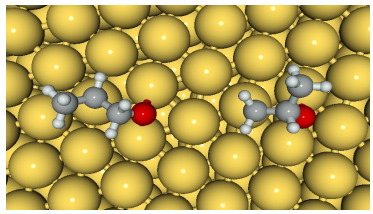

Figure 3: The two different OMMP intermediates, OMMP1 (left) and OMMP2 (right), involved in the primary chemistry of propylene partial oxidation on Au(111).

Table 3: Structure (z and d in Å) and energy barriers (E_{TS} in eV) for transition states involved in the primary chemistry of propylene epoxidation on Au(111). d(C–O) stands for the distance between C_1 and C_2 with O, for the TS toward OMMP1 and OMMP2, respectively.

TS	$\triangle E^{TS}$	z(C_{12})	z(O)	d($C-O$)	d($H-O$)
To OMMP1	0.52	2.759	1.403	2.552	-
To OMMP2	0.78	3.379	1.513	2.366	-
To allyl	0.20	3.361	1.732	-	0.990

ergy barrier for the formation of OMMP1 and OMMP2 implies that OMMP2 can only be formed in the reverse reaction from propylene epoxide product adsorption and not as the result of a direct reaction between propylene and oxygen, as previously found for different metals [9,31]. Interestingly enough, hydrogen stripping to yield adsorbed hydroxyl and allyl species is associated with a small energy barrier (E_{TS} Allyl) of 0.20 eV and the minimum-energy path is associated with a proton transfer from propylene to oxygen. The H-O distance reduces from 2.155 to 0.978 Å, with an intermediate value of 0.990 Å at the TS and the intermediate lays 0.33 eV below the energy of adsorbed reactants. Hence, the experimentally predicted inefficiency of extended gold surfaces [32] for the selective oxidation of propylene is due to the low energy barrier for the hydrogen stripping. Note that the energy difference in the barriers leading to OMMP1 and the allylic radical is so large that including or not the zero point vibration energies is irrelevant.

The present results together to those corresponding to previous work [31] involving propylene epoxidation on Cu(111) and Ag(111) allows us to further investigate the effect of the type of metal surface. In Fig. 6 we plot the calculated values of the reaction energy towards OMMP1 and towards allyl; E_R OMMP1 and E_R Allyl, respectively versus the corresponding energy barriers, E_{TS} OMMP1 and E_{TS} Allyl values. Despite the fact that three points are not enough to extract firm conclusions it is clear that Fig. 6 shows a linear trend indicating that the Brönsted–Evans–Polanyi relationship approximately holds. In order to find the origin of these relationship we remind that the difference in selectivity towards PO of silver and copper surfaces was recently attributed to the different acid–base character of the adsorbed oxygen atom [31]. In the following, we will analyze with more detail the acid–base properties of oxygen adsorbed on coinage metals surfaces and the implications on the primary chemistry of the partial oxidation mechanism and will show that this is indeed directly related to the

UNIVERSITAT ROVIRA I VIRGILI
MODELLING AU CATALYST FROM BULK TO NANOSCALE
Alberto Roldán Martínez
ISBN:978-84-693-7669-0/DL:T-1748-2010

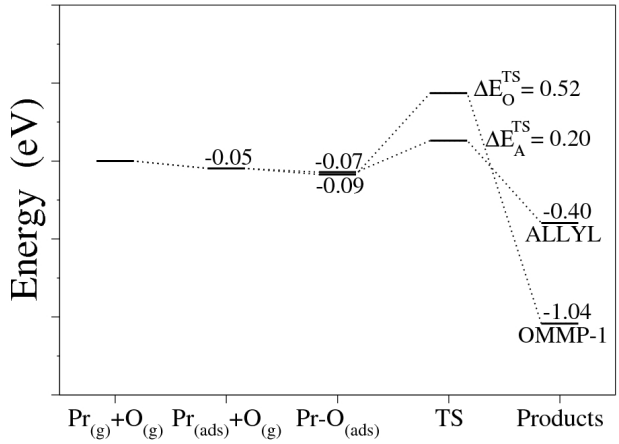

Figure 4: Reaction profile involved in the primary chemistry for propylene partial oxidation on Au(111). The zero energy was taken as the sum of the energies of the surface slab model, gas phase propylene and one half of the gas phase molecular oxygen. Pr +O stands for propylene at infinite distance from the surface having adsorbed atomic oxygen, Pr–O for the situation where the molecule and atomic oxygen are co-adsorbed and OMMP stands for the OMMP1 intermediate.

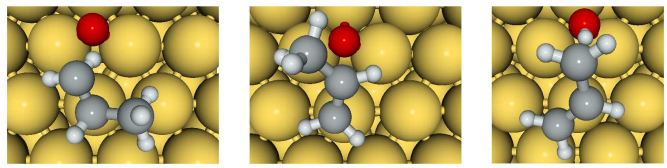

Figure 5: Schematic representations of transition state structures involved in the mechanism. From right to left: TS involved in the formation of OMMP1, OMMP2 and allylic compound.

Brönsted–Evans–Polanyi relationship described above. Let us first consider the formation of the allylic compound. In this reaction step, adsorbed oxygen acts as a Brönsted base, stripping the acidic hydrogen of propylene. Differently, on the reaction step leading to the formation of the OMMP intermediates, oxygen acts as a Lewis acid, receiving electronic density from the double bond of propylene [45].

Therefore, it is the amphoteric character of adsorbed oxygen that rules the competing chemistry toward propylene oxide. We can roughly estimate the acid–base constants in a natural logarithmic scale, PK_b or PK_a, associated to each reaction step, using the Transition State Theory – including only the vibrational degrees of freedom in the necessary partition functions – for the direct and reverse reactions and assuming equilibrium conditions. The corresponding expressions for the acid (OMMP1 formation) and basic (Allyl formations) were obtained by means of the van't Hoff equation as in Eq. (1) and Eq. (2), respectively

$$PK_a = -LnK_a = \frac{\triangle G_R^{OMMP1}}{k_B T} \qquad (1)$$

$$PK_b = \frac{\triangle G_R^{Allyl}}{k_B T} \quad (2)$$

where k_B and T are the Boltzmann constant and the temperature respectively and $\triangle G_R$ stands for the Gibbs free energy of each reaction for the initial (propylene co-adsorbed with oxygen) and final state (OMMP1 or OH plus allyl) involved in the reaction. We can directly relate the Gibbs free energy values with reaction energies (E_R) as in Eq. (3), by neglecting volume and entropic contributions to the Gibbs free energy

$$\triangle G_R = \triangle H_R - T\triangle S_R \approx E_R + E_{R,vib} \quad (3)$$

Regarding Eqs. (1) and (3), and neglecting the vibration contributions to reactions energies ($E_{R,Vib}$), PK values are directly associated with the reaction energies of the competing reaction steps and thus are at the origin of the Brönsted–Evans–Polanyi relationship in Fig. 6 (solid line). In fact, Eqs. (1) and (2) allow us to include an additional PK scale in Fig. 6. For simplicity, we scaled the PK values of Au and Ag with respect to that of Cu as in Eq (4), neglecting also the vibration contribution to $\triangle$PK,

$$\triangle PK_b = \frac{E_R^{Allyl} - E_{R,Cu}^{Allyl}}{k_B T} \quad (4)$$

We find that going from Cu to Au, the amphoteric character of oxygen is drastically changed, being the competing reaction pathways leading to OMMP1 and also to allyl plus OH more exothermic but with different change in the acid and basic character so that O on Au(111) becomes the case with highest basic character. Thus, it is confirmed that the selectivity, driven by the two competing pathways, is related to the acidic–basic character of oxygen: large PK values imply low energy barriers for the OMMP1 and allyl plus OH formation. But the kinetic barriers for each competing pathway have different sensitivity to changes in reaction energy and thus to PK values: a large decrease (∼0.4 eV) is produced in E_{TS} Allyl when going from Cu to Au, while the change in E_{TS} OMMP1 is very small (∼0.1 eV). Hence, the pathway leading to allyl plus OH is much more sensitive to changes on the basic character of adsorbed oxygen than the pathway to OMMP1 is to changes on the oxygen acidic character. According to these results, it is mainly the basic character of oxygen that rules the selective oxidation of propylene on extended gold surface, thus extending and confirming previous findings for the propylene epoxidation reaction on Cu(111) and Ag(111). We have also considered the effect of including vibration contribution to the PK values (Fig. 6, dashed line). We found that, although the PK values for Ag and Au are slightly shifted with respect to Cu, the general trends in Fig. 6 are maintained.

Conclusions

We investigated the effectiveness of extended gold surfaces on the partial oxidation of olefins containing an allylic C-H bond by means of periodic density functional theory based calculations. The analysis of the possible reaction pathways shows that Au(111) surface is inefficient for the selective oxidation of propylene evenwhen pre-covered by atomic oxygen. Results show that the necessary formation of oxametallacycle reaction intermediates on Au is thermodynamically favored but kinetically inhibited. The route for the H-stripping, leading to an adsorbed allyl radical plus adsorbed OH is much more kinetically favored than

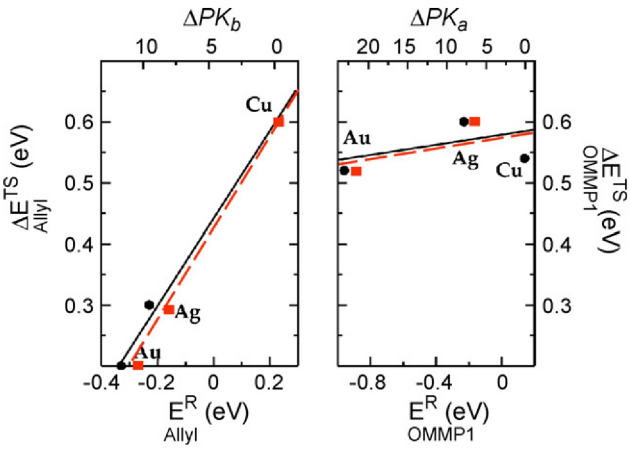

Figure 6: Change in kinetic barriers for the OMMP1 and Allyl formation (E_{TS} OMMP1 and E_{TS} Allyl, respectively) with respect to reaction energy (E_R) for Cu, Ag and Au. The reaction energy values have been translated into a PK scale at 500K. Dashed line includes vibration contributions to the reaction energy, while solid line does not. Lines are included guiding the eye.

the one leading to different oxametallacycle intermediates. Changes on reactivity toward the competing products have been related to changes in the amphoteric character of oxygen and comparison to previous results for the Cu(111) and Ag(111) surface confirms this hypothesis. Our observations strongly suggest that the failure of extended gold surfaces to epoxidize higher alkenes arises from the high sensitivity of the molecular mechanism toward changes in the basic character of adsorbed oxygen.

Acknowledgements

Financial support has been provided by the Spanish Ministerio de Ciencia e Innovación (Projects CTQ2005-08459-CO2-01, CTQ2005-08459-CO2-02 and UNBA05-33-001) and, in part, by Generalitat de Catalunya (Projects 2005SGR-00697, 2005SGR-00104 and 2005 PEIR 0051/69). Part of the computer time was provided by the Centre de Supercomputació de Catalunya, CESCA, and more extensively by the Barcelona Supercomputing Centre, BSC. D.T. acknowledges support by the Generalitat de Catalunya under Grant No. 2006 BP-A 10128 and A.R. thanks the Universitat Rovira i Virgili for the predoctoral fellowship.

References

[1] R.M. Lambert, F.J. Williams, R.L. Cropley, A. Palermo, J. Mol. Catal. A: Chem. 228 (2005) 27.

[2] P. Christopher, S. Linic, J. Am. Chem. Soc. 30 (2008) 11264.

[3] J.G. Serafin, A.C. Liu, S.R. Seyedmonir, J. Mol. Catal. 131 (1998) 157.

[4] S. Linic, M.A. Barteau, J. Am. Chem. Soc. 124 (2002) 310.

[5] S. Linic, M.A. Barteau, J. Am. Chem. Soc. 125 (2003) 4034.

[6] M.L. Bocquet, P. Sautet, J. Cerda, C.I. Carlisle, M. Webb, D.A. King, J. Am. Chem. Soc. 125 (2003) 3119.

[7] M.L. Bocquet, D. Loffreda, J. Am. Chem. Soc. 127 (2005) 17207.

[8] D. Torres, N. Lopez, F. Illas, R.M. Lambert, J. Am. Chem. Soc. 127 (2005) 10774.

[9] D. Torres, F. Illas, J. Phys. Chem. B 110 (2006) 13310.

[10] D.J. Darensbourg, M.W. Holtcamp, Coord. Chem. Rev. 153 (1996) 155.

[11] P. Jannasch, Polymer 41 (2000) 6701.

[12] J. Darensbourg, M.S. Zimmer, Macromolecule 32 (1999) 2137.

[13] S.J. Ainsworth, Chem. Eng. News 2 (1992) 9.

UNIVERSITAT ROVIRA I VIRGILI
MODELLING AU CATALYST FROM BULK TO NANOSCALE
Alberto Roldán Martínez
ISBN:978-84-693-7669-0/DL:T-1748-2010

[14] R.O. Kirk, T.J.Dempsey, M. Grayson, D. Eckroth, H.F.Mark, D.F. Othmer, C.G. Overberger, G.T. Seaborg (Eds.), Kirk-Othmer Encyclopedia of Chemical Technology, vol. 19,Wiley, New York, 1982, p. 246.

[15] H.P.Wulff, F.Wattimenu, US Patent 4021 (1977) 454.

[16] G.F. Thiele, E. Roland, J. Mol. Catal. A: Chem. 117 (1997) 351.

[17] M. Akimoto, K. Ichikawa, E. Echigoya, J. Catal. 76 (1982) 333.

[18] R.L. Cropley, F.J. Williams, O.P.H. Vaughan, A.J. Urquhart, M.S. Tikhov, R.M. Lambert, Surf. Sci. 578 (2005) L85.

[19] T. Hayashi, K. Tanaka, M. Haruta, J. Catal. 178 (1998) 566.

[20] B.S. Uphade, S. Tsubota, T. Hayashi, M. Haruta, Chem. Lett. 27 (1998) 1277.

[21] M.D. Hughes, Y.J. Xu, P. Jenkins, P. McMorn, P. Landon, D.I. Enache, A.F. Carley, G.A. Attard, G.J. Hutchings, F. King, E.H. Stitt, P. Johnston, K. Griffin, C.J. Kiely, Nature 437 (2006) 1132.

[22] M. Turner, V.B. Golovko, O.P.H. Vaughan, P. Abdulkin, A. Berenguer-Murcia, M.S. Tikhov, B.F.G. Johnson, R.M. Lambert, Nature 454 (2008) 981.

[23] H. Kobayashi, Y. Shimodaira, J. Mol. Struct. (THEOCHEM) 762 (2006) 57.

[24] A.M. Joshi,W.N. Delgass, K.T. Thomson, J. Phys. Chem. B 110 (2006) 2572.

[25] M. Haruta, Catal. Today 36 (1997) 153.

[26] M. Haruta, Nature 437 (2005) 55.

[27] M. Valden, X. Lai, D.W. Goodman, Science 281 (1997) 1647.

[28] A.S.K. Hashmi, G.J. Hutchings, Angew. Chem. Int. Ed. 45 (2006) 7895.

[29] See also the reviews in the special issue dedicated to chemistry of nano-gold in Chem. Soc. Rev. (2008) 37.

[30] S. Lee, L.M. Molina, M.J. Lopez, J.A. Alonso, B. Hammer, B. Lee, S. Seifert, R.E. Winans, J.W. Elam,M.J. Pellin, S. Vajda, Angew Chem, Int Ed 48 (2009) 1467-1471.

[31] D. Torres, N. Lopez, F. Illas, R.M. Lambert, Angew. Chem. Int. Ed. 46 (2007) 2055.

[32] X. Deng, B.K. Min, X. Liu, C.M. Friend, J. Phys. Chem. B 110 (2006) 15982.

[33] A. Klust, R.J. Madix, Surf. Sci. 600 (2006) 5025.

[34] M.A. Barteau, Surf. Sci. 600 (2006) 5021.

[35] J.P. Perdew, J.A. Chevary, S.H. Vosko, K.A. Jackson, M.R. Pederson, D.J. Singh, C. Fiolhaiset, Phys. Rev. B 46 (1992) 6671.

[36] P.E. Bloch, Phys. Rev. B 50 (1994) 17953.

[37] H.J. Monkhorst, J.D. Pack, Phys. Rev. B 13 (1976) 5188.

[38] G. Henkelman, B.P. Uberuaga, H. Jonsson, J. Chem. Phys. 113 (2000) 9901.

[39] G. Kresse, J. Furthmuller, Comput. Mater. Sci. 6 (1996) 15.

[40] C.H. Christensen, J.K. Nørskov, J. Chem. Phys. 128 (2008) 182503.

[41] K. Honkala, A. Hellman, I.N. Remediakis, A. Logadottir, A. Carlsson, S. Dahl, C.H. Christensen, J.K. Nørskov, Science 307 (2005) 555.

[42] P. Strasser, Q. Fan, M. Devenney, W.H. Weinberg, P. Liu, J.K. Nørskov, J. Phys. Chem. B 107 (2003) 11013.

[43] B. Hammer, L.B. Hansen, J.K. Nørskov, Phys. Rev. B 59 (1999) 7413.

[44] D. Torres, K.M. Neyman, F. Illas, Chem. Phys. Lett. 429 (2006) 86.

[45] K.P. Volhard, N.E. Schore, Organic Chemistry, Freeman, San Francisco, CA, 1999.

UNIVERSITAT ROVIRA I VIRGILI
MODELLING AU CATALYST FROM BULK TO NANOSCALE
Alberto Roldán Martínez
ISBN:978-84-693-7669-0/DL:T-1748-2010

3.3 One-dimensional systems: Nanowire

"Galaxies and crystals, for example, arise spontaneously by self-assembly; that is, they create themselves unaided from a disordered or featureless initial state."

Paul Davies [3]

The self-assembling of Au nanoparticles to nanowires of different structure has been investigated by means of a periodic approach within density functional theory using an Au_{79} nanoparticle as a building block. The density functional calculations show that the interaction of the Au nanoparticles takes place preferentially along the [111] direction, in agreement with the experimental. The electronic structure of the different Au nanowires studied is found to be intermediate between that of the isolated nanoparticle and that of the bulk metal. This is perhaps not surprising but has important consequences for the chemistry of such nanostructures. Finally, calculations carried out for nanowires built from Cu, Ag and Au nanoparticles containing 38 atoms reveal that the self-assembling mechanism is general but that the strength of the interaction is dictated by the chemical nature of the metal with Au being the coinage metal leading to stronger interaction between the nanoparticles.

[3] Professor at Arizona State University.

UNIVERSITAT ROVIRA I VIRGILI
MODELLING AU CATALYST FROM BULK TO NANOSCALE
Alberto Roldán Martínez
ISBN:978-84-693-7669-0/DL:T-1748-2010

UNIVERSITAT ROVIRA I VIRGILI
MODELLING AU CATALYST FROM BULK TO NANOSCALE
Alberto Roldán Martínez
ISBN:978-84-693-7669-0/DL:T-1748-2010

3.3.1 Growth and properties of Au nanowires

Corresponding to: Roldán, A.; Ricart, J. M.; Illas, F. Molecular Simulation 2009, 35, 1051-1056.

Introduction

The study of materials at the nanoscale is believed to open new fascinating applications and technology and it is generally motivated by the change in physical and chemical properties of these systems compared to their bulk counterpart [1]. For instance, by proper understanding of chemical processes taking place at the nanoscale it is possible to produce crystals with the desired shape and crystalline structure, as recently shown by Yang et al. [2] in the case of titanium dioxide (TiO_2), a compound largely used in heterogeneous catalysis. These authors were able to synthesise anatase nanoparticles with a large percentage of reactive facets. A particularly interesting form of nanostructure is the one that is composed of one dimensional (1D) chains, carbon nanotubes being probably the best known example [3,4] with practical applications already at hand [5]. These 1D nanostructures provide important building blocks for bottom-up approaches because of the multitude of interesting properties that they exhibit, such as their large anisotropy, which makes them ideal candidates for many applications, such as biosensors, logic circuits, fieldeffect transistors and non-volatile memory elements [6–10]. The discovery of carbon nanotubes had a tremendous impact on the field with new materials being discovered almost weekly. Many of the known 1D nanostructures involve semiconducting materials such as oxides [11] or phosphides [12] but metals have also attracted attention. In particular, noble metals such as Au have been the focus of intense research since they possess a lattice configuration comprising a single element, with a simple face-centred cubic (*fcc*) crystalline structure. Also Au nanowires promise applications in nanoelectronics, biomedicine, sensing and catalysis [13,14], especially after the discovery of quantum conductance through individual rows of suspended gold atoms [15]. The Au nanowires and other nanostructures [16–20] with special features such as conductance [21,22] and transport properties [23,24] have been reported and have also been the focus of several theoretical studies [17,25–33].

The synthesis of 1D Au nanostructures without the help of ex situ techniques, such as chemical etching, is desirable not only for fundamental research purposes but also for future nanodevice design and fabrication. For instance, it is likely that Au nanowires will be obtained through a self-assembly oriented attachment growth of suitable nanoparticles. This follows from the fact that nanoparticles may have a large surface-

UNIVERSITAT ROVIRA I VIRGILI
MODELLING AU CATALYST FROM BULK TO NANOSCALE
Alberto Roldán Martínez
ISBN:978-84-693-7669-0/DL:T-1748-2010

to-volume ratio and self-assembling reduces the surface energy thus stabilising the system [6]. Nevertheless, a precise knowledge of the formation mechanism at a microscopic level cannot be achieved easily without the help of theoretical analysis. Recently, the mechanism of Pd nanowires growth by a self-assembling process of nanoparticles of different size has been reported [34]. In the present paper we extend the previous work to study structural and several relevant properties of 1D Au nanostructures built from Au_{79} building block, a cubo-octahedral nanoparticle of 1.5 nm width exhibiting (111) and (100) facets. In particular, we report results for the self-assembly mechanism of Au nanowires grown by interconnecting Au_{79} particles either through the (111) or (100) facets.

Computational approach

The Au nanowires have been studied using the strategy described in a previous work concerning the self-assembling mechanism of Pd nanoparticles [34]. This makes use of the advantages of periodic approaches which allow one to model single molecules, clusters or periodic structures. Single particles have been modelled by placing them into a large enough supercell, with a vacuum space of 1nm in all directions to avoid interactions between species in the neighbouring cells. Nanowires are modelled simply by reducing one of the three directions of the supercell while maintaining the vacuum width in the other two directions. The result is an infinite series on non-interacting nanowires all built from the same structure. This array of infinite nanowires is, of course, an artificial construct resulting from the 3D imposed in the calculation which in turn is a necessary requirement when using a plane wave basis set, which span the whole space with the periodicity imposed by the unit cell chosen. This requirement can be removed by making use of a localised basis set, although this is likely to introduce other problems due to the need to use large basis sets. The use of periodic symmetry also imposes the need to handle the necessary numerical integrations in the reciprocal space. However, the supercells used are sufficiently large to allow one to obtain meaningful results by considering the Γ-point only. The building blocks used to construct the nanowires are compact nanoparticles cut from the *fcc* metal bulk containing 79 atoms. These structures, exhibiting low index planes, provided initial geometries for subsequent geometry optimisation [35–40]. For convenience, the centre of each particle has been placed at the unit cell centre.

The energy of the isolated particles and of the resulting nanowires has been obtained from density functional theory (DFT) based calculations using a plane wave basis set. The optimum structures have been obtained from total energy minimisation. The geometry optimisation and most of the calculations were carried out using the local density approach (LDA) form of the Voskow, Wilk and Nusair exchange-correlation potential [41], and the final energy obtained from a single point calculation using the Perdew–Wang (PW91) [42] implementation of the generalised gradient approach (GGA) to the exchange-correlation potential. For metals, this methodology provides structural results closer to the experiment and has been used extensively for determination of structural properties [38–40]. The effect of core electrons on the valence electron density was described by projector augmented wave (PAW) method [43,44], and the cut-off for the kinetic energy of the plane-wave basis set has been set to 315 eV which has been shown to be sufficient for the

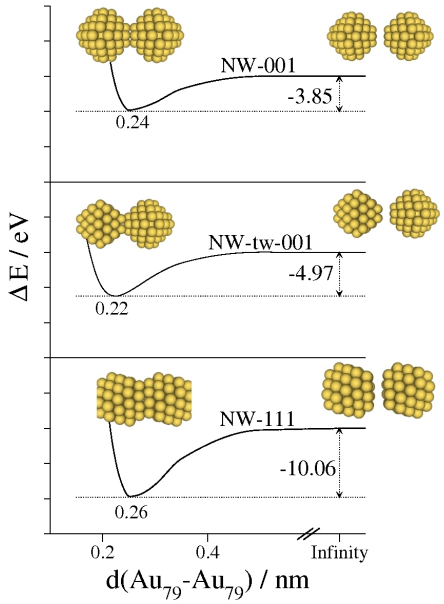

Figure 1: Potential energy curve for the interaction of an infinite chain of Au_{79} nanoparticles as a function of the d(Au_{79}–Au_{79}) distance, the minimum in the curve corresponds to the stable NW-100, NW-tw-100 and NW-111 (see text) nanowire formed. Numbers near arrows stand for the energy difference between optimised nanowires and isolates particles obtained at the GGA//LDA level.

present purposes. A Gaussian smearing technique, with a 0.2 eV width, has been applied to enhance convergence but all energies presented below have been obtained by extrapolating to zero smearing (0 K). All minima on the potential energy surfaces were determined by relaxing the structure until self-consistent forces are lower than 0.01 eV/Å . In the optimisation geometry calculations all atoms were allowed to relax without imposing any constraint. This is at variance with the previous work where some calculations were carried out by fixing the atoms in the particle core and relaxing only those in the interacting facets [34]. All calculations have been carried out using the VASP code [44–46].

Results and discussion

The different nanostructures that can be formed by self-assembling nanoparticles are dictated by the possible surface connections between the nanoparticles. The nanoparticles described in the previous section expose only (111) or (111) and (001) facets depending on whether their shape is octahedral or cubo-octahedral. Consequently, the resulting superstructure, or in this case the resulting nanowire, grows along the [001] or [111] directions. In the first case, the particles assemble through the (001) particle facet [34] and, in the second case, the particles interact through (111) surfaces. From the existing literature concerning gold nanowires there are indications that the nanowire grows preferentially along the [111] direction [6,16,17]. In order to confirm this hypothesis, we study nanowires made by merging nanoparticles so as to contact their (001) facets either in a parallel way [34] or twisting one of the particles 45º along the axis perpendicular to (001) or

UNIVERSITAT ROVIRA I VIRGILI
MODELLING AU CATALYST FROM BULK TO NANOSCALE
Alberto Roldán Martínez
ISBN:978-84-693-7669-0/DL:T-1748-2010

by merging two parallel (111) facets. The resulting nanowires are labelled as NW-001, NW-tw-001 and NW-111, respectively (Figure 1). Note that in the case of the NW-tw-001 nanowire there are two Au_{79} nanoparticles in the unit cell.

The interaction between Au_{79} nanoparticles leads to nanowires with a diameter of the order of 1.5 nm which are similar to those obtained in experiments where the Au nanowires are grown in organic media [16]. This interaction is always attractive with a minimum in the total LDA energy with respect to the interparticle Au_n-Au_n separation. The equilibrium distance appears at distances between 0.22 and 0.26 nm depending on the type of nanowire (Figure 1). This is within the LDA interlayer distance of 0.25 nm meaning that the particles are in quite close contact. This is also in agreement with experimental results for the distance between atomic layers of a single crystalline nanowire grown in organic media along the [111] direction. These nanowires have a diameter of the order of 1.6–2 nm and the interatomic distances estimated from the transmission electron miscroscopy (TEM) images is of the order of 0.23 nm [16,17]. This is not surprising, since it is well-known that GGA tends to overestimate intermetallic distances whereas LDA (VWN) reproduces the Au–Au distance surprisingly well [38]. Conversely, LDA is known to severely overestimate the interaction energies because of the self-interaction problem. This is, in part, rectified by the GGA functionals. Hence, we have estimated the interaction energies from single point PW91 calculations at the LDA optimised structure [38]: this is indicated as GGA//LDA. The energy gain in forming the NW-001 nanowire is of 3.85 eV per Au_{79} unit. For the NW-tw-001 nanowire the interaction is considerably stronger by 4.97 eV per Au_{79} unit as it could be anticipated from the shorter equilibrium distance between the interacting units (0.22 nm). Finally, for the NW-111 nanowire, which links the (111) surfaces of the interacting nanoparticles, the calculated interaction energy is still larger reaching a value of 10.06 eV per Au_{79} unit. The stabilisation energy arises from the increase in the atomic coordination or, alternatively, from the loss of atoms with low-coordination number. This energy may be distributed between the atoms in contact. For the NW-tw-001 nanowire, there are four atoms interacting per side but since the particle is also interacting with one particle per side the stabilisation comes from four atoms per particle. For the NW-tw-001, this leads to a stabilisation of 1.26 eV per contact atom. For the NW-111 nanowire one has 12 atoms in contact and the stabilisation energy per atom is now 0.84 eV per contact atom. The lower value for the interaction energy per contact atom in the NW-111 is easy to understand. Here, the surfaces in contact are the (111) which are the most stable ones and involve atoms with larger coordination number which favour the [111] direction of growth. Note that from the stabilisation energy per contact atom only one would tend to think that the nanowire will grow through the (100) facets. However, proper consideration of the number of interacting atoms in each facet clearly shows that growth through the [111] direction is preferred. Moreover, the fact that the interaction through (111) facets is considerably larger than the one through (100) surfaces is in agreement with experimental evidence that the growth of Au nanowires takes place preferentially along the [111] direction.

Next, we comment on the electronic structure of the Au nanowires as emerging from the density of states (DOS) plots. These are carried out at the

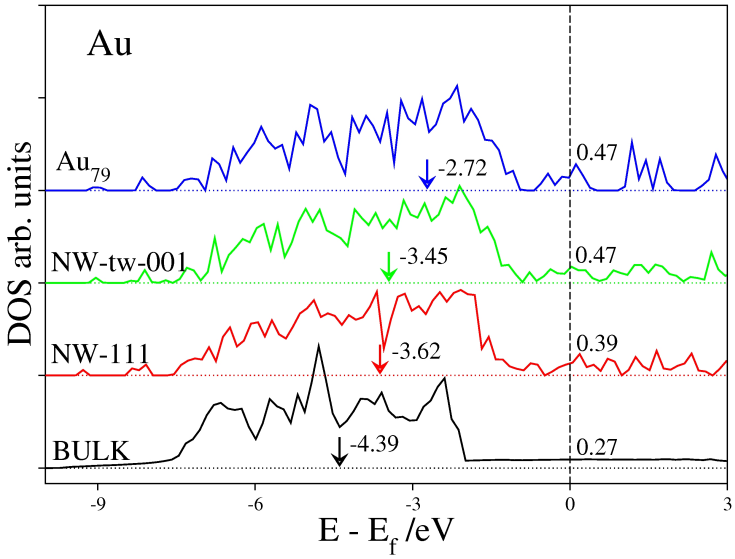

Figure 2: DOS of Au_{79} nanoparticle, NW-tw-001 and NW-111 nanowires and of bulk gold. Arrows indicate the centre of d-band and the numbers near Fermi level are the number of states at this level.

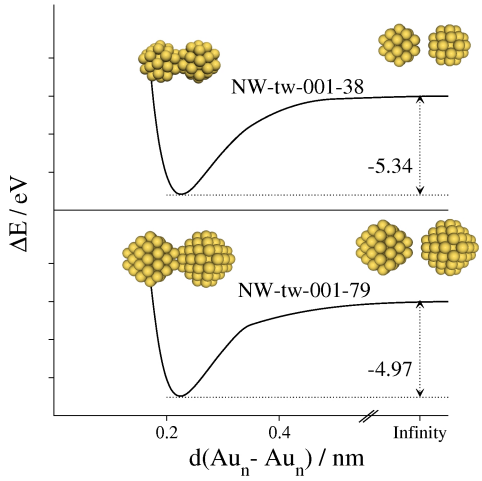

Figure 3: Potential energy curve for the interaction of an infinite chain of Au_{38} and Au_{79} nanoparticles resulting in NW-tw-001 nanowires as a function of the distance between the interacting particles. Numbers near arrows stand for the interaction energy per Au_n unit obtained at the GGA//LDA level.

GGA//LDA level. Nanoparticles made from metal atoms exhibit a semiconductor state because they are usually too small to develop a band structure similar to that of the bulk metal. Hence, Au nanoparticles exhibit a significant DOS near the Fermi level but with a small band gap (0.13 eV) that disconnects electrons to conduction band. Figure 2 shows the evolution of the DOS plots from the isolated Au_{79} nanoparticle to bulk Au passing through the NW-tw-001 and NW-111 nanowires, which are the most stable ones. The DOS in Figure 2 show

that the number of states at the Fermi level decreases in going from the nanoparticle to the bulk with intermediate values for the nanowires. The DOS plots also show that the centre of the d-band, which is a good descriptor of the reactivity of transition metal structures [47], becomes deeper when going from the nanoparticle to the bulk. This is consistent with the fact that the bulk Au is inert whereas Au nanoparticles have a particular catalytic activity. From the DOS plots one can also predict that the reactivity of the nanowires will be intermediate between the isolated nanoparticles and the bulk Au. This is also consistent with the previous work indicating that the extended Au surfaces with less-coordinated Au atoms are able to dissociate molecular hydrogen [48] but the same sites are not able to dissociate molecular oxygen which requires really small particles [49]. Further information about the electronic structure of the Au nanowires studied in the present work can be found from the Bader analysis of the electron density [50]. The Bader analysis has been carried out for the GGA density obtained at the LDA geometry (GGA//LDA) and it reveals several differences between NW-001 and NW-tw-001. In the first case, the connecting atoms have slightly less negative charges than the isolated particle whereas the atoms in the free (001) and (111) facets essentially maintain the charge as in the isolated particle. For the NW-tw-001 nanowire, the connecting atoms are more negatively charged than the corresponding ones in the isolated particle whereas the atoms in the free (001) facets have a more negative charge than in the isolated particle. Finally, for the NW-111 nanowire, the atoms in the (001) facets tend to be more negatively charged than the equivalent ones in the isolated nanoparticle. This analysis shows that the formation of the nanowire induces a significant electronic rearrangement, although the charges in the atoms are always rather small, never exceeding 0.15 eV.

The discussion so far has been centred on Au nanowires built from nanoparticles. At this point it is interesting to explore the influence of the particle size on the self-assembling mechanism and structural properties of the resulting nanowire. Figure 3 compares the potential energy curve for the formation of NW-tw-001 nanowires built from Au_{38} and Au_{79} both with cubo-octahedral shape. The interaction energy per building block unit is 5.38 and 4.97 eV for the nanowires built from Au_{38} and Au_{79} nanoparticles, respectively. Moreover, the minimum of the corresponding potential energy curves also appears at comparable distances. The close similarity between these values strongly suggests that the interaction is dominated by the atoms which are in close contact, four Au atoms in (001) facets in each case. These results strongly suggest that possible differences in the self-assembling process are likely to originate from structural differences between the building blocks, i.e. are of the interacting (001) facets rather than the size of the nanoparticles.

Finally, we consider the effect of changing the metal atom while maintaining the structural unit. To this end, Figure 4 reports the potential energy curves for NW-tw-001 nanowires built from Cu_{38}, Ag_{38} and Au_{38} nanoparticles. The three potential energy curves are also very similar and the main difference is in the strength of the interaction, the largest value corresponding to the Au nanowire (5.34 eV per Au_{38} unit) and the smallest to the Ag nanowire (3.34 eV per Ag_{38} unit) with the Cu one lying in between (4.24 eV per Cu_{38} unit). Hence, one expects that Au nanowires are formed easily and that Ag nanowires

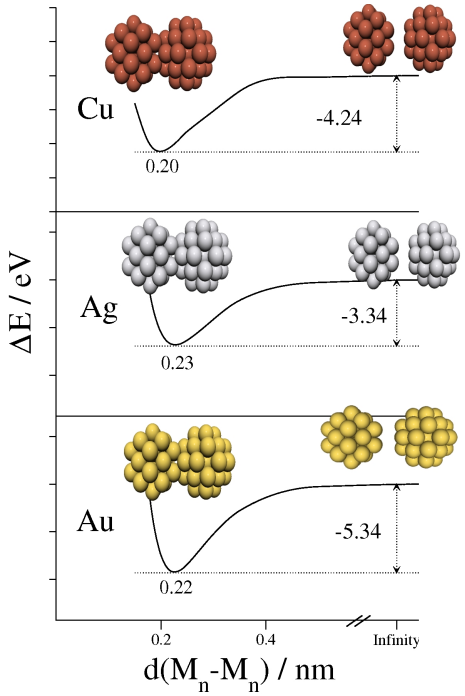

Figure 4: Potential energy curve for the interaction of an infinite chain of Cu_{38}, Ag_{38} and Au_{38} nanoparticles resulting in NW-tw-001 nanowires as a function of the distance between the interacting particles. Numbers near arrows stand for the interaction energy per unit obtained at the GGA//LDA level. The optimum distance (in nm) is given by the numbers below the dotted line.

are the most difficult to form. This is in agreement with the experimental results, indicating that Au nanowires are obtained in a rather simple way [16,17].

Conclusions

The self-assembling of Au nanoparticles into nanowires of different structure has been investigated by means of a periodic approach within DFT following the strategy of previous works on Pd nanowires [34]. The results reported in the present work have been obtained using a Au_{79} nanoparticle as building blocks. However, calculations carried out using a smaller nanoparticle (Au_{38}) as building blocks allow us to conclude that the self-assembling mechanism is general and that the process is dominated by the structural features of the interacting nanoparticles rather than by the particular size of the building block.

The interaction of the Au nanoparticles takes place preferentially along the [111] direction, this is through the (111) facets rather than through the (100) ones which dominate the formation of Pd nanowires. This preference for the growth through the [111] direction is in agreement with the experimental observation and allows us to further validate this computational approach to the study of metallic nanowires.

The electronic structure of the different Au nanowires built from Au_{79} is intermediate between that of the isolated nanoparticle and that of the bulk metal. This is perhaps not surprising but has important consequences for the chemistry of

such nanostructures.

Finally, calculations carried out for nanowires built from Cu, Ag and Au nanoparticles containing 38 atoms reveal that the self-assembling mechanism is general but that the strength of the interaction is dictated by the chemical nature of the metal with Au being the coinage metal leading to stronger interactions between the nanoparticles.

Acknowledgements

A. Roldán thanks Universitat Rovira i Virgili, for supporting his pre-doctoral research. Financial support has been provided by the Spanish Ministry of Science and Innovation (MICINN) (grants FIS2008-02238/FIS and CTQ2008-06549-C02-01). Computational time on the Marenostrum supercomputer of the Barcelona Supercomputing Center is gratefully acknowledged.

References

[1] B. Brushan, Springer Handbook of Nanotechnology, Springer, Berlin, 2007.

[2] H.G. Yang, C.H. Sun, S.Z. Qiao, J. Zou, G. Liu, S. Smith, H.M. Cheng, and G.Q. Lu, Anatase TiO2 single crystals with a large percentage of reactive facets, Nature 453 (2008), pp. 638–641.

[3] S. Iijima and T. Ichihashi, Singel-shell calbon nanotubes of 1-nm diameter, Nature 363 (1993), pp. 603–605.

[4] A. Thess, R. Lee, P. Nikolaev, H.J. Dai, P. Petit, J. Robert, C.H. Xu, Y.H. Lee, S.G. Kim, A.G. Rinzler, D.T. Colbert, G.E. Scuseria, D. Tomanek, J.E. Fischer, and R.E. Smalley, Crystalline ropes of metallic carbon nanotubes, Science 273 (1996), pp. 483–487.

[5] R.H. Baughman, A.A. Zakhidov, and W.A. de Heer, Carbon nanotubes – the route toward applications, Science 297 (2002), pp. 787–792.

[6] N. Wang, Y. Cai, and R.Q. Zhang, Growth of nanowires, Mater. Sci. Eng. R. 60 (2008), pp. 1–51.

[7] Z. Tang, N.A. Kotov, and M. Giersig, Spontaneous organization of single CdTe nanoparticles into luminescent nanowires, Science 297 (2002), pp. 237–240.

[8] M.S. Gudiksen, L.J. Lauhon, J. Wang, D.C. Smith, and C.M. Lieber, Growth of nanowire superlattice structures for nanoscale photonics and electronics, Nature 415 (2002), pp. 617–620.

[9] F. Patolsky and C.M. Lieber, Nanowire nanosensors, Mater. Today 8 (2005), pp. 20–28.

[10] D. Wang, F. Qian, C. Yang, Z. Zhong, and C.M. Lieber, Rational growth of branched and hyperbranched nanowire structures, Nano Lett. 4 (2004), pp. 871–874.

[11] Z.W. Pan, Z.R. Dai, and Z.L. Wang, Nanobelts of semiconducting oxides, Science 291 (2001), pp. 1947–1949.

[12] X.F. Duan, Y. Huang, Y. Cui, J.F. Wang, and C.M. Lieber, Indium phosphide nanowires as building blocks for nanoscale electronic and optoelectronic devices, Nature 409 (2001), pp. 66–69.

[13] M.C. Daniel and D. Astruc, Gold nanoparticles: assembly, supramolecular chemistry, quantum-size-related properties, and applications toward biology, catalysis, and nanotechnology, Chem. Rev. 104 (2004), pp. 293–346.

[14] M. Hu, J. Chen, Z.Y. Li, L. Au, G.V. Hartland, X. Li, M. Marquez, and Y. Xia, Gold nanostructures: engineering their plasmonic properties for biomedical applications, Chem. Soc. Rev. 35 (2006), pp. 1084–1094.

[15] H. Ohnishi, Y. Kondo, and K. Takayanagi, Quantized conductance through individual rows of suspended gold atoms, Nature 395 (1998), pp. 780–790.

[16] N. Pazos-Perez, D. Baranov, S. Irsen, M. Hilgendorff, L.M. Liz- Marzan, and M. Giersig, Synthesis of flexible, ultrathin gold nanowires in organic media, Langmuir 24 (2008), pp. 9855–9860.

[17] A. Halder and N. Ravishankar, Ultrafine single-crystalline gold nanowire arrays by oriented attachment, Adv. Mater. 19 (2007), pp. 1854–1858.

[18] L. Zhang, Y. Fang, and P. Zhang, Experimental and DFT theoretical studies of SERS effect on gold nanowires array, Chem. Phys. Lett. 451 (2007), pp. 102–105.

[19] Z. Huo, C.K. Tsung, W. Huang, X. Zhang, and P. Yang, Sub-two nanometer single crystal Au nanowires, Nano Lett. 8 (2008), pp. 2041–2044.

[20] X. Lu, M.S. Yavuz, H.Y. Tuan, B.A. Korgel, and Y. Xia, Ultrathin gold nanowires can be obtained by reducing polymeric strands of Oleylamine-AuCl complexes formed via aurophilic interaction, J. Am. Chem. Soc. 130 (2008), pp. 8900–8901.

[21] K. Biswas, Y. Qin, M. DaSilva, R. Reifenberger, and T. Sands, Electrical properties of individual gold nanowires arrayed in a porous anodic alumina template, Phys. Stat. Sol. A 204 (2007), pp. 3152–3158.

[22] V. Rodrigues, T. Fuhrer, and D. Ugarte, Signature of atomic structure in the quantum conductance of gold nanowires, Phys. Rev. Lett. 85 (2000), pp. 4124–4127.

[23] C. Wang, Y. Hu, C.M. Lieber, and S. Sun, Ultrathin Au nanowires and their transport properties, J. Am. Chem. Soc. 130 (2008), pp. 8902–8903.

[24] N.A. Melosh, A. Boukai, F. Diana, B. Gerardot, A. Badolato, P.M. Petroff, and J.R. Heath, Ultrahigh-density nanowire lattices and circuits, Science 300 (2003), pp. 112–115.

[25] Y. Zhang, L. Giordano, and G. Pacchioni, Gold nanostructures on TiOx/Mo(112) thin films, J. Phys. Chem. C 112 (2008), pp. 191–200.

[26] E.Z. Da Silva, F.D. Novaes, A.J.R. Da Silva, and A. Fazzio, Theoretical study of the formation, evolution, and breaking of gold nanowires, Phy. Rev. B 69 (2004), pp. 1–11.

[27] L. Xiao, B. Tollberg, X. Hu, and L. Wang, Structural study of gold clusters, J. Chem Phys. 124 (2006), pp. 1–10.

[28] Y. Mokrousov, G. Bihlmayer, and S. Blugel, Full-potential linearized augmented plane-wave method for one-dimensional systems: gold nanowire and iron monowires in a gold tube, Phys. Rev. B 72 (2005), pp. 1–15.

[29] H. Mehrez and H. Guo, Theoretical study of nanowires, Nanowires Nanobelts 1 (2003), pp. 95–124.

[30] J. Nakamura, N. Kobayashi, S. Watanabe, and M. Aono, Structural stability and electronic states of gold nanowires, Surf. Sci. 482 (2001), pp. 1266–1271.

[31] Y. Fujimoto and K. Hirose, First-principles theory for the calculation of electron-transport properties of metallic nanowires, Nanotechnology 14 (2003), pp. 147–151.

[32] S. Zalis, I. Kratochvilova, A. Zambova, J. Mbindyo, T.E. Mallouk, and T.S. Mayer, Combined experimental and theoretical DFT study of molecular nanowires negative differential resistance and interaction with gold clusters, EPJ E 18 (2005), pp. 201–206.

[33] X. Yin, Y. Li, Y. Zhang, P. Li, and J. Zhao, Theoretical analysis of geometry-correlated conductivity of molecular wire, Chem. Phys. Lett. 422 (2006), pp. 111–116.

[34] F. Vines, F. Illas, and K.M. Neyman, On the mechanism of formation of metal nanowires by self-assembly, Ang. Chem. Int. Edit. 46 (2007), pp. 7094–7097.

[35] I.V. Yudanov, R. Sahnoun, K.M. Neyman, N. Rösch, J. Hoffmann, S. Schauermann, V. Johanek, H. Unterhalt, G. Rupprechter, J. Libuda, and H.J. Freund, CO adsorption on Pd nanoparticles. Density functional and vibrational spectroscopy studies, J. Phys. Chem. B 107 (2003), pp. 255–264.

[36] I.V. Yudanov, K.M. Neyman, and N. Rösch, Density functional study of Pd nanoparticles with subsurface impurities of light element atoms, Phys. Chem. Chem. Phys. 6 (2004), pp. 116–123.

[37] K.M. Neyman, R. Sahnoun, C. Inntam, S. Hengrasmee, and N. Rösch, Computational study of model Pd–Zn nanoclusters and their adsorption complexes with CO molecules, J. Phys. Chem. B 108 (2004), pp. 5424–5430.

[38] A. Roldan, F. Vines, F. Illas, J.M. Ricart, and K.M. Neyman, Density functional studies of coinage metal nanoparticles: scalability of their properties to bulk, Theoret. Chem. Acc. 120 (2008), pp. 565–573.

[39] I.V. Yudanov, K.M. Neyman, and N. Rösch, CZO bond scission of methoxide on Pd nanoparticles: a density functional study, Phys. Chem. Chem. Phys. 8 (2006), pp. 2396–2401.

[40] K.M. Neyman, G.N. Vayssilov, and N. Rösch, Transition metal clusters and supported species with metal-carbon bonds from first-principles quantum chemistry, J. Organomet. Chem. 689 (2004), pp. 4384–4394.

[41] S.H. Vosko, L. Wilk, and M. Nusair, Accurate spin-dependent electron liquid correlation energies for local spin density calculations: a critical analysis, Can J. Phys. 58 (1980), pp. 1200–1211.

[42] J.P. Perdew and Y. Wang, Erratum: pair-distribution function and its coupling-constant average for the spin-polarized electron gas [Phys. Rev. B 46, 12 947 (1992)], Phys. Rev. B 56 (1997), p. 7018.

[43] P.E. Blochl, Projector augmented wave method, Phys. Rev. B 50 (1994), pp. 17953–17979.

[44] G. Kresse and D. Joubert, From ultrasoft pseudopotentials to the projector augmented-wave method, Phys. Rev. B 59 (1999), pp. 1758–1775.

[45] G. Kresse and J. Furthmuller, Efficiency of ab-initio total energy calculations for metals and semiconductors using a plane-wave basis set, Comput. Mater. Sci. 6 (1996), pp. 15–50.

[46] G. Kresse and J. Furthmueller, Efficient iterative schemes for ab initio total-energy calculations using a plane-wave basis set, Phys. Rev. B 54 (1996), pp. 11169–11186.

[47] B. Hammer and J.K. Norskov, Theoretical surface science and catalysis – calculations and concepts, Adv. Catal. 45 (2000), pp. 71–129.

[48] A. Corma, M. Boronat, S. Gonzalez, and F. Illas, On the activation of molecular hydrogen by gold: a theoretical approximation to the nature of potential active sites, Chem. Commun. 32 (2007), pp. 3371–3373.

[49] A. Roldan, S. Gonzalez, J.M. Ricart, and F. Illas, Critical size for O_2 dissociation by Au nanoparticles, ChemPhysChem 10 (2009), pp. 348–351.

[50] R.F.W. Bader, Atoms in Molecules: A Quantum Theory, Oxford Science, Oxford, 1990.

UNIVERSITAT ROVIRA I VIRGILI
MODELLING AU CATALYST FROM BULK TO NANOSCALE
Alberto Roldán Martínez
ISBN:978-84-693-7669-0/DL:T-1748-2010

3.4 Zero-dimensional systems: Nanoparticle

"Particles do not exist... the particle concept is just an idealized model of some use in the quantum field theory plane space."

Paul Davies [4]

Density functional plane-wave calculations have been carried out for series particles containing up to 225 (Au) atoms. Full geometry optimization has been performed for all particles starting from the structures created by cuts from the bulk. In line with previous studies, calculated average nearest neighbour distances and cohesive energies of the particles linearly depend on such size-derived parameters as the average coordination number of metal atoms and the inverse of the mean particle radius, respectively. Rather accurate linear extrapolation of the observables under scrutiny to the bulk values has been achieved. Implications of encountered structural peculiarities of the nanoparticles for their reactivity are outlined.

The series of Au nanoparticles as well as extended systems containing low-coordinated sites show that the presence of low-coordinate Au atoms is not enough to dissociate O_2. Strong adsorption of molecular oxygen on Au nanoparticles is a necessary but not sufficient condition for O_2 dissociation, process that has a common pathway for O_2 dissociation on these nanoparticles. Furthermore, there is critical size for Au nanoparticles to dissociate O_2.

A microkinetic model has been developed to describe the evolution of atomic and molecular oxygen on a variety of Au nanoparticles with rate constants derived from density functional calculations. Simulated thermal programmed desorption (TPD) curves are also presented and compared with recent experimental results for Au nanoparticles supported on silica. The present calculations confirm that TPD temperature peaks depend on the particle size, in agreement with experiment, and provide some clues about the chemical composition of the particles used in the experiments.

[4] Professor at Arizona State University.

UNIVERSITAT ROVIRA I VIRGILI
MODELLING AU CATALYST FROM BULK TO NANOSCALE
Alberto Roldán Martínez
ISBN:978-84-693-7669-0/DL:T-1748-2010

UNIVERSITAT ROVIRA I VIRGILI
MODELLING AU CATALYST FROM BULK TO NANOSCALE
Alberto Roldán Martínez
ISBN:978-84-693-7669-0/DL:T-1748-2010

3.4.1 Density functional studies of coinage metal nanoparticles: scalability of their properties to bulk

Corresponding to: Roldan, A.; Vines, F.; Illas, F.; Ricart, J. M.; Neyman, K. M. Theoretical Chemistry Accounts 2008, 120, 565-573.

Introduction

The study of materials at the nanoscale constitutes a rather new and rapidly growing field with implications in industry and catalysis [1–3]. Industrial catalysts are often made of metal particles deposited on some kind of a support [4,5]. Information about how various properties change with size of the nanoparticles appears to be a very important issue. This includes, among other parameters, size-evolution of electronic and geometric structures and, for magnetic systems, also the evolution of magnetic moments. The ultimate goal behind the studies of size- and shape-dependent observables is the possibility to help to tune the reactivity and other particle parameters in a desired direction. One may think of designing metal nanoparticles with a special activity and selectivity towards a given reaction or prepare nanoparticles with particular electric or magnetic properties, which can be used as the basis for new devices.

There have been many experimental studies aimed at unravelling the structure of metal nanoparticles on different supports [6–11]. Several computational studies have also addressed these problems, although in most cases without directly taking the support into account [4,5,12–18]. A considerable effort has been devoted to predict the most stable isomers for a given transition metal nanoparticle of a certain (usually rather small) size; studies of the scalability of properties with the nanoparticle size are also reported [19–22]. As far as the shape is concerned, it has been demonstrated that three-dimensional (3D) metal crystallites cut from metal bulk by low-index planes are adequate starting models [23–29]. The latter provide a tic representation of larger metal nanoparticles present in catalysts and offer some advantages with respect to the more conventional surface science models of two-dimensional (2D) extended surfaces, which lack atoms in a low coordination. In fact, it is well established nowadays that low-coordinated metal atoms of stepped surfaces often exhibit a superior catalytic activity over those of ideal regular surfaces (e.g. [30–40] and references therein). For instance, it has been recently shown that low-coordinated atoms are crucial for the dissociation of molecular hydrogen on gold [41].

A tic and appropriate representation of the nanoparticles involved in supported metal catalysts requires using 3D models in the regime when the properties are scalable (follow a monotonous

trend) with increasing size, so that they eventually converge to the bulk values. The use of scalable models allows one to predict properties of larger particles of a tic size without carrying out rather demanding calculations for them. However, there are two main problems when attempting to build models in the scalable regime. On the one hand, it is not quite clear how large the model particle under scrutiny needs to be to ensure scalability for a particular metal. On the other hand, these model particles can be too large to carry out state-of-the-art density functional (DF) calculations. Until recently, calculations on moderately large metal particles required dedicated codes, which efficiently handle symmetry [42,43]. Lately, it has been suggested to take advantage of the computational efficiency of codes that use plane-wave basis sets and translational symmetry. In this way DF calculations for nanoparticles containing up to ∼200 metal atoms have been reported (see e.g., [22]). Moreover, one can utilize the periodic boundaries to study assembling of nanoparticles and even to model ordered superstructures [44].

In spite of the recent progress outlined above, there is almost no information about the scalable regime for metal nanoparticles other than Pd [20,21,23] and Au [19,20,22]. In this article we present an exhaustive systematic DF study of selected observables of nanoparticles of all three coinage metals and compare them with available results from previous studies. In particular, we focus on the convergence of mean interatomic distances and cohesive (binding) energies of Cu_n, Ag_n and Au_n nanoparticles towards the bulk values with increasing particle size. We also use this data set to re-assess precision of LDA (local-density approximation) and GGA (generalized-gradient approximation) functionals to quantify structural and energetic parameters of (heavy) metal systems.

Computational details

Density functional plane-wave calculations have been carried out with the help of VASP code [45–47] for three series of coinage metal particles M_n (M = Cu, Ag, Au), containing up to 225 atoms. The total energy was computed using either the LDA(VWN) [48] or the GGA(PW91) [49] exchange-correlation functionals. The effect of the core electrons on the valence electron density was described by the projector augmented wave (PAW) method [50,51]. The cut-off for the kinetic energy of the plane-waves has been set to 315 eV throughout, which ensures total energy convergence to better than 10−4 eV. A Gaussian smearing technique with a 0.2 eV width has been applied to enhance convergence but all energies presented in the following have been obtained by extrapolating to zero smearing (0K). Smaller smearing values of 0.05 eV were employed to calculate DOS plots (see Sect. 3.3). Geometry optimization on selected starting geometries (see below) was carried out using a gradient conjugate method until forces on all atoms were less than 0.3 eV/nm. Based on our test calculations, negligibly small spin-polarization effects were ignored throughout, except for spin-polarized energies of the atomic references. Both LDA and GGA functionals are considered to allow one a reasonably accurate description of (heavy) metallic systems (bulk, surfaces and clusters). In general, energies obtained at a GGA level are more precise but LDA is able to provide for such systems better geometries (see e.g. [19]). Therefore, we also performed calculations, in which the GGA energy was evaluated at the LDA geometry. Following the standard notation in molec-

ular calculations, this approach is hereafter denoted as GGA//LDA. It has already proven to give accurate results for heavy metal systems [23,27 and references therein].

Single particles have been modelled by placing them into a large enough supercell, with a minimum vacuum space of 1 nm in all directions to avoid interactions between species in the neighbouring cells. This is a necessary requirement when using a plane wave basis set, which spans the whole space with the periodicity imposed by the unit cell chosen. However, to describe single particles it is sufficient to consider only the Γ-point of the reciprocal space. The centre of each particle has been placed at the unit cell centre. Cutting compact structures by low-index planes from the fcc metal bulk provided initial geometries for optimization. We studied coinage metal species M_n of both octahedral (n = 44, 85 and 146) and cuboctahedral shapes (n = 38, 55, 79, 116, 140, 147, 201 and 225; the latter three only for M = Au). Illustrative examples of Au_n nanoparticles are shown in Fig. 1. Note that geometry optimization always converged to a structure with the same topology, even though no symmetry constraints were imposed. It is worth emphasizing that no attempt has been made to find the most stable isomer for a given particle nuclearity, because our focus is on the properties scalability for particles of the *same fcc structural motif*.

All calculations have been carried out on parallel computers. Smaller M_n (M = Cu, Ag, Au; n < 80) moieties can be routinely calculated on a standard Linux cluster. However, for the larger species a supercomputer is required. In fact, LDA geometry optimization of the particles containing ∼150 atoms typically takes ∼4 CPU hours on 64 processors of the Marenostrum supercomputer.[5] Therefore, rather timeconsuming calculations for the clusters with 147, 201 and 225 atoms were carried out only for Au, assuming similar trends for the corresponding Cu and Ag particles.

Results and discussion

Geometric parameters

Interatomic distances in nanoparticles Cu_n, Ag_n and Au_n as well as the bulk values calculated at LDA and GGA levels are listed in Table 1 and compared with the experimental bulk distances [52–54]. Not unexpectedly [19,20], the LDA distances in all systems under scrutiny are shorter than the corresponding GGA values. Interestingly, differences of the average bond lengths d(GGA)–d(LDA) are not only substantial, ∼8–10 pm, but also rather constant across the series of nanoparticles of different metals. Comparing the calculated and experimental bulk distances one observes overestimated d(GGA) values, deviations of which from experiment increase monotonously from just 2 pm for Cu, via 5 pm for Ag to 7 pm for Au. The latter overestimation is considerable, especially if compared to the precision of the d(LDA) value for Au bulk, exactly matching the experimental distance. The experimental distance for Ag bulk is just in the middle of the d(LDA)-d(GGA) interval and only for Cu does the GGA provide definitely superior accuracy for interatomic distances in coinage metal particles over the LDA distances. These results illustrate some practical consequences of the lack of a sufficiently

[5] For details about the supercomputer architecture see www.bsc.es

UNIVERSITAT ROVIRA I VIRGILI
MODELLING AU CATALYST FROM BULK TO NANOSCALE
Alberto Roldán Martínez
ISBN:978-84-693-7669-0/DL:T-1748-2010

Table 3.4.1: Average nearest-neighbour (d) and minimum/maximum (dmin/dmax, in parentheses) interatomic distances (in pm) of octahedral and cuboctahedral *fcc* Cu_n, Ag_n and Au_n particles of increasing size, characterized by average coordination numbers N_{av}, calculated using LDA(VWN) and GGA(PW91) functionals. The calculated and experimental metal bulk distances are also shown.

n	N_{av}	Cu_n		Ag_n		Au_n	
		LDA	GGA	LDA	GGA	LDA	GGA
38	7.58	242 (239/251)	250 (247/260)	277 (273/288)	287 (284/298)	281 (273/309)	289 (281/316)
44	7.64	243 (237/250)	251 (245/258)	278 (272/278)	288 (281/299)	280 (267/297)	288 (273/306)
55	7.85	243 (231/249)	251 (238/256)	278 (267/285)	288 (277/295)	280 (266/289)	289 (274/299)
79	8.51	244 (238/252)	252 (246/260)	280 (274/289)	290 (283/300)	283 (272/307)	292 (279/322)
85	8.47	244 (234/251)	252 (242/261)	276 (268/288)	290 (278/300)	282 (268/302)	291 (274/314)
116	8.90	245 (237/252)	253 (244/260)	280 (271/288)	290 (282/297)	284 (268/316)	292 (275/329)
140	9.09	245 (237/257)	253 (244/266)	280 (272/294)	291 (282/306)	284 (275/312)	292 (279/326)
146	9.04	245 (236/255)	253 (244/263)	280 (271/292)	291 (282/304)	284 (268/308)	292 (275/321)
147	9.89					283 (266/300)	291 (274/311)
201	9.43					284 (269/306)	292 (277/317)
225	9.49					284 (272/308)	293 (279/321)
bulk	12.00	249	258	284	294	288	295
		256^b		289^b		288^b	

[a] Octahedral starting geometry; cuboctahedral one for all other particles. The shape retained in symmetry-unrestricted optimized structures.

[b] Experimental values from Refs. [52–54]

UNIVERSITAT ROVIRA I VIRGILI
MODELLING AU CATALYST FROM BULK TO NANOSCALE
Alberto Roldán Martínez
ISBN:978-84-693-7669-0/DL:T-1748-2010

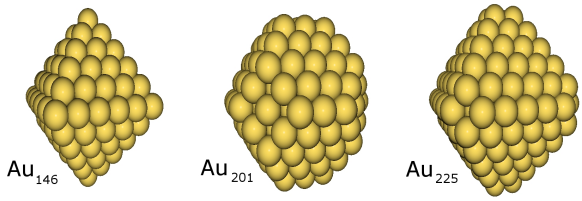

Figure 1: Sketches of selected Au nanoparticles with octahedral (Au_{146}) and cuboctahedral (Au_{201}, Au_{225}) structures.

accurate universal exchange-correlation functional (especially for heavy-element systems), which would be capable of equally precise description of the whole spectrum of observable parameters. We mention in the next section another implication of this problem—deficiencies in a consistent GGA description of the binding energy.

Let us focus on two other useful geometry indicators of the nanoparticles—minimum, d_{min}, and maximum, d_{max}, interatomic distances (Table 1). The difference $\triangle d = d_{max} - d_{min}$ increases smoothly from Cu_n to Au_n species of the same size and for the particles of the same metal with increasing size. For instance, $\triangle$d values for the particles with n = 140 and 146 increase from ~20 pm (Cu_n) and ~22 pm (Ag_n) to ~40 pm (Au_n); at GGA level $\triangle d(Au_n)$ values reach as much as 47 pm. This shows that Au_n particles differ significantly from the Cu_n and Ag_n analogues with respect to the d_{min}/d_{max} distribution. Substantial size of d values, especially for larger particles considered, implies possibilities for noticeable alteration of the properties of atoms involved in the shortest and longest cluster M–M bonds, respectively. In general, the longest M–M bonds in the coinage metal particles are found for some of the surface atoms on (111) facets with some of their subsurface neighbours. It could be interpreted as a consequence of the surface stress that pushes outwards a small part of atoms exposed in the facets, thus leading to pronounced corrugation of the facets. Reactivity of such atoms with adsorbed species may well differ from that of their neighbours on the same facet. This effect should not be overlooked when comparing reactivity of nanoparticle facets with that of extended single-crystal surfaces.

In Fig. 2 we illustrate scaling of the average M–M bond distance d with the cluster size, expressed in terms of the average coordination number N_{av}. The latter is defined as a sum of the coordination numbers of all n atoms of a particle divided by n; for metal bulk N_{av} = 12 (data also included). Both LDA and GGA values are presented. In line with previous scalability studies for transition metal particles [19–21,23], the calculated average bond lengths converge rather rapidly to the corresponding bulk values, clearly manifesting development of the bulk character along each of the M_n series. On the other hand, these data reveal that even the largest nanocrystallite considered here, Au_{225} with its more than 60% of surface atoms and N_{av} value close to 80% of that for the bulk, is still not very close to the bulk limit, despite the LDA and GGA d value is only 4 and 2 pm, respectively, or ~1% shorter than the corresponding bulk value.

One should mention that the correlations of d with N_{av} are linear with a rather high precision, especially for Cu_n and Ag_n. They give the values d extrapolated to the bulk to within 1 pm

UNIVERSITAT ROVIRA I VIRGILI
MODELLING AU CATALYST FROM BULK TO NANOSCALE
Alberto Roldán Martínez
ISBN:978-84-693-7669-0/DL:T-1748-2010

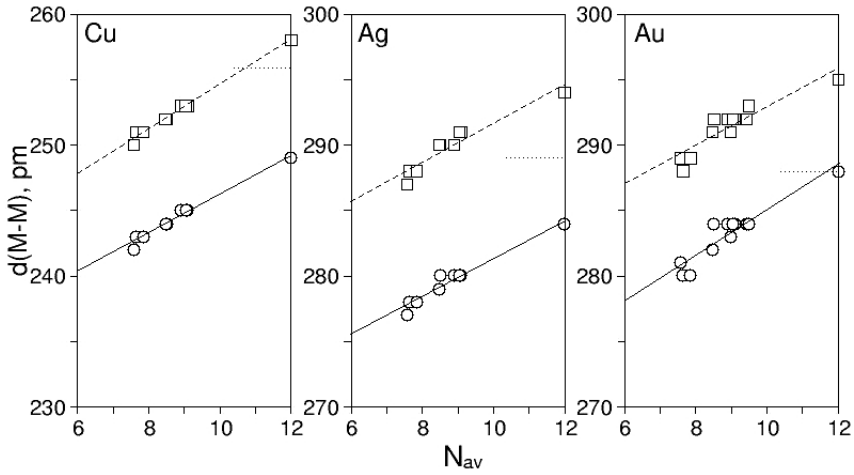

Figure 2: Average nearest-neighbour interatomic distances d(M–M) of coinage metal (M = Cu, Ag, Au) particles M_n and bulk metals as a function of the average coordination number N_{av}. *Circles* and *solid lines* results of LDA(VWN) geometry optimization, *squares* and *dashed lines* correspond to GGA(PW91) geometry optimization. Experimental bulk values are also shown (*dotted lines*). Computed correlations for systems $38 \leq n < \infty$ (pm): $d^{Cu}(LDA) = 1.50 \times N_{av} + 231.4$ ($R^2 = 0.981$), $d^{Cu}(GGA) = 1.70 \times N_{av} + 237.8$ ($R^2 = 0.996$), $d^{Ag}(LDA) = 1.45 \times N_{av} + 266.9$ ($R^2 = 0.978$), $d^{Ag}(GGA) = 1.42 \times N_{av} + 277.5$ ($R^2 = 0.948$), $d^{Au}(LDA) = 1.75 \times N_{av} + 267.4$ ($R^2 = 0.940$), $d^{Au}(GGA) = 1.51 \times N_{av} + 277.9$ ($R^2 = 0.825$).

with respect to those explicitly calculated for the corresponding metal bulk. Interestingly, dispersion of the average distances d over the fitted lines is notably larger for Au_n systems than for other two coinage metals, in particular, at the GGA level. This clear manifestation of the worse scalability of interatomic distances for gold moieties with their size should probably be traced back to its strongly expressed relativistic character and partly related to its trend to form more open (planar) structures, compared to copper and silver [55,56]. Such peculiar structural behaviour of Au_n particles also implies that the onset of the scalable (to bulk) regime for them is postponed to larger sizes compared to congeners of the other two coinage metals, and, more generally, of other, less relativistic metals.

Finally, we compare our calculated interatomic distances with those of previous DF calculations [19,22], which were performed for smaller Au_n particles n $\leq$ 147. Our average GGA bond-lengths d(Au–Au) of Au_n are very close, within 1 pm, to the values recently obtained using the same plane-wave computational technique [22]. However, unclear why d(Au–Au) = 292 pm has been calculated for Au bulk in Ref. [22], i.e. exactly equals to that in the four largest clusters Au_{116}, Au_{140}, Au_{146} and Au_{147} there. Note that our explicitly calculated bulk GGA distance d(Au–Au) is 295 pm, in full agreement with the value derived from our correlations. Probably, this inconsistency is related to the structure optimization approach of bulk gold, employed in Ref. [22]. Of special importance for such "relativistic" element as Au is benchmarking versus data of highly accurate all-electron scalar relativistic calculations [19]. The latter have been undertaken with Oh point-group symmetry and a DF code using Gaussian basis, similar to the code ParaGauss [42, 43]. For the largest fcc cluster studied, Au_{55} [19],

the LDA d(Au–Au) value with exactly the same exchange-correlation functional VWN as we used is 279 pm, i.e. only 1 pm shorter than in the present PAW plane-wave calculations. At GGA level (with a functional distinct from PW91 one used by us), the scalar relativistic d(Au–Au) = 287 pm [19] appears also to be in very good agreement with the presently calculated value of 289 pm having in mind notably different computational procedures employed. Average Au–Au bond lengths extrapolated to the bulk are in Ref. [19] even closer to the corresponding values of this work. Interestingly, both d(LDA) = 283 pm and d(GGA) = 291 pm values for the Au_{147} particle optimized under Ih symmetry constraints [19] match exactly the distances for the cuboctahedral Au_{147} particle (see Table 1).

Bonding energies

Cohesive (binding) energy per atom, E_c, is another important characteristic of nanoparticles. Our results are listed in Table 2, including calculated and experimental [57] values for bulk metals. Similarly to the interatomic distances, we computed and analysed bonding energies for the different particles at both LDA and GGA levels. In line with observations that GGA geometric parameters may appreciably deviate from accurate values, especially for heavy-element systems (see Sect. 3.1), we also examined performance of a combined GGA//LDA approach, according to which GGA energy is computed in a single-point fashion for the geometry optimized at LDA level. Beyond that one has at GGA//LDA level the opportunity to work with often more reliable geometries, such GGA//LDA calculations are faster, because instead of GGA geometry optimization less time-consuming LDA optimization is performed.

From calculated and experimental bulk values of cohesive energy (Table 2) a clear trend in the precision of the LDA and GGA emerges for metals along the group – Cu → Ag → Au. For Cu bulk E_c(GGA) = −3.52eV quantitatively matches the experimental value of −3.50eV [57], whereas at LDA the binding is much too strong, −4.54eV. For Ag bulk, the presently used GGA PW91 furnishes binding energy of −2.56eV, which notably, by 0.40eV (14%), underestimates the experimental energy, −2.96eV [57]. In fact, this rather low precision of GGA for Ag is of comparable size with that of LDA, which features overbinding by 0.67eV. For Au, performance of GGA for the bulk binding energy is even worse, E_c(GGA) = −3.06eV vs. experimental −3.78eV [57], concomitantly, E_c(LDA) = −4.30eV becomes somewhat closer to the experiment. These data illustrate that GGA in the form of one of the most widely used PW91 functional provides rather approximate description of the binding between heavy element atoms, in particular 5d (Au) and, to lesser extend, 4d (Ag) metals. It appears to be a general deficiency of contemporary GGA functionals, not just of the PW91 one [27]. Therefore, the more economic and also often more accurate for geometric parameters combined GGA//LDA description of the metal binding energies may well be considered advantageous for the metals under scrutiny (Table 2): the deviation of E_c(GGA) from the corresponding E_c(GGA//LDA) energy is throughout close to ∼0.05eV (∼5 kJ/mol), which is actually the best "chemical" accuracy that can be presently reached using DFT methods.

The binding per atom in M_n species is gradually strengthening with increasing particle size n, towards the corresponding energy in the bulk (Table 2).

UNIVERSITAT ROVIRA I VIRGILI
MODELLING AU CATALYST FROM BULK TO NANOSCALE
Alberto Roldán Martínez
ISBN:978-84-693-7669-0/DL:T-1748-2010

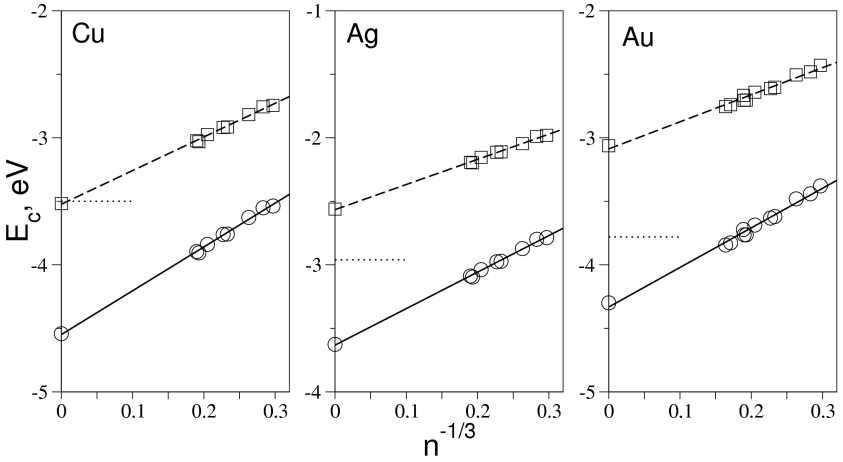

Figure 3: Cohesive energy E_c (eV) per atom of coinage metal (M = Cu, Ag, Au) particles Mn and bulk metals as a function of the inverse of the mean particle radius $R^{-1} \sim n^{-1/3}$. *Circles* and *solid lines* LDA(VWN) energies, *squares* and *dashed lines* GGA(PW91) energies. Experimental bulk values are also shown (*dotted lines*). Computed correlations for $38 \leq n < \infty$: $E_c^{Cu}(LDA) = -4.548 + 3.446 \times n^{-1/3}$ ($R^2 = 0.997$), $E_c^{Cu}(GGA) = -3.552 + 2.643 \times n^{-1/3}$ ($R^2 = 0.997$), $E_c^{Ag}(LDA) = -3.631 + 2.870 \times n^{-1/3}$ ($R^2 = 0.998$), $E_c^{Ag}(GGA) = -2.565 + 1.978 \times n^{-1/3}$ ($R^2 = 0.997$), $E_c^{Au}(LDA) = -4.332 + 3.114 \times n^{-1/3}$ ($R^2 = 0.990$), $E_c^{Au}(GGA) = -3.087 + 2.128 \times n^{-1/3}$ ($R^2 = 0.986$).

However, at variance with the interatomic distances, the binding energy per atom in the nanoparticles of the size considered here is still rather far from the bulk reference, reaching only ∼86% (Cu_{146}, Ag_{146}, Au_{146}) or 90% (Au_{225}) of the latter; the absolute particle bulk energy deviation is quite significant and it ranges from ∼0.3 eV(Au) to ∼0.6 eV(Cu). E_c values of nanoparticles can be extrapolated to the bulk value as a function of the inverse of the mean particle radius R, approximated as $R^{-1} \sim n^{-1/3}$ [19–21,23]. Results of such extrapolations of the LDA and GGA energies calculated for the whole range of M_n clusters, $n \geq 38$, and including the calculated bulk value are shown in Fig. 3. Linearity of the fitted LDA and GGA energy correlations for all three series of metal systems is of rather high accuracy, as manifested by R^2 values close to 1 (see caption of Fig. 3). For most of the calculated E_c values the deviations from the respective fitted values are just ∼0.01eV and only few outliers in the plots of Fig. 3 exhibit slightly larger deviations, limited to ∼0.05eV. The energy correlations for Au, especially GGA one, are slightly less perfect than those for Cu and Ag, but the overall differences are much smaller than we have found for correlations of the interatomic distances (see Sect. 3.1). Thus, the specific character of relativistic metal Au with respect to Cu and Ag appears to manifest less in the particle energetics than in the size-evolution of their M–M distances. Due to the still significant "gap" between the binding energies of computationally tractable moderately large metal particles and of the bulk, the presently derived sufficiently accurate correlations $E_c(n^{-1/3})$ should be useful for prediction of the binding strength for those coinage metal particles, which are still out of the scope of routine DF calculations.

Table 3.4.2: Cohesive energy per atom (E_c, eV) of octahedral and cuboctahedral *fcc* Cu_n, Ag_n and Au_n particles of increasing size, $n \geq 38$, characterized by the inverse of the mean particle radius $R^{-1} \sim n^{-1/3}$, calculated using LDA(VWN) and GGA(PW91) functionals. Calculated and experimental values for the bulk metals are also shown.

N	$n^{-1/3}$	Cu_n			Ag_n			Au_n		
		LDA	GGA	GGA//LDA	LDA	GGA	GGA//LDA	LDA	GGA	GGA//LDA
38	0.297	-3.54	-2.75	-2.71	-2.79	-1.98	-1.93	-3.38	-2.43	-2.38
44[a]	0.283	-3.55	-2.76	-2.72	-2.80	-1.99	-1.94	-3.44	-2.48	-2.43
55	0.263	-3.63	-2.82	-2.78	-2.87	-2.05	-2.00	-3.48	-2.51	-2.46
79	0.233	-3.76	-2.92	-2.87	-2.97	-2.11	-2.06	-3.62	-2.60	-2.55
85[a]	0.227	-3.76	-2.92	-2.88	-2.98	-2.11	-2.06	-3.63	-2.61	-2.56
116	0.205	-3.84	-2.98	-2.93	-3.04	-2.15	-2.10	-3.69	-2.64	-2.59
140	0.193	-3.91	-3.03	-2.99	-3.10	-2.20	-2.14	-3.76	-2.70	-2.65
146[a]	0.190	-3.90	-3.02	-2.98	-3.09	-2.19	-2.14	-3.72	-2.70	-2.65
147	0.189							-3.72	-2.67	-2.62
201	0.171							-3.83	-2.74	-2.69
225	0.164							-3.84	-2.75	-2.70
Bulk	0.000	-4.54	-3.52	-3.47	-3.63	-2.56	-2.49	-4.30	-3.06	-3.01
			-3.50[c]			-2.96[c]			-3.78[c]	

[a] LDA (GGA) notation means that the same LDA (GGA) functional is used both for geometry optimization and cohesive energy calculation; GGA//LDA notation specifies GGA energies calculated in a single point fashion for the LDA-optimized geometries.
[b] Octahedral starting geometry; cuboctahedral one for all other particles
[c] Experimental values from Ref. [57]

UNIVERSITAT ROVIRA I VIRGILI
MODELLING AU CATALYST FROM BULK TO NANOSCALE
Alberto Roldán Martínez
ISBN:978-84-693-7669-0/DL:T-1748-2010

Comparison of the present E_c(GGA) values for Au_n species ($n \leq 147$) with results of another VASP study [22] (introduced first as total energies of Au_n per atom, but subsequently compared with the E_c energies from Ref. [19]) reveals excellent agreement, with average energy deviations of ∼0.01eV. Only for Au_{116} was the value of −2.59eV [22], 0.05eV higher than E_c(GGA) = −2.64eV that we obtained. However, if the energies from Ref. [22] are indeed total energies per atom, they would only fit our energies after a systematic offset by 0.15eV—total spin-polarized PW91 energy of single Au atom. Interestingly, this offset brings the calculated total PW91 energy per atom for Au bulk, −3.20eV [22], in perfect agreement with the corresponding present E_c value −3.06eV (Table 2). Important finding is that our E_c(LDA) values for Au_n species (Table 2) in comparison with those for Au_{38}, Au_{44} and Au_{55} available from all-electron scalar relativistic calculations [19] agree basically quantitatively, with a systematic deviation of only ∼0.05eV, despite considerable differences in the two computational procedures. This justifies that even for such relativistic element as Au the present approximation of relativistic effects at the PAW VASP level is sufficiently reliable also for description of the Au–Au bond energies.

Electronic structure

Finally, we comment on the size dependence of the electronic structure of nanoparticles and how it approaches that of the bulk for all three studied coinage metals. We present and analyse the electronic structure in terms of the density of states (DOS). Note that the DOS peculiarities are responsible for major differences in the particle reactivity and thus could have very important implications for catalysis. Another aspect of even more general interest is how the bulk-like electronic properties are developed for nanoparticles of a particular metal when their size is increasing. In other words, the issue of interest is at which size range the particles start to behave not as large "molecules" with discrete electronic levels but rather as the smallest pieces of bulk featuring metallic electronic structure.

First we examined how the band smearing approximation of VASP (applied to converge electron density) affects the DOS plots. For that we compared DOS plots for Ag nanoparticles and bulk computed with the standard smearing of 0.20eV (see Sect. 2) and reduced one of 0.05eV. The results can be found in the Electronic Supplementary Material (ESM), in Fig. S1. For the bulk Ag and the largest particle Ag_{140} the effect of the smearing value is negligible and minor, respectively. However, for the smallest Ag_{38} species its molecular character is partially hidden when the smearing 0.20 eV is applied. So, we have chosen to plot all DOS with the smearing 0.05 eV. Also, characteristic features of DOS depend on the exchange-correlation functional. We studied this dependence for Ag_n particles and Ag bulk, by comparing DOS plots, positions of the d-band centre and numbers of states at the Fermi level calculated using GGA, GGA//LDA and LDA approaches; the comparison of GGA vs. GGA//LDA estimates the geometry uncertainty, whereas the GGA//LDA vs. LDA comparison (done for the same geometries) reveals a direct effect of the functional. Despite quantitative differences (see ESM, Fig. S2), trends in the DOS plots calculated at the GGA level appear to be representative. Thus, in the following we only discuss the GGA results.

In Fig. 4 GGA DOS plots for se-

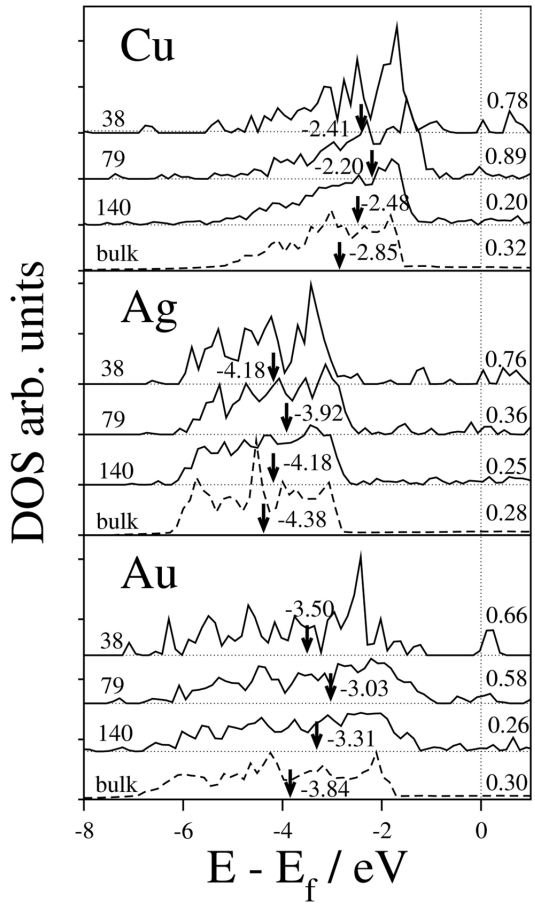

Figure 4: GGA density of states (DOS) plots for selected coinage metal nanoparticles M_n of increasing size (n = 38, 79, 140; M = Cu, Ag, Au; *solid lines*) compared to the corresponding plot for bulk metal M (*dashed line*). *Arrows* and *numbers* near them indicate centres of the valence d-bands. DOS values per atom at the Fermi level E_f are also shown

lected coinage metal nanoparticles M_n of increasing size (n = 38, 79, 140; M = Cu, Ag, Au) are compared to each other and to the plots for the bulk metals. Molecular character of all M_{38} species is clearly seen already at the first glance, for instance, from the quite extended regions of the zero DOS amplitude at the right-hand side of the energy scale; this is contrary to the essentially constant DOS values of bulk metals in these regions. In general, Fig. 4[6] manifests fast enough evolution of the DOS towards the bulk with increasing particle size. An important question is at which size the particles become sufficiently large, so that their DOS parameters monotonously approach those of the bulk. As an indicator of the DOS evolution with particle size we have chosen positions of the centre of valence d-bands, corresponding to the half of the cumulative d-projected density of states integrated till the Fermi level (see vertical arrows and numbers near them in Fig.

[6]See also Fig 5, that was not included in the present paper.

UNIVERSITAT ROVIRA I VIRGILI
MODELLING AU CATALYST FROM BULK TO NANOSCALE
Alberto Roldán Martínez
ISBN:978-84-693-7669-0/DL:T-1748-2010

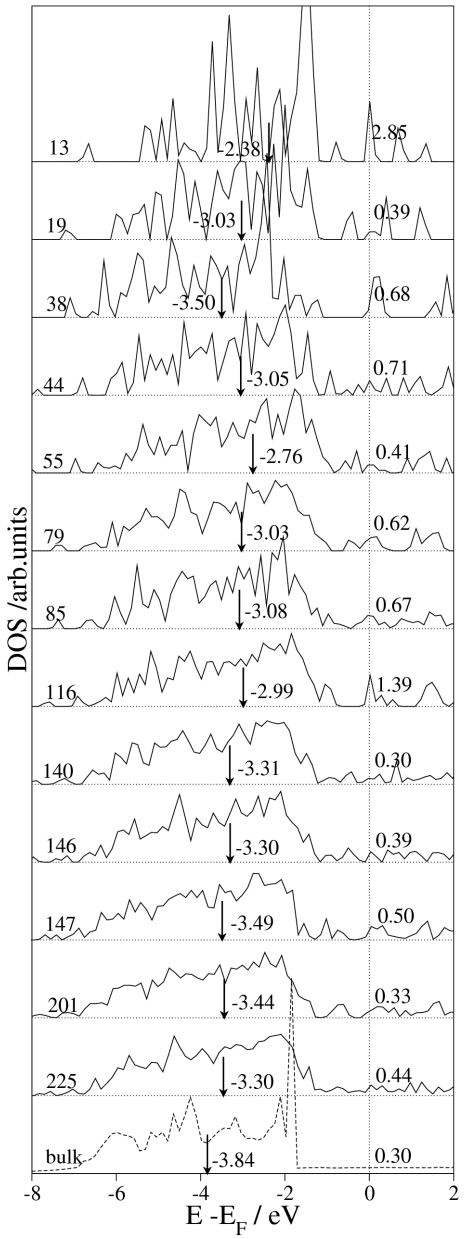

Figure 5: GGA density of states for whole set of Au_n clusters ($n < 225$) and Au bulk.

4). For all M_n species under scrutiny, starting from n = 79, this indicator goes monotonously with increasing n from the values for isolated atoms (not shown) down to the bulk values. On the other hand, the smallest members of the series, M_{38} species, do not follow this trend, in agreement with their above-mentioned molecular character. From this observation one can conclude that for coinage

metal particles the onset of scalable-to-bulk properties (here, based on evolution of DOS parameters) requires about 80 atoms, similarly to what has been found for Pd nanoparticles based on the evolution of the adsorption properties [23]. Finally, DOS values per metal atom calculated for M_n species at the Fermi level E_f , also presented in Fig. 4, provide further evidence for the close similarity of the electronic structure of M_{140} particles and the bulk M as well as for noticeable differences with the electronic structure of M_{38} "molecules". However, this indicator of the electronic structure alteration appears to be less reliable and characteristic than the just discussed centre of the d-band.

Summary and conclusion

Results of systematic density functional plane-wave calculations carried out for series of coinage metal particles containing up to 146 (Cu, Ag) and 225 (Au) atoms are presented. Full LDA and GGA geometry optimization has been performed for all particles starting from octahedral or cuboctahedral structures created by cuts from the metal bulk. Performance of the GGA, LDA and GGA//LDA schemes for the description of geometric and energetic parameters of the metal nanoparticles as well as trends along the group of the Periodic Table is critically evaluated. At variance with 3d metal Cu, GGA does not reveal definitely better accuracy than LDA for heavier 4d metal Ag and, especially, 5d congener Au. Applicability of the combined GGA//LDA scheme is corroborated. In line with previous studies (mainly of Pd and Au nanoparticles), calculated average nearest neighbour distances and cohesive energies of the particles are found to depend linearly on such size-derived parameters as the average coordination number of metal atoms and the inverse of the mean particle radius, respectively. Rather accurate linear extrapolation of the observables under scrutiny to the bulk values has been achieved. However, the scalability for particles made of various elements of the same $d^{10}s^1$ electron configuration differs, e.g. for bond lengths in Au_n species it is noticeably less perfect than in case of Cu_n and Ag_n. The correlations established in this work allow one to quantitatively predict binding energies of coinage metal nanoparticles filling the gap between the currently computationally tractable particles of up to 100–200 atoms and larger ones, parameters of which more closely approach the bulk ones. Particle electronic structure evolution towards the bulk with their increasing size has been discussed; we show that in order for the DOS parameters start to be scalable to those of the bulk the particles should contain about 80 or more coinage metal atoms. Implications of detected structural peculiarities of the nanoparticles for their reactivity are outlined. Especially important for future applications of the plane-wave approach is an excellent agreement of the present interatomic distances and the binding energies of Au_n particles with data of previous benchmark all-electron scalar relativistic calculations. Among advantages of the present plane-wave approach is its applicability in an almost routine fashion and without symmetry restrictions to tically mimic crystallites present in metal catalysts and their reactivity.

Acknowledgements

This article is dedicated to Prof. Nino Russo in the occasion of his 60th birthday. FV and AR thank the Spanish Ministry of Education and Science (MEC) and Universitat Rovira

i Virgili, respectively, for supporting their pre-doctoral research. Financial support has been provided by the MEC (grants CTQ2005-08459- CO2-01, CTQ2005-08459-CO2-02, UNBA05-33-001, HA2006-0102) and the Generalitat de Catalunya (2005SGR00697, 2005SGR-00104, 2005 PEIR 0051/69 and Distinció per a la Promoció de la Recerca Universitària granted to FI). Computational time on the Marenostrum supercomputer of the Barcelona Supercomputing Center is gratefully acknowledged.

References

[1] B. Brushan, Springer Handbook of Nanotechnology, Springer, Berlin, 2007.

[2] H.G. Yang, C.H. Sun, S.Z. Qiao, J. Zou, G. Liu, S. Smith, H.M. Cheng, and G.Q. Lu, Anatase TiO2 single crystals with a large percentage of reactive facets, Nature 453 (2008), pp. 638–641.

[3] S. Iijima and T. Ichihashi, Singel-shell calbon nanotubes of 1-nm diameter, Nature 363 (1993), pp. 603–605.

[4] A. Thess, R. Lee, P. Nikolaev, H.J. Dai, P. Petit, J. Robert, C.H. Xu, Y.H. Lee, S.G. Kim, A.G. Rinzler, D.T. Colbert, G.E. Scuseria, D. Tomanek, J.E. Fischer, and R.E. Smalley, Crystalline ropes of metallic carbon nanotubes, Science 273 (1996), pp. 483–487.

[5] R.H. Baughman, A.A. Zakhidov, and W.A. de Heer, Carbon nanotubes – the route toward applications, Science 297 (2002), pp. 787–792.

[6] N. Wang, Y. Cai, and R.Q. Zhang, Growth of nanowires, Mater. Sci. Eng. R. 60 (2008), pp. 1–51.

[7] Z. Tang, N.A. Kotov, and M. Giersig, Spontaneous organization of single CdTe nanoparticles into luminescent nanowires, Science 297 (2002), pp. 237–240.

[8] M.S. Gudiksen, L.J. Lauhon, J. Wang, D.C. Smith, and C.M. Lieber, Growth of nanowire superlattice structures for nanoscale photonics and electronics, Nature 415 (2002), pp. 617–620.

[9] F. Patolsky and C.M. Lieber, Nanowire nanosensors, Mater. Today 8 (2005), pp. 20–28.

[10] D. Wang, F. Qian, C. Yang, Z. Zhong, and C.M. Lieber, Rational growth of branched and hyperbranched nanowire structures, Nano Lett. 4 (2004), pp. 871–874.

[11] Z.W. Pan, Z.R. Dai, and Z.L. Wang, Nanobelts of semiconducting oxides, Science 291 (2001), pp. 1947–1949.

[12] X.F. Duan, Y. Huang, Y. Cui, J.F. Wang, and C.M. Lieber, Indium phosphide nanowires as building blocks for nanoscale electronic and optoelectronic devices, Nature 409 (2001), pp. 66–69.

[13] M.C. Daniel and D. Astruc, Gold nanoparticles: assembly, supramolecular chemistry, quantum-size-related properties, and applications toward biology, catalysis, and nanotechnology, Chem. Rev. 104 (2004), pp. 293–346.

[14] M. Hu, J. Chen, Z.Y. Li, L. Au, G.V. Hartland, X. Li, M. Marquez, and Y. Xia, Gold nanostructures: engineering their plasmonic properties for biomedical applications, Chem. Soc. Rev. 35 (2006), pp. 1084–1094.

[15] H. Ohnishi, Y. Kondo, and K. Takayanagi, Quantized conductance through individual rows of suspended gold atoms, Nature 395 (1998), pp. 780–790.

[16] N. Pazos-Perez, D. Baranov, S. Irsen, M. Hilgendorff, L.M. Liz- Marzan, and M. Giersig, Synthesis of flexible, ultrathin gold nanowires in organic media, Langmuir 24 (2008), pp. 9855–9860.

[17] A. Halder and N. Ravishankar, Ultrafine single-crystalline gold nanowire arrays by oriented attachment, Adv. Mater. 19 (2007), pp. 1854–1858.

[18] L. Zhang, Y. Fang, and P. Zhang, Experimental and DFT theoretical studies of SERS effect on gold nanowires array, Chem. Phys. Lett. 451 (2007), pp. 102–105.

[19] Z. Huo, C.K. Tsung, W. Huang, X. Zhang, and P. Yang, Sub-two nanometer single crystal Au nanowires, Nano Lett. 8 (2008), pp. 2041–2044.

[20] X. Lu, M.S. Yavuz, H.Y. Tuan, B.A. Korgel, and Y. Xia, Ultrathin gold nanowires can be obtained by reducing polymeric strands of Oleylamine-AuCl complexes formed via aurophilic interaction, J. Am. Chem. Soc. 130 (2008), pp. 8900–8901.

[21] K. Biswas, Y. Qin, M. DaSilva, R. Reifenberger, and T. Sands, Electrical properties of individual gold nanowires arrayed in a porous anodic alumina template, Phys. Stat. Sol. A 204 (2007), pp. 3152–3158.

[22] V. Rodrigues, T. Fuhrer, and D. Ugarte, Signature of atomic structure in the quantum conductance of gold nanowires, Phys. Rev. Lett. 85 (2000), pp. 4124–4127.

[23] C. Wang, Y. Hu, C.M. Lieber, and S. Sun, Ultrathin Au nanowires and their transport properties, J. Am. Chem. Soc. 130 (2008), pp. 8902–8903.

[24] N.A. Melosh, A. Boukai, F. Diana, B. Gerardot, A. Badolato, P.M. Petroff, and J.R. Heath, Ultrahigh-density nanowire lattices and circuits, Science 300 (2003), pp. 112–115.

[25] Y. Zhang, L. Giordano, and G. Pacchioni, Gold nanostructures on TiOx/Mo(112) thin films, J. Phys. Chem. C 112 (2008), pp. 191–200.

[26] E.Z. Da Silva, F.D. Novaes, A.J.R. Da Silva, and A. Fazzio, Theoretical study of the formation, evolution, and breaking of gold

nanowires, Phy. Rev. B 69 (2004), pp. 1–11. [27] L. Xiao, B. Tollberg, X. Hu, and L. Wang, Structural study of gold clusters, J. Chem Phys. 124 (2006), pp. 1–10.

[28] Y. Mokrousov, G. Bihlmayer, and S. Blugel, Full-potential linearized augmented plane-wave method for one-dimensional systems: gold nanowire and iron monowires in a gold tube, Phys. Rev. B 72 (2005), pp. 1–15.

[29] H. Mehrez and H. Guo, Theoretical study of nanowires, Nanowires Nanobelts 1 (2003), pp. 95–124.

[30] J. Nakamura, N. Kobayashi, S. Watanabe, and M. Aono, Structural stability and electronic states of gold nanowires, Surf. Sci. 482 (2001), pp. 1266–1271.

[31] Y. Fujimoto and K. Hirose, First-principles theory for the calculation of electron-transport properties of metallic nanowires, Nanotechnology 14 (2003), pp. 147–151.

[32] S. Zalis, I. Kratochvilova, A. Zambova, J. Mbindyo, T.E. Mallouk, and T.S. Mayer, Combined experimental and theoretical DFT study of molecular nanowires negative differential resistance and interaction with gold clusters, EPJ E 18 (2005), pp. 201–206.

[33] X. Yin, Y. Li, Y. Zhang, P. Li, and J. Zhao, Theoretical analysis of geometry-correlated conductivity of molecular wire, Chem. Phys. Lett. 422 (2006), pp. 111–116.

[34] F. Vines, F. Illas, and K.M. Neyman, On the mechanism of formation of metal nanowires by self-assembly, Ang. Chem. Int. Edit. 46 (2007), pp. 7094–7097.

[35] I.V. Yudanov, R. Sahnoun, K.M. Neyman, N. Rösch, J. Hoffmann, S. Schauermann, V. Johanek, H. Unterhalt, G. Rupprechter, J. Libuda, and H.J. Freund, CO adsorption on Pd nanoparticles. Density functional and vibrational spectroscopy studies, J. Phys. Chem. B 107 (2003), pp. 255–264.

[36] I.V. Yudanov, K.M. Neyman, and N. Rösch, Density functional study of Pd nanoparticles with subsurface impurities of light element atoms, Phys. Chem. Chem. Phys. 6 (2004), pp. 116–123.

[37] K.M. Neyman, R. Sahnoun, C. Inntam, S. Hengrasmee, and N. Ro¨sch, Computational study of model Pd–Zn nanoclusters and their adsorption complexes with CO molecules, J. Phys. Chem. B 108 (2004), pp. 5424–5430.

[38] A. Roldan, F. Vines, F. Illas, J.M. Ricart, and K.M. Neyman, Density functional studies of coinage metal nanoparticles: scalability of their properties to bulk, Theoret. Chem. Acc. 120 (2008), pp. 565–573.

[39] I.V. Yudanov, K.M. Neyman, and N. Rösch, CZO bond scission of methoxide on Pd nanoparticles: a density functional study, Phys. Chem. Chem. Phys. 8 (2006), pp. 2396–2401.

[40] K.M. Neyman, G.N. Vayssilov, and N. Rösch, Transition metal clusters and supported species with metal-carbon bonds from first-principles quantum chemistry, J. Organomet. Chem. 689 (2004), pp. 4384–4394.

[41] S.H. Vosko, L. Wilk, and M. Nusair, Accurate spin-dependent electron liquid correlation energies for local spin density calculations: a critical analysis, Can J. Phys. 58 (1980), pp. 1200–1211.

[42] J.P. Perdew and Y. Wang, Erratum: pair-distribution function and its coupling-constant average for the spin-polarized electron gas [Phys. Rev. B 46, 12 947 (1992)], Phys. Rev. B 56 (1997), p. 7018.

[43] P.E. Blochl, Projector augmented wave method, Phys. Rev. B 50 (1994), pp. 17953–17979.

[44] G. Kresse and D. Joubert, From ultrasoft pseudopotentials to the projector augmented-wave method, Phys. Rev. B 59 (1999), pp. 1758–1775.

[45] G. Kresse and J. Furthmuller, Efficiency of ab-initio total energy calculations for metals and semiconductors using a plane-wave basis set, Comput. Mater. Sci. 6 (1996), pp. 15–50.

[46] G. Kresse and J. Furthmueller, Efficient iterative schemes for ab initio total-energy calculations using a plane-wave basis set, Phys. Rev. B 54 (1996), pp. 11169–11186.

[47] B. Hammer and J.K. Norskov, Theoretical surface science and catalysis – calculations and concepts, Adv. Catal. 45 (2000), pp. 71–129.

[48] A. Corma, M. Boronat, S. Gonzalez, and F. Illas, On the activation of molecular hydrogen by gold: a theoretical approximation to the nature of potential active sites, Chem. Commun. 32 (2007), pp. 3371–3373.

[49] A. Roldan, S. Gonzalez, J.M. Ricart, and F. Illas, Critical size for O_2 dissociation by Au nanoparticles, ChemPhysChem 10 (2009), pp. 348–351.

[50] R.F.W. Bader, Atoms in Molecules: A Quantum Theory, Oxford Science, Oxford, 1990.

UNIVERSITAT ROVIRA I VIRGILI
MODELLING AU CATALYST FROM BULK TO NANOSCALE
Alberto Roldán Martínez
ISBN:978-84-693-7669-0/DL:T-1748-2010

UNIVERSITAT ROVIRA I VIRGILI
MODELLING AU CATALYST FROM BULK TO NANOSCALE
Alberto Roldán Martínez
ISBN:978-84-693-7669-0/DL:T-1748-2010

3.4.2 Critical size for O_2 dissociation by Au nanoparticles

Corresponding to: Roldan, A.; Gonzalez, S.; Ricart Josep, M.; Illas, F. ChemPhysChem 2009, 10, 348-51.

Introduction

Since the earlier discoveries of Haruta,[1] and Goodman,[2] catalysis by gold nanoparticles has become a very active field of research and a continuous source of surprises.[3,4] In fact, from the initial low-temperature catalyzed CO oxidation,[1,2] important discoveries have been made concerning the water–gas shift reaction,[5,6] difficult chemoselective hydrogenations[7] and, even more recently, selective oxidation of olefins with[8] or without initiators.[9] The available literature is colossal but, as pointed out by Hashmi and Hutchings,[3] different groups prepare catalysts in different ways and test them under different conditions. This provides a large amount of important, but not systematic, information. Nevertheless, a common feature from all reported work concerning catalysis by Au supported particles is their small dimension[1,2] with compelling evidence that beyond a certain size gold particles become as inactive as the bulk metal.[3]

The catalytic activity of gold nanoparticles has been attributed to various effects such as the presence of low coordinated atoms, electronic confinement, particle shape, and, more importantly, to support effects (see ref. [3] and references therein). Recently, it has been shown that the activity of Au nanoparticles supported on TiC(001) towards SO_2 splitting is much larger than when supported on MgO or TiO_2.[10] Nevertheless, a guide to synthesis requires proper understanding and disentangling size and support effects. Herein we use a series of models which allow us explore purely size effects alone which thus isolates the particle effects from those introduced by the support.

In the case of hydrogenation reactions it seems clear that the activity of Au nanoparticles is due to the availability of low-coordinated sites that efficiently split molecular hydrogen without noticeable energy barriers.[11] However, in the case of oxidation reactions the information is more scattered with claims that catalytic activity relies on the increase of low-coordinated sites with the decrease of the particle size,[12] although the evidence comes from the study of stepped surfaces and of small Au_{10} clusters only[13] or from indirect experimental support.[14] Wang and Gong[15] found that an icosahedral Au_{32} cluster can dissociate molecular oxygen but without describing the dissociation pathway and the corresponding energy barriers. Barrio et al.[16] also found that small Au clusters (Au_{14}, Au_{25} and Au_{28}) activate O_2 but, again, details about O_2 dissociation are not given. As in the experiments, the models used by

each group are different hampering the extraction of general conclusions. Here, we report results of a systematic density functional theory study (see Methods Section) of the interaction and dissociation of O_2 on a monoatomic Au row (nanorow) model,[11] and on Au_{25}, Au_{38}, Au_{55} and Au_{79} nanoparticles (Figure 1). Previous work[17] has shown that the methodology used leads to results which are very close to those obtained from fully relativistic all electron calculations[18] and that beyond Au_{79} the electronic properties linearly scale to the bulk[17] and, therefore, the catalytic activity dies out.[1–3] Calculations for the interaction of O_2 on the Au(111) and Au(100) single crystal surfaces have been also carried out for comparison.

Computational approach

The nanorow model is constructed from a (5×5) supercell slab model from Au(111) surface with five atomic layers and removing four rows from the first layer and three rows of the second one. The Au nanoparticles chosen in this work are three-dimensional (3D) metal crystallites cut from metal bulk by low-index planes and have the typical cuboctahedral (Au_{38}, Au_{55} and Au_{79}) shape of Au-supported clusters.[3] The Au_{25} is derived from Au_{38} by removing two (100) atomic layers to provide a hemispherical particle also similar to those found in experiments.[3] In this way, the nanoparticles used in the present work have diameter (estimated using the Au covalent radius) in the ∼1.0 to ∼2.0 nm range. Note that all models include low coordinate Au atoms thus allowing one to explore the reactivity towards O_2 as a function of the particle size. The structure of the particles has been fully optimized and O_2 has been added in all possible coordination ways on the facets and edges of the Au models described previously (almost 30 initial geometries have been tried for O_2 on Au_{55}) and the structure fully relaxed again. For each one of the stable coordination modes a vibrational analysis was carried out to reveal that these structures were minima in their corresponding potential energy surface with respect to any displacement of the oxygen atoms. Next, nudged elastic band (NEB) calculations were carried out using these stable structures as starting point and dissociated O_2 (adsorbed atomic O in the corresponding sites) as final state. These calculations allowed us to locate the transition states for the dissociation pathway; which were characterized by appropriate vibrational analysis, and the corresponding energy barriers. All relevant data has been compiled in the Supporting Information. The adsorption and energy barriers discussed hereafter have been all corrected to account for the zero point energy.

Density functional theory based calculations have been carried out for molecular oxygen interacting with various Au nanoparticles and for extended models containing low-coordinated Au atoms as in ref. [11]. Slab models, containing five atomic layers separated by a 10Å vacuum width, have been used to represent the Au(111) and Au(100) surfaces which have also been considered for comparison. The interaction of molecular oxygen with each model and the corresponding dissociative pathway has been studied using a supercell approach with the repeated images separated by a large vacuum width (>10Å) and the energy was evaluated using the PW91 functional. Spin polarization has been tested in a few cases and found to be unimportant, except, obviously for molecular oxygen. Molecular oxygen is adsorbed in all possible ways, all geometries are fully relaxed and the dissociation pathway to adsorbed oxygen atoms deter-

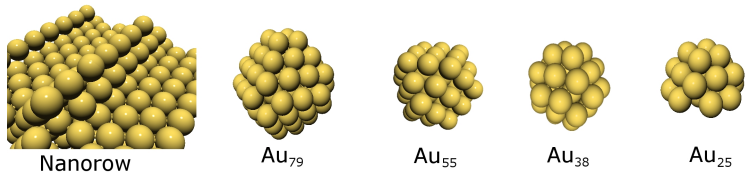

Figure 1: The nanorow and different nanoparticles models used to study O_2 dissociation.

mined by means of the climbing image-nudged elastic band, CI-NEB method.[19] Transition state structures thus located have been characterized by small enough forces in the atoms and a subsequent vibrational analysis. The PAW method[20] was used to represent the inner cores and one electron states were expanded in a plane wave basis with a kinetic cut-off energy of 415 eV. Calculations were performed using the VASP package.[21–23] A proper Monkhorst-Pack[24] grid of special k-points has been used for the calculations on the extended systems whereas only the $\Gamma-$point has been considered for those corresponding to discrete nanoparticles.

Results and discussion

The interaction of O_2 with the different models is quite different from that corresponding to the flat Au(111) surfaces. In fact, the presence of low-coordinates atoms is enough to adsorb O_2 quite strongly. For the nanorow model, two different states are found for chemisorbed O_2 with bonding energies (BE) of 0.56 and 0.92 eV. Four states have been characterized for O_2 on Au_{79} with BEs ranging from 0.12 to 0.31 eV. Thus, a small particle does not necessarily mean a strong interaction. In fact, going to Au_{55} the O_2 BEs range from 0.04 to 0.12 eV. However, the trend changes completely when considering Au_{38} where the bonding energy is between 0.90 and 0.96 eV with four different coordination modes (see Supporting Information). Finally, two strong coordination modes with BEs of 0.48 and 1.33 eV have also been found for O_2 on the Au_{25} nanoparticle. An additional aspect of the structure of O_2 adsorbed in the nanorow and nanoparticle models, which is relevant to catalytic oxidation, involves the interatomic O-O distance (d_{O-O}). In all cases, favorable adsorption is accompanied by a significant increase of d_{O-O} from its gas-phase equilibrium value in the triplet ground state (1.244 calculated and 1.207 from experiment[25]) with values ranging from 1.312 for the nanorow to 1.452 for Au_{38} and 1.462 for Au_{79}. From these results one may argue that, upon adsorption, the O_2 molecule is activated and ready for dissociation. Note, however, calculations show that on the Au(111) and Au(100) surfaces d_{O-O} becomes 1.354 and 1.339 even if adsorption is endothermic and the energy barrier for O_2 dissociation larger than 1.5 eV! Clearly, d_{O-O} cannot be considered as a good predictor of the catalytic activity of these Au systems towards O_2 dissociation. An alternative possibility; which indeed could be used in experiments, consists in analyzing the O-O stretching frequency (ν_{O-O}). Again, interaction of O_2 with the different Au systems results in a significant decrease of the ν_{O-O} with respect to the gas phase reference (1520 cm^{-1} calculated versus 1556 cm^{-1} experimental[25]). Interestingly, the interaction of the O_2 molecule with the nanorow model and with the different nanoparticles leads to a significant shift with values in the 690–1120 cm^{-1} range. Unfortunately, this vibra-

UNIVERSITAT ROVIRA I VIRGILI
MODELLING AU CATALYST FROM BULK TO NANOSCALE
Alberto Roldán Martínez
ISBN:978-84-693-7669-0/DL:T-1748-2010

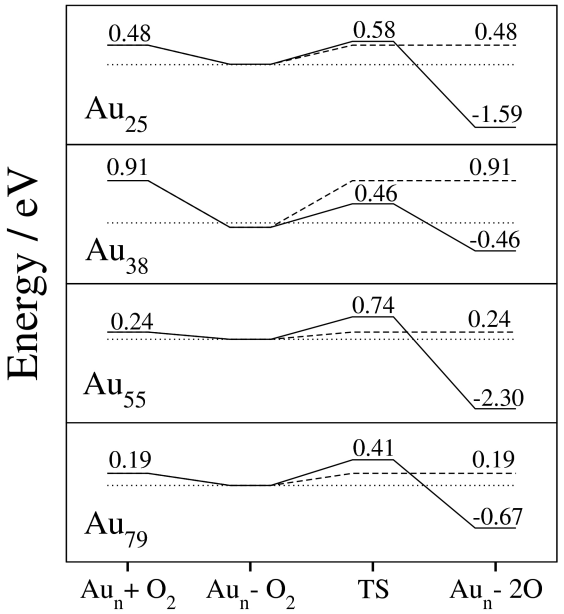

Figure 2: Most favorable energy profile for O_2 dissociation on the Au_{25}, Au_{38}, Au_{55} and Au_{79} nanoparticles. The two products on the right-hand side correspond to O_2 desorption and O(ads)+O(ads), upper and lower, respectively. Note that the zero energy has been set up for the molecular O_2 adsorbed on the corresponding Au nanoparticle. On the right, the dashed lines indicate desorption and the solid lines dissociation.

tional shift cannot be taken as a measure of O_2 activation towards dissociation because a similar shift is calculated when the molecules are placed on the Au(111) and Au(100) slab models. Note, however, that in these cases O_2 adsorption is endothermic and these data cannot be obtained from experiment. Consequently, neither d_{O-O} nor ν_{O-O} can be used to predict the activation of molecular oxygen adsorbed on Au nanoparticles. Therefore, locating the corresponding transition state (TS) and energy barrier (EB) seems to be unavoidable.

For each one of the stable structures in the nanorow model described above, the TS has been located and characterized. The corresponding energy barriers are, 1.44 and 1.57 eV, respectively and, hence, much larger than the energy required to desorb molecular oxygen. This result provides a first important conclusion. Contrarily to the case of H_2, the presence of low-coordinated sites is not enough to dissociate O_2. Next, let us analyze the energy profile for O_2 dissociation on the different nanoparticles. Figure 2, reports the most favorable profile for each substrate and clearly shows that, even in such a case, molecular oxygen dissociation on the isolated, cuboctahedral, Au_{55} and Au_{79} nanoparticles is not favored and molecular desorption will always take place before dissociation. There is compelling evidence that nanoparticles larger than Au_{79} are in the scalable regime and their properties vary linearly with size.[17] Therefore, it is possible to claim that, on those Au nanoparticles, O_2 desorption will also take place before dissociation. A very different situation is found for O_2 dissociation on the smaller Au_{25} and Au_{38} clusters. Let us discuss Au_{38} first since

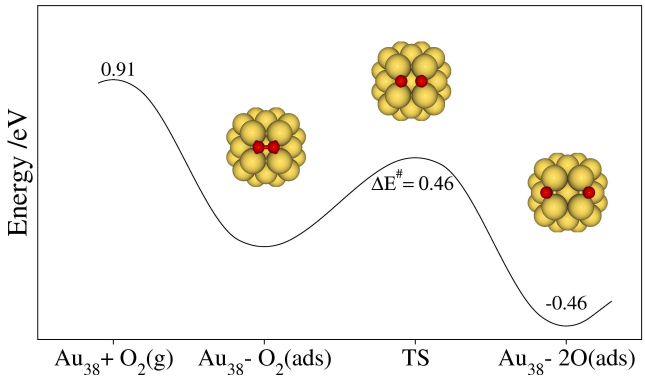

Figure 3: Atomic structure for the most favorable energy profile for O_2 dissociation on the Au_{38} nanoparticle. The zero energy is for the O_2 adsorbed state as in Figure 2.

it has a clear cuboctahedral structure. For the most favorable reaction pathway, the energy barrier for dissociation is 0.46 eV; a value which is similar and even larger to that computed for the Au_{79}. However, the difference is in the adsorption/desorption of molecular O_2, larger (in absolute value) than the energy barrier for Au_{38} and smaller than it for Au_{79}. Hence, large enough adsorption energy is a necessary condition for O_2 dissociation on Au clusters. However, the results for the nanorow model clearly show that this is not sufficient. The case of Au_{25} is also of interest, this cluster does not have a cuboctahedral structure since it is derived from Au_{38} as describe above. In this case the energy difference between the two pathways (desorption and dissociation) is of 0.1 eV only. Hence, a fraction of adsorbed molecules will dissociate and another fraction will desorb. Maintaining the equilibrium between the gas phase and adsorbed molecules will ensure a continuous rate for the dissociation process.

For all nanoparticles investigated in this work, calculations reveal that there is a common feature for the minimum energy pathway: the O_2 molecule is placed with the O atoms above bridge sites of a square in an (100) facet and d_{O-O} increases in such a way that the final state corresponds to O atoms in three-fold hollow sites of the (111) facets (Figure 3). Upon O_2 dissociation, and concomitant adsorption of two oxygen atoms, all particles suffer some degree of deformation which, as expected, increases with increasing the area of the (100) facets. The fact that the minimum energy pathway for the different particles is chemically similar indicates that the larger activity of Au_{25} and Au_{38} towards O_2 dissociation originates from electronic and not from geometric effects only. Indeed, these particles are the ones with larger difference in electronic structure with respect to the bulk as indicated in the density of states plots.[17] In other words, the small number of bulk like atoms is not enough to develop a band structure, and hence the particular electronic structure plays a key role.

Conclusions

In summary, the present theoretical study presents convincing evidence that 1) the presence of low-coordinate Au atoms is not enough to dissociate O_2 ; 2) strong adsorption of molecular oxygen on Au nanoparticles is a necessary but not sufficient condition for O_2 dissociation, 3)

there is a common pathway for O_2 dissociation and 4) there is a critical size for Au nanoparticles to dissociate O_2. This latter point deserves further comments, especially in the view of the recent work by the group of Lambert et al.[9] concerning O dissociation by supported Au nanoparticles derived from the Au_{55} cluster. These authors provide strong experimental evidence that Au nanoparticles derived from Au_{55} and deposited on inert supports are able to dissociate O_2. However, these authors show that the supported particles are spread in a range of sizes. The present results show that bare Au_{55} clusters cannot dissociate O_2. This is in agreement with the experimental evidence that these Au nanoparticles exhibit a particular chemical inertness[26] but seems to contradict the suggestion that they could be especially effective oxidation catalysts.[27] However, the present results are in agreement with the even more recent experimental work of Hutchings et al.[28] showing that subnanometer Au particles supported on FeO_x are active for CO oxidation. Therefore, we are led to the conclusion that the catalytic effect observed by Lambert et al.[9] arises from the presence of Au particles smaller than Au_{55} and we strongly suggest that new experiments are carried out attempting to make use of these smaller particles.

Acknowledgements

AR thanks Universitat Rovira i Virgili, for supporting his pre-doctoral research. Financial support has been provided by the Spanish Ministry of Science and Innovation (MCINN) (grants CTQ2005- 08459-CO2-01, CTQ2005-08459-CO2-02, UNBA05-33-001) and, in part, by the Generalitat de Catalunya (Grants 2005SGR00697, 2005SGR-00104 and 2005 PEIR 0051/69) Computational time on the Marenostrum supercomputer of the Barcelona Supercomputing Center is gratefully acknowledged.

References

[1] M. Haruta, Catal. Today 1997, 36, 153; Nature 2005, 437, 1098.

[2] M. Valden, X. Lai, D. W. Goodman, Science 1997, 281, 1647.

[3] A. Stephen, K. Hashmi, G. J. Hutchings, Angew. Chem. 2008, 118, 8064; Angew. Chem. Int. Ed. 2006, 45, 7896.

[4] See also the reviews in the special issue dedicated to chemistry of nano-gold in Chem. Soc. Rev. 2008, 37.

[5] Q. Fu, H. Saltsburg, M. Flytzani-Stephanopoulos, Science 2003, 301, 935.

[6] J. A. Rodriguez, S. Ma, P. Liu, J. Hrbek, J. Evans, M. Perez, Science 2007, 318, 1757.

[7] A. Corma, P. Serna, Science 2006, 313, 332.

[8] M. D. Hughes, Y. J. Xu, P. Jenkins, P. McMorn, P. Landon, D. I. Enache, A. F. Carley, G. A. Attard, G. J. Hutchings, F. King, E. H. Stitt, P. Johnston, K. Griffin, C. J. Kiely, Nature 2005, 437, 1132.

[9] M. Turner, V. B. Golovko, O. P. H. Vaughan, P. Abdulkin, A. Berenguer- Murcia, M. S. Tikhov, B. F. G. Johnson, R. M. Lambert, Nature 2008, 454, 981.

[10] J. A. Rodriguez, P. Liu, F. Vines, F. Illas, Y. Takahashi, K. Nakamura, Angew. Chem. 2008, 120, 6787; Angew. Chem. Int. Ed. 2008, 47, 6685.

[11] A. Corma, M. Boronat, S. Gonzlez, F. Illas, Chem. Commun. 2007, 3371.

[12] N. Lopez, T. V. W. Janssens, B. S. Clausen, Y. Xu, M. Mavrikakis, T. Bligaard, J. K. Nørskov, J. Catal. 2004, 223, 232.

[13] I. N. Remediakis, N. Lopez, J. K. Nørskov, Angew. Chem. 2005, 117, 1858; Angew. Chem. Int. Ed. 2005, 44, 1824.

[14] X. Deng, B. K. Min, A. Guloy, C. M. Friend, J. Am. Chem. Soc. 2005, 127, 9267.

[15] Y. Wang, X. Gong , J. Chem. Phys. 2006, 125, 124703.

[16] L. Barrio, P. Liu, J. A. Rodriguez, J. M. Campos-Martin, J. L. G. Fierro, J. Phys. Chem. C 2007, 111, 19001.

[17] A. Roldan, F. ViÇes, F. Illas, J. M. Ricart, K. M. Neyman, Theoret. Chem. Acc. 2008, 120, 565.

[18] O. D. Hberlen, S. C. Chung, M. Stener, N. Rösch, J. Chem. Phys. 1997, 106, 5189.

[19] G. Henkelman, B. P. Uberuaga, H. Jonsson, J. Chem. Phys. 2000, 113, 9901.

[20] P. E. Blochl, Phys. Rev. B 1994, 50, 17953.

[21] G. Kresse, J. Furthmller, Phys. Rev. B 1996, 54, 11169.

[22] G. Kresse, J. Hafner, Phys. Rev. B 1993, 47, 558.

[23] G. Kresse, J. Furthmller, Comp. Mater. Sci. 1996, 6, 15.

[24] H. J. Monkhorst, J. D. Pack, Phys. Rev. B 1976, 13, 5188.

[25] K. P. Huber, G. Herzberg, Molecular Spectra and Molecular Structure IV. Constants of Diatomic Molecules 1979, New York, Van Nostrand Reinhold.

[26] G. Schmid, Chem. Soc. Rev. 2008, 37, DOI: 10.1039/b713631p.

[27] H.-G. Boyen, G. Kstle, F. Weigl, B. Koslowski, C. Dietrich, P. Ziemann, J. P. Spatz, S. Riethmller, C. Hartmann, M. Moller, G. Schmid, M. G. Garnier, P. Oelhafen, Science 2002, 297, 1533.

[28] A. A. Herzing, C. J. Kiely, A. F. Carley, P. Landon, G. J. Hutchings, Science 2008, 321, 1331.

UNIVERSITAT ROVIRA I VIRGILI
MODELLING AU CATALYST FROM BULK TO NANOSCALE
Alberto Roldán Martínez
ISBN:978-84-693-7669-0/DL:T-1748-2010

UNIVERSITAT ROVIRA I VIRGILI
MODELLING AU CATALYST FROM BULK TO NANOSCALE
Alberto Roldán Martínez
ISBN:978-84-693-7669-0/DL:T-1748-2010

3.4.3 Influence of the exchange–correlation potential on the description of the molecular mechanism of oxygen dissociation by Au nanoparticles

Corresponding to: Roldan, A.; Ricart, J. M.; Illas, F. Theoretical Chemistry Accounts 2009, 123, 119-126.

Introduction

The discovery that Au nanoparticles with diameter in the range 1–10 nm exhibit unexpected catalytic properties, such as the low temperature oxidation of CO [1–23] has triggered a renewed gold rush [2,4], but now the chemical activity of this noble element and its possible use in practical applications in the chemical industry being the key question. In fact, the possible use of Au in catalysis is now being actively investigated for both heterogeneously and homogeneously catalyzed reactions [5–7]. For the former, significant advances have been achieved in the recent years for various technologically or environmentally relevant reactions. For instance, one can mention carbon–carbon bond formation and reactions of alkynes and alkenes [8–10], the water gas shift reaction catalyzed by Au supported on ceria [11, 12], the challenging chemoselective reduction of nitro groups on mild conditions catalyzed by Au supported on anatase, which, in addition, provides a route for the synthesis of the industrially relevant cyclohexanone oxime from 1-nitro-1-cyclohexene [13] and selective oxidation of olefins by initiators or oxidant agents such as hydrogen peroxide or adsorbed OOH intermediates [14–16] or, even more recently, directly by dioxygen [17].

The analysis of the existing literature reveals that one of the critical parameters is the small dimension of the gold nanoparticles [5] although support effects have been found to play also a key, and more important than earlier imagined, role [18]. For example, the dissociation of SO_2 on Au nanoparticles supported on TiC(100) takes place readily and the process is more efficient than when the Au nanoparticles are supported on TiO_2(110) and this system is in turn much more efficient than when the support consist of MgO(100) [19]. In a similar way, chemoselective hydrogenation of substituted nitroaromatics implies a subtle interaction between the gold nanoparticles and the support [20] and this can be tuned to transform non selective into chemoselective metal catalysts [21]. From these recent contributions it seems clear that the complexity of gold supported catalysts appears to be higher than imagined, being governed not solely by size effects of the supported gold nanoparticle. Therefore, isolating support from particle effects provides a precise knowledge of the intrin-

sic reactivity of nanosized gold nanoparticles that it is likely to open a way to improve the properties of gold supported catalysts. For the hydrogenation reactions, the first step implies molecular hydrogen dissociation and it has been recently shown that the necessary and sufficient condition for this process to occur on gold nanoparticles is the presence of low coordinated gold atoms [22]. This conclusion is derived from density functional theory based calculations carried out on a series of Au nanoparticles and of Au stepped surfaces which show that low coordinated Au atoms efficiently split molecular hydrogen without noticeable energy barriers. Here, the need for nanosized nanoparticles seems to be important just to maximize the number of these active sites. The case of selective oxidation reactions catalyzed by gold nanoparticles seems to be more complicated and the particular activity of Au nanoparticles attributed to different origins. Hence, some authors suggested that the enhanced catalytic activity of small Au nanoparticles is due to the increase of low coordinated sites with the decrease of the particle size [23]. However, these conclusions come from the study of stepped surfaces and of a small Au_{10} cluster only [24] or from a rather indirect experimental evidence [25]. Several other authors have also used density functional theory calculations to address the problem of molecular oxygen dissociation by Au nanoparticles but the available information is quite scattered and non systematic. Thus, Wang and Gong [26] found that an icosahedral Au_{32} cluster is able to dissociate molecular oxygen but the dissociation pathway and the corresponding energy barriers were not reported. A more systematic work is reported by Barrio et al. [27] who also found that small Au clusters (Au_{14}, Au_{25} and Au_{28}) activate O_2 but, again, without providing details about the molecular mechanism of O_2 dissociation. In a recent work, Turner et al. [17] have presented strong experimental evidence that Au nanoparticles derived from Au_{55} are able to dissociate molecular oxygen, the first step toward partial oxidation of styrene by dioxygen. However, these authors have also shown that the supported particles are spread in a range of sizes making it difficult to assign the observed catalytic activity to a particular particle or set of particles. Nevertheless, an important conclusion from this work is the firm conclusion that a sharp size threshold exist for the catalytic activity, and that particles with diameters of $\sim$2 nm and above are completely inactive.

In a recent work, density functional theory based calculations carried out for a series of models including Au nanoparticles, Au stepped and extended surfaces have lead to the conclusion that the presence of low coordinate Au atoms is not enough to dissociate O_2 and that there is a critical size for Au nanoparticles to dissociate O_2 [28]. These conclusions are based on the computed energy barriers obtained for molecular oxygen dissociation as a function of particle size and taking also into account the desorption energy of the adsorbed molecule. Nevertheless, one must be aware of the fact that these calculations are based on a given approximation to the exact unknown exchange–correlation potential and one may wonder whether the use of a different form for this potential may lead to qualitative changes in the description. For chemical reactions on extended metallic surfaces there is compelling evidence that differences in the adsorption energies, which may be large and are inherent to the use of a different form of the exchange–correlation potential, do not imply noticeable changes in the calculated reaction rates [29–31]. In the

present work, we investigate the influence of the exchange–correlation potential on the calculated energy barriers for the dissociation of molecular oxygen on several Au nanoparticles. We will show that, as in the case of extended surfaces [29–31], the adsorption energy depends rather strongly of the particular density functional theory method used. However, this dependence does not largely affect the calculated energy barriers and, as a consequence, previous conclusions about the critical size for molecular oxygen dissociation by Au nanoparticles are further supported.

Computational approach

The effect of the exchange–correlation potential ($E_{xc}[\rho]$) on the description of the molecular mechanism of O_2 dissociation on Au nanoparticles has been studied on Au_{25}, Au_{38} and Au_{79} nanoparticles using periodic density functional theory plane-wave calculations following the procedure previously used in [28]. Single particles have been modeled by placing them in the center of a large enough supercell, with a vacuum space of 1 nm in all directions to avoid interactions between species in the neighboring cells. The use of periodically repeated single particles may seem artificial to readers used to the methods of molecular quantum chemistry but it is a necessary requirement when using a plane-wave basis set, which span the whole space with the periodicity imposed by the chosen unit cell. Nevertheless, this supercell approach has been found to be an efficient way to study the atomic and electronic structure of rather large nanoparticles of coinage metals [32], Pd [33] or of ceria [34–36].

The calculations reported in the present work have been carried out using the VASP code [37, 38] and the total energy has been computed using the local density approach (LDA) to the $E_{xc}[\rho]$ [39], and three different forms of the generalized gradient approach (GGA). These are the widely used functional due to Perdew and Wang (PW91) [40–42], the so-called PBE functional [43] and the revision of the PBE due to Zhang and Yang [44] hereafter referred to as RevPBE. The PBE functional has been introduced to overcome six shortcomings of the PW91 one and includes an accurate description of the linear response of the uniform electron gas, correct behavior under uniform scaling, a smoother potential and a simpler form. The revision of the PBE exchange–correlation functional by Zhang and Yang intended to improve the PBE atomization energies although Hammer et al. [31] have later shown that this functional also leads to improved adsorption energies of atoms and molecules on transition metal surfaces. Here, it is important to point out that Hammer et al. [31] also proposed a slightly different form of the RevPBE, usually termed RPBE, which provides essentially the same results of the RevPBE but, in addition, fulfills the Lieb-Oxford criterion locally. Despite the fact that PW91 and PBE have different analytical forms, it is commonly assumed that they will produce essentially the same results and, consequently, it is hard to find papers where the two functionals are used and compared. However, there is also increasing evidence that these two functionals are not so equivalent when surface effects are present [45]. This is one of the reasons to investigate their performance in the description of molecular oxygen dissociation catalyzed by Au nanoparticles. The effect of the core electrons on the valence electron density was described by projector augmented wave (PAW) method [46] as implemented by Kresse and Joubert [47] and the cutoff

UNIVERSITAT ROVIRA I VIRGILI
MODELLING AU CATALYST FROM BULK TO NANOSCALE
Alberto Roldán Martínez
ISBN:978-84-693-7669-0/DL:T-1748-2010

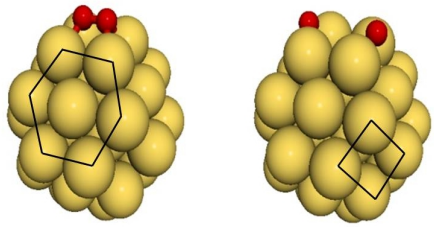

Figure 1: (left) Molecular oxygen adsorbed on Au_{38} (001) facet (square) and (right) atomic oxygen adsorbed on Au_{38} (111) facets (hexagon), respectively

for the kinetic energy of the plane-wave basis set has been set to 415 eV, considering only the Γ-point of the reciprocal space. This is a typical value for the cutoff energy and ensures that, for the purposes of the present work, the calculated energies are sufficiently converged [48–50]. Except for the RevPBE functional, total energy calculations were always carried out using the PAW core potentials derived from the $E_{xc}[\rho]$. For the calculations using the RevPBE functional we used the PBE derived PAW potentials. A Gaussian smearing technique with a 0.2eV width has been applied to enhance convergence but all energies presented below have been obtained by extrapolating to zero smearing (0 K).

The Au_{38} and Au_{79} particles have a cuboctahedral shape and were initially cut from the bulk so as to exhibit low index planes and their atomic structure fully optimized either in absence or presence of molecular oxygen. The Au_{25} particle is just one half of the Au_{38} unit and is representative of a supported particle. From the various possible ways of molecular adsorption and dissociation on different sites of these particles we have always considered the one which was found to be the minimum energy pathway. This involves the adsorption of the O_2 molecule with the O atoms above bridge sites of a square in an (100) facet and, next, the internuclear distance of the molecule (dO–O) increases in such a way that the final state corresponds to O atoms in threefold hollow sites of the (111) facets (Fig. 1). In order to better understand the effect of particle size on the adsorption energy of O_2, calculations were also carried out for a slab model representing the extended Au(001) surface. The Au(001) slab has been constructed using the lattice parameter corresponding to each functional, it contains four atomic layers interleaved with a vacuum width of 1 nm. The two outermost atomic layers have been always relaxed whereas the other two ones are fixed as in the bulk. For the interaction with O_2, a 5×5 supercell was used resulting in a coverage of atomic oxygen of 0.11. For the slab calculations, a $3 \times 3 \times 1$ grid of Monkhorst–Pack special k-points [51] has been used to carry out the integration in the reciprocal space. For such large supercells, this grid of special k-points has been found to be dense enough to produce essentially converged relative energies up to 0.01 eV [48, 49]. Except for the isolated O_2 molecule, calculations have been always carried out without spin polarization. Test calculations for a series of structures have proven that for the Au_n nanoparticles and O_2–Au_n complexes spin polarization effects can be neglected.

Transition state (TS) structures were located through the climbing image nudged elastic band (cNEB) method [52–54]. All minima on the potential energy

surface were relaxed until self-consistent forces were lower than 0.03 eV/Å and TS structures were fully characterized with the pertinent vibration analysis making sure that TS structures show a single normal mode associated with an imaginary frequency. The calculated vibration frequencies were also used to obtain zero point energy (ZPE) corrections. Consequently, all energies reported in the present work include the ZPE correction. Finally, the rate constant for the O_2 dissociation elementary step (k) has been roughly estimated from the TS theory using the calculated vibrational frequencies of reactants and TS species to estimate the entropy contribution to the free energy variation in terms of vibrational partition functions [55]. Hence, where k_B is the Boltzmann constant, T is the absolute temperature, $q^{\#}$ and q are the vibrational partition functions for the TS and initial state, respectively, andE_{barr} is the activation energy of the elementary step corrected with the ZPE.

$$k = \left(\frac{k_B T}{h}\right)\left(\frac{q^{\#}}{q}\right) e^{-\frac{E_{barr}}{k_B T}} \qquad (1)$$

Results and discussion

In order to facilitate the discussion we will consider first the adsorption energy of the oxygen molecule on each nanoparticle and next we will focus on the calculated energy barriers and their dependence on the exchange–correlation potential. Here, let us just add that the calculated values for the equilibrium internuclear distance of the isolated oxygen molecule (dO–O) predicted by the different exchange– correlation potentials (LDA dO–O = 1.218 Å; PW91 dO–O = 1.235 Å and PBE or RevPBE dO–O = 1.244 Å) is quite close to the experimental value which is 1.207 Å[56].

Effect of the exchange–correlation potential on the adsorption energy of molecular and atomic oxygen

The adsorption energy of O_2 on each particle has been obtained from the ZPE corrected energy difference between the Au_n nanoparticle and of O_2 at their equilibrium geometry and the minimum energy of the O_2–Au_n complex. Molecular oxygen has been placed above different sites such as corners, edges and surfaces but the best configuration always correspond to adsorption near the four low-coordinate atoms of the (100) facet. In a similar way we also considered the relative stability of two separated atomic oxygen atoms which, as in the case of the Au(111) surface [49], tend to occupy the three hollow sites of the (111) facets. The structures of the adsorbed molecule and of the separated oxygen atoms provide the starting point for the TS search through the cNEB algorithm.

The optimized adsorption geometries of the O_2–Au_n complex do not exhibit significant differences either with respect to the particle size or with respect to functional, d_{O-O} is 1.46 ± 0.02 Å and the nearest Au–O distance (d_{Au-O}) is 2.27 ± 0.07 Å . The noticeable elongation of the O–O distance is a clear indication of bond weakening, whereas the rather short d_{Au-O} distances seem to indicate a rather strong interaction. However, the calculated values of the adsorption energy (E_{ads}) exhibit noticeable differences with both particle size and exchange–correlation potential. For the LDA functional, the calculated E_{ads} value for Au_{79} is very close to that of the Au(001) surface indicating convergence with respect to cluster size. However, this is not the case for the three GGA functionals which all predict E_{ads} values for Au_{79} quite far from the one corresponding to Au(001). Nevertheless, a word of caution is necessary in the view

UNIVERSITAT ROVIRA I VIRGILI
MODELLING AU CATALYST FROM BULK TO NANOSCALE
Alberto Roldán Martínez
ISBN:978-84-693-7669-0/DL:T-1748-2010

Table 1: Adsorption energy (E_{ads}/eV) for O_2 adsorption on the (001) facets of Au_{25}, Au_{38} and Au_{79} and for LDA, PW91, PBE and RevPBE functional.

	E_{ads}/eV			
	LDA	PW91/ΔLDA[a]	PBE/ΔPW91[b]	RevPBE/ΔPBE[c]
Au_{25}	-0.682	0.024/0.706	0.194/0.218	0.576/0.382
Au_{38}	-1.754	-0.906/0.848	0.719/0.187	-0.278/0.441
Au_{79}	-0.943	-0.191/0.752	0.011/0.202	0.367/0.378
Au(001)	-0.840	0.194/1.034	0.357/0.163	0.805/0.448

Results for the extended Au(001) surface are included for comparison
[a] $\triangle$LDA is the difference in E_{ads} between LDA and PW91
[b] $\triangle$PW91 is the difference between PBE and PW91
[c] $\triangle$PBE is the difference between RevPBE and PBE

of the positive E_{ads} values predicted by the GGA functionals for Au(001) which indicate that O_2 will not adsorb on this surface.

Next, let us consider the effect of the exchange–correlation functional in some more detail. Table 1 summarizes the E_{ads} values obtained for each particle using the different functionals. In general, the E_{ads} values follow the trend LDA>PW91>PBE>RevPBE with the LDA values clearly overestimated since they predict quite a strong adsorption of O_2 on Au(001) in clear disagreement with experiment. The interaction of O_2 with the Au_{25}, Au_{38} and Au_{79} nanoparticles follows the trends described by Hammer et al. [31] for the interaction of oxygen, CO and NO with late transition metal surfaces. Table 1 also reports the difference in adsorption energy on going from one functional to the next. Thus $\triangle$LDA is the difference in E_{ads} between LDA and PW91 whereas $\triangle$PW91 is the difference between PBE and PW91 and $\triangle$PBE the difference between RevPBE and PBE. The analysis of Table 1 shows that the differences in E_{ads} between the different functionals seem to follow a systematic trend with $\triangle$LDA = 0.75 $\pm$ 0.10 eV, $\triangle$PW91 = 0.18 $\pm$ 0.03 eV and $\triangle$PBE = 0.40 $\pm$ 0.04 eV. The differences are large enough to lead to qualitative differences regarding the adsorption energy of O_2 on the three nanoparticles, exothermic or endothermic depending on the exchange–correlation potential except for the Au_{38} particle which is predicted to be the one interacting stronger with this molecule. In spite of these important differences, the trend predicted by the different functionals regarding the effect of the particle size is the same, $E_{ads}(Au_{38})$>$E_{ads}(Au_{79})$>$E_{ads}(Au_{25})$. Strong similarities are also found regarding the charge transfer between the Au nanoparticle and the oxygen molecule which has been estimated using the Bader analysis [57]. The three nanoparticles have core and shell atoms, two shells for Au_{25} and Au_{38} and three for Au_{79}. The Au_{25} particles has five core atoms, four in equatorial plane positive and one near the (001) facet; Au_{38} has six core atoms, four in equatorial plane positive and two perpendiculars to this plane. The interaction with molecular oxygen distorts the Au nanoparticles so that one more shell appears in the radial distribution. Figure 2 (top panel) reports the charge distribution for the Au atoms as a function of the radial distribution. In general, all functionals predict a substantial amount of charge transfer of an approximately -0.9e to the oxygen molecule, the posi-

tive charge on the metal atoms tending to accumulate on those close to the oxygen atoms. The charge distribution per atom as a function of radial atomic distance in Fig. 2 also provides information on how each particle modifies his structure upon adsorption, this is clear from the scattering of dots, in the Au_{25} and Au_{38} particles the gold atoms interacting with oxygen increase the gold–gold distances whereas in the Au_{79} particle the atoms interacting with oxygen get closer to the particle core. In all cases, the Au atoms directly interacting with oxygen acquire some positive charge with the missing electron density being donated to the neighboring metallic atoms.

Effect of the exchange–correlation potential on the energy barrier for O_2 dissociation

Figure 3 displays the energy profile corresponding to the molecular oxygen dissociation pathway as a function of the particle size and for the different exchange–correlation functionals. Let us start the discussion by considering the final state where the two oxygen atoms are well separated. The effect of the exchange–correlation potential on the final state follows almost the same trend described in the previous subsection for the initial state, except for the LDA value for the smallest Au_{25} particle. This is because the presence of adsorbed atomic oxygen has a large effect on the structure of this particle. However, increasing the particles size leads to a considerable decrease in the particle ability to deform and this also influences the d_{O-O} at the TS which decreases with increasing the particle size from $d_{O-O} = 2.02$ Å for Au_{25} to $d_{O-O} = 1.98$ Å and $d_{O-O} = 1.94$ Å , for Au_{38} and Au_{79}, respectively, and for the PW91 functional. The influence of the functional on the TS structure is not very important; LDA gives the smaller d_{O-O} followed by PBE, RevPBE and PW91.

The energy barrier for O_2 dissociation ($\triangle E^{\#}$) is obtained by subtracting the total energy of the Au_n–O_2 complex from the total energy of the TS structure, both corrected by ZPE. From the energy profiles in Fig. 3 and the reported $\triangle E^{\#}$ values we first notice that the PW91 energy barriers are significantly smaller than the one corresponding to the regular Au(111) [50] and the stepped Au(321) surface [58,59] as expected from the well known different reactivity of Au extended surfaces and Au nanoparticles [1–23]. For the case of H_2 dissociation this difference can be explained in terms of low coordinated sites and, hence, it is predicted that Au(321) will be able to dissociate H_2 with a small energy barrier [22]. This is not the case for the O_2 dissociation where recent work has shown that the existence of these low coordinated sites is not enough to dissociate O_2. Therefore, in the case of O_2 dissociation by Au nanoparticles electronic confinement must play a key role.

The influence of the exchange–correlation potential on the energy barriers is really small, especially for the three GGA functionals. In fact the differences do not exceed 0.04 eV for Au_{25} and Au_{38} and 0.08 eV for Au_{79}. The differences between the three GGA barriers and the LDA one are somehow larger but never exceeding 0.15 eV. This is a very important result since it indicates that, for a given system, the energy barrier does not largely depend on the exchange–correlation potential and hence, the qualitative description of the dissociation process remains essentially unchanged. This conclusion is further confirmed by the calculated values of the rate constants for the dissociation step reported in Table 2. However, one must

UNIVERSITAT ROVIRA I VIRGILI
MODELLING AU CATALYST FROM BULK TO NANOSCALE
Alberto Roldán Martínez
ISBN:978-84-693-7669-0/DL:T-1748-2010

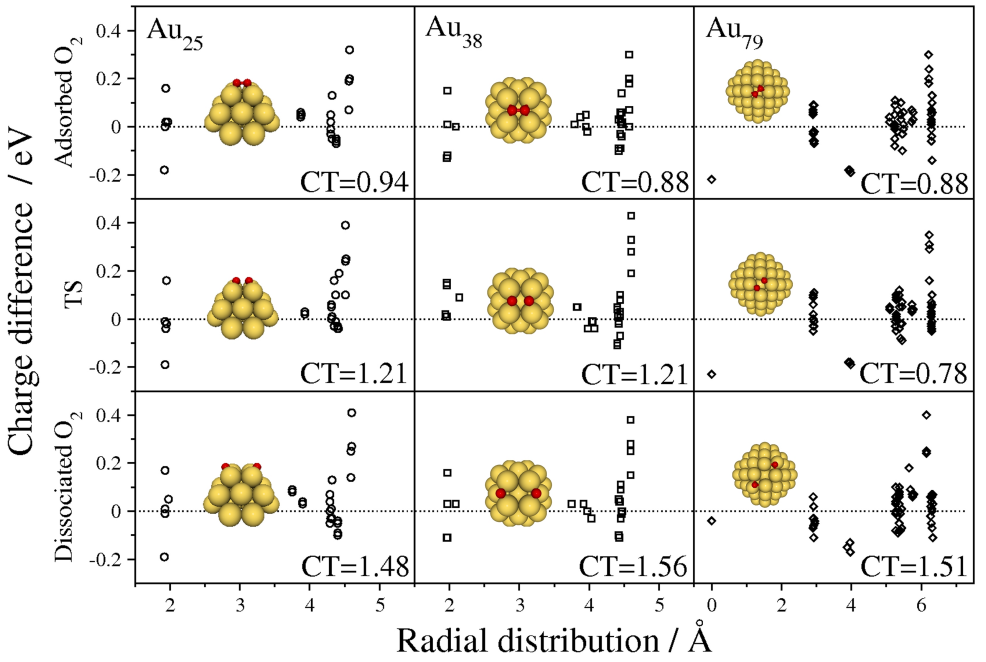

Figure 2: Atomic charges on Au atoms as a function of radial atomic distribution (in angstrom) for the Au_{25}, Au_{38} and Au_{79} particles obtained from the Bader analysis of the PW91 density functional. The total charge transfer (CT) is also shown. The (001) gold atoms interacting with the O_2 molecule are identified with filled points

also realize that molecular oxygen dissociation will only take place when the energy barrier is smaller than the energy required for the molecule to desorb. This is only fulfilled by the Au_{38} particle, in agreement with previous work based on the PW91 only [28], but this conclusion holds also when considering the PW91 and PBE functionals. For the Rev-PBE, the adsorption energy becomes always too small, especially when compared with the energy barrier for dissociation. Nevertheless, for the Au_{38} particle this energy difference becomes 0.19 eV, well within the error bar for chemisorption energies reported for the RevPBE functional [31], indicating that desorption and dissociation may compete and that the later can be effective when the O_2 pressure is enough to maintain a covered surface. Here, an important question concerns the accuracy of the calculated RevPBE adsorption energies. From the work of Hammer et al. [31] one would expect that the RevPBE values are more accurate although one must also admit that this is based in a rather limited database which does not take into account energy barriers nor does it include calculations for nanoparticles. However, the fact that present values have been obtained using the PBE derived PAW core potentials and the rather large difference between the PBE and RevPBE adsorption energies suggest that the latter are probably underestimated.

To end this discussion we will only add that the dissociation process is accompanied by an increase in the charge transfer from the particle to oxygen molecule as indicated in Fig. 2. Here, the influence of the exchange–correlation

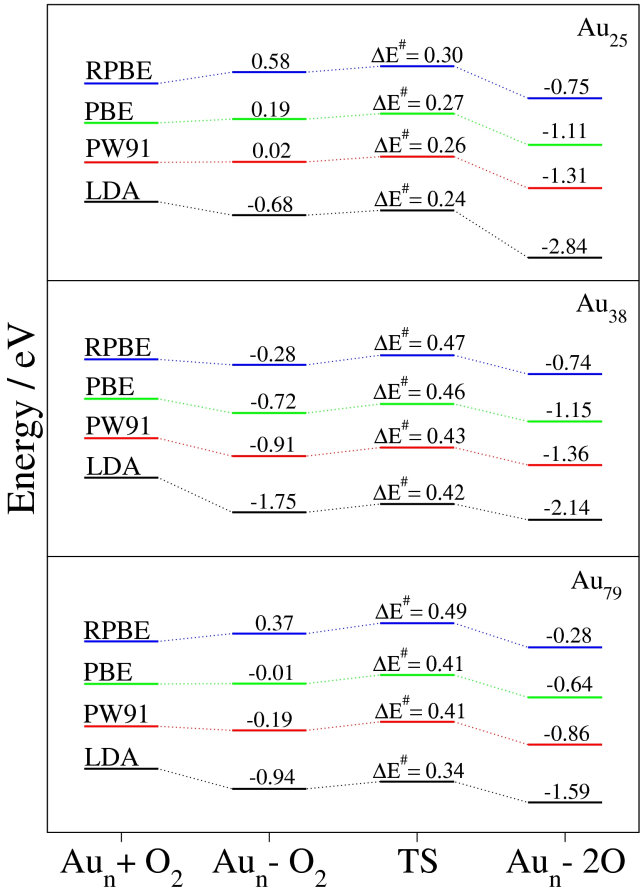

Figure 3: Profile to dissociate O_2 on the (001) particle facets. Furthermore the effect of exchange–correlation was plotted: LDA, PW91, PBE and RevPBE.

functional is less important and will not be further commented. We will only add that the PW91 charge transfer at the TS is the smallest for Au_{79} which seems to be the reason for the high reaction barrier. In fact, the charge transfer increases from 0.94 and 0.88 e in the adsorbed state for Au_{25} to Au_{38} to 1.21 e at the TS but decreases from 0.88 e in the adsorbed state to 0.78 e at the TS for the Au_{79}. However, the charge transfer at the dissociated state is almost the same (∼1.5 e) for all particles.

Conclusions

Density functional calculations carried out for the adsorption and dissociation of molecular oxygen on three Au nanoparticles of modest size (Au_{25}, Au_{38} and Au_{79}) evidences that the adsorption energy is rather strongly dependent on the exchange–correlation functional chosen. The tendency of LDA to strongly overestimate the adsorption energy reported by various authors [60–64] is confirmed for the case of O_2 adsorption on Au nanoparticles. The difference between the predictions of the three GGA functionals is smaller than from these to GGA but no-

Table 2: Calculated rate constants for the dissociation step as a function of the particle size and of the exchange–correlation functional.

	k/s			
	LDA	PW91	PBE	RevPBE
Au_{25}	3.81×10^{8}	1.40×10^{8}	8.94×10^{7}	3.12×10^{7}
Au_{38}	4.32×10^{5}	1.83×10^{5}	6.97×10^{4}	2.04×10^{4}
Au_{79}	1.05×10^{7}	6.34×10^{5}	4.54×10^{5}	1.68×10^{4}

ticeable, the PW91 values being larger than the PBE by roughly 0.20 eV and those are larger than the RevPBE by about 0.35 eV. The deviations are found to be systematic and, hence, the main trends remain unaltered. The influence of the exchange–correlation functional on the energy barriers for O_2 dissociations are, however, much smaller. On the one hand this is a good new since it indicates that, for a given system, the description of this elementary step does not depend on the choice of the functional. On the other hand, this different behavior of chemisorption energies and energy barriers with respect to the exchange–correlation functional has some undesirable effects, especially when the competition between adsorption and dissociation becomes crucial as is the case here for O_2 dissociation on Au nanoparticles. Nevertheless, the calculated results confirm previous work indicating that there is a critical size for the Au nanoparticles to efficiently dissociate O_2 [28]. In fact, PW91 and PBE calculations show that Au_{38} is the only particle where O_2 dissociation clearly dominates over O_2 dissociation whereas RevPBE calculations point to a less clear trend although still indicating that dissociation may occur. This is not the case for the other two Au nanoparticles where all functionals predict that desorption will always take place. Finally, the present calculations provide theoretical support to recent experimental work indicating that direct styrene epoxidation by dioxygen requires really small particles [17], reinforces previous theoretical findings [29] and is in agreement with the even more recent experimental work of Hutchings and colleagues [65] showing that subnanometer Au particles supported on FeO_x are active for CO oxidation.

Acknowledgements

Acknowledgments Alberto Roldán thanks Universitat Rovira i Virgili, for supporting his pre-doctoral research. Financial support has been provided by the Spanish Ministry of Science and Innovation (MICINN) (grants FIS2008-02238/FIS and CTQ2008-06549-C02-01) and, in part, by the Generalitat de Catalunya (Grants 2005SGR00697, 2005SGR-00104 and 2005 PEIR 0051/69). Computational time on the Marenostrum supercomputer of the Barcelona Supercomputing Center is gratefully acknowledged.

References

1. Haruta M (1997) Catal Today 36:153–166.
2. Haruta M (2005) Nature 437:1098–1099.
3. Valden M, Lai X, Goodman DW (1998) Science 281:1647–1650. doi:10.1126/science.281.5383.1647.
4. Nolan SP (2007) Nature 445:496–497. doi:10.1038/445496a.
5. Hashmi ASK (2007) Chem Rev 107:3180–3211.
6. Hashmi ASK, Hutchings GJ (2006) Angew Chem Int Ed Engl 45:7896–7936.
7. See also the reviews in the special issue dedicated to chemistry of nano-gold in (2008) Chem Soc Rev 37.
8. Carrettin S, Guzman J, Corma A (2005) Angew Chem Int Ed Engl 44:2242–2245.

9. Gonzalez-Arellano C, Corma A, Iglesias M, Sanchez F (2006) J Catal 238:497–501.

10. Gonzalez-Arellano C, Abad A, Corma A, Garcia H, Iglesias M, Sanchez F (2007) Angew Chem Int Ed Engl 119:1558–1560.

11. Fu Q, Weber A, Flytzani-Stephanopoulos M (2003) Science 301:935–938.

12. Rodriguez JA, Ma S, Liu P, Hrbek J, Evans J, Perez M (2007) Science 318:1757–1760.

13. Corma A, Serna P (2006) Science 313:332–334.

14. Hughes MD, Xu YJ, Jenkins P, McMorn P, Landon P, Enache DI, Carley AF, Attard GA, Hutchings GJ, King F, Stitt EH, Johnston P, Griffin K, Kiely CJ (2005) Nature 437:1132–1135.

15. Nijhuis TA, Weckhuysen BM (2006) Catal Today 117:84–89.

16. Chowdhury B, Bravo-Suarez JJ, Mimura N, Lu J, Bando KK, Tsubota S, Haruta M (2006) J Phys Chem B 110:22995–22999.

17. Turner M, Golovko VB, Vaughan OPH, Abdulkin P, Berenguer-Murcia A, Tikhov MS, Johnson BFG, Lambert RM (2008) Nature 454:981–983.

18. Corma A, Garcia H (2008) Chem Soc Rev 37:2096–2126.

19. Rodriguez JA, Liu P, Vines F, Illas F, Takahashi Y, Nakamura K (2008) Angew Chem Int Ed Engl 47:6685–6689.

20. Boronat M, Concepcion P, Corma A, Gonzalez S, Illas F, Serna P (2007) J Am Chem Soc 129:16230–16237.

21. Corma A, Serna P, Concepcion P, Calvino JJ (2008) J Am Chem Soc 130:8748–8753.

22. Corma A, Boronat M, Gonzalez S, Illas F (2007) Chem Commun 3371–3373.

23. Lopez N, Janssens TVW, Clausen BS, Xu Y, Mavrikakis M, Bligaard T, Nørskov JK (2004) J Catal 223:232–235.

24. Remediakis IN, Lopez N, Nørskov JK (2005) Angew Chem Int Ed Engl 44:1824–1826.

25. Deng X, Min BK, Guloy A, Friend CM (2005) J Am Chem Soc 127:9267–9270.

26. Wang Y, Gong X (2006) J Chem Phys 125(1–12):124703.

27. Barrio L, Liu P, Rodriguez JA, Campos-Martin JM, Fierro JLG (2007) J Phys Chem C 111:19001–19008.

28. Roldan A, Gonzalez S, Ricart JM, Illas F (2009) Chem Phys Chem 10:348–351.

29. Honkala K, Hellman A, Remediakis IN, Logadottir A, Carlsson A, Dahl S, Christensen SH, Nørskov JK (2005) Science 307:555– 558.

30. Strasser P, Fan Q, Devenney M, Weinberg WH, Liu P, Nørskov JK (2003) J Phys Chem B 107:11013–11021.

31. Hammer B, Hansen LB, Nørskov JK (1999) Phys Rev B 59:7413–7421.

32. Roldan A, Vines F, Illas F, Ricart JM, Neyman KM (2008) Theor Chem Acc 120:565–573.

33. Viñes F, Illas F, Neyman KM (2008) J Phys Chem A 112:8911– 8915. doi:10.1021/jp8014854.

34. Loschen C, Bromley S, Neyman KM, Illas F (2007) J Phys Chem C 111:10142–10145.

35. Migani A, Loschen C, Illas F, Neyman KM (2008) Chem Phys Lett 465:106–109.

36. Loschen C, Migani A, Bromley ST, Illas F, Neyman KM (2008) Phys Chem Chem Phys 10:5730–5738.

37. Kresse G, Furthmuller J (1996) Comput Mater Sci 6:15–50.

UNIVERSITAT ROVIRA I VIRGILI
MODELLING AU CATALYST FROM BULK TO NANOSCALE
Alberto Roldán Martínez
ISBN:978-84-693-7669-0/DL:T-1748-2010

UNIVERSITAT ROVIRA I VIRGILI
MODELLING AU CATALYST FROM BULK TO NANOSCALE
Alberto Roldán Martínez
ISBN:978-84-693-7669-0/DL:T-1748-2010

3.4.4 O_2 adsorption and dissociation on neutral, positively and negatively charged Au_n (n = 5-79) clusters

Corresponding to: Alberto Roldán, Josep Manel Ricart, Francesc Illas, Gianfranco Pacchioni, Phys. Chem. Chem. Phys., 2010, DOI:10.1039/C004110F. Reproduced by permission of the PCCP Owner Societies.

Introduction

The role of reduced dimensionality in determining the properties of metal particles and clusters is a topic which has attracted a lot of attention in the past decades. Beside fundamental interest, these systems offer new perspectives and opportunities to design materials with unprecedented properties. A particular application of nanoparticles is related to the promotion of chemical reactions with reduced energy cost or the removal of pollutants under mild conditions.[1–4] These are typical activities related to catalysis by supported metals. Gold is a rather special system since it is rather inert in massive form while it becomes chemically very active when prepared in the form of small particles. Examples of this unique chemical activity have been reported for low-temperature CO oxidation,[3–5] water–gas shift,[6,7] chemoselective hydrogenations[8] and selective oxidation of olefins,[9,10] just to mention a few.

Despite a large number of theoretical and experimental studies dedicated to the origin of this peculiar chemical activity, the reason why gold becomes so active is still matter of discussion. One aspect which is clear is that the size plays a crucial role, and that for particles of size above a given threshold (typically 2-3 nm) the activity decreases and tends to disappear.[4] In this respect, the main role of the nanoparticle is that to exhibit several low-coordinated and highly reactive sites where reactions occur more easily.[11] For instance, some of us have recently shown the special activity of a particular cluster size, that of Au_{38}, in oxidation reactions.[12] However, other hypotheses have been formulated. For instance it has been suggested that peripheral Au atoms could be cationic in nature and that this may help the activation of dioxygen in a catalytic oxidation process.[13] Other studies seem to suggest more a role of charging the cluster by adding or removing electrons. Also in this case claims have been reported of a higher reactivity related to the formation of cationic gold,[1] as well as studies which show the higher reactivity of anionic gold.[14,15] This apparent contradiction can be partly resolved by mentioning that different kind of gold nanoparticles, oxidized or reduced, can form depending on the reaction under consideration and in particular for different reaction temperatures. Finally, since gold nanoparticles have to be supported on a substrate in order to be used in practical applications, there is clear evidence that this can have a major effect on the particle properties.[16,17] The role of the sup-

port in modifying/activating gold nanoclusters has been studied by comparing properties of oxides like MgO, TiO_2, Al_2O_3, Fe_2O_3,[4,18–21] and more recently, also metal carbides.[22–24] Since most of the supports are oxides, which are characterized by a high complexity and variability of the surface (defects, morphology, phase, etc.), this explains why several contributions have been invoqued to explain the unusual reactivity of gold nanoparticles without reaching a complete consensus.

In this study we report the results of a systematic study of the role of a positive or negative charge on the activation and dissociation of O_2 by a gold nanoparticle. To this end we have considered gold clusters of various sizes, going from the tiny Au_5 cluster to the rather large Au_{79} particle (∼1.4 nm). For larger systems, containing hundred of atoms, it is expected that a full metallic character is reached and no effect will arise from the addition or the removal of one electron to the particle.[25] But for smaller systems this effect has not been investigated in a systematic way yet. In particular, we have considered the interaction of O_2 with the gold clusters (molecular chemisorption) and we have determined the reaction profile leading to oxygen dissociation (energy barrier and stability of the resulting products) as a function of both the size and the charge of the clusters.

The paper is organized as follows. The computational details are described in Section 2. Section 3.1 is dedicated to the intrinsic properties of the naked clusters. In Section 3.2 we describe the adsorption and activation of O_2 interacting with the various clusters, while Section 3.3 is dedicated to the dissociation barrier and final products. Some conclusions are summarized in the last Section.

Computational Details

We performed spin polarized periodic density functional theory (DFT) calculations on the interaction of O_2 with neutral, positively and negatively charged Au_5, Au_{13}, Au_{25}, Au_{38}, Au_{55}, and Au_{79} clusters. The clusters have been placed into the center of a large unit cell, with a vacuum space of 1 nm in all directions in order to avoid interactions between replicas in the various cells. This supercell approach has been found to be an efficient method to study the atomic and electronic structure of rather large nanoparticles of coinage metals.[25] Ionization potential (IP) and electronic affinity (EA) were determined by placing the nanoparticle in a large supercell with at least 1.5 nm vacuum.

The calculations have been carried out within the Kohn–Sham (KS) implementation of DFT using the PW91 version of the generalized gradient approximation (GGA) of the exchange-correlation functional.[26] The effect of the inner electrons on the valence density has been described by the projector augmented wave (PAW) method and the KS valence states have been expanded in a plane-waves basis set with a cutoff for the kinetic energy at 415 eV, considering only the Γ-point of the reciprocal space. This is a typical value for the cutoff energy and ensures that the calculated energies are sufficiently converged and forces among atoms are lower than 0.02 eV/Å^2. A Gaussian smearing technique with a 0.05 eV width has been applied to enhance convergence but all energies presented below have been obtained by extrapolating to zero smearing (0 K).

The largest aggregates, Au_{38}, Au_{55}, and Au_{79}, have a octahedral shape and were initially cut from bulk gold so as to exhibit low-index planes, Fig. 1; Au_{25} is derived from Au_{38} by removing two (100)

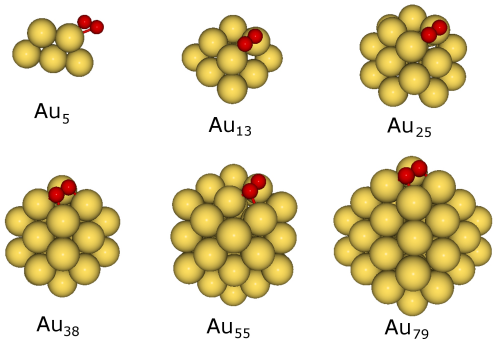

Figure 1: Structures of $Au_n^{(+,0,-)}$ clusters with an adsorbed O_2 molecule (molecular chemisorbed state).

layers; in Au_{13} three (100) layers are removed and the cluster consists of two layers only with 9 and 4 Au atoms each, respectively; Au_5 has a planar trapezoidal structure obtained by combining three equilateral triangles, Fig. 1. Of the various possible ways of O_2 adsorption and dissociation on different sites of these particles, we have always considered the one which was found to correspond to the minimum energy pathway, see Supplementary Information. All calculations have been always carried out with spin polarization. However, given the metallic character of most of the systems considered, only for the smallest clusters a net spin polarization has been found. Since, as it will be shown below, the spin properties are not going to be relevant for the reactivity of the clusters, they will not be discussed in detail.

Transition states (TS) for O_2 dissociation over free Au_n clusters were obtained by means of the computationally intensive climbing-image nudged elastic band (CI-NEB)[27] and DIMER[28] methods. Once the TS structures have been determined, their nature has been verified and characterized with a vibrational analysis. We performed a diagonalization of the corresponding Hessian matrix obtained by numerical difference of analytical gradients, neglecting coupling with the cluster-surface phonons, and making sure that the TS structures show a single normal mode associated with an imaginary frequency.

Results

Electronic properties of bare gold clusters

Before to consider the properties of O_2 molecules adsorbed on the Au_n clusters we briefly discuss their basic electronic properties. All gold structures have been reoptimized for the neutral, positive and negative charge states starting from the initial structures described above. The addition or removal of one electron has little effect on the final geometry. The topology remains the same and only the Au-Au distances are slightly modified. This is true also for the smallest cluster considered, Au_5, where the average distances change at most by 4 pm going from the cation to the anion, Table 1. For the larger clusters the change in average Au-Au separation becomes rapidly very small and for Au_{79} it is completely absent. Au_{55} and Au_{79} have distances close to those of bulk gold.[25]

The adiabatic ionization potential (IP) and electron affinity (AE) of the naked clusters have been determined, Table 1. Previous DFT calculations on the

UNIVERSITAT ROVIRA I VIRGILI
MODELLING AU CATALYST FROM BULK TO NANOSCALE
Alberto Roldán Martínez
ISBN:978-84-693-7669-0/DL:T-1748-2010

Table 1: Average Au-Au distances (d_{Au-Au}), IP and EA for $Au_n^{(+,0,-)}$ clusters.

	d_{Au-Au} /Å				
n	Au^+	Au	Au^-	EA /eV	IP /eV
5	2.68	2.69	2.72	4.11	5.97
13	2.80	2.81	2.82	3.85	5.43
25	2.87	2.88	2.91	4.09	5.09
38	2.89	2.89	2.89	3.66	4.50
55	2.88	2.89	2.89	4.44	5.40
79	2.92	2.92	2.92	4.08	4.73
Bulk Au		2.88[36]		5.1[31]	5.1[31]

properties of Au clusters have shown a linear trend of IP and EA with the reciprocal effective cluster radius defined as $n^{-1/3}$ (n = number of atoms), assuming a spherical droplet model.[29] In our clusters the EA does not change significantly with the cluster size, and even for Au_{79} is about 1 eV below the metal work function; where a direct comparison with the results of ref. is possible (e.g. for Au_{13}, Au_{38} and Au_{55}) the values are very similar despite the use of a different exchange-correlation functional and computational setup. The trend in IP is in line with the expectation since the IP decreases going from Au_5 (5.97 eV) to Au_{79} (4.73 eV). This latter value is slightly below the gold work function, 5.1 eV.[30] The IP values calculated here are consistently lower, by about 1 eV, than those report in ref. 30. Relatively large oscillations are found on EA and IP due to the fact that we are in a non-scalable regime and to the presence of clusters with odd and even number of valence electrons. Au_{38} exhibits the smallers IP, 4.50 eV, followed by Au_{79}, 4.73 eV, Table 1. All other clusters have IP larger than 5 eV. We will see below that this correlates quite well with the level of activation of adsorbed O_2.

O_2 adsorption

In the study of the interaction of O_2 with gold clusters three main quantities have been considered, the O_2 binding energy to the cluster, E_B, the barrier to dissociation, $\triangle E^{\#}$, and the reaction energy when the molecule is dissociated into two O atoms. For clarity these quantities are illustrated in Fig. 2 and reported in Table 2. In this section we discuss only the O_2 adsorption energy, E_B, leaving the other quantities for the next Section. O_2 adsorption on small planar gold clusters only takes place on the cluster periphery, where oxygen can interact with the low-coordinated Au atoms. Due to the odd-even oscillation in the number of valence electrons,[31] some clusters are closed shell while others are open shell, which may results in oscillations in the adsorption properties of a paramagnetic molecule like O_2. Neutral Au_5 binds O_2 via a single O atom by 0.54 eV, Table 2. This is also the configuration found on the closed shell Au_5^+ and Au_5^- units, where the bond strength is slightly decreased, Table 2. This is true in particular for the anion cluster which binds O_2 by 0.39 eV only. On Au_5^+ the O-O bond distance is as in the gas-phase, while a small elongaton, 0.05 Å, is found for neutral and anionic Au_5, Table 3. This elongation reflects a moderate charge transfer from the gold cluster to adsorbed O_2, Table 4. Still, the O_2 ad-molecule cannot be classified as a superoxo species, O_2^-; the small elongation and occupation of the $2\pi^*$ MO is indicative of a partial

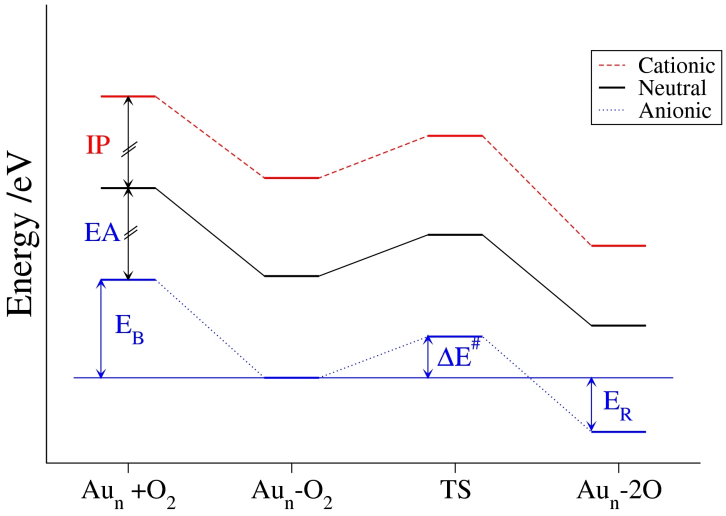

Figure 2: Definition of energies involved in the adsorption and dissociation of an O_2 molecule on gold clusters.

activation of the adsorbed molecule.

After searching for several possible adsorption sites, we found that on Au_{13} O_2 prefers to adsorb on a edge site shared by a (100) and a (111) facets. While the adsorption mode is independent of the cluster charge, the bond strength changes markedly being largest for Au_{13}^- (0.83 eV) and smallest for Au_{13}^+ (0.29 eV). Neutral Au_{13} is in between, with a bond strength of 0.51 eV, Table 2. The O-O bond length clearly follows the trend in adsorption energy, and becomes longer going from Au_{13}^+ (1.32 Å), to Au_{13} (1.34 Å), and to Au_{13}^- (1.39 Å), Table 3. This trend is clearly correlated with the amount of charge transferred from gold to O_2 as estimated with the Bader charge analysis, Table 4. Also in this case, however, we cannot classify the adsorbed O_2 as a superoxo species.

On Au_{25} the preferred adsorption site for O_2 is similar as in Au_{13}, i.e. at the edge between a square and a triangular facet. However, differently from all other clusters considered in this work, here we found that the cluster undergoes a substantial structural rearrangement when the O_2 molecule is adsorbed, see Figure 3. This rearrangement is quite different depending on the charge of the cluster. The strong structural fluxionality suggests that Au_{25} is an intrinsically less stable cluster compared to Au_{13} and to other larger aggregates considered, so that it exhibits an high deformable structure. Of course, also the binding properties vary strongly with charge and associated structural relaxation. On Au_{25}^+ and on neutral Au_{25} the O_2 bond strength is 0.58 and 0.51 eV respectively, practically the same as on neutral Au_{13}, while a much larger interaction takes place on anionic Au_{25}^-, 1.37 eV. This is the same trend found in Au_{13}. The O-O distance, 1.36 Å in Au_{25}^+, 1.32 Å in Au_{25}, and 1.37 Å Au_{25}^-, Table 3, does not show a direct correlation with the bond strength and with the cluster charge for the reasons discussed previously.

On Au_{38} the preferred adsorption site is with the O_2 molecule lying above a (001) face that contains four corner atoms. Each O atom of the molecule is in a bridge position over two Au atoms. The binding is strong for all charge states, be-

UNIVERSITAT ROVIRA I VIRGILI
MODELLING AU CATALYST FROM BULK TO NANOSCALE
Alberto Roldán Martínez
ISBN:978-84-693-7669-0/DL:T-1748-2010

Table 2: Binding energy, E_B, dissociation barrier, $\triangle E^{\#}$, and reaction energy, E_R, for O_2 reacting with $Au_n^{(+,0,-)}$ clusters (see also Fig. 2). All values are in eV.

	Au_n^+			Au_n			Au_n^-		
n	E_B	$\triangle E^{\#}$	E_R	E_B	$\triangle E^{\#}$	E_R	E_B	$\triangle E^{\#}$	E_R
5	-0.47	2.89	0.05	-0.54	2.81	-0.58	-0.39	2.23	-0.90
13	-0.29	1.81	-1.45	-0.51	1.79	-1.46	-0.83	1.66	-1.79
25	-0.58	1.65	-0.61	-0.51	0.53	-1.55	-1.37	1.75	-0.49
38	-0.89	0.46	-0.74	-0.96	0.45	-0.55	-1.07	0.45	-0.59
55	-0.50	0.87	-2.24	-0.23	0.54	-2.32	-0.21	0.88	-2.15
79	-0.32	0.52	-0.68	-0.28	0.42	-0.65	-0.25	0.49	-0.66

ing 0.89 eV on Au_{38}^+, 0.96 eV on Au_{38}, and 1.07 eV on Au_{38}^-, Table 2. Different from Au_{25}, the structure is not deformed by O_2 adsorption, indicating a considerable stability of Au_{38}. As found in the analysis of IP and AE values, Au_{38} appears to be "special" with respect to the other clusters considered, Table 1. This is not only because a strong bonding is found for all charge states, but also because this is connected to a strong activation of the O-O bond, Table 3. In all three cases, in fact, the distance increases by about 0.2 Å with respect to the gas-phase and is typical of a superoxo complex, being around 1.45-1.46 Å. This is clearly induced by a larger charge transfer than on the smaller clusters, see Table 4. Notice that the net charge on O_2, from -0.84 to -0.90 e, Table 4, is not varying significantly with the cluster total charge, $+1$, 0, or -1. This suggests that the shape and possibly the size of the gold nanoparticle are more important than the total electron count. The formation of a superoxo complex seems to be related more to the IP of Au_{38} which is the smallest among the structures considered, Table 1.

Au_{55} has a diameter of $\sim$1.4 nm and as such is representative of the small Au clusters which have been shown to exhibit special catalytic activity.[3,4] Its adsorption properties towards O_2 are very different from those of Au_{38}. The preferred adsorption site is not exactly the same and changes also with the charge state (e.g. on the anionic cluster the O atoms are on-top of Au, and not in bridge positions as on the neutral and positively charged Au_{55} cluster, Fig. 1). But what is more surprising, is that the binding energy of O_2 is rather small for all charge states, in particular the neutral and the anionic ones, where the bonding is 0.2 eV only (it is 0.5 eV on Au_{55}^+, Table 2). These binding energies are the smallest found so far, and indicate how important is the cluster size is in determining the adsorption properties. The O_2 molecule is less activated on Au_{55} than on Au_{38}: the O-O distance is of 1.36 Å on Au_{55}^+ and on Au while is only 1.31 Å on Au_5^-, Table 3. Once more, this is related to the small amount of charge transferred into the $2\pi^*$ of O_2 and to the fact that Au_5 has the highest IP among the clusters considered, nearly 0.8 eV larger than on Au_{38}, Table 1.

Au_{79} is the largest gold cluster considered here. On its surface one can identify six (001) facets; O_2 is bound to one of these facets in a bonding mode which is similar to that found on Au_{38}. The bonding properties, however, are quite different. For all charge states, in fact, the O_2 molecule is weakly bound, from 0.32 eV in Au_{79}^+ to 0.28 eV in Au_{79} and 0.25 eV in Au_{79}^-. This is reminiscent of the situation found in Au_{55}. However,

UNIVERSITAT ROVIRA I VIRGILI
MODELLING AU CATALYST FROM BULK TO NANOSCALE
Alberto Roldán Martínez
ISBN:978-84-693-7669-0/DL:T-1748-2010

Table 3: O-O distance (d_{O-O}) for O_2 molecularly adsorbed $Au_n^{(+,0,-)}$ clusters.

	d_{O-O} /Å		
n	Au_n^+	Au_n	Au_n^-
5	1.250	1.287	1.294
13	1.317	1.340	1.386
25	1.357	1.323	1.374
38	1.450	1.456	1.462
55	1.359	1.364	1.308
79	1.451	1.465	1.477

at variance with Au_{55}, the molecule is elongated and exhibits the typical O_2^- superoxo structure, with O-O distances in the range 1.45-1.48 Å, Table 3, and a net charge close to -1, Table 4. This is the kind of activation found on Au_{38}, where the bond strength was 3-4 times larger. Thus, there is no relation between the net charge transfer, the level of O-O bond activation and the strength of the adsorption bond, while the formation of a superoxo species can be attributed to the relatively low IP of this cluster, Table 1. The presence of a positive or negative charge on a large cluster like Au_{79} has no effect on the bonding characteristics, a result which suggests that in this size regime we are approaching metallic character.

Sumarizing this section, we have seen that on ultrasmall clusters, up to about 20-25 atoms, the presence of a charge has some effect on the bond strength and activation of adsorbed O_2. For Au_{38} the effect is present but small being of about 10% on the adsorption energy and of 0.4% on the bond distances. On the larger clusters (Au_{55} and Au_{79}) the effect of the charge on the adsorption energies is not detectable while there is always an elongation of the O-O bond as one goes from Au_n^+ to Au_n and Au_n^-. What is absolutely clear is that for sizes of the order of about 40 atoms or above, the nuclearity and the shape of the gold cluster are much more important than the charge state, so that completely different bond strengths and activation modes are found for octahedral Au_{38}, Au_{55}, and Au_{79}, independent of their charge.

O_2 dissociation

In this section we discuss the dependence of the energy barrier and the stability of the products of the O-O dissociation (formation of two adsorbed atoms) on the charge and size of the gold clusters. The barrier, $\triangle E^{\#}$, is defined as the energy difference between the minimum of the adsorbed state (reactants) and the TS, Fig. 2; the energy of the products, E_R, is the energy difference with respect to the chemisorbed O_2 state and, as such, does not corresponds to the thermodynamic cost or gain associated to the reaction of separated fragments, O_2 and Au_n, Fig. 2. Except for Au_5, the TS has practically the same form on all clusters considered with the two O atoms bridging Au-Au bonds on a square facet and a typical O-O distance of about 2 Å. This is important since it allows us to disentangle geometrical from electronic effects in determining the effect of the charge on the energy barrier. In the final dissociated state the two O atoms are completely separated and non-interacting (for information about the structure of TS and dissociative adsorption see Supplementary information).

On Au_5 we notice a clear effect of the charge both on the energy barrier and

UNIVERSITAT ROVIRA I VIRGILI
MODELLING AU CATALYST FROM BULK TO NANOSCALE
Alberto Roldán Martínez
ISBN:978-84-693-7669-0/DL:T-1748-2010

Table 4: Net Bader charge on each O for molecularly and dissociatively adsorbed O_2 on $Au_n^{(+,0,-)}$ clusters.

	Charge / e					
n	Au_n^+/O_2	Au_n/O_2	Au_n^-/O_2	$Au_n^+/2O$	$Au_n/2O$	$Au_n^-/2O$
5	-0.02	-0.15	-0.20	-0.61	-0.69	-0.78
13	-0.20	-0.26	-0.36	-0.76	-0.77	-0.81
25	-0.29	-0.23	-0.34	-0.76	-0.77	-0.80
38	-0.42	-0.43	-0.45	-0.79	-0.77	-0.79
55	-0.31	-0.32	-0.21	-0.77	-0.78	-0.78
79	-0.41	-0.44	-0.45	-0.77	-0.77	-0.78

on the stability of the formed products. On the neutral cluster the barrier is very high, 2.81 eV; on Au_5^+ the barrier is even higher, 2.89 eV. On the anion the barrier is lowered by 0.6 eV and becomes 2.23 eV, Table 2. Also the energy of the products is strongly affected by the charge state of the cluster: the two adsorbed O atoms form a strongly charged adspecies, Table 4. Due to the different electron density on the three clusters, Au_5^+, Au_5, and Au_5^-, the products are almost at the same energy of chemisorbed O_2 on Au_5^+, while are 0.58 eV and 0.90 eV more stable, respectively, in Au_5 and Au_5^-, Table 2. Clearly, in such a small cluster the presence of a positive or a negative charge has a stong effect both on the thermodynamics and on the kinetics of the process. When we go to Au_{13} the effect of the charge on the barrier and product stability is definitely smaller. The barrier is of 1.7-1.8 eV, i.e. much lower than on Au_5, and depends only moderately on the charge (the highest barrier, 1.81 eV is found for Au_{13}^+, and the lowest barrier, 1.66 eV, for Au_{13}^-, thus confirming that the additional electron lowers the barrier, although to a much smaller extent than in Au_5, Table 2). In the final products the O atoms occupy a three-fold position and have a similar stability in Au_{13}^+ and Au_{13}, and a higher stability on Au_{13}^-, Table 2. Also in this case, the presence of extra electrons favors the bonding with the highly electronegative O atoms and lowers the total energy of the dissociative state.

Au_{25} has a somehow special behavior. As we mentioned in the previous Section, this can be ascribed to the intrinsic instability of this cluster which leads to substantial modifications of the original structure during the reaction. In fact, both the TS and the final structure where O_2 is dissociated exhibit a large structural rearrangement which varies as a function of the cluster charge. For this reason the computed $\triangle E^{\#}$ and E_R values have little meaning since they reflect, more than the intrinsic reactivity of a charge state, the tendency to minimize the energy of the cluster. This results in values of $\triangle E^{\#}$ and E_R which do not correlate at all with the cluster charge, nor can be related to a specific property of this nuclearity, Table 4. The largest barrier, 1.75 eV, is found for Au_{25}^-, the smallest one for Au_{25} (0.53 eV); on Au_{25}^- however, the dissociative state is the least stable, -0.49 eV, which does not correlated at all with the presence of the extra charge. For this reason Au_{25} will be no longer discussed.

The next cluster considered is Au_{38}. Here the barrier is very small, less than 0.5 eV, and surprisingly similar for all charge states, Table 2. Also the products of the reaction show a similar energy gain with respect to the chemisorbed state, with values going from -0.55 eV for

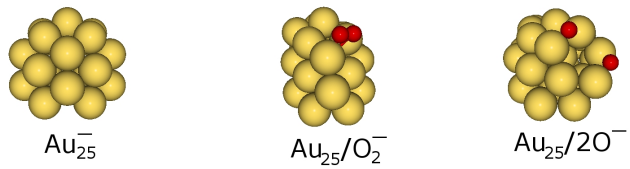

Figure 3: Structure of the bare Au_{25}^- cluster and of the Au_{25}/O_2^- and $Au_{25}/2O^-$ complexes.

neutral Au_{38} to -0.74 eV for Au_{38}^+ and -0.59 eV for Au_{38}^-, Table 2. This confirms the conclusions reached by analyzing the O_2 adsorption properties on this cluster: the presence of a positive or negative charge has little effect on the reaction profile. On the other hand, for this cluster size and shape, the dissociation reaction appears to be very favorable with energy barriers which are about one fifth of those found on the small Au_5 cluster. The reasons for the special behavior of Au_{38} are not entirely clear, but must be ascribed to the nature of the frontier orbitals and of the electron density of this cluster which appear to be particularly favorable for O_2 dissociation.

Au_{55} is characterized by very weak O_2 adsorption (0.2-0.5 eV, Table 2); the energy barriers to dissociation, from 0.54 to 0.88 eV (Table 2), are always higher than the adsorption energy but the variations with cluster charge are modest. In the final dissociative state the total energy is considerably lower, by more than 2 eV, than the O_2 chemisorbed state. The last case examined is that of Au_{79}. As in Au_{55} the O_2 molecule is weakly bound on all charge states. However, at variance with Au_{55}, the O-O molecule is elongated and forms spontaneously a superoxo complex. This is expected to favor the dissociation, and indeed the computed barriers are always below 0.5 eV (0.52 eV for Au_{79}^+, 0.42 eV for Au_{79}, and 0.49 eV for Au_{79}^-, Table 2). Thus, it is confirmed that the effect of the total cluster charge on the barrier is negligible for large Au clusters. On the other hand, the formation of a superoxo species in Au_{79} (Table 3) favors the dissociation. The barriers, in fact, are similar to those computed for Au_{38} which is the other cluster where a superoxo species is formed. E_R for Au_{79} is relatively small, about -0.7 eV, and again not dependent on the charge. The E_R value for Au_{79} is much smaller than that found on Au_{55} (about -2.2/-2.3 eV) and similar as for Au_{38}. The reason lies in the different structural response to the formation of two isolated O atoms: while on Au_{55} there is a strong relaxation which stabilizes the final products, the minor flexibility of Au_{38} and Au_{79} results in small relaxation (the cluster behaves more like an extended surface). Thus, in addition to the electronic effects that contribute to determine the cluster reactivity, like for instance the high IP of Au_{55}, one has to take into account also structural effects. Often, a clear distinction of the importance of these two terms, electronic and structural effects, is not simple.

Discussion and conclusions

From the data reported above, the following trends emerge. First of all, the systematic study of the reactivity of gold nanoclusters towards oxygen shows that systems containing several tens of atoms, up to Au_{79} at least, belong to the non scalable regime typical of clusters and nanostructures. The adsorption prop-

UNIVERSITAT ROVIRA I VIRGILI
MODELLING AU CATALYST FROM BULK TO NANOSCALE
Alberto Roldán Martínez
ISBN:978-84-693-7669-0/DL:T-1748-2010

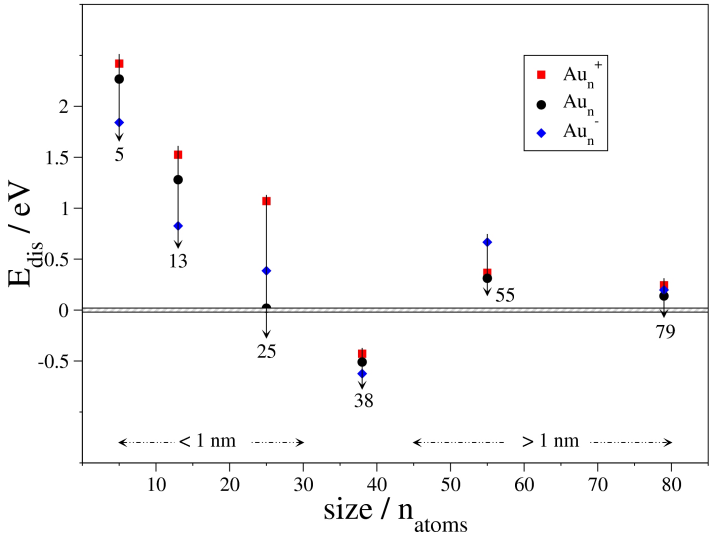

Figure 4: Plot of the dissociation energy, $E_{dis} = [E(Au_n) + E(O_2)] - \triangle E^{\#}$, as a function of cluster size and cluster charge. Negative E_{diss} values indicate that the O_2 can be dissociated by a given cluster, positive values indicate that desorption will take place instead of dissociation (see also Fig. 2 for definitions).

erties and reaction profiles depend very strongly on the size of the cluster considered. For example, going from Au_{38} to Au_{55} one moves from a very reactive cluster ideally suited to promote oxidative processes to a rather unreactive structure which is unable to properly activate the O-O bond. Just to mention another example, while the structure of Au_{25} adopted here resulted to be rather unstable, fluxional and easy to deform, a cluster like Au_{38} has a special stability which strongly reduces the atomic rearrangements induced by oxygen adsorption. This confirms that mass selection of specific cluster sizes is a desirable objective in the design of a new generation of catalysts since every size can exhibit peculiar properties.[15]

Coming to the main purpose of this study, i.e. verify the importance of positively or negatively charged gold clusters compared to their neutral counterparts in the activation of O_2, the calculations show that the effect is significant for ultra-small clusters containing less than 20 atoms like Au_5 and, to less extent, Au_{13}. On Au_5 the presence of a negative charge is beneficial since it lowers the activation barrier and stablizes the final products. Still, the computed barrier is very high (> 2 eV) indicating that this cluster will be inactive in promoting oxygen dissociation. Of course, things could change completely if a small cluster is deposited on an active substrate, an aspect which has been addressed in other studies.[15,32,33] An effect of the extra charge is found also on Au_{13} where, again, the barrier to dissociation is lower on the anionic form (by 0.13 eV compared to the neutral cluster). Also the binding and the activation of the O_2 molecule are more efficient on Au_{13}^- than on neutral Au_{13}. On both Au_5 and Au_{13} the presence of a positive charge does not seem to have a beneficial effect, neither on the O_2 binding nor on the barrier. This is consistent with the fact that the O_2 bond activation is related to the electron transfer

from the cluster to the adsorbate. The effect of the charge state cannot be easily evaluated on Au_{25} because of its great flexibility. Here it seems that a negative charged cluster helps O_2 chemisorption, but the corresponding dissociation barrier is rather high. Also considering that we cannot exclude the existence of more stable minima for $Au_{25}O_2$, no conclusion about the role of the charge can be derived from this system.

The situation is quite clear when we analyze the largest Au_{38}, Au_{55}, and Au_{79} clusters. Here the results (adsorption geometry and bond strength, barrier heigth, products stability, etc.) are essentially independent of the charge state of the cluster. While this can be expected for a cluster like Au_{79}, with nearly 900 valence electrons, it is not so clear that also a cluster of about 40 atoms will be unaffected by the addition or removal of one electron. On the other hand, the present results clearly indicate that for this cluster size there is no significant variation in cluster properties as a function of the charge state.

The calculations indicate also that some cluster sizes exhibit special behavior towards O_2 dissociation. In particular, a viable reaction requires that the barrier for dissociation, $\triangle E^{\#}$, should be smaller in absolute value of the adsorption energy, E_B, or, in other words, should be below the reference energy of the non-interacting fragments, see Fig. 2. When this is not the case, an increase in temperature to overcome the barrier instead of leading to a dissociation process will result in O_2 desorption. In Fig. 4 we have plotted a new quantity, the dissociation energy, E_{dis}, as a function of the cluster nuclearity for all charge states. E_{dis} is defined as:

$$E_{diss} = [E(Au_n) + E(O_2)] - \triangle E^{\#}$$

A negative value of E_{dis} indicates a favorable process (energy of the reactants higher than the energy of the TS, Fig. 2), and viceversa.[35] The plot of Fig. 4 clearly shows that of all gold clusters considered, only Au^{38} has the characteristics to give rise to oxygen dissociation (negative E_{dis}). For all other clusters the O-O bond dissociation is not a viable process. Of course, other oxidation mechanisms are possible, like for instance the direct interaction of the activated O_2 molecule with CO or another organic substrate.[14,15,32]

In conclusion, we have demonstrated that charging of gold clusters has pronounced effects for very small sizes up to about 20-25 atoms. When the size goes beyond about 40 atoms, size and shape effects appear to have a much more pronounced effect on the reactivity than the total cluster charge.

Acknowledgements

AR thanks Universitat Rovira i Virgili, for supporting his pre-doctoral research. Financial support has been provided by Spanish MICINN (grants FIS2008-02238/FIS and CTQ2008-06549-C02-01) and in part by Generalitat de Catalunya (grants 2009SGR1041, 2009SGR00462 and XRQTC) and by COST Action D41 "Inorganic oxides: surfaces and interfaces". Computational time has been generously provided by the Barcelona Supercomputing Center.

References

1 A. Stephen, K. Hashmi and G. J. Hutchings, Angew. Chem., Int. Ed., 2006, 45, 7896.

2 See also the reviews in the special issue dedicated to chemistry of nano-gold in Chem. Soc. Rev. 2008, 37.

3 M. Haruta Catal Today. 1997, 36, 153.

4 M. Valden, X. Lai, D. W. Goodman Science 1998, 281, 1647.

5 A. A. Herzing, C. J. Kiely, A. F. Carley, P. Landon and G. J. Hutchings, Science , 2008, 321, 1331.

6 Q. Fu, H. Saltsburg and M. Flytzani-Stephanopoulos, Science , 2003, 301, 935.

7 A. Rodriguez Jose, P. Liu, J. Hrbek, J. Evans and M. Perez, Angew Chem Int Ed Engl, 2007, 46, 1329.

8 A. Corma and P. Serna, Science, 2006, 313, 332.

9 M. D. Hughes, Y. J. Xu, P. Jenkins, P. McMorn, P. Landon, D. I. Enache, A. F. Carley, G. A. Attard, G. J. Hutchings, F. King, E. H. Stitt, P. Johnston, K. Griffin and C. J. Kiely, Nature, 2005, 437, 1132.

10 M. Turner, V. B. Golovko, O. P. H. Vaughan, P. Abdulkin, A. Berenguer-Murcia, M. S. Tikhov, B. F. G. Johnson and R. M. Lambert, Nature, 2008, 454, 981.

11 N. Lopez and J. Norskov, J. Am. Chem. Soc. 2002, 124, 11262.

12 A. Roldan, S. Gonzalez, M. Ricart Josep and F. Illas, ChemPhysChem, 2009, 10, 348.

13 G. C. Bond and D. T. Thompson, Gold Bull., 2000, 33, 41.

14 A. Sanchez, S. Abbet, U. Heiz, W. D. Schneider, H. Haekkinen, R. N. Barnett and U. Landman, J. Phys. Chem. A, 1999, 103, 9573.

15 B. Yoon, H. Hakkinen, U. Landman, A. S. Worz, J. M. Antonietti, S. Abbet, K. Judai, U. Heiz Science. 2005, 307, 403.

16 M. Haruta J. New Mater. Electrochem. Syst. 2004, 7, 163.

17 I. N. Remediakis, N. Lopez, J. K. Norskov Appl. Catal. A: General. 2005, 291, 13.

18 D. Pillay, G. S. Hwang Phys Rev B. 2005, 72, 205422.

19 S. S. Lee, C. Y. Fan, T. P. Wu, S. L. Anderson J. Am. Chem. Soc. 2004, 126, 5682.

20 F. Boccuzzi, A. Chiorino, M. Manzoli, P. Lu, T. Akita, S. Ichikawa, M. Haruta J. Catal. 2001, 202, 256.

21 L. M. Molina, B. Hammer Phys. Rev. Lett. 2003, 90, 206102.

22 J. A. Rodriguez, P. Liu, F. Viñes, F. Illas, Y. Takahashi and K. Nakamura, Angew. Chem. Int. Ed., 2008, 47, 6685.

23 J. A. Rodriguez, P. Liu, Y. Takahashi, K. Nakamura, F. Viñes and F. Illas, J. Am. Chem. Soc., 2009, 131, 8595.

24 E. Florez, L. Feria, F. Vines, J. A. Rodriguez, F. Illas J. Phys. Chem. C. 2009, 113, 19994.

25 A. Roldan, F. Vines, F. Illas, J. M. Ricart and K. M. Neyman, Theor. Chem. Acc., 2008, 120, 565.

26 A. Roldan, J. M. Ricart, F. Illas Theor. Chem. Acc. 2009, 123, 119.

27 G. Henkelman, B. P. Uberuaga, H. Jonsson J. Chem. Phys. 2000, 113, 9901.

28 G. Henkelman, H. Jonsson J Chem Phys. 1999, 111, 7010.

29 O. D Haberlen, S. C. Chung, M. Stener, N. Rösch J Chem Phys 1997, 106, 5189.

30 C. Jackschath, I. Rabin, W. Schulze Zeitschrift Fur Physik D-Atoms Molecules and Clusters 1992, 22, 517.

31 B. Yoon, H. Hakkinen, U. Landman J. Phys Chem A 2003, 107, 4066.

32 G. Pacchioni, S. Sicolo, C. Di Valentin, M. Chiesa, E. Giamello, J. Am. Chem. Soc., 2008, 130, 8690.

33 A. Roldan, J. M. Ricart, F. Illas, G. Pacchioni, J. Phys. Chem. C, ID: jp-2010-017357.R1

34 B. Hammer, L. B. Hansen, J. K. Noskov, Phys. Rev. B 1999, 59, 11.

35 D. R. Lide, CRC Handbook of Chemistry and Physics, Taylor and Francis, Florida, 2007.

UNIVERSITAT ROVIRA I VIRGILI
MODELLING AU CATALYST FROM BULK TO NANOSCALE
Alberto Roldán Martínez
ISBN:978-84-693-7669-0/DL:T-1748-2010

3.4.5 Theoretical simulation of temperature programmed desorption of molecular oxygen on isolated Au nanoparticles from density functional calculations and microkinetics models

Introduction

The discoveries of Haruta[1] and Goodman[2] concerning catalysis by gold nanoparticles have triggered a new research field in catalysis[3] with important potential implications in chemical reactions of technological[4] interest. In the past few years several important contributions were made involving catalysts based on supported Au nanoparticles. In particular we mention the work of Fu et al. concerning the water gas shift reaction catalyzed by Au nanoparticles supported on ceria,[5] of Corma et al. about selective hydrogenation of nitroaromatics[6] and about the synthesis of aromatic azo compounds from anilines and nitroaromatics catalyzed by Au,[7] and of Turner et al.[8] showing that it is possible to epoxidize styrene directly by dioxygen employing Au nanoparticles, derived from Au_{55}, supported on SiO_2. The increasing control over the nanoparticle size distribution led Ono and Roldan-Cuenya to prepare Au nanoparticles with two different distributions ($\sim$1.5 and $\sim$5 nm) and to deposit them on TiO_2 and SiO_2 supports.[9] This preparation allowed these authors to study the formation of gold oxide on the two types of Au nanoparticles and also to carefully analyze O_2 desorption thereon.[10] The thermal programmed desorption (TPD) experiments of Ono et al.[10] are in agreement with previous results by Bondzie et al.,[11] but the better control about particle size allowed them to show that, after exposure to atomic oxygen at room temperature, the O_2 desorption temperature peak depends on the nanoparticle size. Nevertheless, it is important to point out that the underlying desorption kinetics has been the subject of some controversy[12,13] and has been found to be more complex[10] than anticipated in the original work of Ono and Roldan-Cuenya.[9]

The experimental studies discussed above constitute without a doubt a fundamental step toward an improved control of the reactivity of Au nanoparticles with a concomitant gain of fundamental understanding. Nevertheless, several open questions remain which require further research. For instance, a key aspect is the structure and physical nature of the active site, although it is also important to disentangle particle and support effects as well as to separately investigate the effects related to particle size and particle morphology. The careful ex-

UNIVERSITAT ROVIRA I VIRGILI
MODELLING AU CATALYST FROM BULK TO NANOSCALE
Alberto Roldán Martínez
ISBN:978-84-693-7669-0/DL:T-1748-2010

periments designed by Chen and Goodman contributed to clarify some aspects by showing that a supported Au monolayer is more reactive than a bilayer.[14] Note that even with the current rather extreme control over particle size, experiments provide information about a certain particle distribution range, and it is difficult to assign the observed reactivity to a particular type of nanoparticle. Another related problem is the chemical composition of the supported Au particle. One may, for instance, wonder to which extent the particle contains oxide species,[15] as evidenced by the work of Ono and Roldan-Cuenya,[9] and which is the role of these species in the catalytic process. A related question concerns the precise oxidation state of Au atoms as suggested by Fu et al. for the water gas shift reaction catalyzed by Au supported on ceria[5] and by Abad et al. for the selective oxidation of alcohols.[16]

Theoretical techniques offer an alternative and complementary approach because one can make use of models designed specifically to focus on a given feature. For instance, it is possible to isolate a particle from support effects by considering either the particle alone or the naked support or both. This strategy has been successfully used in a recent study of the chemoselective hydrogenation of nitro groups in nitroaromatic compounds catalyzed by Au supported on TiO_2.[17] Theoretical models have also been employed to show that molecular hydrogen dissociation on Au can easily take place at lowcoordinate sites[18,19] whereas molecular oxygen dissociation on Au does not occur when the nanoparticles exceed a certain size.[20,21] In the case of molecular oxygen interacting with Au nanoparticles, the density functional theory (DFT) calculations of Roldan et al.[20,21] provide a molecular picture for the results of Turner et al. concerning epoxidation of styrene on Au nanoparticles supported on SiO_2 directly by dioxygen, which strongly suggests that molecular oxygen dissociation occurs in an initial step.[8] Moreover, the calculated adsorption/desorption energies and activation energies for molecular oxygen dissociation on Au nanoparticles of increasing size provide the necessary information to carry out a microkinetic analysis of the adsorption, dissociation, and recombination steps taking place above the Au nanoparticles which are relevant to the experimental work of Turner et al.,[8] and, with the appropriate conditions, it also allows one to compare to the experimental TPD measurements of Ono and Roldan-Cuenya,[10] thus providing an unbiased interpretation of the experimental results.

Nanoparticle Models and Computational Details

A systematic study of the interaction and dissociation of O_2 on Au_{25}, Au_{38}, Au_{55}, and Au_{79} nanoparticles has been carried out employing DFT techniques. Recently, it has been shown[22] that the computational setup employed in this work to study Au nanoparticles leads to results which are very close to those obtained from fully relativistic density functional all-electron calculations.[23] These results also evidence that beyond Au_{79} the electronic properties linearly scale to the bulk with subsequent loss of catalytic activity. The Au_{25}, Au_{38}, Au_{55}, and Au_{79} nanoparticles are three-dimensional metal crystallites cut from metal bulk through low-index planes and often have the typical cuboctahedral (Au_{38}, Au_{55}, and Au_{79}) shape of Au supported clusters except for Au_{25} which is derived from Au_{38} by removing two (100) atomic layers to provide a hemispherical particle similar to those found in experiments

UNIVERSITAT ROVIRA I VIRGILI
MODELLING AU CATALYST FROM BULK TO NANOSCALE
Alberto Roldán Martínez
ISBN:978-84-693-7669-0/DL:T-1748-2010

Figure 1: Schematic representation of the structures of the Au_{25}, Au_{38}, Au_{55}, and Au_{79} nanoparticles models used to study O_2 dissociation, O + O recombination, and desorption thereon.

(see Figure 1). Therefore, the nanoparticles used in the present work have diameters (estimated using the Au covalent radius) in the ∼1.0-∼1.5 nm range, and thus they are in the size range in the experiments of Turner et al.[8] and also cover at least the smallest type of particle studied by Ono and Roldan-Cuenya.[9,10] In all cases, O_2 has been added in such a way that dissociation follows the most favorable pathway.[20] The density functional calculations have been carried out using a supercell approach with the repeated images separated by a large vacuum width (>10 Å) and using the VASP package.[24–26] The one-electron states were expanded in a plane wave basis with a kinetic cutoff energy of 415 eV, whereas the PAW method[27] has been used to take into account the effect of the inner cores on the valence density. For these finite systems only the Γ-point of the reciprocal space needs to be considered. The total energy has been evaluated using the PW91 exchange-correlation potential; recent work has shown that, for the cases of interest in the present work, PBE and RevPBE potentials also lead to similar results.[21] Spin polarization has been tested in a few cases and found to be unimportant. The atomic structure of each one of the O_2-Au_n (n = 25, 38, 55, 79) systems has been fully relaxed, and the dissociation pathway to adsorbed oxygen atoms has been determined by means of the climbing image-nudged elastic band, the CI-NEB method.[28] The stationary points have been characterized by proper frequency analysis. Adsorption and barrier energies discussed hereafter have been all corrected to account for the zero point energy. The rate constant for a given elementary step (see below) is derived from conventional classical harmonic transition state theory of Evans-Polanyi-Eyring[29] as in eq 1

$$k = \left(\frac{k_B T}{h}\right)\left(\frac{q^{\#}}{q}\right) e^{-\frac{E_{barr}}{k_B T}} \qquad (1)$$

where k_B is the Boltzmann constant, T is the temperature, h is the Planck constant, $q^{\#}$ is the partition function of the transition state, q is the partition function of the reactants, and E_a is the activation energy. Partitions functions include translational, rotational, vibrational, and electronic contributions with the usual approximations.

Microkinetic Model

In order to provide an adequate framework to better compare theory and experiment, a microkinetic model is proposed which takes into account the adsorption and desorption of molecular oxygen on Au nanoparticles as well as the dissociation and recombination steps as indicated below:

Adsorption/Desorption of O_2 with rate constants k_1 (direct) and k_2 (inverse)

$$O_2(g) + 4* \leftrightarrow O_2(ads)$$

Dissociation/recombination of O_2 with rate constants k_3 and k_4

UNIVERSITAT ROVIRA I VIRGILI
MODELLING AU CATALYST FROM BULK TO NANOSCALE
Alberto Roldán Martínez
ISBN:978-84-693-7669-0/DL:T-1748-2010

Table 1: Hertz-Knudsen Adsorption Rate Constant (k_1) from Eq 3, Zero Point Energy Corrected Energy Barriers ($E_{a,i}$), Transition State Theory Calculated Pre-Exponential Factors, and Rate Constants at 300 K (cf. Eq 1) for the Desorption (i) 2), Molecular Oxygen Dissociation (i) 3), and Atomic Oxygen Recombination (i) 4) Steps on Au_{25}, Au_{38}, Au_{55}, and Au_{79} Nanoparticles.

	Au_{25}	Au_{38}	Au_{55}	Au_{79}
$k_1/(s \cdot ML^4)^{-1}$	554.2	607.2	678.5	624.5
$E_{a,2}$ /eV	0.48	0.91	0.30	0.19
A_2	3.18×10^{15}	9.47×10^{15}	6.77×10^{15}	1.08×10^{16}
k_2/s^{-1}	2.70×10^{7}	5.75	7.33×10^{10}	6.66×10^{12}
$E_{a,3}$ /eV	0.55	0.43	0.73	0.41
A_3	2.19×10^{12}	3.56×10^{12}	4.37×10^{12}	3.99×10^{12}
k_3/s^{-1}	1055.69	1.82×10^{5}	2.84	6.34×10^{5}
$E_{a,4}$ /eV	1.59	0.46	2.30	0.67
A_4	9.95×10^{12}	6.07×10^{11}	1.15×10^{13}	6.08×10^{12}
$k_4/(s \cdot ML)^{-1}$	1.06×10^{-23}	6.68×10^{-4}	1.96×10^{-38}	4.80×10^{-6}

$$O_2(ads) + 4* \leftrightarrow 2O(ads)$$

where the state of each component is given in parentheses and "*" indicates a free site on the nanoparticle surface. To be consistent with the dissociation reaction pathway where molecular oxygen takes place on the (001) facets of the cuboctahedral nanoparticles, we consider that one adsorbed oxygen atom occupies two sites and, hence, O_2 adsorption requires four sites. Consequently, the coverage of free sites becomes $\theta^* = 1 - 4\theta_{O_2} - 2\theta_O$. Thus, full occupation of sites at the (001) facets by O_2 corresponds to a molecular oxygen coverage θ_{O_2} of 0.25 ML, whereas $\theta_{O_2} = 0.05$ ML means occupation of 20% of these sites. Note, however, that atomic oxygen desorption is not considered because the large adsorption energy makes the event very unlikely. A further simplification concerns atomic oxygen diffusion through the nanoparticle surface and interaction between nanoparticles which has been neglected.

For the kinetic model consisting of the two reversible elementary steps described above, it follows that the concentration of each component as a function of time is governed by the following set of differential equations:

$$\frac{dP_{O_2}}{dt} = -k_1 \cdot P_{O_2}\theta_*^4 + k_2 \cdot \theta_{O_2}$$

$$\frac{d\theta_{O_2}}{dt} = k_1 \cdot P_{O_2}\theta_*^4 - k_2 \cdot \theta_{O_2} - k_3 \cdot \theta_{O_2} - k_4 \cdot \theta_O^2 \quad (2)$$

$$\frac{d\theta_O}{dt} = 2k_3 \cdot \theta_{O_2} - 2k_4 \cdot \theta_O^2$$

The transition state theory rate constants for the dissociation and recombination steps are obtained from eq 1 with values obtained from the density functional calculations. For the adsorption process we assume that there is no activation barrier, and the rate constant is estimated from the classical Hertz-Knudsen relation[30]

$$k = \frac{1}{(2\pi \cdot m \cdot k_B T)^{1/2}} A_{cat} \quad (3)$$

where A_{cat} is the area per active site. Finally, for the desorption step one assumes that the transition state is infinitely close to the desorbed state. In practice, this means using the partition functions for the free molecule for $q^{\#}$ in

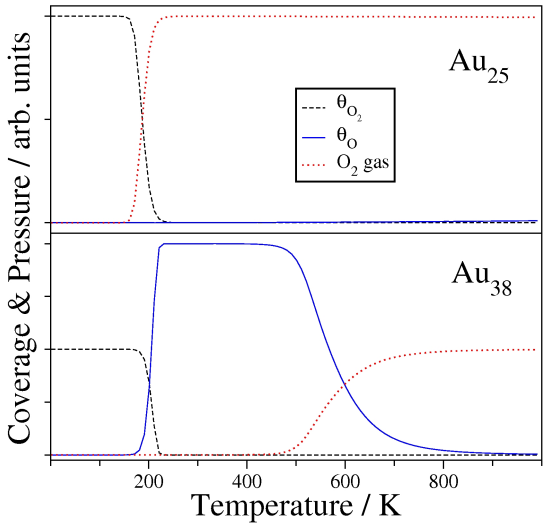

Figure 2: Atomic and molecular oxygen evolution for an initial O_2 coverage of 0.10 ML (40% of occupancy) on Au_{25} and Au_{38} at the zero limit of external pressure. Time of measurement is 1 ms.

eq 1 but with two degrees of freedom in the translational partition function because the third is taken as the reaction coordinate for desorption. Relevant information concerning the values of the reaction rate constants used in the present work is reported in Table 1.

Numerical integration of the set of differential equations has been carried using standard recipes and different sets of initial conditions. Results from the numerical simulation are discussed in the next section.

Results and discussion

In this section we discuss two different series of microkinetic simulations based on the rate constants derived from the DFT calculations and reported in Table 1. The first series attempts to explore the reactivity of Au nanoparticles toward O_2 dissociation including the four elementary steps described in the previous section and is motivated by the work of Turner et al.[8] evidencing direct epoxidation of styrene by dioxygen by Au nanoparticles supported on SiO_2. Consequently, this series assumes that the Au nanoparticles are in contact with a given amount of O_2 in the gas phase. Let us recall that the interaction of O_2 with Au nanoparticles is extremely influenced by the particle size that it is largely favored on low-coordinated Au atoms at the (001) facets. The second series of simulations attempts to compare to the experimental TPD data of Ono et al.[10] Therefore, this second series starts from atomic oxygen adsorbed at the Au nanoparticles with no molecular oxygen in the gas phase.

Let us start the discussion by considering the first series of microkinetic simulations which consider that O_2 is present in the gas phase. Figure 2 shows the coverage of atomic and molecular oxygen as a function of the temperature and also the O_2 pressure in the gas phase for the Au_{25} and Au_{38} particles for a reaction time of 1 ms. Note that the effect of the temperature is taken into account in the corresponding rate constants, and, hence, the reaction time starts to count assuming that the sample has been heated up to

UNIVERSITAT ROVIRA I VIRGILI
MODELLING AU CATALYST FROM BULK TO NANOSCALE
Alberto Roldán Martínez
ISBN:978-84-693-7669-0/DL:T-1748-2010

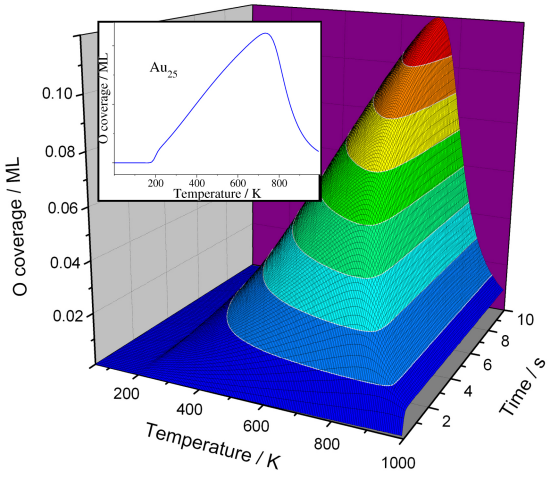

Figure 3: Atomic oxygen evolution on Au_{25} as a function of temperature (from 1 to 1000 K) and time (from 0 to 10 s) for an initial O_2 coverage of 0.10 ML. Atomic and molecular oxygen partial pressure evolution for a reaction time of 8 s is shown in the inset.

this temperature. For Au_{25} one can readily see that the desorption rate reaches its maximum at around 200 K and that the atomic oxygen coverage is essentially zero in the 0-400 K temperature range. Au_{38} activation of adsorbed O_2 occurs below the energy threshold for molecular desorption, and atomic oxygen is available on the surface for a rather large temperature range, which confirms the conclusions reached from the analysis of the potential energy surface for O_2-2O on Au_{38}[20] and supports the hypothesis of Turner et al.[8] that these types of particles are the ones that are active for styrene epoxidation. On particles larger than Au_{38}, it is found that desorption takes place at low temperature, simply because the dissociation energy barrier is too large compared to the desorption energy.

In order to better analyze the reaction kinetics occurring in the smallest Au_{25} nanoparticle, we present in a three-dimensional plot (Figure 3) of the atomic oxygen coverage as a function of both the temperature and the reaction time. Figure 3 shows that the atomic oxygen coverage is significant for large reaction times even at rather high temperatures. In fact, the inset reports the atomic oxygen evolution with respect to the temperature and shows that this reaches a maximum at $\sim$750 K for a reaction time of 8 s. This is because larger reaction times contribute to accumulate adsorbed atomic oxygen because molecular desorption and dissociation reactions are practically at equilibrium. Therefore, once atomic oxygen is formed, it remains adsorbed up to temperatures higher than 750 K. Only beyond this temperature and for sufficiently large reaction times, the recombination step starts to decrease the amount of atomic oxygen available at the nanoparticle surface. For the larger Au_{55} and Au_{79} particles, the microkinetic analysis shows that atomic oxygen is not present even at high temperatures and even after much larger reaction times. In any case, the global process concerns molecular oxygen adsorption/desorption because in the present study atomic oxygen, in principle avail-

UNIVERSITAT ROVIRA I VIRGILI
MODELLING AU CATALYST FROM BULK TO NANOSCALE
Alberto Roldán Martínez
ISBN:978-84-693-7669-0/DL:T-1748-2010

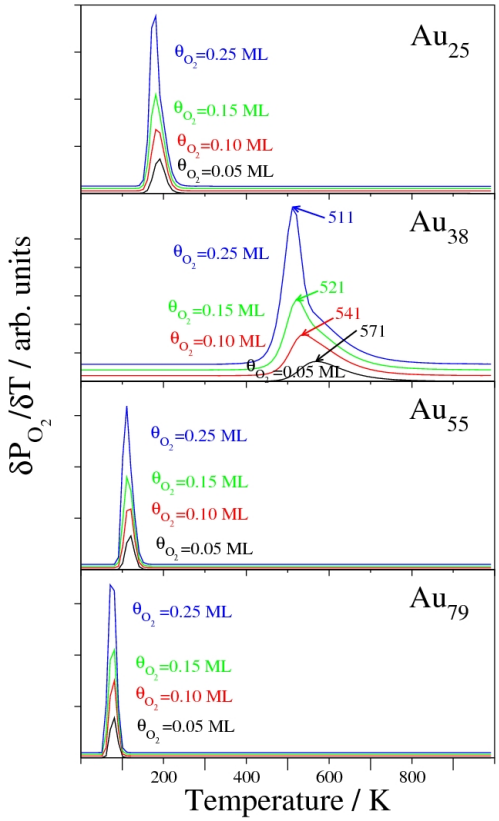

Figure 4: Simulated TPD curves for O_2 desorption on Au_{25}, Au_{38}, Au_{55}, and Au_{79} nanoparticles for a reaction time of 1 ms at different initial coverage values. In the case of Au_{38} the maximum desorption temperature peaks are indicated.

able for a subsequent reaction with other reactants as in the styrene epoxidation studied by Turner et al.,[8] can only recombine and then desorb as O_2.

The evolution of O_2 with temperature can be monitored by a computational simulation of the temperature programmed desorption (TPD) curves although these cannot be directly compared to the experimental measurements of Ono and Roldan-Cuenya[9,10] because the initial conditions are different. Figure 4 reports the simulated TPD spectra of molecular oxygen on the various Au nanoparticles considered in the present work and for various O_2 coverage values. The figure plots the derivative of the O_2 partial pressure with respect to the temperature; this corresponds to an experimental situation where O_2 is continuously pumped. The desorption peaks indicate the temperature at which the O_2 pressure variation reaches its maximum, which is directly related to the adsorption energy. From Figure 4 it is also clear that for the Au_{55} nanoparticle O_2 desorption takes place below 150 K, whereas for Au_{25} the desorption peak takes place at 200 K and only for Au_{38} the desorption maximum is above room temperature, between 500 and 600 K, depending on the initial coverage.

The dependence of the desorption temperature peak with coverage is ana-

UNIVERSITAT ROVIRA I VIRGILI
MODELLING AU CATALYST FROM BULK TO NANOSCALE
Alberto Roldán Martínez
ISBN:978-84-693-7669-0/DL:T-1748-2010

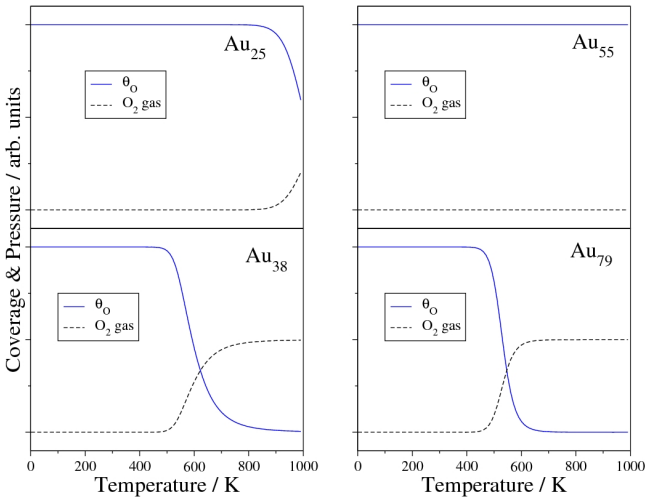

Figure 5: Atomic and molecular oxygen evolution on Au_{25}, Au_{38}, Au_{55}, and Au_{79} starting from atomic oxygen adsorbed at the Au nanoparticles (0.1 ML) for a reaction time of 1 ms.

lyzed in some more detail in Figure 4 for the case of the Au_{38} nanoparticle. The TPD simulated curves show that increasing coverage results in lower temperature for the TPD maximum desorption peak. Hence, for Au_{38} at full coverage (θ_{O_2} = 0.25 ML) the desorption peak occurs at 511 K, whereas for a 20% occupancy of active sites (θ_{O_2} = 0.05 ML) it rises up to 571 K. Furthermore, the TPD peaks for Au_{38} show a flat tail toward higher temperatures because the recombination step is much slower than the desorption one, and it leads to a pseudosecond- order desorption process.

Let us now discuss the second series of microkinetic simulations aimed at comparing the present calculated results with the accurate and careful experiments of Ono and Roldan-Cuenya.[9,10] Nevertheless, it is necessary to remember that the experimental preparation used by these authors is likely to lead to particles with a metallic Au core and oxide shell and that the precise chemical composition is unknown. Figure 5 presents the evolution of atomic and molecular oxygen for each one of the Au nanoparticles considered in the present work. The simulations in Figure 5 start from a situation where only atomic oxygen is present at the surface of the Au nanoparticles. Here, molecular oxygen desorption is only possible after recombination toward adsorbed O_2, but this step requires a high temperature to overcome the rather large barrier. Figure 5 shows that the particle size has a strong influence on the temperature desorption, in agreement with the simulations discussed above. For Au_{38} and Au_{79}, O_2 desorption starts at roughly 500 K, whereas for Au_{25} it requires reaching a much higher temperature and for Au_{55} it practically does not occur in the range of temperatures explored.

Finally, Figure 6 reports the simulated TPD starting from a situation in which the particles are covered by different amounts of atomic oxygen. Let us recall that with the present definition, a coverage of $\vartheta_O = 0.50$ ML represents full coverage since all active sites for O_2 dissociation are occupied. We already mentioned that this is, of course, a simplification of the model which ignores atomic oxygen diffusion to the (111) facets of the

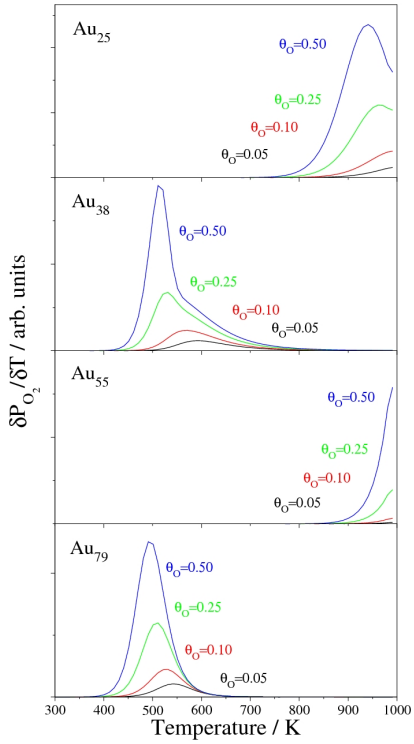

Figure 6: Simulated TPD curves for O_2 desorption on Au_{25}, Au_{38}, Au_{55}, and Au_{79} nanoparticles for a reaction time of 1 ms at different initial coverage values and starting from adsorbed atomic oxygen.

Au nanoparticles. The present results for the simulated TPD in Figure 6 agree qualitatively with experimental findings in the sense that the TPD peak depends strongly on the particle size and it is independent of the support. Note that in the simulated TPD, particle size effects are even larger than in the experiment. Moreover, the calculated and experimental positions of the TPD peak for the particles in the 1.5 nm range are remarkably close. This is an indication that the assumptions in the microkinetic model used in the present work are tic. In particular, the close similarity between the simulated TPD for the Au_{38} and Au_{79} particles and the experimental results for the smaller ($\sim$1.5 nm) nanoparticles suggests that the particles used in the experiment are still mainly metallic. Note also that the energy barrier for atomic oxygen recombination is especially large for Au_{25} and Au_{55} and this is the origin of the TPD peak at a rather high temperature obtained for these two particles. This is not surprising since these nanoparticles are far from the scalable range where the properties of particles follow a monotonous trend.

Conclusions

A microkinetic model based on density functional calculated rate constants has been presented for the evolution of atomic and molecular oxygen on Au nanoparticles which takes into account molecular adsorption/desorption as well as dissociations/recombination chemical reactions. Two series of simulations have

UNIVERSITAT ROVIRA I VIRGILI
MODELLING AU CATALYST FROM BULK TO NANOSCALE
Alberto Roldán Martínez
ISBN:978-84-693-7669-0/DL:T-1748-2010

been considered which are related to the work of Turner et al. for styrene epoxidation by dioxygen[8] and to the work of Ono and Roldan-Cuenya on Au nanoparticles.[10] In the first series we consider explicitly the presence of molecular oxygen in the gas phase, whereas the second one starts from a situation where only atomic oxygen is present. The first series of simulations confirms that, upon O_2 adsorption, atomic oxygen may be present at the surface of small Au nanoparticles (Au_{25} and Au_{38}) and hence may provide the oxidizing agent for styrene epoxidation, whereas for larger particles (Au_{55} and Au_{79}) desorption always takes place before dissociation even for large reaction times. The simulated TPD for the second series evidences that the position of the TPD peaks strongly depends on the particle size, which is in qualitative agreement with experimental findings. The rather close agreement between calculated and TPD also suggest that Au nanoparticles in the 1.5 nm range are likely to be metallic and therefore much harder to oxidize that the larger (5 nm) ones.[31]

Acknowledgement

A.R. thanks Universitat Rovira i Virgili for supporting his predoctoral research. Financial support has been provided by Spanish MICINN (grants FIS2008-02238/FIS and CTQ2008-06549-C02-01) and in part by Generalitat de Catalunya (grants 2009SGR1041, 2009SGR00462, and XRQTC). Computational time has been generously provided by the Barcelona Supercomputing Center.

References

(1) Haruta, M. Catal. Today 1997, 36, 153.

(2) Valden, M.; Lai, X.; Goodman, D. W. Science 1998, 281, 1647.

(3) See also the reviews in the special issue dedicated to chemistry of nanogold in Chem. Soc. ReV. 2008, 37.

(4) Hughes, M. D.; Xu, Y. J.; Jenkins, P.; McMorn, P.; Landon, P.; Enache, D. I.; Carley, A. F.; Attard, G. A.; Hutchings, G. J.; King, F.; Stitt, E. H.; Johnston, P.; Griffin, K.; Kiely, C. J. Nature 2005, 437, 1132.

(5) Fu, Q.; Saltsburg, H.; Flytzani-Stephanopoulos, M. Science 2003, 301, 935.

(6) Corma, A.; Serna, P. Science 2006, 313, 332.

(7) Grirrane, A.; Corma, A.; Garcı´a, H. Science 2008, 322, 1661.

(8) Turner, M.; Golovko, V. B.; Vaughan, O. P. H.; Abdulkin, P.; Berenguer-Murcia, A.; Tikhov, M. S.; Johnson, B. F. G.; Lambert, R. M. Nature 2008, 454, 981.

(9) Ono, L. K.; Roldan-Cuenya, B. J. Phys. Chem. C 2008, 112, 4676.

(10) Ono, L. K.; Roldan-Cuenya, B. J. Phys. Chem. C 2008, 112, 18543.

(11) Bondzie, V. A.; Parker, S. C.; Campbell, C. T. J. Vac. Sci. Technol., A 1999, 17, 1717. Erratum: Ibid 2008, 26, 1546.

(12) Gottfried, J. M. J. Phys. Chem. C 2008, 112, 16721.

(13) Ono, L. K.; Roldan-Cuenya, B. J. Phys. Chem. C 2008, 112, 16723.

(14) Chen, M. S.; Goodman, D. W. Science 2004, 306, 252.

(15) Campbell, C. T. Science 2004, 306, 234.

(16) Abad, A.; Concepcion, P.; Corma, A.; Garcia, H. Angew. Chem., Int. Ed. 2005, 44, 4066.

(17) Boronat, M.; Concepcion, P.; Corma, A.; Gonzalez, S.; Illas, F.; Serna, P. J. Am. Chem. Soc. 2007, 129, 16230.

(18) Corma, A.; Boronat, M.; Gonzalez, S.; Illas, F. Chem. Commun. 2007, 3371.

(19) Boronat, M.; Illas, F.; Corma, A. J. Phys. Chem. A 2009, 113, 3750.

(20) Roldan, A.; Gonzalez, S.; Ricart, J. M.; Illas, F. ChemPhysChem 2009, 10, 348.

(21) Roldan, A.; Ricart, J. M.; Illas, F. Theor. Chem. Acc. 2009, 123, 119.

(22) Roldan, A.; Vines, F.; Illas, F.; Ricart, J. M.; Neyman, K. M. Theor. Chem. Acc. 2008, 120, 565.

(23) Haberlen, O. D.; Chung, S. C.; Stener, M.; Rösch, N. J. Chem. Phys. 1997, 106, 5189.

(24) Kresse, G.; Furthmueller, J. Phys. ReV. B 1996, 54, 11169.

(25) Kresse, G.; Hafner, J. Phys. ReV. B 1993, 47, 558.

(26) Kresse, G.; Furthmuller, J. Comput. Mater. Sci. 1996, 6, 15.

(27) Blochl, P. E. Phys. ReV. B 1994, 50, 17953.

(28) Henkelman, G.; Jonsson, H. J. Chem. Phys. 2000, 113, 9978.

(29) Henkelman, G.; Uberuaga, B. P.; Jonsson, H. J. Chem. Phys. 2000, 113, 9901.

(30) Laidler, K. J. Chemical Kinetics, third ed.; Harper Collins: New York, 1987.

(31) Boyen, H. G.; Kastle, G.; Weigl, F.; Koslowski, B.; Dietrich, C.; Ziemann, P.; Spatz, J. P.; Riethmuller, S.; Hartmann, C.; Moller, M.; Schmid, G.; Garnier, M. G.; Oelhafen, P. Science 2002, 297, 1533.

UNIVERSITAT ROVIRA I VIRGILI
MODELLING AU CATALYST FROM BULK TO NANOSCALE
Alberto Roldán Martínez
ISBN:978-84-693-7669-0/DL:T-1748-2010

Summary and concluding remarks

In this thesis we have carried out a systematic study of gold structures as well as adsorption of different molecules on Au surface and nanoparticles. We have used a plane-wave DFT method and periodic models implemented in VASP. The key steps to understand the catalytic phenomena are derived from the characterization of structures, adsorption modes and nature of the adsorbate-substrate interaction, reaction energies and reaction barriers. Our work was aimed at completing experimental observations and providing additional data.

We have focused our attention on the different structures of Au: bulk, surfaces, nanowires and nanoparticles. The gold catalytic activity has been studied towards the partial oxidation of propene and oxygen activation-dissociation on the $Au(111)$ surface and cuboctahedral nanoparticles respectively.

Three-Dimensional gold

We have carried out the study of gold bulk to obtain a right background on its description. This background is useful to prepare future gold structures such as surface or nanoparticles.

The parameter of unit cell (a_0) of Au derived by LDA(VWM) exchange-correlation functional (4.07 Å) is closer to experimental one (4.07 Å) than the obtained by GGA(PW91) (4.17 Å). It is accepted that GGA overestimate the distances.

The bulk modulus (B_0) is difficult to reproduce accurately due to the several approximations done along its calculation. Nevertheless experimental value (220 GPa) is close to derived by LDA(VWM) differing by $26\,GPa$. Although both functional used LDA(VWM) and GGA(PW91) are below the experimental, the last differs by 75 GPa.

Finally, the cohesive energies (E_{coh}) carried out with LDA(VWM) and GGA(PW91) are far from experimental value (-3.78 $eV/atom$) by $0.52\,eV/atom$ and $0.72\ eV/atom$ respectively.

Gold bulk structure is rather well described by local density approximation exchange-correlation functional. However, LDA faults on the interaction energy description; nevertheless, to solve this poor description we can carry out a single point calculation over well described LDA geometries with GGA functional, this approximation is so-called GGA//LDA.

UNIVERSITAT ROVIRA I VIRGILI
MODELLING AU CATALYST FROM BULK TO NANOSCALE
Alberto Roldán Martínez
ISBN:978-84-693-7669-0/DL:T-1748-2010

Two-Dimensional gold

We have checked several adsorption position and orientation of propene molecule on bare and oxigenated $Au(111)$ surface to study the partial oxidation of this molecule. To carry out this study we have followed a methodology used for the same process on $Ag(111)$ and $Cu(111)$ [166, 167].

On both Au surfaces, bare and oxygenated, the propene molecule adsorbs almost parallel to the surface by a weak interaction and without important structural distortions. The adsorption energy slightly increases by the presence of oxygen adatoms.

In agreement with the literature, the partial oxidation of propene by co-adsorbed oxygen atom takes place through two different ways: via oxametallacycle (OMMP) or via allyl formation. A detailed analysis of our results shows that both pathways are thermodynamically favorable but oxametallacycle falls below allyl compound by 0.64 eV. Nevertheless the pathway towards oxametallacycle formation has a barrier energy of 0.52 eV, which is larger than the barrier towards allyl formation (0.20 eV). Therefore OMMP formation is kinetically disabled whereas the favorable process is the H-stripping by the basic O-adatom leading to allyl radical and adsorbed OH. The secondary reaction step burns allyl to CO_2 and H_2O as well as Cu and Ag done [35, 11, 15].

Thus, the partial oxidation of propene towards propene oxide is an unfavorable pathway on oxygenated $Au(111)$ as a catalyst, in agreement with experimental results [15]. The amphoteric character of oxygen adatom on s^1d^{10} metals and the results of propene oxidation on these regular surfaces suggest that we could tune the reaction profile to desired products.

One-Dimensional gold

We have studied the growth mechanism of metal nanowires by nanoparticle self-assembly. This study was carried out taking advantage of periodic methodology provided by plane-waves [143]. The GGA//LDA approach methodology has been used to obtain an accurate description of geometries by LDA(VMW) and interaction energies by GGA(PW91) functional.

Besides merging metallic particles in a parallel way along [001] growth direction as Ref. [143] does for Pd, we have checked two other different mechanism: adding nanoparticles twisted 45^{o} with respect to the other and following the [111] growth direction by merging (111) nanoparticle faces.

All mechanisms are favorable thermodynamically. Nevertheless the Au_{79} self-assembly growth mechanism along [111] direction provides a major energy gain (10.06 eV). After it, twisted mechanism gains 4.97 eV and finally the parallel way gains 3.85 eV. The experimental distance between nanowire fragments differs in the most favorable mechanism by 0.03 nm, using Au_{79} as a nanowire piece, along [001] direction the twisted mechanism differs by -0.01 nm and means parallel addition by 0.01 nm.

These results suggest that nanoparticles interaction is dominated by raising coordination. For instance, when Au_{79} is added by [111] direction, the coordination number increase on 12 atoms instead of the 4 atoms on [001] mechanism.

Besides the anisotropy that Au nanowires present, their density of states (DOS) show many similitudes with the DOS of bulk, indicating a certain chemical inertness

and stability that reinforces the applicability in electronic devices. Many other properties can be derived from this kind of study such as Young modulus and transport properties [49, 48].

Zero-Dimensional gold

Nanoparticles structure

We have carried out the study of a set of gold nanoparticles containing up to 225 atoms. These nanoparticles are comparable in size with the experimental supported ones [168, 169, 170, 171, 172, 173, 174, 58]. The starting structure of these nanoparticles is provided by cutting the Au bulk through low index facets leading to octahedral and cuboctahedral shapes [57]. These moieties have been placed in the center of a large enough cell to avoid interaction between replicated nanoparticles. The basis set is provided by the plane-waves approach which is applicable in an almost routine fashion and without symmetry restriction to ticalliy mimic crystallites present in metal catalyst. Also the use of spherical droplet model has been proved to be quite useful in rationalizing the dependence on cluster size properties [65].

The convergence of nanoparticle properties toward its bulk value is simply given by the rate of decreasing influence of the surface compared to the bulk part as the cluster size grows [175, 176, 65]. Then, appealing to a liquid droplet model, distances can be rationalized in terms of an increasing pressure with decreasing droplet radios due to the surface tension. Nevertheless we have shown that the scalability for particles made of various elements differs in bond lenght. In Au_n species (n>38), the scalability is noticeable less perfect ($R^2_{(LDA)} = 0.940$) than for Ag_n ($R^2_{(LDA)} = 0.978$) and Cu_n ($R^2_{(LDA)} = 0.981$) for the same range of clusters.

The cohesion energy trend-line obtained from the same particles range shows a linear scalability towards bulk as a function of nanoparticles radius using both LDA and GGA functionals. The last one shows a closer results with experimental bulk value. For Cu and Ag the correlation trend-lines are $R^2_{(GGA)} = 0.997$ and $R^2_{(GGA)} = 0.997$ respectively, and for Au $R^2_{(GGA)} = 0.986$.

The d-band center on density of states (DOS) goes monotonously to bulk values with increasing the particle size, for all species under scrutiny. Otherwise, the smallest members of the set do not follow this trend due to their molecular character. The similarities to DOS bulk is shown from clusters containing at least 80 atoms.

From a general point of view, the results illustrate some practical consequences of the lack of a sufficiently accurate universal exchange-correlation functional (especially for heavy-element systems), which would be capable of equally precise description of the whole spectrum of observable parameters. However, especially important for future applications, the present interatomic distances of Au_n particles obtained with plane-wave approximation is in excellent agreement with data of previous benchmark all-electron scalar relativistic calculations [65].

Reactivity of gold nanoparticles

The Au nanoparticles interaction with molecules has been studied following the same model and methodology than for the study of their structures: the nanoparticles are placed in the center of large enough cell. We have studied the O_2 adsorption and

UNIVERSITAT ROVIRA I VIRGILI
MODELLING AU CATALYST FROM BULK TO NANOSCALE
Alberto Roldán Martínez
ISBN:978-84-693-7669-0/DL:T-1748-2010

dissociation on a set of cuboctahedral Au_n nanoparticles ($n = 13, 25, 38, 55, 79$), and planar Au_5 moiety.

Small nanoparticle properties often show considerable oscillations with size and shape because the finite cluster models represent insufficiently the surface electronic structure [177]. Otherwise, the electron confinement into a restricted volume produces a quantum size effects in the cluster electronic structure. The quantum effect appears to be responsible for the unexpected catalytic properties of the nanoscaled Au system [178].

One may advance a chemical argument based on unsaturated bonds as expressed by the fact that the average coordination number decreases with cluster size [179]. From a general perspective, the coordination argument alone helps us to understand why Au particles must be small to be reactive: A condition is the existence of a sizable driving force for capturing a molecule, for instance O_2. This only occurs at very special places, namely, edges or vertex [180].

Hence, the structure of the nanoparticles set were optimized and O_2 was added in all possible coordination ways on the facets and edges described above, for O_2 on Au_{55} has been tried almost 30 initial geometries. As the molecule approaches to the nanoparticle, it loses its magnetic moment and becomes trapped in a superoxo state with an enlarged bond length [180]. This is consistent with the fact that the O_2 bond activation is related to the electron transfer from the cluster to the molecule.

Nanoparticles of modest size (Au_{25}, Au_{38} and Au_{79}) evidence that the O_2 adsorption energy is rather strongly dependent on the exchange–correlation functional chosen. The tendency of LDA to strongly overestimate the adsorption energy reported by various authors [181, 182, 183, 184, 185] as well as our work. Otherwise PW91 adsorption energies are shorter than the PBE by roughly 0.20 eV and those are shorther than the RevPBE by about 0.35 eV. The correlations established in our work allow one to quantitatively predict binding energies of coinage metal nanoparticles filling the gap between the currently computationally tractable particles of up to 100–200 atoms and larger ones. The influence of the exchange–correlation functional on the energy barriers for O_2 dissociation are, however, much smaller. On the one hand this is a good new since it indicates that, for a given system, the description of this elementary step does not depend on the choice of the functional.

The adsorption properties and reaction profiles depend very strongly on the size of the cluster considered. For example, going from Au_{38} to Au_{55} one moves from a very reactive cluster ideally suited to promote oxidation processes to a rather unreactive structure. Hence, we have analyzed the Au_{38}, Au_{55}, and Au_{79} clusters showing that results are essentially independent of the charge state of the cluster in agreement with experiment.The charge effect is significant for ultra-small clusters containing less than 20 atoms like Au_5 and, to less extent, Au_{13}.

The dissociative adsorption is predicted to induce large relaxations in the gold part of the complex. It could be detected by mobility measurements or electron diffraction spectroscopy such as high-resolution photoelectron spectroscopy which in this case should reveal typical $Au - O$ bond frequencies.

In summary, our theoretical studies present convincing evidence that:

1. Strong adsorption of molecular oxygen on Au nanoparticles is a necessary but not sufficient condition for O_2 dissociation.

UNIVERSITAT ROVIRA I VIRGILI
MODELLING AU CATALYST FROM BULK TO NANOSCALE
Alberto Roldán Martínez
ISBN:978-84-693-7669-0/DL:T-1748-2010

2. The presence of low coordinate Au atoms is not enough to dissociate O_2.

3. There is a common pathway for O_2 dissociation where the energy barrier is almost equal.

4. There is a critical size for Au nanoparticles to dissociate O_2.

5. The effect of the oxidation state on medium size Au_n is negligible on adsorption and on energy barrier.

The dissociation barriers are quite large for ultra small clusters, of the order of 1 eV or more over the desorption limit [55]. This is in agreement with the experimental evidence that these Au nanoparticles exhibit a particular chemical inertness [186]. In particular, a viable reaction requires that the barrier for dissociation should be smaller in absolute value of the adsorption energy, this is the case of Au_{38} that adsorbs O_2 with a binding energy of 1 eV meanwhile the barrier to overcome is around 0.50 eV.

Rate constants based on a microkinetic model has been presented for the evolution of atomic and molecular oxygen on Au nanoparticles. This model takes into account molecular adsorption/desorption as well as dissociation/recombination chemical reactions. Two series of simulations have been considered which are related to the work of *Turner et al.* for styrene epoxidation by dioxygen [23] and to the work of *Ono* and *Roldan-Cuenya* on Au nanoparticles [187].

These series of simulations confirms that, upon O_2 adsorption, atomic oxygen may be present at the surface of small Au nanoparticles (Au_{25} and Au_{38}) and hence may provide the oxidizing agent for alkene epoxidation, whereas for larger particles (Au_{55} and Au_{79}) desorption always takes place before dissociation even for large reaction times. Therefore, the position of the TPD peaks strongly depends on the particle size.

In conclusion, we have demonstrated that charging of gold clusters has pronounced effects for very small sizes up to about 20-25 atoms. When the size goes beyond about 40 atoms, size and shape effects appear to have a much more pronounced effect on the reactivity than the total cluster charge. The oxidation state of these Au clusters does not modify significantly the catalytic activity, nor critical size.

UNIVERSITAT ROVIRA I VIRGILI
MODELLING AU CATALYST FROM BULK TO NANOSCALE
Alberto Roldán Martínez
ISBN:978-84-693-7669-0/DL:T-1748-2010

4.1 Introducció, objectius i conclusions en Català

Els processos catalítics sobre superfícies metàl·liques són de gran importància, no només per a la indústria, sinó també per a la vida diària. Per això, és interessant millorar el coneixement a nivell elemental dels processos de fisisorció, quimisorció, difusió molecular i ruptura o formació d'enllaços. Això exigeix les tècniques experimentals més avançades i les descripcions teòriques disponibles: espectroscòpia, química computacional i mecanismes cinètics. Altrament, els perfils de reacció són de gran importància per a entendre com tenen lloc els processos al món macroscòpic. En particular, en aquesta tesi ens centrem en l'or, les seves diferents estructures i la seva activitat catalítica. La química computacional pot ser un suport important per als investigadors, fent més fàcil la interpretació de fenòmens a nivell molecular, i per a predir propietats interessants dels sistemes en estudi.

Or sòlid

L'or ha fascinat la humanitat des que es va descobrir, essent el més noble dels metalls, no es desenllustra quan s'exposa a l'atmosfera i reté la seva brillantor per sempre.

Per als químics, fins fa poc, l'or ha presentat molt poc interès, encara que fascinava als alquimistes abans que comencés la química moderna. La raó és la seva inactivitat química com a metall, cosa que proporcionava oportunitats molt limitades a l'hora d'obrir una nova química. En vista d'això, la química de l'or era pràcticament nul·la i, típicament, a qualsevol llibre de text de química el capítol que tractés d'or ho feia de manera molt breu.

Superfícies d'or

L'ús d'or com a catalitzador metàl·lic ha estat descartat històricament a causa de la seva baixa reactivitat. Les superfícies d'or són altament inactives per a dissociar la molecular d'oxigen, una fase clau en moltes reaccions d'oxidació com l'oxidació parcial d'alquens [1]. L'oxidació parcial d'aquests produeix, entre d'altres components, l'epòxid, un apreciat producte per a moltes indústries. Aquest compost és un reactiu químic intermediari i s'utilitza principalment en la fabricació de poliols polièter, glicols de propè, èters de glicol i glicols de polialquens. Els epòxids dels alquens més simples, etè i propè, tenen una gran i creixent demanda, l'òxid d'etè (EO) té un consum mundial aproximat de 20 milions de tones per any i l'epòxid de propè (PO) de més de 6 milions de tones per any.

L'òxid de propè es produeix tradicionalment mitjançant la clorhidrina, un compost obtingut a partir del propè i del clor en presència d'aigua, aquest mètode però, produeix una gran quantitat de residus [2, 3, 4]. Altres tècniques fan sevir l'oxidació electroquímica en ànodes de Pt, o l'oxidació fotoquímica sobre catalitzadors basats en SiO_2 [5]; tanmateix, les selectivitats no són suficientment altes, un 50% la més alta [6], encara que s'ha vist que alguns catalitzadors comercials operen amb selectivitats d'un 80%.

L'estudi de l'epoxidació d'un alquè mitjançant la catàlisi heterogènia en ultra alt buit (UHV) depèn de l'ús d'olefines de pes molecular elevat amb barreres de desorció per damunt la barrera per a la oxidació [7], per exemple, l'estirè s'utilitza per estudiar l'etè, ja que són anàlegs químicament però l'estirè té un pes molecular més alt i una

desorció a una temperatura més alta [8, 9, 10, 11, 12]. L'oxidació parcial d'estirè a òxid d'estirè s'ha observat en $Ag(100)$ [9], $Ag(111)$ [8, 12], $Cu(110)$ [13], $Cu(111)$ [14], i últimament, els catalitzadors basats en l'or han atret una atenció considerable a causa de la seva utilitat potencial per a reaccions d'oxidació, incloent-hi l'epoxidació de propè [15].

L'espècie responsable de l'oxidació en la catàlisi heterogènia ha estat un tema de debat en la comunitat científica. Bàsicament, s'han plantejat dues hipòtesis, la primera és que el dioxigen adsorbit fos l'agent epoxidant mentre que els àtoms d'oxigen adsorbits eren responsables de la combustió [16]. La hipòtesi alternativa, basada en mesures clàssiques, era que tota la química estava causada per l'oxigen atòmic [17]. Senzilles mesures sobre monocristalls van demostrar que els àtoms d'oxigen adsorbits reaccionaven amb l'etè adsorbit sobre una superfícies d'argent per a produir l'epòxid i també productes de la combustió [18]. Això conclou que els àtoms d'oxigen són els responsables tant de la combustió com de l'oxidació selectiva dels alquens coadsorbits [19, 20, 21, 7, 15].

Així doncs, la coordenada de reacció en el procés d'oxidació ha d'incloure l'adsorció i dissociació de la molècula d'oxigen, on la barrera d'activació sembla jugar un paper crucial per a determinant la cinètica de reacció global [20, 21]. La dissociació d'oxigen molecular es dóna en molts elements metàl·lics de forma pràcticament immediata produint oxigen atòmic adsorbit, aquests metalls normalment modifiquen fortament l'estructura electrònica de les molècules orgàniques coadsorbides causant-hi la combustió [23].

Està establert que les superfícies d'or són inactives front l'adsorció d'oxigen a no ser que estigui activat per la deposició de oxigen atòmic o hi hagi la suficient energia com per a trencar el doble enllaç de la molecula [188, 189, 190]. Alguns mètodes de preparació d'oxigen preadsorbit a la superfície utilitzen NO_2 ja que permet un control acurat del recobriment d'O a la superfície, mentre que evita problemes potencials de contaminació degut a les altes pressions [7, 24]; una altra possibilitat es aplicar el feix d'àtoms d'oxigen produïts a partir d'una font de plasma [25]; exposar la superfície a ozó [26], o mitjançant la dissociació tèrmica d'O_2 gasós [27].

L'oxigen atòmic pot servir tant com a reactiu electrofílic en enllaços dobles carboni-carboni [28, 29] com a reactiu nucleòfil, atacant l'àtom de C en els hidrocarburs [30, 31]. S'ha mostrat que en $Ag(110)$ [32], $Ag(111)$ [33] i $Cu(111)$ [34] el propè, i uns altres alquens, s'adsorbeixen amb el doble enllaç gairebé paral·lel a la superfície [35].

Un assumpte important per a entendre el mecanisme d'epoxidació d'alquens és la natura dels intermedis de reacció. Hi ha dos camins possibles per a l'addició d'oxigen a l'enllaç $C = C$: un és quan l'àtom d'O forma enllaços amb dos àtoms de C simultàniament. Però, els estudis, tan teòrics com experimentals, proporcionen evidències que l'addició és seqüencial amb la formació d'un intermedi oxametal·locíclic [38, 36, 37, 21, 39, 20, 40]. En el cas de l'òxid d'estirè, l'existència de dos pics clars de desorció proporcionen l'evidència de dos configuracions diferents del oxametal·locicle [7].

Els oxametal·locicles són intermediaris a l'epòxid o a l'acetaldehid, l'últim essent identificat com el primer pas al a combustió total [37, 21]. Així doncs, la selectivitat per a l'epoxidació d'alquens està determinada pels dos camins de reacció i la diferència entre les seves energies lliures d'activació [37]. L'aldehid és deriva de

l'intermediari que es forma mitjançant la inserció d'oxigen a l'enllaç $C-H$ al·lílic. L'altre mecanisme es creu que implica l'addició de l'oxigen atòmic quimisorbit a l'enllaç $C=C$ [41]. Tanmateix, els catalitzadors d'argent no són gaire eficaços com a catalitzadors de l'epoxidació d'alquens amb enllaços $C-H$ al·lílics perquè la combustió predomina front a l'epoxidació. Un exemple és l'epòxid d'etè sobre un catalitzador de Ag amb selectivitats al voltant d'un 80%, mentre que per a l'epòxid de propè ocorre només amb un 5% [42]. L'oxidació d'estirè en $Au(111)$ amb oxigen quimisorbit produeix selectivament l'òxid d'estirè, àcid benzoic, i àcid benzo-acètic, oxidat selectivament només en un 20% [27]. L'adsorció de l'òxid d'etè s'espera que sigui més forta als metalls del grup VII, els quals finalment condueixen a la destrucció de l'alquè. Aquest argument és coherent amb les observacions fetes sobre $Pd(110)$ [44, 45], $K/Ni(111)$ [46], i $Pt(111)$ [47] en el qual l'adsorció d'òxid d'etè ocasionava la seva destrucció i la formació de CO i H en $Pt(111)$ i $Pd(110)$ o acetaldehid en $K/Ni(111)$ [20, 21].

En $Au(111)$ hi han dos camins de reacció possibles per a formar un intermedi d'òxid al·lílic quan el propè és activat per l'oxigen: l'òxid d'al·lil es podria formar mitjançant l'oxigen que activa l'hidrogen al·lílic seguit per l'addició de l'oxigen a l'al·lil o mitjançant la inserció de l'oxigen al $C-H$ seguit per la transferència de l'hidrogen al·lílic a l'oxigen [15]. La presència d'àtoms d'H al·lílics als alquens produeix espècies adsorbides d'al·lil i d'$O-H$, impedint l'oxidació selectiva i conduint només a la combustió [35]. Quan els àtoms d'hidrogen al·lílics són presents (propè, al·lil-benzè i els seus isòmers), el coure continua catalitzant l'oxidació selectiva eficaçment, mentre que l'argent simplement crema aquests alquenes al·lílics [35, 11, 15]. Els resultats teòrics impliquen que la diferència clau entre l'argent i el coure resideix a la química primària: l'argent afavoreix l'extracció de l'hidrogen al·lílic i el coure la formació del metal·locicle. Aquesta diferència suggereix que els intents de millora la selectivitat dels catalitzadors de coure s'hauria de centrar sobre els processos químics primaris, possiblement canviant l'estructura i/o la composició del metall. L'extracció dels àtoms d'hidrogen és induïda pel caràcter bàsic de l'oxigen adsorbit.

En l'estat de transició que porta a l'òxid d'etè, la distancia $C-O$ per a l'estat de transició en Au és similar a l'estructura sobre Ag i és similar als reactius, mentre que en coure, aquesta distància és significativament més curta [167], fet que podria ser útil per a uns altres estudis sobre l'oxidació d'alquens.

L'oxidació parcial de propè també és provocada per l'oxigen atòmic adsorbit sobre $Au(111)$, tanmateix, l'epoxidació no és el camí més favorable [15], pel contrari, és prefereix l'activació de l'enllaç al·lílic $C-H$ que condueix a l'aldehid, que s'oxida posteriorment. Llavors, l'epòxid de propè no es forma a partir de l'oxidació de propè sobre $Au(111)$, degut a l'activació fàcil dels enllaços $C-H$ al·lílics[15].

Nanofils d'Or

Els sistemes unidimensionals, com els fils, han atret un interès enorme per les seves propietats dependents de la mida. Tot i així, unes quantes àrees exigeixen més desenvolupament, en particular, la fabricació de materials 1D amb estructures atòmiques fetes a mida i el seu muntatge en nanoaparells funcionals són encara desafiaments essencials per als científics.

Avui dia, els científics es centren en la investigació sobre la formació de nanofils

UNIVERSITAT ROVIRA I VIRGILI
MODELLING AU CATALYST FROM BULK TO NANOSCALE
Alberto Roldán Martínez
ISBN:978-84-693-7669-0/DL:T-1748-2010

metàl·lics, semiconductor i d'òxids de metall fent èmfasi en la caracterització estructural de la nucleació, creixement inicial, defectes i estructures d'interfície, així com sobre l'anàlisi teòric de la formació de nanocristalls i la seva reactivitat i estabilitat. Hi ha unes quantes tècniques de creixement auto-organitzades: vapor-líquid-sòlid, deposició química de vapor assistida per òxids, ablació làser, evaporació tèrmica, etc. [48]. Per a desenvolupar nanofils metàl·lics, es pot utilitzar l'auto-acoblament, basat en l'adhesió de nanopartícules de grans relacions superfície-volum [49]. Així, els nanofils es fan pas a pas, afegint nanopartícules i reduint la seva energia superficial.

Les nanoestructures 1D desenvolupades exhibeixen fenòmens de creixement inusuals i propietats inesperades, per exemple direccions de creixement depenent del diàmetre i de la temperatura, transformacions estructurals per efectes fototèrmics i transformacions de fase provocades per la reacció de contacte de punt en nanofils ultra prims de semiconductors. Els nanofils metàl·lics són components per a sistemes nanoelectrònics que exhibeixen propietats òptiques altament modificables que els fan candidats atractius. Les nanoestructures d'Au unidimensionals, especialment els ultra prims (diàmetre $< 2\,nm$), són de gran interès a causa de les seves propietats de transport inusuals i tenen aplicacions prometedores en electrònica a nanoescala i sensors.

En el cas dels nanofils d'or, la direcció de creixement més favorable termodinàmicament és la [111], cosa raonable per a metalls *fcc* [50, 51, 52]. Experimentalment els nanofils d'Au tenen un espaiat entre capes de 2.35 Å que es correspon al pla (111) del cristall d'or. Els pics de difracció de raig-X confirmen que els nanofils estan compostos per or pur [50, 53, 51, 52] i mostren una estructura de barra torçada [51].

El seu comportament inert i l'alta conductivitat fan els nanofils d'Au un candidat ideal com a connector d'aparells moleculars. A temperatura ambient, un nanofil d'Au exhibeix una conducció d'electrons i un comportament òhmic convencional. Per exemple un fil de $9\,nm$ amb una llargada de $450\,nm$ té una resistència de $1.85\,k\Omega$ sense correcció de la constant de resistència. Això correspon a una resistivitat de $260\,ohm \cdot nm$, molt més baixa que la dels fils d'Au policristal·lins ($1000\,ohm \cdot nm$) [49].

Nanopartícules

El nombre de publicacions anuals que tracten sobre nanopartícules fa obvi que el camp ha aconseguit una importància substancial i un cert grau de maduresa. És un camp de recerca actiu de gran interès actual, del que de vegades s'esperen grans expectatives.

Les propietats interessants i de vegades inesperades dels materials canvien quan la seva mida s'apropa a l'escala nanomètrica. Les propietats diferents dels materials ultra petits van ser conegudes pels artesans per a generar efectes de gebre en les superfícies de ceràmica. Les nanopartícules metàl·liques amb ressonàncies de plasmó en el rang visible de l'espectre són interessants com a pigments, però va ser *Michael Faraday* qui va fer la primera descripció en termes científics de les propietats òptiques de metalls a escala nanomètrica.

Hi ha una àmplia varietat de mètodes sintètics per a obtenir nanopartícules: mètodes de moltura, mètodes en fase gas, síntesi en fase líquida, etc. A més de la mida de partícula hi han altres aspectes a tenir en compte per a obtenir nanopartícules de

qualitat, la distribució de mides ha de ser poc dispersa, hi ha d'haver un control directe de la funcionalització de la superfície, i s'ha de suprimir el procés d'aglomeració ja que la formació d'un sòlid sempre està afavorida respecte a la formació de partícules amb un àrea relativa gran, enllaços insaturats i llocs de coordinació desocupats. Dels diferents mètodes de síntesis de catalitzadors d'or suportat amb una alta dispersió, el mètode de deposició col·loïdal és una alternativa atractiva degut a que permet desacoblar les partícules sintetitzades i dipositar-les sobre un suport.

El factor decisiu per a la utilització de nanopartícules en catàlisi és la gran relació de l'àrea respecte al volum, amb un nombre gran de centres catalíticament actius en la superfície i un relatiu baix nombre d'àtoms inactius a l'interior. Com es poden obtenir fàcilment les nanopartícules d'or de diferents mides i formes, aquestes juguen un paper central en avançar en el coneixement de les propietats catalítiques que depenen de la mida i de la forma, per exemple, es poden preparar *in situ* nanopartícules d'or polièdriques amb una activitat excepcional, mitjançant una reducció amb àcid cítric o citrat en condicions suaus i sense utilitzar emulsionants.

Les diferencies entre nanopartícules i el sòlids macroscòpic es poden assignar qualitativament a diferents propietats:

- Propietats que depenen de la superfície: També les presenten els materials macroscòpic, però són dominants en nanopartícules degut a la relació volum-superfície.
- Propietats que depenen de la mida: Moltes propietats de les nanopartícules són degudes a la seva petita mida. Entre elles hi han capes transparents, efectes d'interferència, nanopartícules superparamagnètiques.
- Efectes quàntics que depenen de la mida: L'estructura electrònica de les partícules està influenciada per la mida. Això és degut a la transició entre els nivells d'energia definits d'un àtom o molècula a les bandes disperses de col·lectius d'àtoms i, finalment, de materials sòlids.

Estructura de les nanopartícules

Com les reaccions catalitzades tenen lloc sobre la superfície, l'àrea catalítica accessible es correlaciona amb el rendiment del material. En el cas dels metalls nobles, l'avantatge és obvi. Retrospectivament, la catàlisi heterogènia és un dels primers exemples de rellevància industrial de les nanopartícules. Un altre exemple és l'increment dràstic de la reactivitat química de les nanopartícules al disminuir el diàmetre de la partícula.

La caracterització de les nanopartícules és necessària per a comprendre i controlar la síntesi d'aquestes i les seves aplicacions. La caracterització es pot fer amb una varietat de tècniques que provenen, principalment, de la ciència de materials. Tècniques comuns són la microscòpia electrònica (TEM, SEM), la microscòpia de força atòmica (AFM), la microscòpia d'efecte túnel (STM), l'espectroscòpia fotoelectrònica de raig X (XPS) i la difracció de pols de raig X (XRD), entre d'altres.

Investigadors en l'estructura de les nanopartícules d'or des 2 a 20 àtoms van mostrar que la transició d'estructura planar a estructura tridimensional és dóna als 13 àtoms. Per a sistemes més grans, els isòmers de més baixa energia són els que tenen una estructura tetraèdrica amb base piramidal, la següent estructura més estable és

una amorfa [55, 56]. Així, les partícules tridimensionals són models prometedors per a interpretar les dades experimentals de les nanopartícules amb bona caracterització i àmpliament usades com a model catalític. La configuració més estable termodinamicament dels sistemes més petits es determina amb l'energia lliure de la cares superficials i la interfase amb el suport, l'estructura de la partícula doncs, es pot construir mitjançant el model de construcció de *Wulff* [57]. Aquest model assumeix que la distancia a la superfície d'un pla específic al centre de l'estructura és proporcional a l'energia superficial, així una superfície que tingui una energia petita la distancia al centre serà petita i aquest pla tallarà als altres per a formar el poliedre.

Per a modelitzar les nanopartícules, els cristalls tridimensionals tallats directament del bulk metàl·lic per plans de baix índex són una bona estructura inicial donant models catalítics realístics i apropiats [58, 59, 60, 61, 62, 63, 64]. En el cas dels metalls *fcc* exposen cares (111) i (001) donant estructures octaèdriques, cuboctaèdriques i icosaèdriques. Per a la partícula Au_{13}, la simetria cuboctàedriques és la més estable mentre que per a Au_{55} la més estable és la icosaèdrica, encara que la diferencia d'energia amb la cuboctadrica és força petita, 0.1 eV [65]. Com a primera aproximació es pot negligir les interaccions metall-substracte i considerar la partícula aillada [58].

El descobriment de l'estructura de Au_{55} estabilitzada per fosfines, l'any 1981, va marcar l'inici del desplaçament des la ciència clàssica dels col·loides a la nanotecnologia química. La habilitat d'obtindre nanopartícules d'or extremadament estables en solució aquosa va fer renéixer l'ús de l'or en aplicacions de ciència de la vida.

Des d'un punt de vista qualitatiu, molts dels fenòmens trobats en la química de l'or són experimentalment ben diagnosticats i amb una interpretació teòricament complerta, però les dades quantitatives, tal com les energies d'enllaç o la seva dependència amb les distancies interatòmiques són encara escasses. Això fa que una avaluació rigorosa de les propietats físiques sigui força difícil i encara es requereixen més estudis. Un cop aquestes limitacions hagin estat superades, pot tindre lloc un progrés ràpid amb prometedores aplicacions en nanociència i materials que continguin components d'or.

Un dels objectius de la ciència de les nanoestructures és esclarir com les diferents propietats observades difereixen dels valors del sòlid. Les partícules lliures són normalment estudiades en fase gas mitjançant feixos moleculars supersònics i estan caracteritzades per diferents tècniques espectroscòpiques. Les partícules nues poden ser útils per a estudiar la transició entre els àtoms o molècules i l'estat sòlid. Incrementant la mida de les partícules, les propietats segueixen una tendència monòtona que eventualment convergeix als valors del sòlid. L'ús de models d'escalabilitat ens permeten predir propietats de partícules més grans, d'una mida real, sense portar a terme els costosos càlculs computacionals.

Reactivitat de les nanopartícules

Un significant nombre de processos de catàlisis heterogènia es dóna sobre metalls de transició suportats sobre algun òxid metàl·lic. En la nanociència de l'or la dependència de la mida amb l'estructura electrònica dels materials té una importància central i ha acaparat molta atenció per la capacitat catalítica de les seves nanopatícules.

Haruta i col·laboradors van demostrar que una selectivitat alta en l'oxidació het-

erogènia del propè es podia portar a terme per l'or suportat sobre òxid de titani [67]. Diferents reaccions poden ser atribuïdes a les partícules d'or, tal com la formació de herbicides, nombrosos polímers, compostos de química fina o la reducció funcional de compostos nitroaromàtics a derivats de l'anilina, els quals són importants intermedis per als productes farmacèutics. *Serna* i *Corma* van mostrar com les nanopartícules d'Au sobre substrats de TiO_2 or Fe_2O_3 catalitzaven la hidrogenació de compostos nitrogenats sota condicions de reacció suaus amb una alta selectivitat [68].

Fent servir el mètode de deposició col·loïdal, es poden preparar petites partícules d'or en un rang de 1 a 5 nm [69, 70] encara que *Herzing* i col·laboradors han mostrat que les especies actives en catalitzadors de Au/FeO_x consisteixen en partícules subnanomètriques. La determinació del nombre exacte d'àtoms en aquestes estructures és complicat, per factors tals com la petita contracció de l'enllaç Au–Au [71].

Alguns estudis experimentals de les estructures de l'or a nanoescala sobre MgO han mostrat, en força casos, que les partícules creixen perfectament regulars, les quals porten a estructures determinades pel model de *Wulff* [72]. Aquestes partícules acostumen a adsorbir-se sobre vacants d'oxigen en el cas de la superfície de $MgO(100)$, on la interacció amb aquest centre de color comporta una transferència electrònica parcial. La interacció partícula-suport determina l'amplada i la posició de la banda d de l'or en la regió d'energia, a més, la flexibilitat de l'estructura de les partícules juga un paper molt important en la adsorció de reactius i la disminució de les barreres energètiques d'activació [73]. La partícula Au_{20} suportada en $MgO(100)$ amb moltes vacants d'oxigen incrementa sorprenentment l'activitat oxidativa de la partícula [74].

Hi ha hagut molt debat respecte a la natura dels llocs actius en les partícules d'Au suportades. Alguns autors senyalen els llocs entre el metall i el suport com una regió d'alta activitat, així que al decrèixer la mida de les partícules incrementa l'activitat global per l'augment de la zona d'interfase [75, 76]. La natura electrònica de les partícules més petites s'espera que estigui molt influenciada per la natura del suport, especialment per l'existència de llocs amb defectes. Tots els investigadors estan d'acord que l'activitat catalítica de l'or suportat s'incrementa quan més petita és la partícula, i la porció d'àtoms en contacte amb el suport s'incrementa al igual que la influencia del suport a la naturalesa electrònica d'aquest àtoms d'or. Aquest efecte esdevé molt significant quan el diàmetre de la partícula és menor de $2\,nm$ el qual coincideix amb una millora dramàtica de l'activitat. Ni les propietats electròniques de la interfase ni la banda de valència de les partícules ha estat investigat per separat experimentalment. S'ha d'especificar que els nanocristalls d'or no suportats són actius per a les reaccions d'oxidació [66].

Recentment *Valden* i col·laboradors han sugerit que l'anormalment alta activitat de les nanopartícules d'or es degut a l'efecte quàntic. Ho van demostrar amb microscòpia atòmica d'efecte túnel sobre partícules amb forma de disc suportades en una superfície de TiO_2, on la reactivitat depenia fortament de l'altura del disc [77]. Per exemple, un catalitzador de Au/CeO_2 amb partícules de mida $\leqslant 1\,nm$ és més actiu que aquell que contenen partícules més grans [78], a més un altre catalitzador de Au/FeO_x va mostrar que l'origen de l'activitat està associat a partícules de $\sim 0.5\,nm$ de diàmetre [71]. Es va mostrar teòricamentque una partícula d'Au_{10} aïllada era activa per catalitzar l'oxidació de CO per sota la temperatura normal.

Així doncs, les propietats catalítiques de les nanopartícules depenen del suport, del mètode de preparació i de la mida de la partícula [77]. Esbrinar aquesta de-

pendència és el motor de motivació per a molts científics i ingeniers. Hi han diferents claus a considerar:

- L'abundància relativa de llocs amb baixa i alta coordinació en funció de la mida de la partícula [80].
- Les interaccions metall-suport [74, 81].
- L'estructura electrònica de les partícules més petites [82].

Un dels processos catalítics més estudiats és l'oxidació de CO per O_2, el qual s'ha vist que té una alta activitat en nanopartícules d'Au de entre 2 i 5 nm suportats sobre òxids metàl·lics tal com TiO_2, Fe_2O_3, CeO_2, Co_3O_4 a baixes temperatures, però per sota de 70 °C només es dóna quan la mida de la partícula és inferior a 1 nm [70]. L'activitat de les partícules d'or és molt sensible a la seva estructura determinant les característiques amb l'interfase i la proporció de llocs de baixa coordinació que juguen un paper evident [75].

Degut a l'alta activitat en reaccions d'oxidació s'ha estudiat la reactivitat de les partícules d'Au amb oxigen, encara que no s'ha obtingut res clar del treballs realitzats sobre el mecanisme de dissociació. S'ha mostrat que hi ha una interacció entre O_2 i partícules super petites, tan neutres com iòniques [73, 83]. Aquesta energia d'interacció és més gran en partícules aniòniques, on es presenta un comportament diferent depenent del nombre parell-imparell d'electrons en funció del nombre d'àtoms. El mecanisme d'enllaç implica una transferència de carga a l'oxigen amb la corresponent activació de l'enllaç a estat superoxo [73]. L'adsorció d'oxigens atòmic produeix una gran relaxació en el sistema d'or, el qual es pot detectar mitjançant mesures de mobilitat dels àtoms o per espectroscòpia de difracció d'electrons. La interacció de la molècula d'oxigen amb partícules molt petites també es dóna, encara que de forma més dèbil i sense induir l'activació de l'enllaç [73].

També s'han estudiat teòricament partícules més grans que uns quants àtoms, i amb l'aproximació DFT s'ha investigat la seva interacció amb la molècula d'oxigen, concluïnt que l'adsorció sobre Au_{24} depèn de la forma i el nombre de coordinació dels àtoms interactuants [85]. A més, s'ha vist que Au_{55} interacciona molt dèbilment amb la molècula d'O_2 però que les artícules Au_{13} ho fan de forma substancial [86]. Quan la partícula esta suportada, estudis teòrics sugereixen que l'interfase és el lloc més poblable d'adsorció [87, 88].

En qualsevol cas, la molècula adsorbida es troba activada com a espècie peroxo amb un l'enllaç altament debilitat comparat amb la molècula en fase gas [74]. La natura d'aquesta activació del sistema oxigen-or continua incert i es necessiten mesures cinètiques detallades per a determinar el seu paper en mecanismes de reacció.

Objectius d'aquesta tesi

Aquesta tesi té com a objectius estudiar diferents estructures d'or i la seva activitat catalítica mitjançant la teoria del funcional de la densitat per a sistemes periòdics. Inclou el sòlid, la superfície bidimensional d'or i la seva activitat catalítica cap a l'epoxidació de propè, l'auto assemblatge de nanopartícules resultant una estructura monodimensional i també nanopartícules i la seva activitat catalítica en l'activació d'O_2.

Els resultats intenten aprofundir en el coneixement de la matèria condensada: la seva estructura i reactivitat. Hem intentat també ser útils per a nous investigadors a més de proporcionar un guia breu per a preparar sistemes de diferents dimensions per al seu tractament teòric.

Els objectius generals d'aquest treball són:

- Modelitzar les estructures metàl·liques del sòlid, superfície, nanofils i nanopartícules.
- Estudiar la interacció adsorbat-metall i establir les propietats d'adsorció.
- Caracteritzar estructures que són mínims energètics o punts de sella mitjançant l'anàlisi de les freqüències de vibració.
- Simular els perfils de reaccions i determinar els estats de transició que conecten els diferents mínims energètics.
- Simular reaccions sobre un catalitzador en condicions reals utilitzant models microcinètics.

En el cas de les nanopartícules intentarem proporcionar una aproximació per a unir el buit entre l'estructura electrònica de les molècules i la ciència de l'estat sòlid.

UNIVERSITAT ROVIRA I VIRGILI
MODELLING AU CATALYST FROM BULK TO NANOSCALE
Alberto Roldán Martínez
ISBN:978-84-693-7669-0/DL:T-1748-2010

Conclusions

En aquesta tesis s'ha portat a terme un estudi sistemàtic de diferents estructures d'or així com l'adsorció de diferents molècules sobre la superfície i les nanopartícules, mitjançant un codi periòdic i la teoria del funcional de la densitat (DFT) implementat en VASP. La caracterització d'estructures proporciona el pas clau per a entendre els fenòmens catalítics, els modes d'adsorció i la natura de la interacció adsorbat-estructura, les energies i barreres de reacció. El treball presentat completa les observacions experimentals i proporciona dades addicionals.

Or en tres dimensions

S'ha portat a terme l'estudi del sòlid d'or per a obtenir una descripció computacional correcta. Aquest coneixement és necessari per a preparar altres estructures com les superfícies o les nanopartícules.

El paràmetre de la cel·la unitària (a_0) d'Au obtingut mitjançant el funcional d'intercanvi-correlació LDA(VWM) (4.07 Å) és més proper a l'experimental (4.07 Å) que l'obtingut mitjançant GGA(PW91) (4.17 Å), resultat esperat ja que el GGA sobreestima les distancies interatòmiques.

El mòdul de sòlid (B_0) és difícil de reproduir acuradament degut a les aproximacions que es fan al llarg del seu càlcul. El seu valor experimental (220 GPa) és proper a l'obtingut per LDA(VWM) diferenciant-se en 26 GPa, encara que els dos funcionals provats, LDA(VWM) i GGA(PW91), estan per sota de l'experimental, l'últim per 75 GPa.

Finalment, les energies de cohesió (E_{coh}) obtingudes amb LDA(VWM) i GGA (PW91) s'allunyen de l'experimental (-3.78 $eV/atom$) per 0.52 $eV/atom$ o 0.72 $eV/atom$ respectivament.

L'estructura de l'or està ben descrita mitjançant l'aproximació LDA(VWM) encara que a aquest funcional li manca una descripció adequada de l'energia d'interacció. Per a resoldre aquest problema es poden fer servir altres funcionals o una aproximació que consisteix en aplicar un càlcul puntual amb el funcional GGA, per exemple, sobre l'estructura obtinguda amb LDA(VWM), en aquest cas rebria el nom de GGA//LDA.

Or en dos dimensions

Hem comprovat diferents posicions y orientacions per a l'adsorció de la molècula de propè sobre la superfície neta o oxigenada d'$Au(111)$ per a estudiar l'oxidació parcial d'aquesta molècula.

A les dues superfícies, neta o oxigenada, l'adsorció de la molècula de propè és dèbil i en una posició paral·lela a la superfície, pràcticament sense distorsions de la molècula. En el cas de la superfície oxigenada, l'energia d'adsorció és lleugerament superior.

D'acord amb la literatura, l'oxidació parcial de la molècula de propè per l'oxigen atòmic adsorbit té lloc mitjançant dos possibles camins de reacció: l'oxametal·locicle (OMMP) o via la formació de l'al·lil. Una anàlisi detallada dels resultats indica que els dos camins són favorables termodinàmicament però que l'oxametal·locicle està 0.64 eV per sota l'al·lil, encara que té una barrera energètica de 0.52 eV, més alta

que per a formar l'al·lil (0.20 eV). Per tan, la formació de l'OMMP està impedida cinèticament mentre que l'extracció de l'H pel O bàsic és el camí favorable, donant el radical al·lílic i OH. La reacció secundaria de l'al·lil és la seva combustió tal com succeeix amb Cu i Ag [11, 35, 15].

Així i d'acord amb els resultats experimentals, l'oxidació parcial del propè a l'òxid de propè sobre una superfície d'$Au(111)$ com a catalitzador és un procés desafavorit [15].

Or en una dimensió

S'ha estudiat el mecanisme de creixement de nanofils metàl·lics a partir de l'auto-acoblament de nanopartícules. Per a portar-lo a terme s'ha fet servir l'aproximació GGA//LDA, obtenint una descripció geomètrica acurada i unes energies d'interacció obtingudes a partir del funcional GGA(PW91).

Hem comprovat tres tipus de mecanismes: seguint la direcció de creixement [001] i acoblant nanopatícules paral·lelament o amb una torsió de 45^{o} i seguint la direcció [111] adjuntant les nanopartícules per les cares (111).

Les distancies obtingudes entre els fragments del nanofil, nanopartícules de Au_{79}, són molts properes a l'experimental (0.23 nm). El mecanisme que creix seguint la direcció [111] només varia en 0.03 nm, i dels que segueixen la direcció [001] amb acoblament paral·lel, 0.01 nm, o amb una torsió de 45^{o}, -0.01 nm.

Tots els mecanismes són favorables termodinàmicament però el més probable és el que segueix la direcció de creixement [111], amb una estabilització energètica de 10.06 eV, mentre que els altres no superen els 5 eV.

Aquest resultats suggereixen que la interacció entre nanopartícules es dominada pel nombre de coordinació. Per exemple, el mecanisme més favorable incrementa la coordinació de 12 àtoms mentre que els altres només a 4 àtoms de la nanopartícula Au_{79}. A més a més de la anisotropia que presenten el nanofils de Au, la seva densitat d'estats (DOS) mostra similituds amb la DOS del sòlid indicant un cert caràcter inert, cosa que reforça la seva aplicació.

Or en cero dimensions

Estructura de les nanopartícules

S'ha portat a terme l'estudi d'un conjunt de nanopartícules de fins a 225 àtoms, les quals són comparables a les nanopartícules suportades experimentalment [168, 169, 170, 171, 172, 173, 58, 174], l'estructura inicial de les quals prové de tallar l'or sòlid tridimensional per plans de baix índex de *Miller* donant estructures octaèdriques i cuboctaèdriques que segueixen el model de construcció de *Wulff* [57]. Aquestes nanopartícules es disposen al centre d'una cel·la suficientment gran per a evitar interaccions amb partícules veïnes i s'optimitzen mitjançant ones planes sense restricció geomètrica, aquesta metodologia ha demostrat ser correcta per a simular estructures reals.

La convergència de les propietats de les nanopartícules cap als valors del sòlid ve donada simplement pel decreixement de la influència de la superfície i l'augment dels àtoms de l'interior a mida que el sistema creix [175, 176, 65]. Així, apel·lant al model de gota, les distancies interatòmiques poden relacionar-se en termes d'increment de

UNIVERSITAT ROVIRA I VIRGILI
MODELLING AU CATALYST FROM BULK TO NANOSCALE
Alberto Roldán Martínez
ISBN:978-84-693-7669-0/DL:T-1748-2010

la pressió amb el decreixement del radi de la gota degut a la tensió superficial. Tot i així, els nostres resultats mostren que la escalabilitat de les nanopartícules de diferents metalls es diferencien respecte a la llargària de l'enllaç, l'or s'escala pitjor que el coure o l'argent.

De la densitat d'estats de les espècies estudiades, el centre de la banda d tendeix paulatinament cap al sòlid a l'augmentar la mida de les partícules, per altra banda, les partícules més petites no segueixen aquesta tendència degut al seu caràcter molecular. És a partir de ∼80 àtoms que les propietats electròniques de les nanopartícules s'escalen al valor del sòlid.

Des d'un punt de vista general, els resultats mostren les conseqüències de la manca d'un funcional d'intercanvi-correlació suficientment acurat i universal capaç de descriure adequadament el total dels paràmetres observables, especialment per a elements més pesants. Cal remarcar, però, que la metodologia aplicada amb l'aproximació de les ones planes resulta en excel·lent concordança amb altres resultats obtinguts amb una metodologia *full-electron*, més costosa computacionalment.

Reactivitat de les nanopartícules

El comportament de les nanopartícules d'or amb altres molècules s'ha estudiat amb els models i la metodologia trobats anteriorment per n=5, 13, 25, 38, 55, 79.

Les propietats de les nanopartícules petites mostren sovint un comportament oscil·latori amb la mida i l'estructura degut a que aquests models representen de manera insuficient l'estructura electrònica [177]. Per altra banda l'efecte quàntic de la mida causat pel confinament de l'electró en un volum determinat sembla ser responsable de les propietats catalítiques inesperades dels sistemes d'Au [191].

Es pot argumentar que al disminuir la mida de la nanopartícula s'incrementa la reactivitat i també la presencia d'àtoms metàl·lics insaturats [179]. Des d'una perspectiva general, l'argument de la coordinació ajuda a entendre perquè les nanopartícules han de ser petites per a que siguin reactives. Una condició és que existeixi una força capaç de capturar les molècules, cosa que succeeix només a determinats llocs: arestes o vèrtexs [180].

Així, les nostres nanopartícules van ser optimitzades sense restriccions estructurals, on l'oxigen es va disposar en totes les posicions de baixa coordinació. Quan la molècula O_2 s'aproxima a la superfície perd el seu moment magnètic i queda atrapada en forma de superoxo allargant la distancia d'enllaç [180]. Això és consistent amb el fet que l'activació d'oxigen comporti una transferència electrònica des de la partícula a l'oxigen.

Les nanopartícules Au_{25}, Au_{38}, Au_{79} evidencien que l'energia d'adsorció de l'oxigen és dependent del funcional d'intercanvi-correlació. La tendència de l'LDA a sobreestimar la interacció és coneguda, per altra banda les descripcions amb PW91 són aproximadament 0.20 eV més petites que amb el funcional PBE i aquestes 0.35 eV que amb RevPBE. Les relacions establertes pels nostres resultats permeten omplir el buit entre les nanopartícules tractades i les d'una mida intractable computacionalment.

Les propietats d'adsorció i els perfils de reacció depenen fortament de la mida de la nanopartícula considerada. Per exemple, anant de Au_{38} a Au_{55}, la primera és molt adequada per a promoure processos d'oxidació mentre que l'altra és altament

inert. Així, varem analitzar els resultats d'aquestes partícules i els de Au_{79}: la geometria d'adsorció, la distancia d'enllaç, les barreres energètiques i l'estabilitat dels productes, que són essencialment independents de l'estat d'oxidació de la partícula, en concordança amb l'experiment. Contràriament, la carga de la partícula té gran importància quan aquesta té una mida reduïda.

L'estudi teòric realitzat presenta evidencies convincents que:

- La presència d'àtoms de baixa coordinació no és suficient per a dissociar O_2.
- Una adsorció forta de la molècula d'oxigen sobre les nanopartícules és una condició necessària però no suficient per a la dissociació d'aquesta.
- Hi ha un camí de reacció de més baixa energía comú per a tots els sistemes tractats i amb una barrera similar.
- Hi ha una mida de partícula crítica capaç de dissociar l'O_2.
- L'efecte de l'estat d'oxidació de les nanopartícules d'una mida moderada és negligible en l'adsorció i en la barrera energètica.

Les barreres de dissociació són força altes per a les partícules molt petites, de l'ordre d'1 eV o més per sobre del límit de desorció [55], cosa que està d'acord amb l'experiment i evidencien la inactivitat d'aquestes partícules [186]. En particular, una reacció viable necessita que la barrera de dissociació hagi de ser més petita en valor absolut que l'energia de desorció, com és el cas de Au_{38}.

S'ha desenvolupat també un model microcinètic, basat en constants de velocitat obtingudes mitjançant el funcional de la densitat per a estudiar l'evolució de l'oxigen atòmic i molecular tenint en compte l'adsorció-desorció i la dissociació-recombinació com a reaccions químiques. Les dos series de simulacions realitzades confirmen que tan l'oxigen molecular com l'atòmic estan presents a la superfície de les nanopartícules Au_{25} i Au_{38} mentre que a les d'una mida major la desorció té lloc abans que la dissociació.

UNIVERSITAT ROVIRA I VIRGILI
MODELLING AU CATALYST FROM BULK TO NANOSCALE
Alberto Roldán Martínez
ISBN:978-84-693-7669-0/DL:T-1748-2010

UNIVERSITAT ROVIRA I VIRGILI
MODELLING AU CATALYST FROM BULK TO NANOSCALE
Alberto Roldán Martínez
ISBN:978-84-693-7669-0/DL:T-1748-2010

List of publications

1. Roldan, A.; Vines, F.; Illas, F.; Ricart, J. M.; Neyman, K. M., *Density functional studies of coinage metal nanoparticles: scalability of their properties to bulk.* Theoretical Chemistry Accounts **2008**, 120, (4-6), 565-573.

2. Roldan, A.; Torres, D.; Ricart, J. M.; Illas, F., *The chemistry of chlorine on Ag(111) over the sub-monolayer range. A density functional theory investigation.* Surf. Sci. **2008**, 602, (15), 2639-2642.

3. Roldan, A.; Gonzalez, S.; Ricart J. M.; Illas, F., *Critical size for O_2 dissociation by Au nanoparticles.* Chemphyschem **2009**, 10, (2), 348-51.

4. Roldan, A.; Ricart, J. M.; Illas, F., *Influence of the exchange-correlation potential on the description of the molecular mechanism of oxygen dissociation by Au nanoparticles.* Theoretical Chemistry Accounts **2009**, 123, (1-2), 119-126.

5. Roldan, A.; Ricart, J. M.; Illas, F., *Growth and properties of Au nanowires.* Molecular Simulation **2009**, 35, (12&13), 1051-1056.

6. Roldan, A.; Torres, D.; Ricart, J. M.; Illas, F., *On the effectiveness of partial oxidation of propylene by gold: A density functional theory study.* Journal of Molecular Catalysis a-Chemical **2009**, 306, (1-2), 6-10.

7. Roldan, A.; Novell, G.; Ricart, J. M.; Illas, F., *Theoretical Simulation of Temperature Programmed Desorption of Molecular Oxygen on Isolated Au Nanoparticles from Density Functional Calculations and Microkinetics Models.* Journal of Physical Chemistry C **2010**, 114, (11), 5101-5106.

8. Roldan, A.; Boronat, M.; Corma, A.; Illas, F., *Theoretical Confirmation of the Enhanced Facility to Increase Oxygen Vacancy Concentration in TiO_2 by Iron Doping.* Journal of Physical Chemistry C **2010**, 114, (14), 6511-6517.

9. Roldan, A.; Ricart, J.M.; Illas, F.; Pacchioni, G.; "*O_2 Activation by Au_5 Clusters Stabilized on Clean and Electron-Rich MgO Stepped Surfaces*", Journal of Physical Chemistry C **2010**, ID: jp-2010-017357.R1

10. Roldan, A.; Ricart, J.M.; Illas, F.; Pacchioni, G.; "*O_2 adsorption and dissociation on neutral, positively and negatively charged Au_n (n = 5-79) clusters*", Physical Chemistry Chemical Physics **2010**, 12, 10723-10729.

11. Víctor Antonio de la Peña O'Shea, Iberio de P. R. Moreira, Alberto Roldan, Francesc Illas; "*Electronic and magnetic structure of bulk cobalt: the α, β and ε-phases from density functional theory calculations*", Journal of Chemical Physics **2010**, 133.

12. Roldan, A.; Ricart, J. M.; Illas, F., *"Origin of the size dependence of Au nanoparticles towards molecular oxygen dissociation"*, Theoretical Chemistry Accounts. No: TCAC-D-10-00191.

Bibliography

[1] Lambert, R. M.; Pacchioni, G. *Chemisorption and Reactivity on Supported Clusters and Thin Films: Towards an Understanding of Microscopic Processes in Catalysis.* Sicily, 1997.

[2] Darensbourg, D. J.; Holtcamp, M. W. *Coordination Chemistry Reviews*, **1996**, *153*, 155–174.

[3] Darensbourg, D. J.; Zimmer, M. S. *Macromolecules*, **1999**, *32*(7), 2137–2140.

[4] Jannasch, P. *Polymer*, **2000**, *41*(18), 6701–6707.

[5] Yoshida, H.; Tanaka, T.; Yamamoto, M.; Funabiki, T.; Yoshida, S. *Chemical Communications*, **1996**, (18), 2125–2126.

[6] Hayashi, T.; Tanaka, K.; Haruta, M. *Journal of Catalysis*, **1998**, *178*(2), 566–575.

[7] Klust, A.; Madix, R. J. *Journal of the American Chemical Society*, **2006**, *128*(4), 1034–1035.

[8] Hawker, S.; Mukoid, C.; Badyal, J. P. S.; Lambert, R. M. *Surface Science*, **1989**, *219*(3), L615–L622.

[9] Williams, F. J.; Bird, D. P. C.; Palermo, A.; Santra, A. K.; Lambert, R. M. *Journal of the American Chemical Society*, **2004**, *126*(27), 8509–8514.

[10] Deng, X. Y.; Friend, C. M. *Journal of the American Chemical Society*, **2005**, *127*(49), 17178–17179.

[11] Lambert, R. M.; Williams, F. J.; Cropley, R. L.; Palermo, A. *Journal of Molecular Catalysis a-Chemical*, **2005**, *228*(1-2), 27–33.

[12] Klust, A.; Madix, R. J. *Surface Science*, **2006**, *600*(23), 5025–5040.

[13] Cowell, J. J.; Santra, A. K.; Lindsay, R.; Lambert, R. M.; Baraldi, A.; Goldoni, A. *Surface Science*, **1999**, *437*(1-2), 1–8.

[14] Santra, A. K.; Cowell, J. J.; Lambert, R. M. *Catalysis Letters*, **2000**, *67*(2-4), 87–91.

[15] Deng, X. Y.; Min, B. K.; Liu, X. Y.; Friend, C. M. *Journal of Physical Chemistry B*, **2006**, *110*(32), 15982–15987.

[16] Sachtler, W. M. *Catalysis Reviews*, **1970**, *4*(1), 27–33.

[17] Force, E. L.; Bell, A. T. *Journal of Catalysis*, **1975**, *40*(3), 356–371.

[18] Grant, R. B.; Lambert, R. M. *Langmuir*, **1985**, *1*(1), 29–33.

[19] Serafin, J. G.; Liu, A. C.; Seyedmonir, S. R. *Journal of Molecular Catalysis A-Chemical*, **1998**, *131*(1-3), 157–168.

[20] Linic, S.; Barteau, M. A. *Journal of the American Chemical Society*, **2002**, *124*(2), 310–317.

[21] Linic, S.; Barteau, M. A. *Journal of the American Chemical Society*, **2003**, *125*(14), 4034–4035.

[22] Katayama, T.; Sekiba, D.; Mukai, K.; Yamashita, Y.; Komori, F.; Yoshinobu, J. *Journal of Physical Chemistry C*, **2007**, *111*(41), 15059–15063.

[23] Turner, M.; Golovko, V. B.; Vaughan, O. P. H.; Abdulkin, P.; Berenguer-Murcia, A.; Tikhov, M. S.; Johnson, B. F. G.; Lambert, R. M. *Nature*, **2008**, *454*(7207), 981–U31.

[24] Bare, S. R.; Griffiths, K.; Lennard, W. N.; Tang, H. T. *Surface Science*, **1995**, *342*(1-3), 185–198.

[25] Kim, J.; Dohnalek, Z.; Kay, B. D. *Journal of the American Chemical Society*, **2005**, *127*(42), 14592–14593.

[26] Min, B. K.; Alemozafar, A. R.; Pinnaduwage, D.; Deng, X.; Friend, C. M. *Journal of Physical Chemistry B*, **2006**, *110*(40), 19833–19838.

[27] Deng, X.; Min, B. K.; Guloy, A.; Friend, C. M. *Journal of the American Chemical Society*, **2005**, *127*(25), 9267–9270.

[28] Roberts, J. T.; Madix, R. J. *Journal of the American Chemical Society*, **1988**, *110*(25), 8540–8541.

[29] Valcarcel, A.; Clotet, A.; Ricart, J. M.; Illas, F. *Chemical Physics*, **2005**, *309*(1), 33–39.

[30] Capote, A. J.; Madix, R. J. *Surface Science*, **1989**, *214*(1-2), 276–288.

[31] Crew, W. W.; Madix, R. J. *Journal of the American Chemical Society*, **1993**, *115*(2), 729–736.

[32] Solomon, J. L.; Madix, R. J.; Stohr, J. *Journal of Chemical Physics*, **1990**, *93*(11), 8379–8382.

[33] Huang, W. X.; White, J. M. *Surface Science*, **2002**, *513*(2), 399–404.

[34] Street, S. C.; Gellman, A. J. *Journal of Physical Chemistry B*, **1997**, *101*(8), 1389–1395.

[35] Cropley, R. L.; Williams, F. J.; Vaughan, O. P. H.; Urquhart, A. J.; Tikhov, M. S.; Lambert, R. M. *Surface Science*, **2005**, *578*(1-3), L85–L88.

[36] Medlin, J. W.; Barteau, M. A. *Journal of Physical Chemistry B*, **2001**, *105*(41), 10054–10061.

[37] Linic, S.; Barteau, M. A. *Journal of Catalysis*, **2003**, *214*(2), 200–212.

[38] Jones, G. S.; Mavrikakis, M.; Barteau, M. A.; Vohs, J. M. *Journal of the American Chemical Society*, **1998**, *120*(13), 3196–3204.

[39] Wu, G.; Stacchiola, D.; Kaltchev, M.; Tysoe, W. T. *Surface Science*, **2000**, *463*(2), 81–92.

[40] Piao, H.; Enever, M. C. N.; Adib, K.; Hrbek, J.; Barteau, M. A. *Surface Science*, **2004**, *571*(1-3), 139–145.

[41] Gleaves, J. T.; Sault, A. G.; Madix, R. J.; Ebner, J. R. *Journal of Catalysis*, **1990**, *121*(1), 202–218.

[42] Akimoto, M.; Ichikawa, K.; Echigoya, E. *Journal of Catalysis*, **1982**, *76*(2), 333–344.

[43] Torres, D.; Lopez, N.; Illas, F.; Lambert, R. M. *Angewandte Chemie-International Edition*, **2007**, *46*(12), 2055–2058.

[44] Shekhar, R.; Barteau, M. A. *Surface Science*, **1996**, *348*(1-2), 55–66.

[45] Shekhar, R.; Barteau, M. A.; Plank, P. V.; Vohs, J. M. *Surface Science*, **1997**, *384*(1-3), L815–L822.

[46] Nieber, B.; Benndorf, C. Ups and hreels investigation of ethylene-oxide and potassium coadsorption ni(111). pp 341–346, 1992.

[47] Campbell, C. T.; Paffett, M. T. *Surface Science*, **1986**, *177*(2), 417–430.

[48] Wang, N.; Cai, Y.; Zhang, R. Q. *Materials Science & Engineering, R: Reports*, **2008**, *R60*(1-6), 1–51.

[49] Wang, C.; Hu, Y.; Lieber, C. M.; Sun, S. *Journal of the American Chemical Society*, **2008**, *130*(28), 8902–8903.

[50] Halder, A.; Ravishankar, N. *Advanced Materials*, **2007**, *19*(14), 1854–1858.

[51] Pazos-Perez, N.; Baranov, D.; Irsen, S.; Hilgendorff, M.; Liz-Marzan, L. M.; Giersig, M. *Langmuir*, **2008**, *24*(17), 9855–9860.

[52] Huo, Z.; Tsung, C. k.; Huang, W.; Zhang, X.; Yang, P. *Nano Letters*, **2008**, *8*(7), 2041–2044.

[53] Sajanlal, P. R.; Sreeprasad, T. S.; Nair, A. S.; Pradeep, T. *Langmuir*, **2008**, *24*(9), 4607–4614.

[54] Lu, X.; Yavuz, M. S.; Tuan, H.-Y.; Korgel, B. A.; Xia, Y. *Journal of the American Chemical Society*, **2008**, *130*(28), 8900–8901.

[55] Hakkinen, H.; Abbet, W.; Sanchez, A.; Heiz, U.; Landman, U. *Angewandte Chemie-International Edition*, **2003**, *42*(11), 1297–1300.

[56] Barnard, A. S.; Curtiss, L. A. *ChemPhysChem*, **2006**, *7*(7), 1544–1553.

[57] Wulff, G. *Zeitschrift Fur Krystallographie Und Mineralogie*, March 1901, *34*(5/6), 449–530.

[58] Yudanov, I. V.; Sahnoun, R.; Neyman, K. M.; Rösch, N. *Journal of Chemical Physics*, **2002**, *117*(21), 9887–9896.

[59] Yudanov, I. V.; Sahnoun, R.; Neyman, K. M.; Rösch, N.; Hoffmann, J.; Schauermann, S.; Johanek, V.; Unterhalt, H.; Rupprechter, G.; Libuda, J.; Freund, H.-J. *Journal of Physical Chemistry B*, **2003**, *107*(1), 255–264.

[60] Yudanov, I. V.; Neyman, K. M.; Rösch, N. *Physical Chemistry Chemical Physics*, **2004**, *6*(1), 116–123.

[61] Neyman, K. M.; Sahnoun, R.; Inntam, C.; Hengrasmee, S.; Rösch, N. *Journal of Physical Chemistry B*, **2004**, *108*(17), 5424–5430.

[62] Neyman, K. M.; Vayssilov, G. N.; Rösch, N. *Journal of Organometallic Chemistry*, **2004**, *689*(24), 4384–4394.

[63] Neyman, K. M.; Inntam, C.; Gordienko, A. B.; Yudanov, I. V.; Rösch, N. *Journal of Chemical Physics*, **2005**, *122*(17), 174705/1–174705/9.

[64] Yudanov, I. V.; Neyman, K. M.; Rösch, N. *Physical Chemistry Chemical Physics*, **2006**, *8*(20), 2396–2401.

[65] Haberlen, O. D.; Chung, S. C.; Stener, M.; Rösch, N. *Journal of Chemical Physics*, **1997**, *106*(12), 5189–5201.

[66] Comotti, M.; Della Pina, C.; Matarrese, R.; Rossi, M. *Angewandte Chemie-International Edition*, **2004**, *43*(43), 5812–5815.

[67] Haruta, M. *Catalysis Today*, **1997**, *36*(1), 153–166.

[68] Corma, A.; Serna, P. *Science*, **2006**, *313*(5785), 332–4.

[69] Stephen, A.; Hashmi, K.; Hutchings, G. J. *Angewandte Chemie, International Edition*, **2006**, *45*(47), 7896–7936.

[70] Jia, C.-J.; Liu, Y.; Bongard, H.; Schüth, F. *Journal of the American Chemical Society*, **2010**, *132*(5), 1520–1522.

[71] Herzing, A. A.; Kiely, C. J.; Carley, A. F.; Landon, P.; Hutchings, G. J. *Science*, **2008**, *321*(5894), 1331–1335.

[72] Molina, L. M.; Hammer, B. *Applied Catalysis, A: General*, **2005**, *291*(1-2), 21–31.

[73] Yoon, B.; Hakkinen, H.; Landman, U. *Journal of Physical Chemistry A*, **2003**, *107*(20), 4066–4071.

[74] Sanchez, A.; Abbet, S.; Heiz, U.; Schneider, W. D.; Haekkinen, H.; Barnett, R. N.; Landman, U. *Journal of Physical Chemistry A*, **1999**, *103*(48), 9573–9578.

[75] Molina, L. M.; Hammer, B. *Journal of Catalysis*, **2005**, *233*(2), 399–404.

[76] Bond, G. C.; Thompson, D. T. *Gold Bulletin*, **2000**, *33*(2), 41–51.

[77] Valden, M.; Lai, X.; Goodman, D. W. *Science*, **1998**, *281*(5383), 1647–1650.

[78] Tabakova, T.; Boccuzzi, F.; Manzoli, M.; Sobczak, J. W.; Idakiev, V.; Andreeva, D. *Applied Catalysis B-Environmental*, **2004**, *49*(2), 73–81.

[79] Lopez, N.; Norskov, J. K. *Journal of the American Chemical Society*, **2002**, *124*(38), 11262–11263.

[80] Mavrikakis, M.; Stoltze, P.; Norskov, J. K. *Catalysis Letters*, **2000**, *64*(2-4), 101–106.

[81] Sterrer, M.; Yulikov, M.; Fischbach, E.; Heyde, M.; Rust, H. P.; Pacchioni, G.; Risse, T.; Freund, H. J. *Angewandte Chemie-International Edition*, **2006**, *45*, 2630–2632.

[82] Mills, G.; Gordon, M. S.; Metiu, H. *Journal of Chemical Physics*, **2003**, *118*(9), 4198–4205.

[83] Yoon, B.; Hakkinen, H.; Landman, U.; Worz, A. S.; Antonietti, J. M.; Abbet, S.; Judai, K.; Heiz, U. *Science*, **2005**, *307*(5708), 403–407.

[84] Barrio, L.; Liu, P.; Rodriguez, J. A.; Campos-Martin, J. M.; Fierro, J. L. G. *Journal of Physical Chemistry C*, **2007**, *111*(51), 19001–19008.

[85] Luo, C.; Fa, W.; Dong, J. *Journal of Chemiscal Physics*, **2006**, *125*(8), 084707.

[86] Barton, D. G.; Podkolzin, S. G. *Journal of Physical Chemistry B*, **2005**, *109*(6), 2262–2274.

[87] Rasmussen, M. D.; Molina, L. M.; Hammer, B. *Journal of Chemical Physics*, **2004**, *120*(2), 988–997.

[88] Molina, L. M.; Rasmussen, M. D.; Hammer, B. *Journal of Chemical Physics*, **2004**, *120*(16), 7673–7680.

[89] Chorkendorff, I.; Niemantsverdriet, J. W. *Concepts of Modern Catalysis and Kinetics*. Wiley-VCH, Weinheim, 2005.

[90] Doke, C. B.; Plummer, E. W. *Frontiers in Surface Science and Interface Science*, volume 500. Elsevier Science, first edition, 2002.

[91] Born, M.; Oppenheimer, R. *Annalen Der Physik*, **1927**, *84*(20), 0457–0484.

[92] Hehre, W. J.; Radom, L.; Schleye, P. V.; Pople, J. A. *Ab Initio Molecular Orbital Theory*. Wiley-interscience, New York, 1986.

[93] Andrés, J. M.; Beltrán, J. *Química teórica y computacional*. Castelló, 2000.

[94] Parr, R. G.; Yang, W. *Density-functional theory of atoms and molecules*. New York, 1989.

[95] Koch, W.; Holthausen, M. C. *A Chemist's Guide to Density Functional Theory*. Weinheim, 2000.

[96] Thomas, L. H. *Proceedings of the Cambridge Philosophical Society*, **1927**, *23*, 542–548.

[97] Hohenberg, P.; Kohn, W. *Physical Review B*, **1964**, *136*(3B), B864.

[98] Kohn, W.; Sham, L. J. *Physical Review*, **1965**, *140*(4A), 1133.

[99] Vosko, S. H.; Wilk, L.; Nusair, M. *Canadian Journal of Physics*, **1980**, *58*(8), 1200–11.

[100] Becke, A. D. *Journal of Chemical Physics*, **1986**, *84*(8), 4524–4529.

[101] Perdew, J. P. *Physical Review B*, **1986**, *34*(10), 7406–7406.

[102] Perdew, J. P.; Yue, W. *Physical Review B*, **1986**, *33*(12), 8800–8802.

[103] Perdew, J. P.; Burke, K.; Ernzerhof, M. *Physical Review Letters*, **1996**, *77*(18), 3865–3868.

[104] Perdew, J. P. *Physical Review B*, **1986**, *33*(12), 8822–8824.

[105] Lee, C. T.; Yang, W. T.; Parr, R. G. *Physical Review B*, **1988**, *37*(2), 785–789.

[106] Becke, A. D. *Physical Review A*, **1988**, *38*(6), 3098–3100.

[107] Becke, A. D. *Journal of Chemical Physics*, **1993**, *98*(7), 5648–5652.

[108] Becke, A. D. *Journal of Chemical Physics*, **1993**, *98*(2), 1372–1377.

[109] Gorling, A. *Physical Review Letters*, **1999**, *83*(26), 5459–5462.

[110] Anderson, P. W. *Physical Review*, **1961**, *124*(1), 41–53.

[111] Anisimov, V. I.; Zaanen, J.; Andersen, O. K. *Physical Review B*, **1991**, *44*(3), 943–954.

[112] Deeth, R. J.; Fey, N. *Journal of Computational Chemistry*, **2004**, *25*(15), 1840–1848.

[113] Fouqueau, A.; Casida, M. E.; Daku, L. M. L.; Hauser, A.; Neese, F. *Journal of Chemical Physics*, **2005**, *122*(4), 044110–044123.

[114] Kresse, G.; Hafner, J. *Physical Review B*, **1993**, *48*(17), 13115–13118.

[115] Kresse, G.; Hafner, J. *Physical Review B*, **1993**, *47*(1), 558–561.

[116] Kresse, G.; Hafner, J. *Physical Review B*, **1994**, *49*(20), 14251–14269.

[117] Kresse, G.; Furthmueller, J. *Physical Review B: Condensed Matter*, **1996**, *54*(16), 11169–11186.

[118] Cohen-Tannoudji, C.; Dui, B.; Lalöe, F. *Mecanique quantique*. Herman, Paris, 1973.

[119] Blochl, P. E. *Physical Review B*, **1994**, *50*(24), 17953–17979.

[120] Vanderbilt, D. *Physical Review B*, **1990**, *41*(11), 7892–7895.

[121] Kresse, G.; Joubert, D. *Physical Review B: Condensed Matter and Materials Physics*, **1999**, *59*(3), 1758–1775.

[122] Payne, M. C.; Teter, M. P.; Allan, D. C.; Arias, T. A.; Joannopoulos, J. D. *Reviews of Modern Physics*, **1992**, *64*(4), 1045–1097.

[123] Arfken, G. B.; Weber, H. J. *Mathematical Methods for Physicists.* Academic Press, Estados Unidos, 2005.

[124] Johnson, D. D. *Physical Review B*, **1988**, *38*(18), 12807–12813.

[125] Pulay, P. *Chemical Physics Letters*, **1980**, *73*(2), 393–398.

[126] Press, W. H.; Flannery, B. P.; Teukolsky, S. A.; Vetterling, W. T. *Numerical Recipes in C: The Art of Scientific Computing.* Cambridge University Press, 1992.

[127] Jonsson, H.; Mills, G.; Jacobsen, K. W. *Nudged Elastic Band Method for Finding Minimum Energy Paths of Transitions, Classical and Quantum Dynamics in Condensed Phase Simulations.* World Scientific, Singapore, 1998.

[128] Henkelman, G.; Jonsson, H. *Journal of Chemical Physics*, **1999**, *111*(15), 7010–7022.

[129] Komornicki, A.; McIver, J. W. *Journal of the American Chemical Society*, **1976**, *98*(15), 4553–4561.

[130] Marsden, J.; Tromba, A. *Cálculo vectorial.* Madrid, 5 edition, 2004.

[131] Atkins, P. *Química física.* Panamericana, Madrid, 8 edition, 2008.

[132] Bader, R. F. W.; Gillespie, R. J.; Macdougall, P. J. *Journal of the American Chemical Society*, **1988**, *110*(22), 7329–7336.

[133] Bader, R. F. W. *Atoms in Molecules - A Quantum Theory.* Oxford University Press, Oxford, 1990.

[134] Bader, R. F. W. *Physical Review B*, **1994**, *49*(19), 13348–13356.

[135] Bader, R. F. W.; Popelier, P. L. A.; Keith, T. A. *Angewandte Chemie-International Edition in English*, **1994**, *33*(6), 620–631.

[136] Ashcroft, N. W.; Mermin, N. D. *Solid State Physics.* New York, 1976.

[137] Sauer, J. *Chemical Reviews*, **1989**, *89*(1), 199–255.

[138] Illas, F.; Sousa, C.; Gomes, J.; Clotet, A.; Ricart, J. in *Theoretical Aspects of Heterogeneous Catalysis*, Netherlands, S., Ed., volume 8, pp 149–181. Elsevier, Holland, 2002.

[139] Gil, A.; Clotet, A.; Ricart, J. M.; Kresse, G.; Garcia-Hernandez, M.; Rosch, N.; Sautet, P. *Surface Science*, **2003**, *530*(1-2), 71–86.

[140] Bagus, P.; Illas, F. in *Encyclopedia of Computational Chemistry*, Sons, J. W. ., Ed., volume 4, pp 2870–2887. P. v. R. Schleyer, N. L. Allinger, T. Clark, J. Gasteiger, P. A. Kollman, H. F. Schaefer III, P. R. Schreiner, Chichester, UK, 1998.

[141] Pacchioni, G. *Heterogeneous chemistry reviews.* Wiley Interscience, 1996.

[142] Roldan, A.; Torres, D.; Ricart, J. M.; Illas, F. *Surf. Sci.*, **2008**, *602*(15), 2639–2642.

[143] Vines, F.; Illas, F.; Neyman, K. M. *Angewandte Chemie, International Edition*, **2007**, *46*(37), 7094–7097.

[144] Loschen, C.; Bromley, S. T.; Neyman, K. M.; Illas, F. *Journal of Physical Chemistry C*, **2007**, *111*, 10142–10145.

[145] Roldan, A.; Gonzalez, S.; Ricart Josep, M.; Illas, F. *Chemphyschem*, **2009**, *10*(2), 348–51.

[146] Carrasco, J.; Illas, F.; Bromley, S. T. *Physical Review Letters*, **2007**, *99*(23).

[147] Blanco, J.; Linarte, R. *Catálisis: Fundamentos y aplicaciones industriales.* Trillas, México, 1 edition, 1976.

[148] Sabatier, P. *La Catalyse in Chemie Onargique.* Libraire Polytechnique, Paris, 1913.

[149] Frankenburg, W. *The catalytic synthesis of ammonia from nitrogen and hydrogen*, volume III of *Catalysis.* Reinhold, New York, 1955.

[150] Chinchen, C.; Davis, P.; Sampson, R. *The historical development of catalytic oxidation process*, volume 8 of *Catalysis-Science and Technology.* Springer, Berlin, 1987.

[151] Natta, G. *Synthesis of methanol*, volume III of *Catalysis.* Reinhold, New York, 1955.

[152] Sinfelt, J. H. *Surface Science*, **2002**, *500*(1-3), 923–946.

[153] Levine, I. N. *Fisicoquímica*, volume Volumen 2. Madrid, 5 edition, 2004.

[154] Eyring, H. *Journal of Chemical Physics*, **1935**, *3*(2), 107–115.

[155] Evans, M. M. G. Polanyi. *Transactions of the Faraday Society*, **1935**, *31*(1), 0875–0893.

[156] Gilbert, R. G.; Smith, S. C. *Theory of Unimolecular and Recombination Reactions.* Blackwell Science Inc, 1990.

[157] Cortright, R. D.; Dumesic, J. A. in *Advances in Catalysis*, Gates, B. C.; Knoezinger, H., Eds., volume 46. Academic Press, 2001.

[158] Gokhale, A. A.; Kandoi, S.; Greeley, J. P.; Mavrikakis, M.; Dumesic, J. A. *Chemical Engineering Science*, **2004**, *59*(22-23), 4679–4691.

[159] Lynggaard, H.; Andreasen, A.; Stegelmann, C.; Stoltze, P. *Progress in Surface Science*, **2004**, *77*(3-4), 71–137.

[160] Lide, D. R. *CRC Handbook of Chemistry and Physics.* Taylor and Francis, Florida, 87th edition, 2007.

[161] Elliot, S. *Physics of Amorphous Materials.* Longman, 2nd revised edition edition edition, 1990.

[162] J. R. Hook, H. E. H. *Solid State Physics.* Wiley, 2 edition edition, 1991.

[163] Samsonov, G. *Handbook of the physicochemical properties of the elements.* IFI/Plenum, New York, 1968.

[164] Wang, L. L.; Cheng, H. P. *Physical Review B*, **2004**, *69*(16), 165417–165429.

[165] Wang, L. L.; Cheng, H. P. *Physical Review B*, **2004**, *69*(4), 045404–045413.

[166] Torres, D.; Lopez, N.; Illas, F.; Lambert, R. M. *Journal of the American Chemical Society*, **2005**, *127*(31), 10774–10775.

[167] Torres, D.; Illas, F. *Journal of Physical Chemistry B*, **2006**, *110*(27), 13310–13313.

[168] Baumer, M.; Freund, H.-J. *Progress in Surface Science*, **1999**, *61*(7-8), 127–198.

[169] Dellwig, T.; Rupprechter, G.; Unterhalt, H.; Freund, H. J. *Physical Review Letters*, **2000**, *85*(4), 776–779.

[170] Frank, M.; Baumer, M. *Physical Chemistry Chemical Physics*, **2000**, *2*(17), 3723–3737.

[171] Libuda, J.; Meusel, I.; Hoffmann, J.; Hartmann, J.; Piccolo, L.; Henry, C. R.; Freund, H. J. *Journal of Chemical Physics*, **2001**, *114*(10), 4669–4684.

[172] Rupprechter, G. *Physical Chemistry Chemical Physics*, **2001**, *3*(21), 4621–4632.

[173] Unterhalt, H.; Rupprechter, G.; Freund, H. J. *Journal of Physical Chemistry B*, **2002**, *106*(2), 356–367.

[174] Giorgi, J. B.; Schroeder, T.; Baumer, M.; Freund, H. J. *Surface Science*, **2002**, *498*(1-2), L71–L77.

[175] Vermaak, J. S.; Mays, C. W.; Kuhlmann.D. *Surface Science*, **1968**, *12*(2), 128–133.

[176] Skala, L.; Kunne, L.; Fritsche, H. G.; Muller, H. *Physica Status Solidi B-Basic Research*, **1982**, *114*(2), 439–448.

[177] Hermann, K.; Bagus, P. S.; Nelin, C. J. *Physical Review B*, **1987**, *35*(18), 9467–9473.

[178] Boyen, H. G.; Kastle, G.; Weigl, F.; Koslowski, B.; Dietrich, C.; Ziemann, P.; Spatz, J. P.; Riethmuller, S.; Hartmann, C.; Moller, M.; Schmid, G.; Garnier, M. G.; Oelhafen, P. *Science*, **2002**, *297*(5586), 1533–1536.

[179] Kruger, S.; Vent, S.; Nortemann, F.; Staufer, M.; Rosch, N. *Journal of Chemical Physics*, **2001**, *115*(5), 2082–2087.

[180] Molina, L. M.; Hammer, B. *Physical Review B*, **2004**, *69*(15), 155424– 155446.

[181] Hammer, B.; Jacobsen, K. W.; Norskov, J. K. *Physical Review Letters*, **1993**, *70*(25), 3971–3974.

[182] White, J. A.; Bird, D. M.; Payne, M. C.; Stich, I. *Physical Review Letters*, **1994**, *73*(10), 1404–1407.

[183] Hammer, B.; Scheffler, M.; Jacobsen, K. W.; Norskov, J. K. *Physical Review Letters*, **1994**, *73*(10), 1400–1403.

[184] Philipsen, P. H. T.; Tevelde, G.; Baerends, E. J. *Chemical Physics Letters*, **1994**, *226*(5-6), 583–588.

[185] Hu, P.; King, D. A.; Crampin, S.; Lee, M. H.; Payne, M. C. *Chemical Physics Letters*, **1994**, *230*(6), 501–506.

[186] Schmid, G. *Chemical Society Reviews*, **2008**, *37*(9), 1909–1930.

[187] Ono, L. K.; Cuenya, B. R. *Journal of Physical Chemistry C*, **2008**, *112*(47), 18543–18550.

[188] Miller, J. T.; Kropf, A. J.; Zha, Y.; Regalbuto, J. R.; Delannoy, L.; Louis, C.; Bus, E.; Van Bokhoven, J. A. *Journal of Catalysis*, **2006**, *240*(2), 222–234.

[189] Van Bokhoven Jeroen, A.; Louis, C.; Miller Jeffrey, T.; Tromp, M.; Safonova Olga, V.; Glatzel, P. *Angewandte Chemie-International Edition*, **2006**, *45*(28), 4651–4.

[190] Zhang, C.; Yoon, B.; Landman, U. *Journal of the American Chemical Society*, **2007**, *129*(8), 2228–2229.

[191] Boyen, H. G.; Herzog, T.; Kastle, G.; Weigl, F.; Ziemann, P.; Spatz, J. P.; Moller, M.; Wahrenberg, R.; Garnier, M. G.; Oelhafen, P. *Physical Review B: Condensed Matter and Materials Physics*, **2002**, *65*(7), 075412/1–075412/5.

UNIVERSITAT ROVIRA I VIRGILI
MODELLING AU CATALYST FROM BULK TO NANOSCALE
Alberto Roldán Martínez
ISBN:978-84-693-7669-0/DL:T-1748-2010

UNIVERSITAT ROVIRA I VIRGILI
MODELLING AU CATALYST FROM BULK TO NANOSCALE
Alberto Roldán Martínez
ISBN:978-84-693-7669-0/DL:T-1748-2010

List of Figures

UNIVERSITAT ROVIRA I VIRGILI
MODELLING AU CATALYST FROM BULK TO NANOSCALE
Alberto Roldán Martínez
ISBN:978-84-693-7669-0/DL:T-1748-2010

List of Tables

UNIVERSITAT ROVIRA I VIRGILI
MODELLING AU CATALYST FROM BULK TO NANOSCALE
Alberto Roldán Martínez
ISBN:978-84-693-7669-0/DL:T-1748-2010

UNIVERSITAT ROVIRA I VIRGILI
MODELLING AU CATALYST FROM BULK TO NANOSCALE
Alberto Roldán Martínez
ISBN:978-84-693-7669-0/DL:T-1748-2010

UNIVERSITAT ROVIRA I VIRGILI
MODELLING AU CATALYST FROM BULK TO NANOSCALE
Alberto Roldán Martínez
ISBN:978-84-693-7669-0/DL:T-1748-2010

UNIVERSITAT ROVIRA I VIRGILI
MODELLING AU CATALYST FROM BULK TO NANOSCALE
Alberto Roldán Martínez
ISBN:978-84-693-7669-0/DL:T-1748-2010